Role of the collagen receptor DDR1 in epithelial morphogenesis and polarisation



Pia Pernille Søgaard
St Catherine's College

Supervisors
Dr Yoshifumi Itoh
Dr Linda Troeberg

Matrix Biology Group
Kennedy Institute of Rheumatology
Nuffield Department of Orthopaedics, Rheumatology and Musculoskeletal Sciences
University of Oxford

Thesis submitted for the degree of Doctor of Philosophy to University of Oxford
Trinity 2017

Approximate word count: 45,014

Abstract

Thesis title: Role of the collagen receptor DDR1 in epithelial tubulogenesis and polarisation

Candidate: Pia Pernille Søgaard, St Catherine's College

Degree: Doctor of Philosophy (DPhil), Trinity 2017

During development of epithelial organs, epithelial cells collectively migrate and invade into their surroundings to form complex 3D structures, such as the tubular ducts and alveoli of the mammary gland. A prerequisite for coordinating such collective movement is apicobasal cell polarity. This polarity divides the plasma membrane of epithelial cells into an apical domain towards the lumen of structures and a basal domain facing the matrix. Polarity is essential for the functionality of epithelial tissues and signals from the surrounding matrix are known to participate in its establishment. In contrast, loss of polarity has been associated with progression of diseases such as cancer. During epithelial tubulogenesis, the pro-invasive enzyme MT1-MMP is regulated according to apicobasal polarity. This regulation is essential for tubulogenesis to occur and restricts MT1-MMP activity to the tip of protruding tubules by ensuring that the enzyme only localises to the basal, matrix-abutting cell surface in this location. Signals from fibrillar collagen I contribute to regulating the polarised distribution of MT1-MMP. How such signals are transmitted and influence polarised trafficking is however not understood.

In this study, I found that inhibition of the collagen receptor DDR1 disturbed the apicobasal distribution of MT1-MMP in MDCK cells. In 3D environments, DDR1 inhibition blocked MT1-MMP-dependent tubulogenesis of epithelial cells, which instead formed compact, multi-layered aggregates. Furthermore, polarisation of the epithelial cell membrane into an apical and a basal domain failed in absence of DDR1 signalling,

suggesting that DDR1 affects establishment of epithelial polarity. In support of this, the effects of DDR1 signalling on apicobasal polarity were not limited to MT1-MMP-dependent morphogenesis, but also proved essential for polarisation of cells during 3D morphogenesis that did not require ECM degradation.

An investigation of signalling downstream of DDR1 in establishment of apicobasal polarity revealed this to involve modulation of cytoskeletal tension. Inhibition of DDR1 in 2D culture of MDCK cells thus increased ROCK-dependent phosphorylation of MLC along cell-cell junctions, suggesting that DDR1 can suppress ROCK activity. Importantly, the ROCK-suppressing function of DDR1 contributed to establishment of polarity in MDCK cells in 3D matrices, where inhibition of ROCK activity rescued the formation of polarised cysts in absence of DDR1 signalling.

The role of DDR1 in epithelial organisation was reflected in the epithelium of the mammary gland of lactating DDR1-null mice, which had smaller alveoli with a diffuse distribution of basement membrane components compared to wild type mice. Furthermore, DDR1 inhibition attenuated formation of milk-producing mammospheres during lactogenic differentiation of mammary epithelial cells *in vitro* in a ROCK-dependent manner. This suggests that the ROCK-suppressing function of DDR1 observed in MDCK cells is important for morphogenesis of other epithelial cell types as well.

Overall, this study suggests that DDR1 signalling contributes to epithelial polarisation and morphogenesis in a manner involving regulation of cytoskeletal organisation, at least partly through regulation of ROCK activity.

Acknowledgements

I would first of all like to thank my supervisor Dr Yoshi Itoh for giving me the chance to take on this exciting project as a PhD student in his lab. Yoshi has been an engaged, demanding and fun supervisor to work for. I am grateful to him for always taking the time to explain, discuss, troubleshoot and encourage. Yoshi's enthusiasm for science is contagious and his ability to push you to always do better has made my time in his lab incredibly instructive. I would also like to thank my co-supervisor Dr Linda Troeberg for providing great advice and guidance on my project and the PhD experience in general as well as for all her useful feedback during the write-up of my thesis.

I would like to thank Noriko, the best teacher that any student could hope to have in the lab, for all her help, guidance, tips and tricks, and not least for fun stories and laughter at lunchtime. The Itoh lab and the rest of the matrix biology group at the Kennedy Institute has been an incredibly friendly and fun environment to work in, and I would like to thank past and present members for help, support and friendship during my time here.

I would like to thank Professor Karl Matter at UCL for offering his expert knowledge on the regulation of the cytoskeleton and junctions in epithelial cells as well as providing lab space and guidance for measuring transepithelial resistance. The two weeks I spent in his lab were instrumental for discovering the involvement of RhoA-ROCK signalling downstream of DDR1.

My time in Oxford would not have been the same without Stephanie, Sandy and George and all the other fantastic housemates and friends I met at Old Road 43. The comfort of coming home to a house full of friends, the company whilst cooking and

complaining about failed experiments and the fun weekends we have shared have been essential for making my time here in Oxford so enjoyable. Furthermore, I am grateful to friends and family in Denmark, particularly my parents, Sigrid, Nanna, Sarah and Jakob, for all their support, emails, phone calls and visits that have lifted me up, when I felt homesick.

Last but not least I would like to thank my partner Aslak for sharing this UK adventure with me and for providing me with a constant source of support and happiness as well as amazing dinners after long days in the lab.

Table of contents

List of Figures **10**
List of Tables **11**
Abbreviations **12**
Declaration **15**

Chapter 1: Introduction **16**

1.1 Epithelial tissue and morphogenesis 17
1.1.1 Epithelial organisation 17
1.1.2 Establishment of epithelial polarity 21
1.1.3 Role of ECM receptors in establishing and orienting apicobasal polarity 27
1.1.4 Epithelial polarisation and morphogenesis in 3D environments 29

1.2 Role of the collagen receptor DDR1 in epithelial polarity and morphogenesis 34
1.2.1 Structure and function of DDR1 34
1.2.2 Biological roles of DDR1 signalling 38
1.2.3 Role of DDR1 in epithelial morphogenesis 42

1.3 Matrix degradation during epithelial morphogenesis 46
1.3.1 Membrane type I matrix metalloproteinase (MT1-MMP) 47
1.3.1 Role and regulation of MT1-MMP in epithelial tubulogenesis 50

1.4 Aims of this thesis 55

Chapter 2: Materials and methods **58**

2.1 Reagents 59

2.2 Molecular biology 59
2.2.1 General solutions 63
2.2.2 Cloning of MT1-pHluorin-RFP 63
2.2.3 Restriction digestion 65
2.2.4 DNA fragment purification 65
2.2.5 Blunt-ending of DNA 65
2.2.6 Ligation of DNA fragments into pJET, pSG5, pCEP4 and pCEP4-neo 65
2.2.7 Transformation of bacteria by electroporation 66
2.2.8 DNA isolation from small-scale culture (mini-prep) by alkaline lysis with SDS 66
2.2.9 RT-PCR 67

2.3 SDS-PAGE and western blotting 67
2.3.1 General solutions 67
2.3.2 Preparation of cell lysates 68
2.3.3 SDS-PAGE gel composition and procedure 69
2.3.4 Western blotting procedure 70

2.4 Cell biology 70
2.4.1 Culture of cell lines 70
2.4.2 Cryopreservation and thawing 71
2.4.3 Transfection of plasmid DNA 72
2.4.4 siRNA transfection of MDCK cells 73
2.4.5 Generation of MDCK cell lines stably expressing plasmid DNA 73
2.4.6 Transduction of MDCK cells with adenovirus 73

2.4.7 Transduction of MDCK cells with lentivirus 74
2.4.8 Generation of MDCK cell lines stably expressing shRNA 75
2.4.9 Culture of cells on gelatin-coated coverslips and culture inserts 75
2.4.10 Gelatin degradation assay in 2D culture 75
2.4.11 Culture of cells on collagen I-coated coverslips and culture inserts 76
2.4.12 Collagen degradation assay in 2D culture 76
2.4.13 Immunoprecipitation of DDR1 77
2.4.14 TER measurements 78
2.4.15 Standard tubulogenesis assay 78
2.4.16 Tubulogenesis assay on microcarrier beads 79
2.4.17 Lactogenic differentiation of HC11 cells to form mammospheres. 80
2.4.18 Branching morphogenesis of primary mammary organoids 81

2.5 Immunocytochemistry 82

2.6 Immunohistochemistry (IHC) 84

2.7 Imaging and analysis 86
2.7.1 Image Processing and analysis 87
2.7.2 Statistical analysis 87

Chapter 3: Collagen signalling through DDR1 plays a role in establishment of apicobasal polarity during epithelial 3D morphogenesis 88

3.1 Introduction 89

3.2 Results 90
3.2.1 HGF induces MDCK cells to undergo MMP-dependent tubulogenesis in 3D collagen I matrices 90
3.2.2 MT1-pHluorin-RFP: A tool to study surface localisation of MT1-MMP during 3D tubulogenesis 92
3.2.3 MT1-MMP localises to the basal surface of cells at the tip of protruding tubules during HGF-induced epithelial tubulogenesis 97
3.2.4 HGF induces a collagen-dependent change in the apicobasal distribution of MT1-MMP in polarised monolayers of MDCK cells 99
3.2.5 Inhibition of signalling from the collagen receptor DDR1 disturbs the polarised distribution of MT1-MMP 102
3.2.6 Alteration of MT1-MMP distribution upon inhibition of DDR1 is functionally significant 105
3.2.7 DDR1 is required for HGF-induced, MMP-dependent tubulogenesis of MDCK cells 106
3.2.8 DDR1 signalling is required for tubulogenesis of MDCK and MCF-10A cells in a modified tubulogenesis assay on microcarrier beads 109
3.2.9 DDR1 inhibition disturbs the distribution of apicobasal markers and lumen formation during MMP-dependent epithelial tubulogenesis 112
3.2.10 DDR1 is required for lumen formation and polarisation during HGF-independent formation of cysts by MDCK and CaCO-2 cells 116

3.3 Discussion 119

Chapter 4: Signalling downstream of DDR1 in epithelial polarisation and morphogenesis 126

4.1 Introduction 127

4.2 Results 127

4.2.1 Identification of molecules involved in DDR1 signalling using chemical inhibitors 128

4.2.1.1 Inhibitor screening suggests PKCαβ as signalling molecules downstream of DDR1 128

4.2.1.2 Inhibition of PKCαβ disturbs polarisation and lumen formation in MDCK and CaCO-2 cells similarly to inhibition of DDR1 131

4.2.1.3 Inhibition of PKCα and -β attenuates tubulogenesis on microcarrier beads and prevents increased collective invasion by MDCK-DDR1 cells 133

4.2.1.4 Generation of MDCK lines with stable knock-down of PKCα or -β 134

4.2.1.5 Knockdown of PKCα or β in MDCK cells does not recapitulate the effect of chemical inhibition of PKCα and β on epithelial tubulogenesis 137

4.2.2 Analysis of DDR1-mediated effects on epithelial organisation in 2D culture to find downstream targets with effects on polarity. 139

4.2.2.1 DDR1 inhibition does not disturb apicobasal polarity in monolayers of MDCK cells 139

4.2.2.2 DDR1 inhibition delays the formation of a mature, polarised monolayer of MDCK cells 140

4.2.2.3 DDR1 inhibition increases ROCK-dependent ppMLC at cell-cell junctions.. 144

4.2.2.4 DDR1 localises to adherens junctions in MDCK cells 147

4.2.2.5 Inhibition of ROCK activity rescues lumen formation and polarisation during cyst formation. 148

4.2.2.6 Inhibition of ROCK restores the polarised distribution of MT1-MMP in inert polarised MDCK cells, but prevents the HGF-induced increase in MT1-MMP at the basal cell surface 151

4.2.2.7 Inhibition of ROCK activity does not rescue lumen formation and polarisation during cyst formation upon inhibition of PKCα and β 153

4.3 Discussion 154

Chapter 5: DDR1 contributes to morphogenesis and differentiation of mammary epithelium 162

5.1 Introduction 163

5.2 Results 164

5.2.1 Mammary gland tissue from DDR1-null mice has smaller ducts and displays diffuse distribution of basement membrane markers 164

5.2.2 Inhibition of DDR1 attenuates branching morphogenesis of primary mammary organoids 166

5.2.3 DDR1 inhibition attenuates formation of mammospheres by HC11 cells in response to lactogenic stimulation in a ROCK-dependent manner 169

5.2.4 DDR1 inhibition causes increased ROCK activity in HC11 cells 171

5.2.5 ROCK inhibition promotes production of β-casein in the absence of DDR1 signalling 172

5.2.6 β-casein staining is not decreased in lactating DDR1-null mice 174

5.3 Discussion 175

Chapter 6: General discussion and future prospects 182

Chapter 7: References 196

Chapter 8: Appendix 208

8.1 Supplementary tables 208

List of Figures

Chapter 1

Figure 1. Diagrammatic representation of types of epithelium.. 18
Figure 2. Junction complexes in the polarised epithelial cell..... 20
Figure 3. Distribution of the major polarity complexes in polarised epithelial cells. 22
Figure 4: An example of the intertwined roles of polarity complexes and RhoGTPases. 24
Figure 5. Organisation of phosphatidylinositide-phosphate lipids and the microtubule cytoskeleton in polarised epithelial cells. 25
Figure 6. Lumen formation and tubular morphogenesis by epithelial cells in 3D. ... 33
Figure 7. Structure of DDR1 and predicted binding partners.. 35
Figure 8. Selected signalling pathways downstream of DDR1 41
Figure 9. Structure of MT1-MMP. 48

Chapter 2

Figure 10. Cloning strategy to create pSG5-MT1F-pHluorin-RFP 64

Chapter 3

Figure 11. HGF induces scattering of MDCK cells in 2D 90
Figure 12. HGF induces MMP-dependent tubulogenesis by MDCK cells in 3D collagen I 91
Figure 13. MT1F-pHluorin-RFP: A tool for specific detection of MT1-MMP at the cell surface..... 93
Figure 14. MT1-pHluorin-RFP can be visualised at the cell membrane at neutral, but not acidic extracellular pH. 95
Figure 15. MT1F-pHluorin-RFP displays functional gelatinase activity. 96
Figure 16. Generation of MDCK-MT1pH cells. 98
Figure 17. HGF- induces a collagen-dependent increase in basal localisation of MT1-MMP at the basal cell surface 101
Figure 18. Inhibition of DDR1 disturbs the polarised distribution of MT1-MMP . 104
Figure 19. Increased localisation of MT1-MMP to the basal surface in the absence of DDR1 signalling is functionally significant 106
Figure 20. DDR1 is required for tubulogenesis in 3D 108
Figure 21. DDR1 is required for tubulogenesis on microcarrier beads and may positively affect collective invasion 112
Figure 22. DDR1 inhibition leads to disorganised apicobasal polarity during HGF-induced tubular morphogenesis..... 116
Figure 23. DDR1 is required for lumen formation and polarisation in MMP-independent morphogenesis 118

Chapter 4

Figure 24: Screening of signalling pathway inhibitors in MDCK tubulogenesis assay.. 130
Figure 25: Apicobasal polarity of epithelial cells is disturbed by inhibition of PKCα and –β during tubulogenesis in 3D matrices 132
Figure 26. Inhibition of PKCα and -β prevents HGF-induced tubulogenesis and attenuates increased collective invasion by MDCK-DDR1 cells..... 133
Figure 27. Stable knockdown of PKCα and –β in MDCK cells 136
Figure 28. Knockdown of PKCα does not inhibit tubulogenesis 138

Figure 29 DDR1 inhibition does not disturb polarity in MDCK cells in 2D culture 140
Figure 30. Inhibition of DDR1 causes a delay in maturation of epithelial monolayers 143
Figure 31: DDR1 inhibition causes increased ROCK activity at cell-cell-junctions 147
Figure 32. DDR1 localises to adherens junctions 148
Figure 33. Inhibition of ROCK activity rescues formation of polarised cysts in absence of DDR1 signalling 149
Figure 34. Inhibition of ROCK does not restore HGF-induced tubulogenesis of MDCK cells in absence of DDR signalling 151
Figure 35. ROCK inhibition prevents recruitment of MT1-MMP to the basal cell surface with consequence for collagen degradation 152
Figure 36. Inhibition of ROCK signalling does not rescue lumen formation and polarisation in the absence of PKCα and β signalling 154

Chapter 5

Figure 37. DDR1-null mice have altered epithelial organisation in the mammary gland 166
Figure 38. DDR1 inhibition attenuates branching morphogenesis of primary, mammary epithelial organoids 168
Figure 39. Inhibition of ROCK rescues attenuated mammosphere formation upon inhibition of DDR1 signalling 170
Figure 40. Inhibition of DDR1 increases ROCK activity in HC11 cells 172
Figure 41. Inhibition of ROCK rescues DIP-induced β-casein expression in the absence of DDR1 signalling. 173
Figure 42. β-casein expression is not decreased in lactating DDR1-null mice 174

List of Tables

Chapter 2

Table 1. List of cell lines used in this thesis 71

Chapter 8

Table 1S. Summary of statistic analysis in chapter 4, **Figure 34**A 207

Chapter 8

Table 2S. Summary of statistic analysis in chapter 5, **Figure 38**C 207

Abbreviations

2D	2-dimensional
3D	3-dimensional
aa	Amino acid
Ad-MT1F	Adenoviral vector encoding flag-tagged MT1-MMP
ADAM	A disintegrin and metalloproteinase
α-SMA	α smooth muscle actin
AMIS	Apical initiation site
aPKC	Atypical protein kinase C
APS	Ammonium persulphate
bFGF	Fibroblast growth factor basic
BSA	Bovine serum albumin
CaCO-2	Human colon adenocarcinoma cells
Cat	Catalytic domain
Cdc42	Cell division cycle 42
CIP	Calf intestinal phosphatase
CLSM	Confocal laser scanning microscope
COS-7	Chinese hamster ovary cells
ddH2O	Double distilled water
DDR	Disoidin domain receptor
DDR1ΔC	DDR1, deleted cytoplasmic domain
DIP	Dexamethasone, insulin and prolactin
DMEM	Dulbecco's modified eagle medium
DMSO	Dimetyl sulfoxide
DNA	Deoxyribonucleic acid
EB1	End binding 1
ECM	Extracellular matrix
EDTA	Ethylenediaminetetraacetic acid
EGF	Epidermal growth factor
EMT	Epithelial to mesenchymal transition
ERK	Extracellular signalling related protein kinase
ERM	Ezrin/radixin/myosin
FAK	Focal adhesion kinase
FCS	Foetal Calf serum
FRET	Förster resonance energy transfer
G418	Neomycin
GFP	Green fluorescent protein
GM6001	Ilomastat
GP135	Glycoprotein 135
GPI	Glycosylphosphatidylinositol
h	Hour
HA	Hyaluronic acid
HC11	Mammary epithelial cells
HE	Hematoxilin/Eosin
HEK293	Human embryonic kidney cells

HGF	Hepatocyte growth factor
Hpx	Hemopexin domain
HRP	Horse radish peroxide
IgG	Immunoglobulin G
IHC	Immunohistochemistry
IHC	Immunohistochemistry
ILK	integrin-linked kinase
IMDM	Iscove's DMEM
JAM	Junctional adhesion molecule
kb	Kilo base
kDa	Kilo Dalton
LB	Luria-Bertani medium
MAP	Mitogen-activated protein kinase
MCF10-A	Michigan Cancer Foundation-10 A
MDCK	Madin Darby canine kidney cells
MEK	MAP/ERK kinase
min	Minute
MLC	Myosin light chain
MMP	Matrix metalloproteinases
mRFP1	Monomeric RFP1
MT-MMP	Membrane type matrix metalloproteinase
MT1-MMP	Membrane type 1 matrix metalloproteinase
MT1-pHluorin-RFP	MT1-MMP tagged with pHluorin and mRFP1
MT1-RFP	MT1-MMP tagged with mRFP1
MT1F	MT1-MMP with FLAG-tag
MT1F	Flag-tagged MT1-MMP
MT1F-RFP	MT1-MMP with FLAG-tag and RFP-tag
NFkappaB	Nuclear factor kappaB
NT	Non-targeting
NT-shRNA	Non-targeting shRNA
NT-siRNA	Non-targeting siRNA
P/S	Penicillin/Streptomycin
PAGE	Polyacrylamide electrophoresis
PAP	Pre-apical patch
Par1-6	Partitioning protein 1-6
PBS	Phosphate-buffered saline
PCR	Polymerase Chain Reaction
PI-P	Phosphoinositide phosphate
PI3K	Phosphoinositide 3-kinase
PIP2	Phosphoinositide (4,5) phosphate
PIP3	Phosphoinositide (3,4,5) phosphate
PKC	Protein kinase C
ppMLC	Diphosphorylated MLC (Thr18/Ser19)
PrlR	Prolactin receptor
PTEN	Phosphatease and tensin homolog
PVDF	Polyvinylidene difluoride

RFP	Red fluorescent protein
Rho	Ras homolog gene family
RhoGAP	RhoGTPase-activating protein
RhoGEF	Rho guanine exchange factor
ROCK	Rho associated kinase
RPM	Rotations per minute
RPMI	Roswell Park Memorial Institute (cell culture medium)
RTK	Receptor tyrosine kinase
s	Second
SDCM	Spinning disc confocal microscope
SDS	Sodium dodecyl sulphate
shRNA	Short hairpin RNA
siRNA	Short interfering RNA
Src	Sarcoma tyrosine kinase
STAT	Signal transducer and activator of transcription
TBS	Tris-buffered saline
TE	Tris-EDTA buffer
TEMED	Tetramethylethylendiamine
TER	Transepithelial resistance
TF	Transcription factor
TIMP	Tissue inhibiotrs of metalloproteinases
TM	Transmembrane
v/v	Volume per volume
w/v	Weight per volume
WAP	Whey acidic protein
ZO1	Zonula occludens 1

Declaration

This dissertation is the result of my own work. All collaborations have been acknowledged in the appropriate place within the text.

Chapter 1 Introduction

1.1 Epithelial tissue and morphogenesis

1.1.1 Epithelial organisation

An organism is protected from its external environment by continuous layers of epithelial cells lining both inner and outer surfaces exposed to the exterior world. Such epithelial layers perform a variety of functions ranging from mechanical barriers (e.g. the skin), absorption (e.g. nutrients are absorbed across the intestinal epithelium and transported into the blood stream), secretion (e.g. hormones and lubricating fluids are secreted in glands), diffusion (e.g. oxygen is taken up across the alveolar epithelium in the lung) and excretion (e.g. waste products are secreted across the renal epithelium in the kidney, and CO2 is excreted in the lungs)[1].

In accordance with the variety of functions of epithelial tissues, the organisation of each epithelium is optimised for its specialised function. For example, flat squamous epithelial cells are found in the alveoli of the lung, where the epithelium is optimised to provide a large surface area of thin cells to allow efficient diffusion of oxygen from the airspace to the bloodstream (**Figure 1A**)[1]. Secretory cells often take on a cuboidal appearance (**Figure 1B**), whereas absorptive cells in regions subjected to more wear and tear frequently have a columnar morphology (**Figure 1C**)[1]. The upper airways are covered by pseudostratified, ciliated cells, which are specialised to transport mucous away from the lungs towards the pharynx by the beating movement of cilia (**Figure 1D**)[1]. This clears dust and pathogens from the airways. Additionally, whereas epithelium can consist of a single monolayer (like in the previous examples), it can also form thick, multi-layered tissues (**Figure 1E**). The keratinised, stratified epidermis of the skin is an example of such multi-layered epithelium, which is specialised to withstand physical insult, dehydration and pathogen entry (**Figure 1E**)[1]. In this thesis, I will mainly describe my research on the epithelial cell line Madin Darby Canine Kidney (MDCK) cells, which

form a simple cuboidal epithelium. Additionally, I will describe my research on mammary epithelial cells, focusing on the function of the luminal, columnar cells of mammary alveoli.

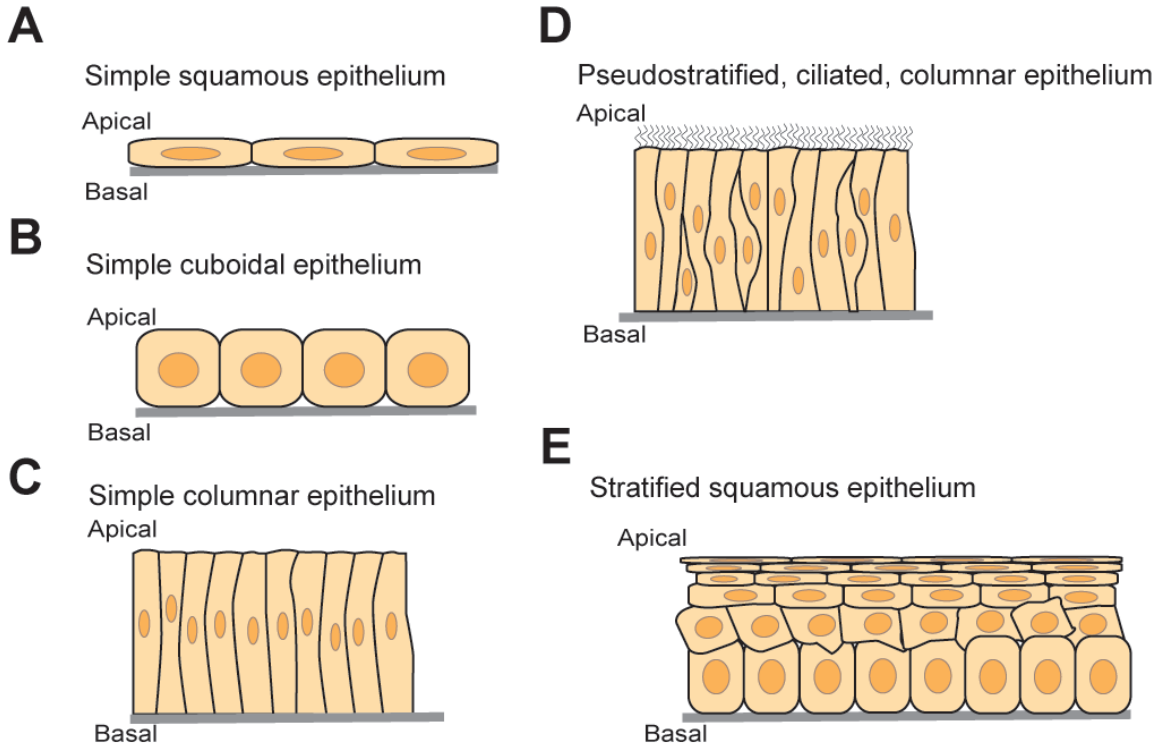


Figure 1. Diagrammatic representation of types of epithelia. A) Simple squamous epithelium is optimised for efficient diffusion, and found in tissues where such permeability is needed, such as the alveoli of the lung and epithelium of glomeruli. **B**) Simple cuboidal epithelium typically performs secretion and/or absorption for example in the renal tubules and glandular ducts. **C**) Simple columnar epithelium is also optimised for absorption and secretion, but is thicker than cuboidal epithelium and thus better able to withstand wear and tear. As such it is found in the intestinal epithelium where absorption as well as a high degree of wear and tear occurs. **D**) Pseudostratified, ciliated, columnar epithelium. A pseudostratified epithelium displays staggered localisation of the nuclei, but all cells reside on the basement membrane and the epithelium is as such a true simple epithelium despite giving the impression of stratification. Cilia provide the epithelium with the ability to transport mucous secretions, for example in the upper airways. **E**) Stratified squamous epithelium is a multi-layered epithelium, where only one layer of cells attach to the basement membrane. This epithelium is optimised to withstand mechanical insult and provide efficient barrier function. The skin is an example of a stratified epithelium, where cells become filled with keratin as they travel from the proliferating basal layer towards the flatter outermost layers.

Epithelial polarity

Common to all epithelial cells is the polarisation of the cell membrane into an apical membrane facing the free surface and a basolateral domain towards the extracellular matrix (ECM)-abutting surface (**Figure 2**)[2]. The result is a cell with a polarised distribution of lipids, proteins and organelles along its apicobasal axis[2]. The

border between the apical and basal membrane domain is formed by the tight junctions, which are composed of transmembrane proteins including occludins, claudins and junctional adhesion molecules (JAMs), as well as cytoplasmic plaque proteins including the adaptor protein zonula occludens 1 (ZO1) and other proteins linking to cytosolic components such as GTPases, kinases and transcription factors (**Figure 2**)[3]. The transmembrane tight junction proteins link neighbouring plasma membranes to each other and create a tight seal rendering the epithelium highly impermeable to paracellular diffusion[3]. Tight junctions also inhibit intramembranous diffusion of membrane-bound molecules, thus aiding in maintaining the distinct composition of the two membrane domains[3]. The adaptor proteins of tight junctions link to the actin cytoskeleton (**Figure 2**)[4]. Basal to the tight junctions, the adherens junctions connect neighbouring cells extracellularly through homophilic interactions between the transmembrane cadherin proteins of adjacent cells (**Figure 2**)[4]. Intracellularly, cadherins link to the actin cytoskeleton via catenin proteins (**Figure 2**)[4]. The actin cytoskeleton at the level of the adherens junctions is organised into a circumferential band of actomyosin, which through its contractile abilities regulate epithelial cell shape and transmit forces between neighbouring cells[4]. Most basally, the desmosomes connect neighbouring cells and anchor intracellular intermediate filaments to the plasma membrane (**Figure 2**)[5]. Hemidesmosomes connect cells to the underlying basement membrane via integrins, and together with desmosomes play a role in conferring the high resistance of epithelia to mechanical tear forces (**Figure 2**)[5]. In addition, lateral gap junctions create channels allowing for the rapid passage of small molecules between the cytoplasm of neighbouring cells (**Figure 2**)[3].

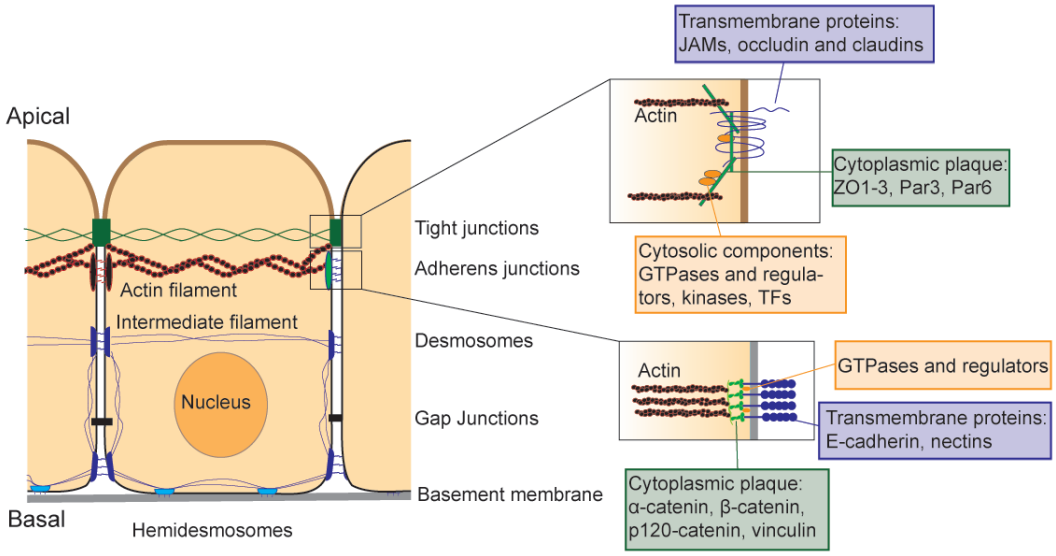


Figure 2. Junction complexes in the polarised epithelial cell. Epithelial cells reside on a basement membrane (grey) towards which their basal side is oriented, whereas the apical side faces the free surface. A number of specialised junctions connect epithelial cells to one another and the underlying ECM. From the apical side these are the tight junctions, adherens junctions, desmosomes and hemidesmosomes. To the right are shown enlarged schematics of the tight and adherens junctions with listed examples of their constituent proteins. JAMs: junctional adhesion molecules, TF: transcription factor.

In addition to flat epithelia like the skin, epithelium *in vivo* is often organised into complex three-dimensional (3D) structures such as the ball-shaped alveoli of lungs and secretory units of glands, as well as tubular structures in organs such as the kidney, mammary glands and lungs. Such tubular networks can mediate transportation of fluids and nutrients between different body compartments as well as provide large surface areas for exchange of ions, nutrients, gases etc.[6,7,8]. Epithelial tubes are composed of a polarised layer of epithelial cells surrounding a central lumen. The apical side of the cells is presented to the lumen, whereas the basal side faces the ECM[9,8]. The functionality of such epithelial organs relies on this polarity, and establishment and orientation of polarity during epithelial morphogenesis is thus essential during development. However, the mechanisms regulating the polarisation process in a 3D context are not fully understood[8].

1.1.2 Establishment of epithelial polarity

Epithelial polarisation initially requires specialised polarity complexes to be distributed asymmetrically along the apicobasal axis. In addition, cues from neighbouring cells and the surrounding environment through cell-cell and cell-ECM adhesions contribute to guiding the division of the cell membrane into distinct membrane domains[10]. Such membrane domains acquire a specific lipid composition, which, together with adhesion and polarity complexes as well as dynamic rearrangements of the cytoskeleton, facilitates polarised endo- and exocytic trafficking. Such polarised trafficking further contributes to the asymmetric distribution of proteins in the cell[10]. Polarisation is thus a complex process requiring coordination and cooperation of several cellular processes. Whilst much of our understanding of polarity, particularly polarisation during development, originates from important studies in *Drosophila*, *Xenopus* and *C. elegans*, I will in this chapter focus on mechanisms of polarisation in mammalian cells.

Polarity complexes

Three major polarity complexes are involved in establishment of epithelial polarity: the Par (Cdc42-Par3-Par6-aPKC), Crumbs (Crumbs-PALS-PATJ) and Scribble (Scribble-Dlg-Lgl) complexes (**Figure 3A**)[11]. These complexes are distributed asymmetrically within the cell with the Par and Crumbs complexes working apically and Scribble functioning basolaterally (**Figure 3A**). The Par complex can further be subdivided into the Par3-aPKC complex, which localises at the tight junctions and the apical Cdc42-Par6-aPKC (**Figure 3A**)[11]. Additional Par proteins with important functions in polarity exist, including the laterally located kinase, Par1, and the 14-3-3 protein Par5[2]. The asymmetric distribution of polarity proteins is one of the earliest steps of the polarisation process and relies on the ability of these proteins to mutually exclude each other from distinct membrane domains[11]. For example, atypical protein kinase C (aPKC)

is recruited to the apical domain by the Crumbs complex, where it excludes basolateral proteins including Par1 (**Figure 3B**). Conversely, Par1 localises in the basolateral domain and excludes apical proteins from the basolateral membrane including Par3 (**Figure 3B**). Exclusion of membrane proteins by both aPKC and Par1 depends on their ability to phosphorylate mislocalised proteins (**Figure 3B**, left). Such phosphorylations then recruit Par5, which enables dissociation of the mislocalised, phosphorylated protein from the plasma membrane (**Figure 3B**, right)[2]. Regulation of Par1 and -3 in this manner is depicted in **Figure 3B**.

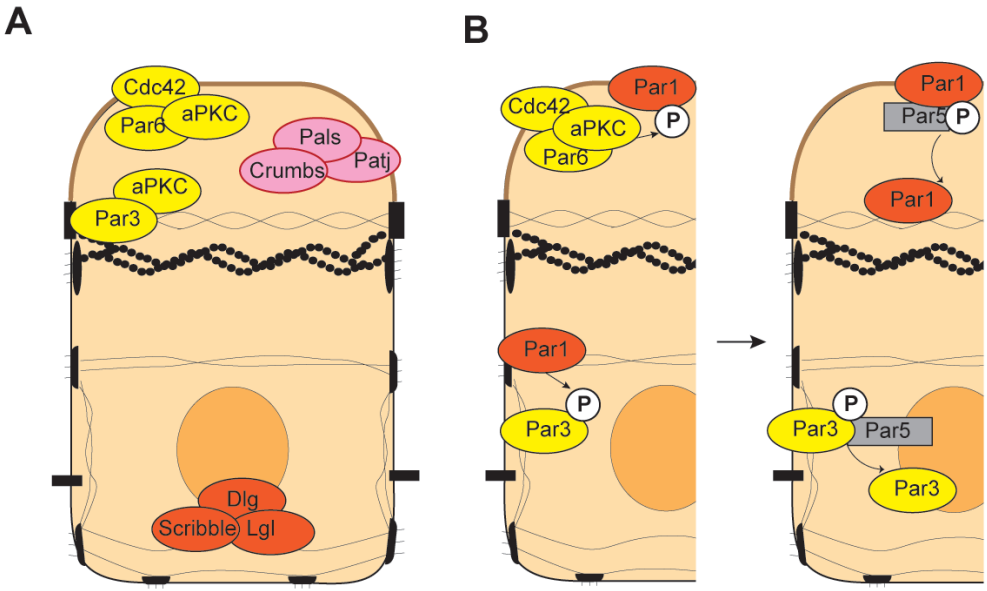


Figure 3. Distribution of the major polarity complexes in polarised epithelial cells. A) Epithelial cells have three major polarity complexes, namely the Par (Cdc42-Par3-Par6-aPKC), Crumbs (Crumbs-PALS-PATJ) and Scribble (Scribble-Dlg-Lgl) complexes[11]. The Par (yellow) and Crumbs (pink) localise apically, whereas Scribble (red) functions basolaterally. The Par complex is further divided into Par6-aPKC-Cdc42 and Par3-aPKC. These complexes contribute to epithelial polarisation through local recruitment of proteins regulating cytoskeletal organisation, lipid distribution and vesicle transport[11]. **B)** The polarised distribution of the polarity complexes is established early in the polarisation process. Their asymmetric distribution at least partly relies on their ability to mutually exclude each other from their domains[2]. Left: Mislocalised Par1 at the apical membrane is phosphorylated by aPKC. Similarly mislocalised Par3 at the basolateral membrane is phosphorylated by Par1[2]. Right: the phosphorylation on the mislocalised proteins recruits Par5, which dissociates the proteins from the cell membrane, and thus allows them to relocalise appropriately. Such mechanisms continuously contribute to removing mislocalised proteins and thus maintain the polarised protein distribution[2].

The asymmetric distribution of polarity complexes further contributes to the polarised distribution of other proteins by recruiting them to distinct locations in the cell. This includes proteins that ensure a polarised distribution of membrane lipids, regulators of vesicle transport as well as cytoskeletal regulators including RhoGTPases and modulators of their activity[2].

Role of RhoGTPases in orienting apicobasal polarity

RhoGTPases are a family of small signalling molecules of the Ras superfamily, which can cycle between a GTP-bound active state and a GDP-bound inactive state[12]. The intrinsic GTPase activity of RhoGTPases can thus switch the protein off by converting it to the GDP-bound state. The GDP/GTP-bound state of RhoGTPases is further controlled by regulatory proteins such as Rho GTPase activating proteins (RhoGAPs), which stimulate the intrinsic RhoGTPase activity. In addition, Rho guanine exchange factors (RhoGEFs) promote the release of GDP from RhoGTPases to allow binding of GTP[2]. RhoGTPases control processes such as cytoskeletal organisation, membrane trafficking and cell-ECM interactions, which are crucial for the polarisation process. In line with this, RhoGTPases are an important group of effector molecules downstream of the polarity complexes, which can regulate RhoGTPases by locally recruiting RhoGAPs and -GEFs[11]. As such, the 3 prototypical RhoGTPases RhoA, Cdc42 and Rac1 have all been assigned important functions during polarisation[11]. Cdc42 forms part of the Par polarity complex and is involved in generating apical membrane identity and maintaining the apical, cortical actin meshwork[13]. It is thus indispensable for lumen formation in 3D culture[13]. Rac1 is associated with signalling through integrins and affects orientation of polarity[14,15]. RhoA activity is found both at the apical and basal domains and controls cytoskeletal contraction, cell shape and migration[11]. Additionally, RhoA-mediated contractility is

involved in bending the plasma membrane during vesicle fusion, and thus contributes to vesicular trafficking.

Par proteins and RhoGTPases have intertwined roles in the polarisation process. Par3 can for example associate with the RhoGEF Tiam1/2, which in complex with aPKC-Par6-Cdc42 activates Rac1 (**Figure 4**, left)[16]. Spatial restriction on this activation of Rac1 is conferred by RhoA-ROCK signalling, which phosphorylates Par3 (**Figure 4**, middle) and leads to dissociation of Par3-Tiam1/2 from the Par6-aPKC complex resulting in inactivation of Rac1 (**Figure 4**, right)[16]. RhoA-ROCK signalling can thus locally turn off Rac1 activity.

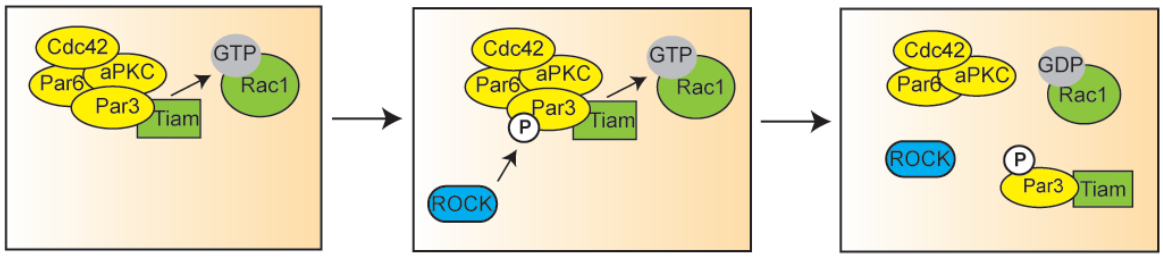


Figure 4: An example of the intertwined roles of polarity complexes and RhoGTPases. The Par complex can locally activate Rac1 by recruiting the Rac1-activating RhoGEF Tiam. This activation can be abolished by RhoA-ROCK mediated phosphorylation of Par3, which leads to dissociation of Par3 and Tiam from the Par complex and thus switches off Rac1 activation in the localisation of the Par complex[16].

Polarised distribution of membrane lipids

Phosphatidylinositol-phosphates (PI-P) are signalling phospholipids, which constitute 1% of lipids in the plasma membrane[2,11]. These lipids vary with regards to number and location of phospho groups in the inositol ring. Membrane domains have a specific PI-P composition, which is regulated by the local presence of PI kinases and phosphatases in organelles and membrane domains. For example the PI-3 kinase (PI3K) associates with E-cadherin in the adherens junctions and enhances production of $PI(3,4,5)P_3$ (PIP3), which consequently recruits E-cadherin[2,11]. Such feedback loops result in PIP3 exclusively being found in the basolateral domain of MDCK cells (**Figure 5A**)[2,11]. In contrast, the phosphatase PTEN is associated with the tight junctions via the

Par3-aPKC complex where it promotes formation of $PI(4,5)P_2$ (PIP2) in the apical domain (**Figure 5A**)[11]. These signalling lipids can then dock other proteins, which bind to specific PI-P motifs and thereby contribute to the polarised distribution of proteins across membrane domains[2]. Furthermore, these lipids are important for polarised trafficking[17]. Disturbing the polarised distribution of PI-Ps by inhibiting the factors that maintain it, e.g. PTEN, causes mistargeting of apical proteins to the basolateral surface and prevents lumen formation in 3D[13].

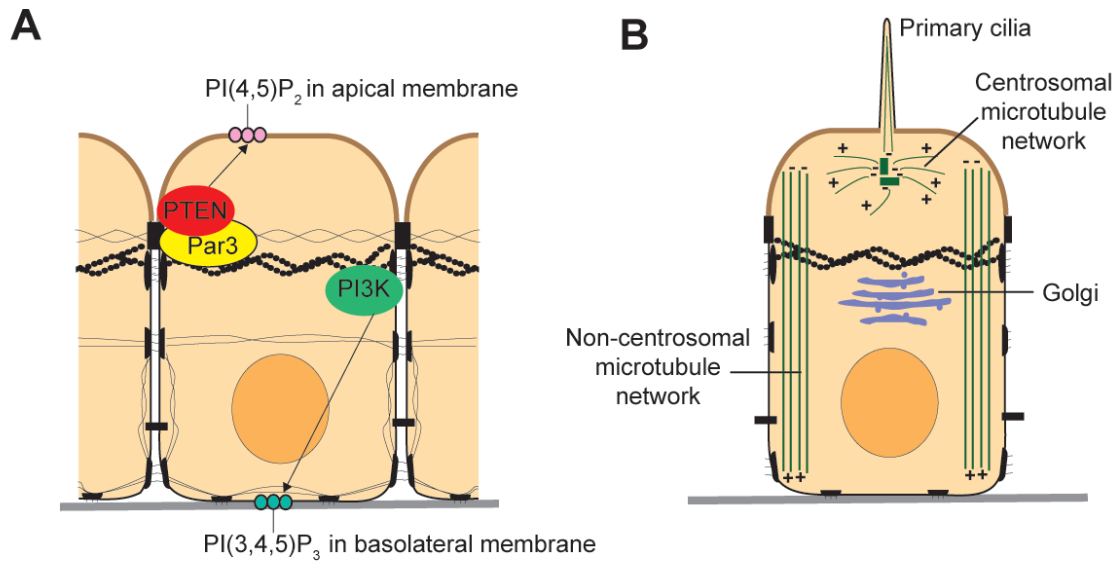


Figure 5. Organisation of phosphatidylinositide-phosphate lipids and the microtubule cytoskeleton in polarised epithelial cells. A) PI-P lipids have a polarised distribution in epithelial cells, which is regulated by PI kinases and phosphatases. PI3K localises in adherens junctions and promotes accumulation of $PI(3,4,5)P_3$ in the basolateral membrane, whereas PTEN in tight junctions promotes the presence of $PI(4,5)_2$ in the apical membrane. This distribution of PI-Ps is required for the polarised recruitment of proteins to the plasma membrane[11]. **B**) A centrosomal and a non-centrosomal microtubule network are found in epithelial cells. The majority of microtubules belong to the non-centrosomal network, which dominates as epithelial cells differentiate. Plus ends of microtubules in the centrosomal network radiate towards adherens junctions and the primary cilia, whereas the non-centrosomal network runs along the lateral plasma membrane with plus-ends towards the basal surface and minus-ends towards the apical surface[18].

Organisation of the cytoskeleton during epithelial polarisation

Both the actin and microtubule cytoskeleton of epithelial cells undergo extensive reorganisation during polarisation. Adherens junctions play an important role in organising the actin cytoskeleton within epithelial cells and in coordinating this organisation between neighbouring cells. Conversely, junction formation and

maintenance also rely on dynamics of the actin cytoskeleton[2]. Local RhoA activity has for example been reported to promote junction formation through effects on actomyosin contractile activity[19], and tight junction barrier function can similarly be modulated by actomyosin tension[3]. Furthermore, the actin cytoskeleton contributes to vesicle trafficking by acting as tracks for vesicle transport along the apical membrane and facilitating vesicle-membrane fusion[18].

Vesicle transport primarily occurs along the microtubules, and microtubule organisation is thus central for polarised trafficking. Vesicles are transported towards either the plus- or the minus-end of microtubules depending on their associated motor proteins[17,18]. The orientation of microtubules is thus critical for polarised trafficking and accordingly the microtubule network is more stable in epithelial cells than in non-polarised cell types[2]. Epithelial cells have both a centrosomal and a non-centrosomal microtubule network with the majority of microtubules belonging to the non-centrosomal network (**Figure 5B**)[18]**.** The centrosomal network is organised by the apically located centrosome with plus-ends radiating towards adherens junctions and the primary cilium (**Figure 5B**)[18]. The primary cilium is a specialised epithelial structure with sensory and signalling functions and constitutes its own subdomain of the apical membrane[18]. Its biogenesis involves both the Par and Crumbs complexes in addition to the centrosomal microtubule network[18]. The non-centrosomal network runs along the apicobasal axis at the cellular cortex with plus-ends towards the basal surface and minus-ends towards the apical surface (**Figure 5B**)[18]. The non-centrosomal microtubule network becomes dominant as epithelial cells go from sub-confluent to confluent[18]. Microtubule organisation in epithelial cells is responsible for the supranuclear positioning of the Golgi apparatus as well as correct localisation of both sorting and recycling endosomes[2].

1.1.3 Role of ECM receptors in establishing and orienting apicobasal polarity

Role of the ECM in orientation of polarity

Despite detailed knowledge of the molecular machinery that contributes to the establishment of polarity, there are still many open questions as to how the epithelial polarity programme is executed[2,9,11,20]. An important element for initiation of the polarisation process appears to be the initial establishment of an apicobasal axis. This relies at least in part on cues from the extracellular environment mediated through contacts with neighbouring cells as well as recognition of the ECM[2]. The immediate ECM underlying a polarised epithelial monolayer is the basement membrane, which is a 100 nm thin sheet of specialised ECM including laminin, collagen IV and proteoglycans[21]. Formation of a fully functional basement membrane requires both secretion and correct assembly of basement membrane components along the basal cell surface[21]. Initial establishment of polarity and basement membrane deposition are thus intertwined processes[21]. However, whereas it is clear that different organisms and epithelial organs deposit basement membrane via different mechanisms, the overall understanding of the process remains limited[20].

The importance of basement membrane assembly is underlined by its disruption through inhibition of β1-integrin or Rac1 causing disorganisation of epithelial polarity in MDCK cells in 3D collagen I[14,15]. Interestingly, addition of exogenous laminin, but not collagen IV, can rescue orientation of polarity[14]. This may be connected to the finding that laminin deposition precedes collagen IV deposition and is thought to be required for its assembly[21,22].

Role of ECM-receptors in orientation of polarity

Epithelial cells bind basement membrane components via cell surface receptors including integrins, dystroglycan and the receptor tyrosine kinase discoidin domain

receptor 1 (DDR1)[20,23]. β1-integrin is known to be important for orienting apicobasal polarity in epithelial cells[20]. β1-integrin mediates these effects via recruitment of a range of cytoskeletal adapters, including vinculin and talin and signalling molecules such as integrin-linked kinase (ILK) and focal adhesion kinase (FAK)[20]. Such integrin-associated complexes contribute to regulating cytoskeletal organisation and signalling in response to recognition of the surroundings. In accordance with a role of β1-integrin in orienting apicobasal polarity, lack of β1-integrin disturbs polarisation during cystogenesis of epithelial cells in 3D collagen I [15,24]. This is due to excessive activity of the RhoA-ROCK-myosin pathway, and knockdown of RhoA can thus rescue correct apicobasal polarity in absence of β1-integrin signalling[24].

MDCK cells in suspension culture form cysts with inverted polarity. The fact that cysts with inverted polarity in suspension culture still maintain cell-cell junctions and an asymmetric distribution of molecules and lipids suggests, that polarisation and orientation of polarity to some extend are regulated independently[11]. The orientation of polarity in these structures is reoriented in a β1-integrin-dependent manner upon their transfer to a collagen matrix[15,25,26]. This function of β1-integrin relies on its activation of Rac1, which promotes laminin assembly along the collagen-abutting cell surface causing it to gain basal membrane identity[15]. In the above example, β1-integrin is activated by collagen I and consequently promotes basement membrane assembly at the collagen-abutting cell surface[20]. Laminin in an assembled basement membrane can, however, also activate β1-integrin to provide polarising cues for epithelial cells[20]. These different roles of β1-integrin require it to pair with different α-subunits, and its role as a collagen receptor is thus mediated in cooperation with the α1, α2 or α11-integrin subunits, whereas its role as a laminin receptor occurs in complex with the α3 subunit[20]. β1-integrin thus plays several crucial roles in orienting epithelial polarity *in vitro*[14,27]. *In vivo*, the requirement of β1-

integrin for correct apical polarity during morphogenesis is underlined by the conditional knockout of β1-integrin in luminal mammary epithelial cells; this causes aberrant tubular morphogenesis of ducts and alveoli in the mammary gland of pregnant female mice[27,28].

While the role of integrins in establishing polarity has been extensively studied, less is known about other ECM receptors. Dystroglycan has been reported to contribute to laminin-induced polarisation in mammary epithelial cells[29], however, its role in polarisation of MDCK cells has not been well characterised. Mice lacking DDR1 also display defects in branching morphogenesis of the mammary gland[30,31]. DDR1-null mice have similar morphological defects to those induced by ablation of β1-integrin, but additionally display deficient lactation postpartum[30]. *In vitro*, DDR1 has been implicated in tubular morphogenesis of MDCK cells[32]. Whether this role for DDR1 in epithelial morphogenesis includes effects on epithelial polarity has not been established. Since this will be addressed in this thesis, a detailed background to this collagen receptor will be provided in the second section of this chapter (Section **1.2**).

1.1.4 Epithelial polarisation and morphogenesis in 3D environments

Much work contributing to our understanding of epithelial cell polarity has been conducted using epithelial cell lines, such as MDCK cells, growing in 2D culture on artificial supports such as coverslips or culture inserts[11]. Such cells receive strong polarisation cues because of the asymmetric nature of their environment with a substratum on one side and free medium on the other side[11]. In contrast, a more symmetric ECM will surround cells undergoing morphogenesis in tissues *in vivo* and cues to orient polarity will thus differ from the 2D situation.

MDCK cells in a 3D collagen I matrix is a frequently used model to study lumen formation and polarisation in 3D environments *in vitro*[11]. This requires cells to proliferate or migrate to form clusters, which then establish fluid-filled, hollow lumens between

them[33]. MDCK cells can further be induced to undergo tubular morphogenesis by addition of hepatocyte growth factor (HGF)[34,35], and can thus also be used to study epithelial polarisation during tubulogenesis. These models have provided important inputs to our understanding of epithelial polarisation in 3D environments.

An important concept governing epithelial cell behaviour in 3D is that cells appear to always attempt to establish 3 distinct membrane regions: an ECM-abutting basal side, a lateral domain along cell-cell contacts and an apical domain facing a free surface[11]. This is based on a variety of experimental observations including that cells lacking an apical domain will establish one by generating a lumen in a region of contact with a neighbouring cell[11]. In the absence of such contacting regions, a pseudo-lumen can be created within the cell itself in the form of vacuoles containing apical proteins[11]. Furthermore, cells that are not in contact with the ECM and thus lack a domain with basal identity, will undergo apoptosis[11]. These observations underpin our understanding of the central role of cell-cell adhesions and cell-ECM contacts in the establishment and orientation of polarity[25,26].

Lumen formation in 3D matrices

Lumen formation can occur in several ways depending on the model system. For single MDCK cells in 3D culture, apical proteins will initially be distributed equally along the ECM-abutting surface[11,25] (**Figure 6A**). Proliferation of cells will lead to establishment of cell-cell contacts and an apical membrane initiation site (AMIS) will form at these points of contact (**Figure 6A**). Apical proteins such as GP135, aPKC, Cdc42 are transported to the AMIS from the ECM-abutting surfaces via Rab-dependent vesicle transport[36] (**Figure 6A**). As the AMIS matures, it develops into a pre-apical patch (PAP), which is sealed off by junctional complexes between the two cells' membranes[36] (**Figure 6A**). The PAP is enriched in actin and actin-binding proteins such as Ezrin-Radixin-

Moesin (ERM) proteins, which are transported from the ECM-abutting surface in a β1-integrin-dependent manner[37]. Cdc42 plays an important role in maintaining this actin network, which can anchor apical proteins to the apical membrane via various actin-associated adaptor proteins and thus contributes to polarisation[10]. As the apical membrane matures, the membranes between the two cells will be pushed apart by electrostatic repulsion generated by negative charges on apical proteins such as sialic acid on GP135[9]. RhoA-ROCK-mediated contraction further separates the apical membranes[9]. Apicobasal polarity is in this way established at the 2-cell stage in 3D culture. Continuous proliferation of cells surrounding a lumen extends the size of the lumen and the number of cells surrounding it (**Figure 6A**). Such proliferation must occur in a regulated manner, in terms of the mitotic spindle being oriented, so that the plane of division is perpendicular to the axis of apicobasal polarity[9]. As an open lumen forms between multiple cells, the junctions that sealed off the pre-apical patch are separated into tight and adherens junctions, leading to cells having clearly defined apical, lateral and basal surfaces[10] (**Figure 6 A**). Expansion of the open lumen between multiple cells requires the pumping of water from the ECM into the lumen. This process is regulated by osmotic pressure, ion channels, permeability-modulating claudins and paracellular permeability[9].

The model for lumen formation by MDCK cells described above is referred to as "hollowing"[10]. In contrast to this, 3D cultures of mammary epithelial acini are thought to form lumens through a process referred to as "cavitation", which involves formation of cellular aggregates through extensive proliferation, followed by apoptosis of cells not in contact with the ECM[10,11].

Tubulogenesis

Once a lumen is established, tubulogenesis requires further proliferation, migration and invasion to create tubular networks. For MDCK cells, such remodelling

induced by HGF requires cells to transiently lose their polarised organisation and instead proliferate and migrate to form epithelial chains and cords[38,39] (**Figure 6B**). Such chains and cords maintain cell-cell junctions, but lack the division of the plasma membrane into clearly defined apical and basal domains[39] (**Figure 6B**). De novo lumens are established within cords, which eventually coalesce to form continuous lumens as tubulogenesis proceeds[39] (**Figure 6B**). Tubulogenesis thus relies on the mechanisms described for lumen formation above, but additionally requires proliferation, invasion and reorganisation of adhesions and the cytoskeleton[11]. HGF signalling activates a number of pathways, which contribute to these cellular events[40]. For example, activation of ERK via Ras promotes proliferation, whereas PI3K activation stimulates survival[40]. Both pathways additionally affect organisation of the cytoskeleton and cell adhesions[40]. Modulation of RhoGTPase activity is another important contributor to the reorganisation required during tubulogenesis and HGF activates both Rac and RhoA[41]. Furthermore, expression of mutant forms of RhoA, Rac and Cdc42 all disturb tubulogenesis[42]. RhoA mediates these effects, at least partially, via its downstream effector ROCK, which has been shown to affect the number and length of branches formed during tubulogenesis[38].

Besides regulation of cell morphology and signalling, tubulogenesis requires remodelling of the ECM to facilitate extension of new tubular structures into the surrounding matrix. Such degradation is mediated by matrix metalloproteinases (MMPs), particularly the transmembrane MMP, MT1-MMP[43]. The role of MT1-MMP in tubulogenesis will be discussed below (Section **1.3**)

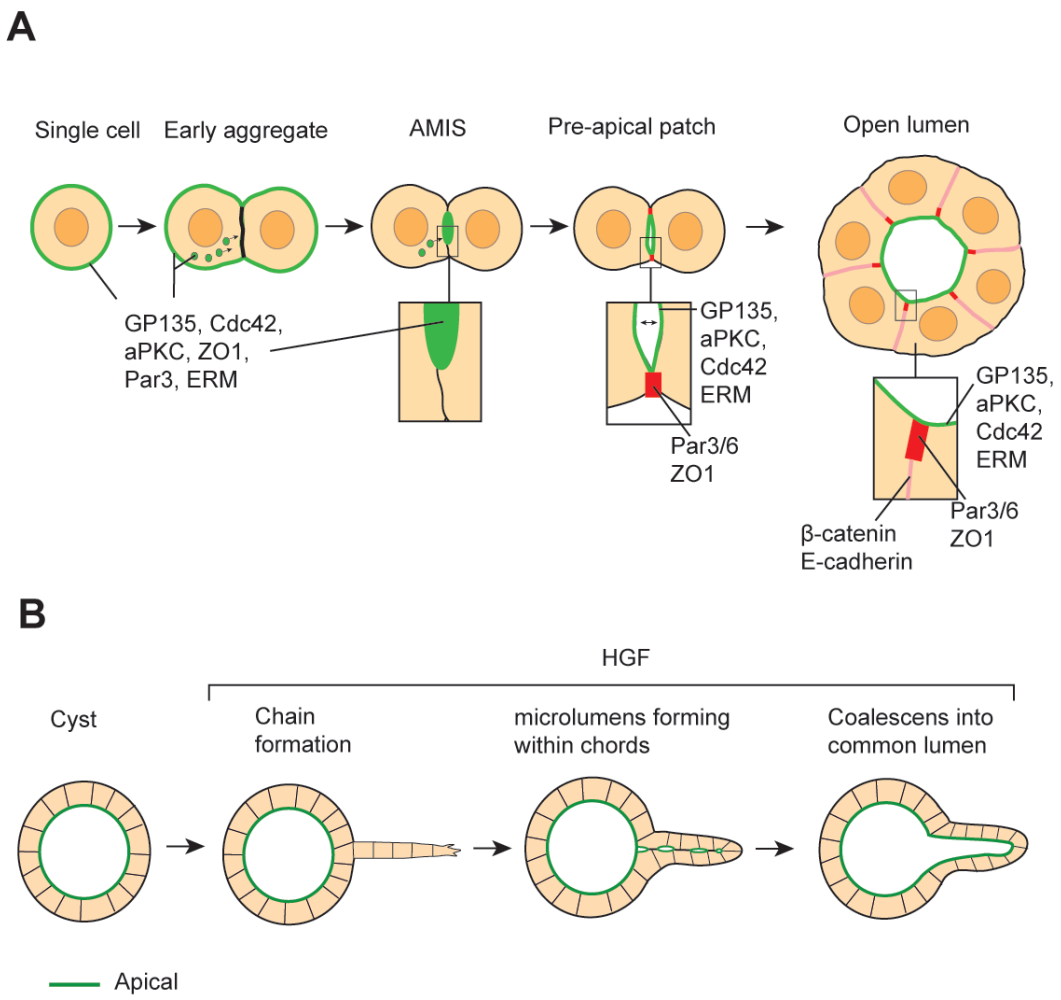


Figure 6. Lumen formation and tubular morphogenesis by epithelial cells in 3D. A) Apical proteins (green, examples of proteins are listed) are distributed along the ECM-abutting surface of single cells in 3D environments[11,25]. These proteins are endocytosed from the cell-ECM surface and transported to points of contact between cells in early aggregates. This area becomes the apical membrane initiation site (AMIS). The AMIS develops into a pre-apical patch (PAP), which is sealed off by junctional complexes between the two cells' membranes (red)[36]. Electrostatic repulsion and cytoskeletal contraction separate the two cell membranes as the PAP matures[9]. Continuous proliferation will extend the lumen size. As an open lumen forms between multiple cells, the junctions that sealed off the pre-apical patch are separated into tight (red) and adherens junctions (pink), leading to cells having clearly defined apical, lateral and basal surfaces[10]. **B)** A model for tubulogenesis by MDCK cells is depicted[39]. Upon HGF stimulation, chains of cells extend from existing cysts. This requires cells to partially lose the division of the cell membrane into an apical and a basal domain, whilst retaining cell-cell junctions. Proliferation expands these chains into cords, and microlumens occur de novo within these cords. Such lumens coalesce to form a central lumen, which eventually becomes continuous with the original cyst lumen[39].

1.2 Role of the collagen receptor DDR1 in epithelial polarity and morphogenesis

1.2.1 Structure and function of DDR1

The receptor tyrosine kinases (RTK) DDR 1 and -2 were discovered in the early 1990s by homology cloning[44]. These RTKs contain a discoidin domain in their extracellular region as well as long cytosolic, juxtamembrane domains[44]. The ligand for these receptors was unknown until 1997, when two groups independently discovered that both DDR1 and -2 are activated by collagens[45,46]. In the study by Vogel et al.[45], DDR1 was found to be phosphorylated in response to Matrigel, and collagen IV was identified to be the component responsible for this activation. Additionally, collagen I-III and V were found to activate DDR1[45]. DDR2 was found to be activated by collagen I-III and V, but not IV[45]. Later, collagen X was found to be an additional ligand for DDR2[47]. The native conformation of collagen was established to be important for DDR activation, since heat-denatured collagen (gelatin) was unable to activate the receptors[45].

The expression pattern of DDR1 and -2 differs, with DDR1 primarily being expressed in epithelial cells and DDR2 in mesenchymal cells[48]. Five isoforms of DDR1 (DDR1a-e) exist, which vary in the length of their cytosplasmic domains. DDR1a and –b are widely expressed and differ by the presence of an extra 37 amino acid sequence in the cytoplasmic domain of DDR1b[44]. DDR1d and –e are truncated forms of DDR1, which lack the cytoplasmic kinase domain[44]. DDR2 only has one isoform, which has about 50% sequence identity to DDR1[44]. DDR1 contains an extracellular region with a discoidin and a discoidin-like domain followed by a juxtamembrane domain and a transmembrane domain (**Figure 7A**). Several glycosylation sites are present in the discoidin-like and juxtamembrane domains. Intracellularly, the large juxtamembrane domain with

phosphorylation sites is followed by the kinase domain, which contains additional phosphorylation sites[44] (**Figure 7A**). Both DDR1 and -2 form constitutive dimers[49,50].

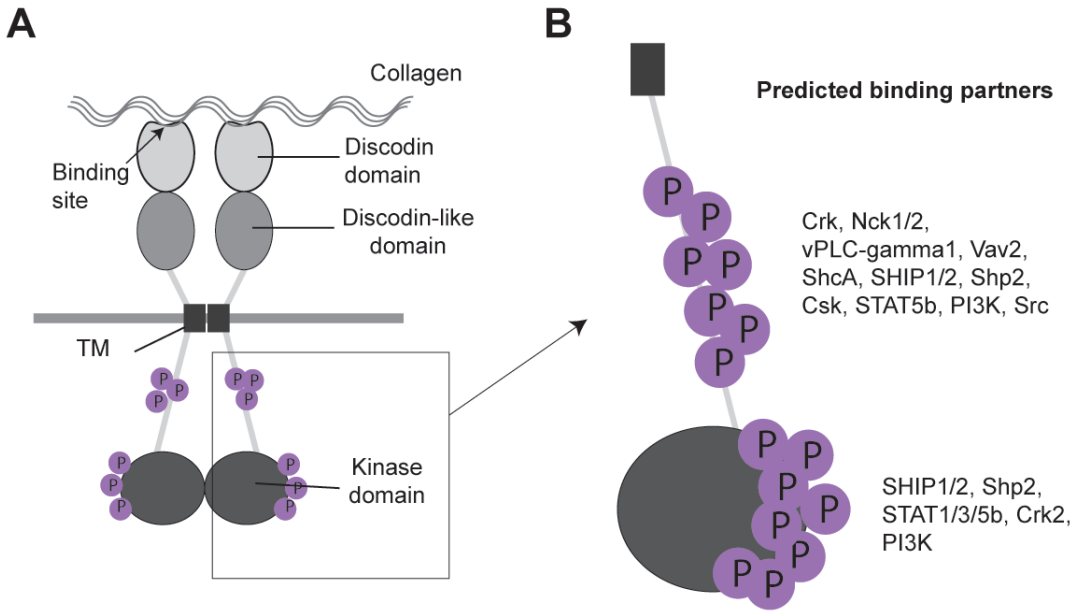


Figure 7. Structure of DDR1 and predicted binding partners. A) DDR1 consists of an extracellular region with a discoidin and a discoidin-like domain followed by a juxtramembranous domain and a transmembrane region. The discoidin-like and juxtamembrane domains contain glycosylation sites. The intracellular part of DDR1 consist of a large juxtamembrane domain followed by the kinase domain. These both contain phosphorylation sites[44]. **B**) 7 and 8 validated phosphorylation sites exist in the juxtamembrane and kinase domain respectively[44]. Potential binding partners with SH2 and PTB domains binding to phospho-residues in each region as predicted by a proteomic study[51] are listed according to Leitinger 2014[48].

Collagen binding and activation of DDR1

DDR1 binds collagen through its discoidin domain. The binding site for DDR1 in collagen has been mapped by using libraries of triple–helical collagen II and III peptides[52]. This revealed a GVMGFO motif to be recognised by DDR1, which is similar to what was previously found for DDR2[53]. This motif is also present in the α-chains of collagen I and can thus also explain binding to this collagen type[52]. Importantly, crystallographic analysis of DDR2 binding to collagen revealed that DDR2 simultaneously interact with the GVMGFO motif in two of the three chains in triplehelical collagen[54], thus providing a potential explanation to why denatured collagen does not activate DDRs[44]. 5 amino acids in a region outside of the GVMGFO binding

pocket are thought to be involved in binding of DDR1 to collagen IV, since mutation of the corresponding residues in DDR2 allows DDR2 to bind collagen IV[52].

The kinetics of receptor phosphorylation upon collagen binding to DDRs are unusually slow compared to other RTKs[44]. While conventional RTKs are activated within seconds or minutes of stimulation before the signal rapidly becomes downregulated, DDRs are activated slowly and the phosphorylation is sustained for hours[44]. The mechanism for this slow and sustained activation of DDRs is not understood. Furthermore, it remains unclear how collagen binding causes activation of the kinase domain. There is no obvious structural alteration of DDR1 upon collagen binding, and the long flexible juxtamembrane domains would make it difficult for binding of collagen at the ectodomain to be directly translated into conformational changes in the kinase domain[44,48]. Many RTKs are activated by ligand-induced dimerisation[55]. However, DDR1 has been found to exist as constitutive, ligand-independent dimers by cross-linking and immunoprecipitation studies and FRET microscopy[49,50]. Using FRET microscopy, DDR1 has been found to oligomerise in response to collagen stimulation[50] and it is possible that collagen-induced high-order clustering of the receptor contributes to its activation. Since collagen forms a high-order complex fibril structure, DDR1 could be clustered due to the multiple binding sites in its ligand. However, collagen does not need to be in the fibrillar state to activate DDR1, since triple-helical-mimetic peptides can mediate activation[52]. Lateral association of DDR1 dimers was recently found to mediate phosphorylation in trans between dimers, suggesting that clustering indeed is part of the activation mechanism for DDR1. Interestingly, phosphorylation was independent of kinase activity of the receiver dimer, and DDR1 dimers lacking the ectodomain were also recruited to and phosphorylated in such receptor clusters[56].

Regulation of DDR1 activity

DDRs are unusual RTKs in that their ligands are ECM components and thus continuously present in the cells' surroundings[44]. Little is known about the degree to which the DDR1 activating motifs of collagen are exposed in an intact healthy tissue *in vivo*. It is possible that activating motifs only become exposed by damage- or remodelling-induced changes to the ECM. DDR2 was recently found to be more readily activated by partially damaged cartilage compared to intact cartilage[57]. As DDR1 shares the same binding motifs within collagen, it is likely that DDR1 activation similarly is induced by partial damage of tissue *in vivo.*

Additional levels of regulation, besides activation, ensure timely downregulation of DDR signalling. Endocytosis of ligand-bound receptor from the cell surface is a common way for RTK activity to be downregulated[58]. Signalling can then either continue from endosomes or be immediately terminated[58]. Endocytosis of YFP-tagged DDR1 has been reported to occur within the time frame of DDR1 phosphorylation after collagen exposure, suggesting that DDR1 may exhibit endosomal signalling[50]. This was however not shown for un-tagged DDR1 and has not been addressed in other studies. The role of endocytosis in regulating DDR1 activity thus remains unclear[48].

Metalloprotease-dependent shedding is known to release the ectodomain of DDR1. Depending on the cell type studied, this can happen both constitutively and in response to collagen stimulation[59]. Shedding downregulates signalling from DDR1 and can release or prevent its binding to the ECM[48]. Collagen-dependent shedding of DDR1 has been shown to be mediated by ADAM10 in HEK293, MCF-7 and A431 cells, where it contributes to downregulation of DDR1 signalling[60]. Shedding of DDR1 was found to be important for cell migration with decreased migration on collagen observed upon expression of a shedding-resistant DDR1-mutant. Knockdown of DDR1 also reduced

migration, suggesting that both attachment and detachment of DDR1 to the ECM are important for migration[60]. Another study found overexpression MT1-MMP to result in spontaneous DDR1 shedding in COS-7, T47D and HCC1806 cells[61]. This study did however not address if endogenous MT1-MMP is responsible for DDR1 shedding.

It is unclear which and how phosphatases contribute to the regulation of DDR1. Inhibition of phosphatase activity by pervanadate treatment leads to increased levels of DDR1 phosphorylation being detected[51], suggesting that endogenous phosphatases can dephosphorylate DDR1. Further studies are however required to determine the biological significance of such regulation as well identifying specific phosphatases involved.

1.2.2 Biological roles of DDR1 signalling

DDR1-null mice phenotype

DDR1-null mice are viable and fertile, but adult males and females are 10%/35% smaller than wild type littermates respectively[30]. Female DDR1-null mice display inefficient blastocyst implantation with implantation only occurring in 20% of females[30]. Furthermore, DDR1-null females that give birth fail to produce milk and are thus unable to nurture their offspring[30]. This defective lactation is a result of aberrant mammary gland differentiation during pregnancy and early onset of involution postpartum[30]. Failed mammary gland differentiation of DDR1-null mice may involve disruption of the lactogenic signalling cascade, since DDR1-null mammary epithelial cells show reduced activation of STAT5 upon lactogenic stimuli[31]. In line with this role for DDR1 in lactogenic differentiation of the mammary gland, the expression of DDR1 has been shown to increase during normal pregnancy and lactation in wild type mice, with a drop in its expression occurring at the onset of involution[30]. A delay in ductal growth in the mammary glands during puberty is furthermore seen in DDR1-null mice. At this time point, terminal end buds are enlarged and the mammary epithelium is hyperproliferative[30].

Besides changes in the mammary epithelium, increased stromal deposition of collagen I is found in the glands of DDR1-null mice[30]. Knockout of DDR1 thus severely affects the mammary gland at time points where active remodelling occurs, suggesting that DDR1 is important for morphogenic processes *in vivo*.

In addition to a phenotype of the mammary gland, DDR1-null mice have been reported to display a thickening of the glomerular basement membrane in the kidney, leading to mild proteinuria[62]. In models of the kidney diseases Alports syndrome, glomerulonephritis and unilateral ureteral obstruction, inhibition of DDR1 has conversely been found to be protective against proteinuria and disease progression[63,64]. DDR1 thus appears to play important roles for kidney function in both health and disease.

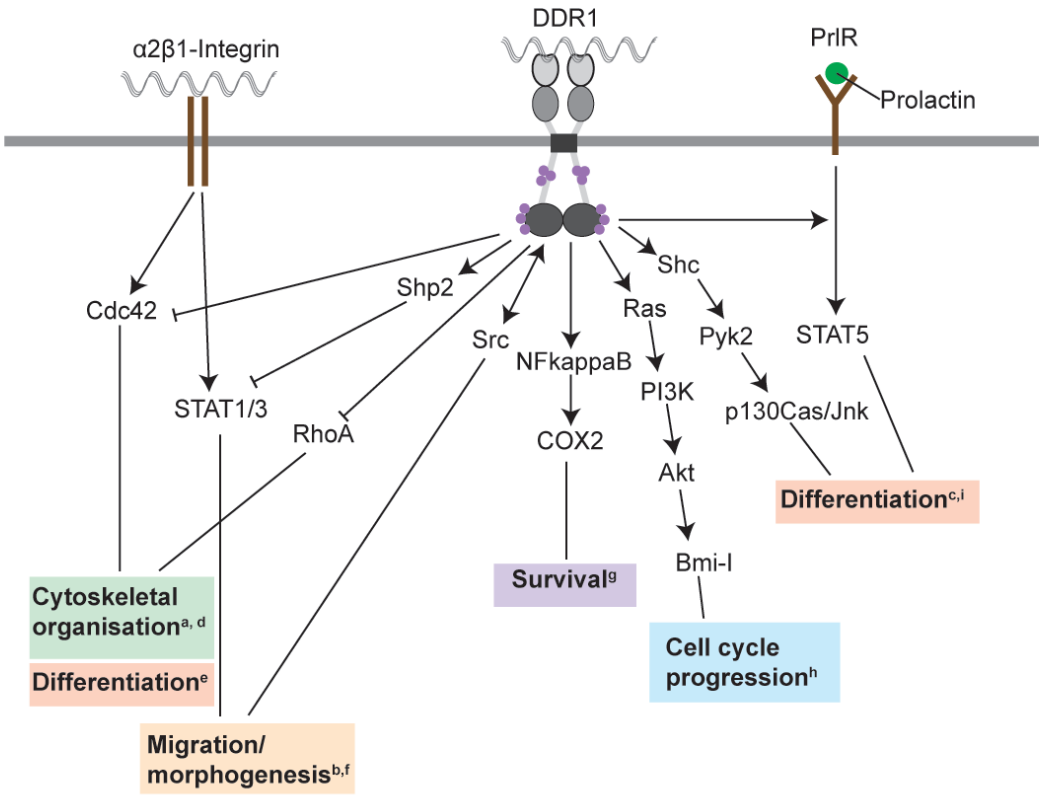
DDR1-null mice have additionally been reported to have structural defects in the inner ear, including the organ of Corti, leading to impaired hearing[65]. DDR1 was found to colocalise with myosin IIA in the inner ear, leading to the proposal that DDR1 may regulate mechanical forces in this organ[66]. This hypothesis was however based exclusively upon colocalisation of DDR1 and myosin IIA in certain cell types, which displayed altered morphology in DDR1-null mice[66]. Further studies should thus validate if DDR1 indeed regulates tension in these cells.

Signalling downstream of DDR1

Signalling pathways through DDR1 and their biological implications are not well understood and have been linked to a number a cellular functions including survival, differentiation and migration[23,48]. Like other RTKs, DDR1 is phosphorylated upon activation and can then dock a number of adaptor and signalling molecules including the adapters Nck2 and ShcA, the phosphatases Shp1 and -2 and kinases including PI3K and Src[48] (**Figure 7B** depicts predicted interaction partners from a proteomic study[51], whereas **Figure 8** depicts a number of reported DDR1 signalling pathways). The association of

Shp2 with DDR1 prevents β1-integrin mediated activation of STAT1 and -3 in MDCK cells[67] (**Figure 8**). In contrast, DDR1 promotes prolactin-induced activation of STAT5 in mammary epithelial cells[31] (**Figure 8**). Survival and proliferation have been shown to be affected by DDR1 via NFκB and PI3K respectively (**Figure 8**)[68,69]. Epithelial cell morphology and differentiation have been shown to be affected by DDR1 through a number of signalling molecules (**Figure 8**)[70–73]. These functions in epithelial organisation may have importance for the role of DDR1 in epithelial morphogenesis and will be discussed further in the next section. DDR1 has also been associated with MAP kinase signalling in a number of studies, however, the reported effects of DDR1 and the cellular outcome varies between cell types and studies[48] and signalling via MAP kinases are therefore not included in **Figure 8**.

DDR signalling has additionally been found to affect tissue remodelling through promoting MMP expression[59]. For example, collagen-induced activation of DDR2 leads to increased MT1-MMP expression and activity in fibroblasts[57]. DDR1 has been found to promote expression of particularly MMP-2 and MMP-9 in a range of malignant cell lines with positive effects on cellular invasion[59]. Additionally, DDR1 depletion has been found to downregulate MMP-7 expression in human bronchial epithelial cells, with consequences for epithelial repair[74]. The molecular mechanisms behind these effects on MMP expression are not well established.



Cytoskeletal organisation
[a]DDR1 inhibits epithelial cell spreading via suppression of Cdc42[70]

[d]Overexpression of DDR1in epithelial cells suppresses levels of GTP-bound RhoA with inhibitory effect on stress fibre formation[73]

Migration
[b]DDR1 supresses β1-integrin mediated activation of STA1/3 with inhibitory downstream effects on migration and tubulogenesis in MDCK cells[67]

[f]DDR1 activation increases cell migration via Src activation in smooth muscle cells. Conversely, Src also promotes DDR1 phosphorylation[75]

Survival
[g]DDR1 activates COX2 via NFκB to enhance chemoresistance of epithelial breast cancer cells[68]

Epithelial differentiation
[c]DDR1 is required for prolactin induced activation of STAT5 and downstream activation of beta-casein transcription during lactogenic differentiation of HC11 cells[31]

[e]DDR1 counteracts endocytosis of E-cadherin from junctions via suppresion of Cdc42 and thereby promotes junction stabilisation and differentiation of epithelial cells[71]

[i]DDR1 promotes EMT and thereby loss of the differentiated epithelial phenotype by activating N-cadherin expression via Shc/Pyk2/p130-Cas/Jnk signalling in pancreatic adenocarcinoma cells[72]

Proliferation
[h]DDR1 stimulates cell renewal of mouse embryonic stem cells vis Ras-PI3K/Akt-Erk-Bmi-I signalling[69]

Figure 8. Selected signalling pathways downstream of DDR1. Signalling pathways downstream of DDR1 and receptors with intercepting pathways are depicted. The biological implications of the pathways are indicated and further details provided in the coloured boxes below the diagram[31,67–73,75].

1.2.3 Role of DDR1 in epithelial morphogenesis

DDR1 as a regulator of cytoskeletal organisation and morphology in epithelial cells

As described in Section **1.1.2**, Chapter 1, cytoskeletal rearrangements are important during polarisation and morphogenesis of epithelial cells, and DDR1 has been associated with these processes by a number of studies. As such, DDR1 has been found to suppress cell spreading and stress fibre formation[67,70,71]. This role of DDR1 may in MDCK cells occur in opposition to collagen-induced β1-integrin-dependent spreading and involve suppression of Cdc42 activity[70] (**Figure 8**). However, DDR1 has in other cell types been reported to increase Cdc42 activity[76]. In addition to Cdc42, DDR1 has also been found to modulate RhoA activity, suggesting that multiple RhoGTPases may function downstream of DDR1. In MDA-MB-231 cells, DDR1 was thus shown to decrease stress fibre formation through suppression of RhoA activity[73] (**Figure 8**). In line with this, DDR1 was found to suppress actomyosin contraction along cell-cell junctions of A431 cells by decreasing the activity of the RhoA effector ROCK[77]. Additionally, direct effects of DDR1 on myosin activity may affect actomyosin-mediated tension[66,78,79]. In MCF-7 cells, activation of DDR1 was thus reported to stimulate complex formation between DDR1 and myosin IIA[78]. This interaction was confirmed in MDA-MB-231 and NIH3T3 cells, where ectopic expression of DDR1 in cells cultured on collagen increased the formation of myosin IIA-containing filaments as well as the activating phosphorylation of serine-19 in myosin IIA[78]. Furthermore, DDR1 expression increased migration and inhibited spreading of NIH3T3 cells in a manner depending on myosin activity[78]. However, given that DDR1 is not normally expressed by fibroblasts, this role of DDR1 should be validated in cells that express DDR1 endogenously. Increased myosin activation upon overexpression of DDR1 in NIH3T3 fibroblasts was also demonstrated in a study addressing the importance of the DDR1-myosin IIA interaction for remodelling

and alignment of collagen fibres both *in vitro* and during attenuated wound healing *in vivo*[79]. This study surprisingly found DDR1 to be co-expressed with α-smooth muscle actin (α-SMA) in wounded tissue and to be expressed by fibroblasts in periodontal ligaments[79]. DDR1 was found to promote collagen remodelling and alignment during generation of fibrotic tissue[79]. The reason for this unusual expression of DDR1 in fibroblasts was, however, not addressed in this study.

In addition to controlling cytoskeletal organisation, DDR1 also affects epithelial cell morphology by localising to cell-cell junctions where it stabilises E-cadherin[71,80–82]. Overexpression of DDR1 thus causes increased half-life of E-cadherin in the cell membrane, whereas knockdown of DDR1 reduces the stability of adherens junctions[71,81,82]. This decrease in junction stability was associated with a rearrangement of the cortical actin bundles into disorganised stress-fibres[71,82]. Stabilisation of E-cadherin at the adherens junctions by DDR1 was in one study reported to be mediated via inhibition of Cdc42-dependent endocytosis of E-cadherin[71], whereas another study found DDR1 to mediate this effect by decreasing α2β1-integrin-dependent Src activation[82]. Junctional stability of E-cadherin may thus depend on a balance of DDR1 and α2β1-integrin-mediated signalling.

Role of DDR1 in epithelial morphogenesis and invasion

As described previously (Section **1.2.2**), DDR1 plays important roles during morphogenesis *in vivo*, however, the mechanisms by which DDR1 contributes to guiding such events are not well understood. *In vitro*, DDR1 has functions in tubular morphogenesis by MDCK cells as suggested by overexpression of dominant negative DDR1 preventing tubular morphogenesis[32]. Overexpression of full-length DDR1a or –b, on the other hand, also affected tubulogenesis and led to formation of shorter tubules with fewer branches[32,67].

In line with a role for DDR1 in epithelial morphogenesis in 3D environments, DDR1 was found to promote collective invasion by A431 spheroids[77]. This was mediated through its role in coordinating cytoskeletal tension within groups of cells[77]. This effect on cytoskeletal organisation was in 2D culture mediated through interaction of DDR1 with components of the Par polarity complex Par3 and -6, which suppressed junctional ROCK activity and thus decreased actomyosin-mediated contraction[77]. A DDR1-Par3 signalling axis was later found to play an attenuating role in invasion of the pancreatic ductal adenocarcinoma cell line CD18[83]. Knockdown of the heterotrimeric G-protein Gα13 in this cell line reduced MT1-MMP-driven invasion and increased cell-cell adhesion[83]. Knockdown of both DDR1 and Par3 reversed these effects, suggesting that DDR1-Par3 signalling has a cell adhesion-promoting role and can suppress MT1-MMP-driven invasion. Cells that otherwise migrated as half-moon shaped cells with front-rear polarity lost this cytoskeletal organisation and increased junctional localisation of Par3 upon Gα13 knockdown, whereas DDR1 knockdown caused Par3 to relocalise away from cell-cell junctions[83]. This role of DDR1 in regulating Par3 localisation is consistent with the study in A431 cells[77], although opposite outcomes for invasion efficiency were observed. This discrepancy may be due to DDR1 playing different roles in different modes of cellular invasion. The promoting role of DDR1 was thus seen during collective invasion A431 cells with an adherent, epithelial phenotype[77], whereas the invasion-supressing function was seen in an assay where cells invade as de-differentiated single cells[83].

Role of DDR1 in epithelial polarity

Given the role of DDR1 in organising epithelial cell morphology through effects on cytoskeletal organisation and junction stability, it is tempting to speculate that DDR1 can affect epithelial polarity. Despite the central role of Par3 in polarity, neither of the above studies addressed whether DDR1-Par3 signalling had any significance for apicobasal polarity. DDR1 has however been associated with the process of epithelial-to-mesenchymal transition (EMT), albeit with contradicting results[72,73,83–88]. Briefly, EMT is a process occuring during development as well as in malignant progression of poorly differentiated cancers[89]. During EMT, epithelial cells lose cell-cell adhesion and gain a more mesenchymal-like, motile phenotype, which requires the cells to lose apicobasal polarity[89]. A role for DDR1 in this process could thus link the receptor to establishment and/or maintainance of polarity.

DDR1 has been implicated in collagen-induced EMT-like changes in pancreatic ductal carcinoma cells[84]. Similarly, DDR1 promotes EMT and invasive behaviour in gastric cancer cell lines and colorectal carcinoma cells[85,86] . In contrast, DDR1 is downregulated during induction of EMT in MCF-10A cells, primary human bronchial epithelial cells and MDCK cells[73,87,88]. Interestingly, suppression of DDR1 was accompanied by an increase in DDR2 expression during induction of EMT in MDCK cells[88]. Modulating DDR1 expression did not affect the expression of EMT markers in neither H-Ras-transformed MCF10A or MDA-MB-231 cells, suggesting that downregulation of DDR1 does not drive EMT in these cells[73]. There are thus pronounced discrepancies between the reported roles of DDR1 in EMT and apart from a DDR1-Shc-Pyk2 signalling axis described in pancreatic ductal adenocarcinoma cells[72], the mechanism by which DDR1 signalling may contribute to EMT is unknown. It thus

remains unclear if DDR1 can contribute to either establishment or maintenance of the polarised epithelial phenotype.

DDR1 has thus been implicated in regulation of epithelial cell morphology, EMT, migration and invasion. This combined with the frequent finding of DDR1 being upregulated in a range of human, epithelial cancers, has led to DDR1 being proposed as a potential therapeutical target[59]. However, our understanding of DDR1 function in epithelial cells under pathological as well as physiological conditions remains incomplete. Further efforts to understand the basic biology of DDR1 in epithelial morphogenesis are necessary to provide a foundation for assessment of DDR1 as a valid therapeutical target in the future.

1.3 Matrix degradation during epithelial morphogenesis

Cells in a multicellular organism are surrounded by ECM, which provides a scaffold to maintain the structure of tissues. The ECM further functions as a barrier, provides cells with survival signals and sequesters growth factors and other molecules to form an appropriate microenvironment according to the specialised function of the tissue[90]. Cell behaviour is directly affected by the cell's surroundings through signalling induced by ECM-receptors on the cell surface[91]. However, cells also affect their immediate environment through degradation, synthesis and reorganisation of ECM components. Such processes must occur during morphogenic events when cells are extending new structures into existing ECM[91]. For example, tubulogenesis requires cells to degrade surrounding matrix in order to create space into which new tubules can extend.

To degrade ECM, epithelial cells utilise proteinases that belong to the matrix metalloproteinase (MMP) family of zinc-binding metalloproteinases[91]. In humans 23 MMPs have been identified and can be classified into soluble MMPs or membrane-type MMPs (MT-MMPs)[92]. MT-MMPs are associated with the plasma membrane through

either a transmembrane domain (MT1-, MT2-, MT3- and MT5-MMP) or a GPI-anchor (MT4- and MT6-MMP)[92]. Soluble MMPs are secreted and thought to diffuse into the surrounding ECM, whereas MT-MMPs act on the cell surface[91]. MT-MMPs are therefore considered to be optimal for ECM degradation in the pericellular environment to promote cellular invasion, whilst soluble MMPs may be more useful for degradation of ECM in wider areas as seen during tissue resorption[91]. MMPs can be inhibited by the 4 endogenous tissue inhibitors of matrix metalloproteinases (TIMPs), which are present in the extracellular environment[92]. TIMP-1, -2, -3 and -4 inhibit all soluble MMPs and GPI-anchored MT-MMPs, whereas transmembrane MT-MMPs are not inhibited by TIMP-1 at physiological concentrations[92].

Tubulogenesis by MDCK cells in a 3D collagen I matrix requires ECM degradation to occur at the tip of tubules that are extending into the collagen matrix[93]. In line with this requirement for spatially confined ECM degradation, MT1-MMP has been found to be the key enzyme mediating collagen degradation during this process[94,43].

1.3.1 Membrane type I matrix metalloproteinase (MT1-MMP)

Structure and function of MT1-MMP

MT1-MMP shares the general domain structure of MT-MMPs and thus consists of a signal peptide, a pro-domain, a catalytic domain, linker 1, a hemopexin (Hpx) domain, linker 2, a transmembrane domain and a short cytosplasmic domain (**Figure 9**)[92]. MT1-MMP degrades a number of ECM components including collagen I-III, laminin 1 and 5, fibronectin, vitronectin, fibrin and aggrecan[95]. Collagen I is the most abundant ECM component in our body, and only MMP1, -2, -8, -13 and MT1-MMP can degrade it at neutral pH[95].

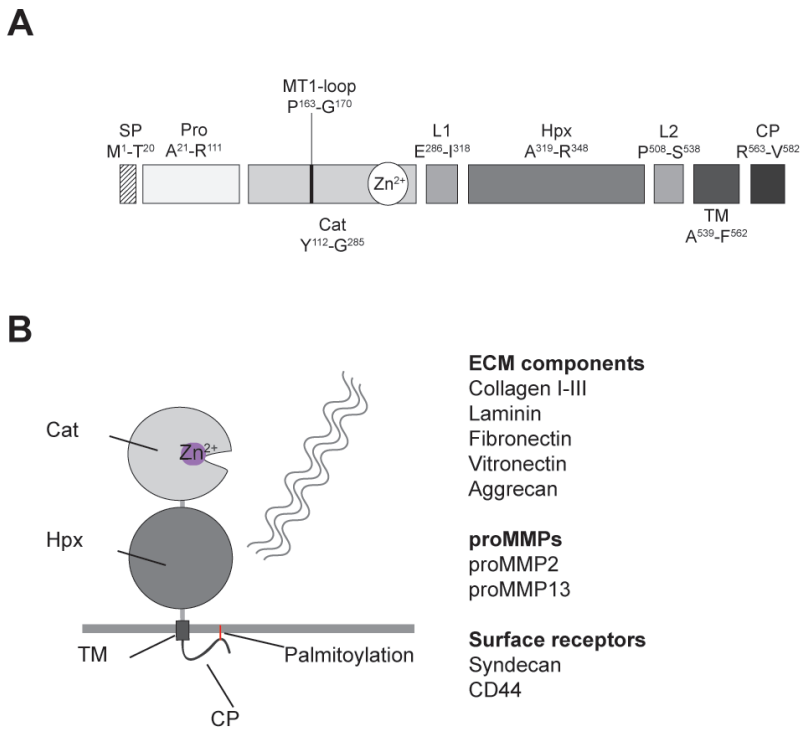


Figure 9. Structure of MT1-MMP. A) Sequence of MT1-MMP: MT1-MMP is synthesised with a signal peptide (SP), a pro-domain (Pro), a catalytic domain (Cat), Linker 1 (L1), a hemopexin domain (Hpx), Linker 2 (L2), a transmembrane domain (TM) and a short cytosplasmic domain (CP). The pro-domain of MT1-MMP is cleaved by furin during secretion, so that active MT1-MMP is expressed at the cell surface[95]. The catalytic domain of MT1-MMP contains an 8 amino acid sequence termed MT-loop, which is found in transmembrane MMPs and has been found to be important for controlling the localisation of MT1-MMP[93,96]. Linker 1 contains sites for O-glycosylations, whereas the Hpx domain mediates homodimerisation of MT1-MMP[95]. **B)** Cartoon of MT1-MMP in the plasma membrane. A selection of substrates is listed to the right.

MT1-MMP-null mice show phenotypes associated with aberrant matrix turnover in connective tissues including severe bone defects and fibrosis of soft tissues[97]. While new-born MT1-MMP-null mice are of similar size to wild type littermates, severe defects begin to show during postnatal development: growth is attenuated, bone defects appear and mice die after 7-13 weeks[97]. Another study reported MT1-MMP-null mice to die earlier (3 weeks of age), but otherwise reported similar bone defects in addition to defective vascularisation of bones and impaired corneal angiogenesis[98]. MT1-MMP thus appears to be a crucial enzyme for matrix remodelling during postnatal development. However, the enzyme is also known to play pivotal roles in matrix remodelling in pathogenic settings such as arthritis[92], ischemic myocardium post-infarction[99], artheroclerosis[100], pathogenic angiogenesis[101] and cancer[102].

In addition to directly degrading ECM components, MT1-MMP can promote ECM degradation indirectly by activating zymogen forms of other MMPs, including proMMP-2 and -13[95]. Particularly the activation of proMMP-2 is considered to be important for cancer cell invasion, since activated MMP-2, in contrast to MT1-MMP, can cleave the basement membrane component collagen IV, which is a necessary step for epithelial cancers to invade into stromal tissue[95,102–104]. For activation of proMMP-2, MT1-MMP forms a homodimer on the cell surface via its Hpx and TM domains[105,106]. One of the MT1-MMP molecules in the dimer binds TIMP-2, which recruits proMMP-2 through an interaction between the C-terminal domain of TIMP-2 and the Hpx domain of proMMP-2. The TIMP-2-free MT1-MMP in the complex can then cleave off the pro-domain of MMP-2[95,105]. This model is supported by defective MMP-2 activation in TIMP-2 knockout mice[107]. MT1-MMP was also shown to activate proMMP-13 on the cell surface[108], but the detailed mechanism behind this is not understood.

In addition to promoting ECM degradation, MT1-MMP can cleave cell surface molecules including the hyaluronan receptor CD44, EphA2, αV-, α3- and α5-integrin, ADAM9, Notch ligand Delta-like 1 and the transmembrane heparan sulfate (HS) proteoglycan syndecan 1[95,109–111]. Such cleavage can modulate intracellular signalling by attenuating signalling from active receptors, removing ligands at the cell surface and by generating biologically active molecules in the form of shed ectodomains. Furthermore, shedding of ECM receptors can release cell adhesion and promote cell migration[90]. For example, MT1-MMP can shed CD44 with pro-migratory consequences in breast and pancreatic carcinoma cells[112]. MT1-MMP also affects the clearing of various molecules from the extracellular space including MMPs and TIMPs, by cleaving the endocytic receptor low-density lipoprotein receptor-related protein 1 (LRP1)[113]. Besides cleaving membrane-bound molecules, MT1-MMP, can generate biologically active peptides by

cleaving ECM components. An example of this is the release of EGF-like domains from the basement membrane component laminin-5 γ2 chain, which bind the EGF receptor erbB1 to enhance motility in human carcinoma cells[114].

1.3.1 Role and regulation of MT1-MMP in epithelial tubulogenesis

Role of MT1-MMP in epithelial tubulogenesis and invasion

Kadono et al[43] identified MT1-MMP as the enzyme mediating collagen degradation during tubulogenesis of MDCK cells in 3D collagen I matrices. They found that a broad-spectrum MMP inhibitor abrogated tubulogenesis and further specified that TIMP-2, but not -1 can inhibit the process[43]. This pattern of inhibition is selective to transmembrane type MT-MMPs of which MT1-MMP is the only member with the ability to degrade collagen I[92]. Accordingly, downregulation of MT1-MMP by anti-sense mRNA expression abrogated HGF-induced tubulogenesis by MDCK cells[43]. A study by Hotary et al. confirmed that MT1-MMP is the only collagen-degrading MMP with the capacity to promote invasion of MDCK cells into collagen I[94]. Proteolytic activity of MT1-MMP was also shown to be required for branching morphogenesis of the mammary epithelial cell line Eph4 in dense collagen I matrices[115]. Interestingly, MT1-MMP expression in the mammary gland is high during development and pregnancy where tubular morphogenesis occurs, whereas it is downregulated in the fully differentiated lactating gland[115,116]. This suggests that MT1-MMP may contribute to epithelial tubulogenesis *in vivo*. However, the extent to which MT1-MMP is expressed and active in epithelial cells undergoing tubulogenesis in the mammary gland remains controversial[115–117].

During tubulogenesis of MDCK cells, MT1-MMP mediates ECM degradation at the tip of extending tubules to facilitate the invasion of these structures into the surrounding matrix[95]. During this process, the activity and expression of MT1-MMP are thought to be under tight regulation. However, in pathological conditions, disruption of

these regulatory mechanisms can activate aberrant MT1-MMP-driven migration and invasion and lead to progression of disease. Understanding the mechanisms behind regulation of MT1-MMP during invasion in epithelial tubulogenesis may thus provide insight to the function of the enzyme during pathological invasion.

Regulation of MT1-MMP expression in epithelial cells

Despite MT1-MMP being implicated in both physiological and pathological events, mechanisms regulating transcription of the MT1-MMP gene are not well understood[111]. Culturing MDCK cells in 3D collagen I has been shown to induce expression of MT1-MMP[43]. While HGF stimulation in this model induced MT1-MMP driven tubulogenesis, it did not further affect MT1-MMP expression, suggesting that HGF can modulate MT1-MMP activity post-translationally[43]. Our group has recently shown that fibrillar collagen can induce the expression of MT1-MMP in human dermal and synovial fibroblasts via signalling through DDR2[57]. DDR2 is not expressed in MDCK cells, and the mechanism of collagen-mediated upregulation of MT1-MMP thus remains unknown in these cells. Upregulation of MT1-MMP has been observed upon induction of EMT in MDCK cells either through expression of the oncogene v-Src or overexpression of MEK[118,119]. This was accompanied by enhanced cell migration and invasion[118,119]. In the transformed, but well-differentiated epithelial cell line, MCF-7, induction of EMT by expression of the transcription factor Snail1 similarly upregulated MT1-MMP expression[120]. Whilst not revealing mechanistic details on transcription of the MT1-MMP gene, these studies confirm the association between high MT1-MMP expression and enhanced motile behaviour of epithelial cells. In line with this, MT1-MMP was shown to be upregulated in mammary epithelial cells in the active, motility-dependent growth phase, while the formation of cell-cell contacts in a resting, confluent monolayer of these cells reduced MT1-MMP expression[121].

Posttranslational regulation of MT1-MMP activity in epithelial cells

In addition to expression levels, MT1-MMP activity can be controlled by several layers of posttranscriptional regulation including activation, trafficking, recycling and degradation of the enzyme in the cell[92]. Furthermore, the presence of TIMPs in the extracellular environment can locally modulate MT1-MMP activity[92]. Modulation of TIMP expression has been shown to affect branching morphogenesis in the mammary gland[122], suggesting that this type of regulation may function *in vivo*.

A central mechanism by which cells regulate MT1-MMP activity is by controlling its localisation. MT1-MMP must localise to the leading edge of migrating cells in order to mediate pro-migratory and invasive functions and regulation of a polarised distribution of MT1-MMP on the cell surface is thus crucial to its function[95]. Such spatial regulation of MT1-MMP varies between specific cellular contexts. In migrating cells in 2D culture, MT1-MMP localises to lamellipodia. It has been shown that localisation of the enzyme to lamellipodia is achieved by interaction of its Hpx domain with CD44 and its cytoplasmic domain with ERM proteins[123,124]. A recent study from our group showed that localisation of MT1-MMP to focal adhesions sites is independent of the cytoplasmic domain and rather relies on the 8 amino acid MT-Loop region in the catalytic domain of MT1-MMP[96]. In many cancer cells, single cell migration involves localisation of MT1-MMP to invadopodia, which are specialised membrane protrusions that extend into the ECM where they mediate focal ECM degradation. Invadopodia are thought to be important for cancer cell invasion and are characterised by co-localisation of proteins such as cortactin, TKS-5, actin and MT1-MMP[102,125]. In collectively invading cells, such as MDCK cells undergoing tubulogenesis, spatial regulation of MT1-MMP becomes more complex since MT1-MMP-dependent matrix degradation must be coordinated across multicellular

structures to only occur at the leading edge of cells at the tip of extending tubules[93]. The detailed mechanism behind this is not well understood.

The localisation of MT1-MMP on the cell surface relies both on targeted vesicle transport and endocytosis of the enzyme[95]. The molecular mechanisms regulating this in epithelial cells are not well understood at present. I will thus briefly summarise general mechanisms from studies in other cell types below:

MT1-MMP can be internalised via both caveolin[126] and clathrin-mediated endocytosis[127]. Overexpression of MT1-MMP mutants defective in clathrin-dependent internalisation did not affect its localisation to the leading edge in CHO cells, but failed to promote cell migration and invasion into Matrigel[127]. This is potentially due to a need for continuous internalisation of MT1-MMP at the leading edge, replacing MT1-MMP molecules that have been inactivated (e.g. by TIMPs)[127]. In line with this, MT1-MMP has a short half-life of less than 30-minutes on the cell surface and has been found primarily to be internalised at the adherent edge[127]. Silencing of caveolin 1 has also been reported to inhibit MT1-MMP-dependent ECM degradation by MDA-MB-231 cells[126]. In contrast to this, overexpression of palmitoylation-defective mutants of MT1-MMP, which can be internalised by caveolin, but not clathrin, failed to promote migration of HT1080 cells. This would suggest that caveolin-dependent internalisation cannot support cell migration[128]. The relative role of endocytic pathways for MT1-MMP may thus vary between different cell types. Endocytosed MT1-MMP can either be degraded in lysosomes or recycled back to the cell surface[95]. Recycling-deficient MT1-MMP can still promote migration and invasion, suggesting that recycled MT1-MMP is not a major contributor to these processes[95].

Besides endocytosis of MT1-MMP, targeted secretion of MT1-MMP at the cell surface is a way to control its localisation. In MDA-MB-231 cells, Rab8 was reported to promote exocytic trafficking of MT1-MMP towards sites of attachment to collagen I[129]. An extensive body of literature has focused on the trafficking of MT1-MMP to invadopodia, however, to what extent this reflects trafficking of MT1-MMP in non-malignant, epithelial cells is unclear.

Regulation of MT1-MMP according to apicobasal polarity during epithelial tubulogenesis

Whereas polarised trafficking of MT1-MMP in migrating cells typically refers to trafficking of MT1-MMP to the leading rather than trailing edge, trafficking of MT1-MMP in polarised epithelial cells is regulated according to the apicobasal polarity[93]. Our group has reported that the default secretory pathway of MT1-MMP in inert epithelial cells is towards the apical cell membrane, thus restricting access of the enzyme to the ECM at the basal surface[93]. Stimulation with HGF resulted in increased localisation of MT1-MMP at the basal cell membrane, which was accompanied by increased degradation of the underlying collagen matrix[93]. Both the Hpx domain and the loop region of MT1-MMP were required for this basal localisation[93]. TGFβ signalling was found to affect this trafficking in a bi-phasic manner, with low concentrations promoting basal localisation and high concentrations preventing it[93]. This spatial regulation of MT1-MMP in 2D culture of MDCK cells was demonstrated to be consistent in 3D culture, where MT1-MMP localised to the basal, ECM-abutting surface of cells at the tip of extending tubules where matrix degradation must occur. In other locations, MT1-MMP remained at the apical surface[93]. The ability of cells to localise MT1-MMP to the basal domain was found to be essential for HGF-induced tubulogenesis[93]. Regulation of MT1-MMP localisation according to apicobasal polarity thus appears to be an important mechanism for

controlling MT1-MMP activity in non-transformed epithelial cells. However, further studies are required to understand the mechanisms behind this regulation and whether signals from the ECM are involved.

1.4 Aims of this thesis

Epithelial tubes form core functional units of epithelial organs including the kidney, lungs and mammary gland. Apicobasal polarity is essential for the functionality of epithelial tubes and is furthermore required for the spatial regulation of MT1-MMP. This regulation ensures that the pro-invasive activity of the enzyme is restricted to the tips of developing tubules. MT1-MMP-driven invasion is important in both physiological and pathological conditions, and studying how localisation of the enzyme to the ECM-abutting, basal surface is induced at the tip of extending tubules may provide insight to the regulation of the enzyme in early stages of malignant invasion.

Preliminary data in the Itoh lab have shown that the substrate MDCK cells are cultured on affects the apicobasal distribution of MT1-MMP and specifically suggests a role for collagen I in this regulation (PhD thesis by previous student of Dr Itoh, Dr Sarah Weaver). This implies that a collagen receptor may be involved. Such signalling from a collagen receptor could either directly affect the polarised trafficking of MT1-MMP or mediate its effect on MT1-MMP distribution through a role in guiding the orientation of apicobasal polarity during 3D morphogenesis. Indeed, ECM receptors, such as β1-integrin, have previously been shown to be crucial for establishment of polarity by epithelial cells in 3D environments including mammary epithelial cells and MDCK cells[20].

The effect of collagen on the polarised distribution of MT1-MMP was found to be specific to collagen I in its fibrillar rather than denatured state (PhD thesis by previous student of Dr Itoh, Dr Sarah Weaver). Based on the selective activation of DDRs by

fibrillar collagen[44], these receptors are interesting candidates to convey this signal. Given the importance of polarised trafficking of MT1-MMP during tubulogenesis, a collagen receptor involved in its spatial regulation could likely affect such morphogenic processes. In line with this, DDR1 has been reported to play a role in tubular morphogenesis of MDCK cells *in vitro*[32] and in the mammary gland *in vivo*[30]. However, the role and downstream signalling of DDR1 in epithelial morphogenesis is not well understood, and it has not been addressed whether this role involves effects on apicobasal polarity and polarised trafficking of molecules such as MT1-MMP. DDR1 has been reported to affect growth, migration and invasion of epithelial cancer cells[59] and an increased understanding of its basic biology in physiological morphogenesis may provide insight to the function of this receptor in pathogenic conditions.

It is thus the aim of this thesis to investigate if signalling through DDR1 contributes to regulating the polarised trafficking of MT1-MMP and whether such signalling affects the ability of epithelial cells to polarise and undergo morphogenesis in 3D matrices.

Aims:

- to investigate the role of DDR1 in spatial regulation of MT1-MMP and its implications for epithelial morphogenesis in 3D matrices
- to identify candidate signalling pathways downstream of DDR1 in epithelial morphogenesis and polarisation
- to investigate if the *in vitro* observation, that DDR1 plays a role in epithelial organisation, is reflected in the function of DDR1 in the mammary gland *in vivo*

Findings in this thesis may contribute to our understanding of how signalling from DDR1 contributes to guiding physiological morphogenesis of polarised epithelial cells in

3D environments. Such insights may contribute to future identification of pathways which can be bypassed or disturbed to activate disorganised epithelial morphogenesis and invasion in pathological settings such as cancer.

Chapter 2 Materials and methods

2.1 Reagents

Chemicals	Supplier	Catalog #
Ammediol Triton X-100	ACROS ORGANICS (Belgium)	
Paraformaldehyde (PFA)	AGAR Scientific (Essex, UK)	
Butanol	Alfa Aesar, Fisher Scientific (Lancashire, UK)	
Ethanol Hydrochloric acid (HCl) Methanol Sucrose	Fisher Scientific (Londonborough, UK)	
sodium carbonate (NaCO3)	MerckMillipore (Hertfordshire, UK)	
sodium dodecyl sulphate (SDS)	MP Biomedical, LLC (France)	
2-mercaptoethanol Ammonium chloride (NH4Cl) Ammonium persulphate Bovine serum albumin (BSA) Bromophenyl Blue Calcium chloride (CaCl2) Chloroform Ethylenediaminetertraacetic acid (EDTA) Glutaraldehyde Tetramethylenediamine (TEMED) Trizma base Tween 20	Sigma-Aldrich (Dorset, UK)	
Acetic acid Glycerol Glycine	VWR PROLABO CHEMICALS (Leicestershire, UK)	

Molecular Biology Reagents	Supplier	Catalog #
LB Agar LB Broth	Invitrogen (ThermoFisher) (Lutterworth, UK)	
Gene Pulser Cuvette	Biorad (Hertfordshire, UK)	165-2086
GelRed	Biotium (Belgium)	41003
Carbenicillin Kanamycine	MerckMillipore (Hertfordshire, UK)	69101

Bacteriological Petri dish	ThermoFisher Scientific	-
CloneJet kit for ligation into pJET1.2 vector	(Lutterworth, UK)	K1231
Dreamtaq Polymerase		EP0702
FastAP		EF0654
FastDigest restriction enzymes		-
GeneJet Gel Extraction kit		K0692
Phusion High-Fidelity Polymerase		F5495
Rapid DNA ligation kit		K1422
T4 DNA Polymerase		EO0061
Ultrapure agarose		16500-500

Primary antibodies	**Supplier**	**Catalog #**
Rbαcollagen IV (IHC: 1:50)	Abcam (Cambridge, UK)	ab6586
MαGM130 (IF: 1:200)		ab52649
RbαLaminin (IHC: 1:50)		ab11575
RbαMLC (WB: 1:1000)		ab92721
RbαMT1-MMP (EP1264Y, loop) (WB: 1:2000)		ab51074
MαE-cadherin (IF: 1:300)	BD Biosciences (Oxford, UK)	610181
RbαPKCα (WB 1:500)	Cell Signalling (Belgium)	2056S
RbαppMLC (Thr18/Ser19) (IF: 1:200, WB: 1:1000)		36745
MαGP135 (3F2/D8 hybridoma supernatant) (IF: 1:10)	Developmental Studies Hybridoma Bank (Iowa, USA)	3F2/D8-f
MαpY (4G10) (WB: 1:1000)	Millipore (Hertfordshire, UK)	05-321
GαDDR1 (ecto domain) (WB: 1:1000)	R&D Systems	AF2396
Mαβ-casein (IHC: 1: 100)	Santa Cruz (Heidelberg, Germany)	sc-166520
RbαDDR1 (cytoplasmic) (WB: 1:1000, IF: 1:100)		sc-532
MαFLAG M1/M2 (WB: 1:1500)	Sigma-Aldrich (Dorset, UK)	F3040/F1804
RbαLaminin (IF: 1:150)		L9393
MαZO1 (IF: 1:400)	ZYMED (ThermoFisher Scientific) (Lutterworth, UK)	33-9100

SDS-PAGE and immunoblotting	**Supplier**	**Catalog #**
Anti-RB IgG VeriBlot secondary ab (HRP)	Abcam (Cambridge, UK)	ab131365
Trans-Blot Turbo Transfer System	Biorad (Hertfordshire, UK)	-
Okadaic acid	Calbiochem (Hertfordshire, UK)	459620
HRP-linked secondary antibodies	DAKO (Denmark)	-
Western Blue. Stabilised Substrate for Alkaline Phosphatase	Promega (Southhampton, UK)	S3841
30% Acrylamide	Severn Biotech (Worcester, UK)	20-2100
Proteinase cocktail	Sigma-Aldrich (Dorset, UK)	P8340
Sodium orthovanadate		36508
Pageruler Plus Prestained Protein Ladder	ThermoFisher Scientific (Lutterworth, UK)	20610

RT-PCR	Supplier	Catalog #
High Capacity cDNA Reverse Trascription Kit	AB applied biosystems (ThermoFisher Scientific) (Lutterworth, UK)	438814
RNAqueous Micro Kit	Invitrogen (Thermo Fisher Scientific) (Londonborough, UK)	AM1931

Cell Culture and biology	Supplier	Catalog #
Y-27632	Abcam (Cambridge, UK)	ab120129
Blebbistatin		B0560
PureCol bovine collagen solution	Advanced Biomatrix Inc.	5065
GM6001 (Ilomastat)	Calbiochem (Hertfordshire, UK)	364205
PKCβ inhibitor		539654
PKCα/β inhibitor (go6976)		365250
MEK inhibitor (PD325901)		444966
Bisindolylmaleimide		203290
Src inhibitor (PP2)		
Wortmannin	Cell Signalling	9951
10 cm^2 tissue culture plate	CellStar (Greinar Bio-one)	664-160
H1152	ChemCruz (Texas, USA)	sc-203592
6, 12, 24 and 48-well plates	Corning or Falcon (Fisher scientific)	-
Corning CellBIND culture plates	CoStar	3336
SMARTvector Human Lentiviral PRKCA shRNA	Dharmacon (GE Life Sciences) (Buckinghamshire, UK)	V3SH7590-230785791
SMARTvector Human Lentiviral PRKCB shRNA		V3SH7590-226289937
12/24-well culture inserts (0.8 μm pore)	Falcon, Fisher Scientific (Lutterworth, UK)	353182/353097
DMEM/F12	Gibco by life technologies	11320-074
Heatinactivated fetal bovine serum	(Paisley, UK)	10500
IMDM		12440-053
Penicillin streptomycine		15140-122
OptiMEM		31985-062
IBIDI μ-slide (8-well)	IBIDI	9093
Lipofectamine 2000	Invitrogen (ThermoFisher	11668-019
RNAiMax	Scientific) (Lutterworthm UK)	13778
dog PKCα siRNA		5445944
dog PKCβ siRNA		5458653
Dynabeads ProteinG		10004D
DMEM	Lonza Biowhitaker (Slough, UK)	BE12-6045
RPMI 1640 media		BE12-1115F
Trypsin-EDTA		BE17-16113
Glass-bottom 12-well plate	MatTek	P12G-1.D-14G
TransIT-2020	Mirus Bio LCC (Wisconsin, USA)	MIR5405

Type I Collagen (Cellmatrix type I-A)	Nitta Gelatin (Japan)	-
Neomycine (G418)	PAA Laborotories (Leeds, UK)	P11-012
Prolactin (murine)	PeproTech (London, UK)	315-16
hEGF HGF Insulin	R&D Systems (Abingdon, UK)	
Cytodex3 microcarrier beads	Sigma-Aldrich (Dorset, UK)	C3275-10G
Type A gelatin from porcine skin		G2625
Cloning cylinders, glass		C1059-IEA
10X RPMI-1650 media		R1145
sterile dimethyl sulphoxide (DMSO)		D5879
Collagenase from Clostridium Histolyticum		C5138
Trypsin from Porcine Pancreas		T4499
bFGF		F0291
Dexamethasone		D4902
ON-TARGETplus Non-targeting Pool	ThermoFisher Scientific (Lutterworth, UK)	D0018-10-50
DDR1-IN-1	Kindly supplied by Prof. Nathaniel Gray (Harvard, USA) TOCRIS Bioscience	5077
Hygromycine B	TOKU-E (Belgium)	H011

Immunocytochemistry/histochemistry	**Supplier**	**Catalog #**
DAKO ARK Peroxidase for Mouse Primary Ab	DAKO (Denmark)	K3954
Prolong Diamond Anti-fade mounting medium Alexa dye-conjugated Phalloidin (Alexa dyes used: 568 nm and 660) (IF: 1:250) Alexa-dye-conjugated secondary antibodies (IF 1:2000) All secondary antibodies produced in goat, unless used with goat primary antibodies in which case antibodies raised in donkey were used. Alexa dyes used: 488 nm, 568 nm and 660	Molecular Probes (ThermoFisher Scientific) (Lutterworth, UK)	P36961 - -
DPX Mountant for Histology	Sigma-Aldrich (Dorset, UK)	6522
Menzel-gläser Microscope slides	ThermoFisher Scientific (Lutterworth, UK)	ISO 8037/1
Peroxidase Substrate Kit DAB VectaStain ABC Kit Biotinylated secondary antibodies	Vector Laboratories (California, USA)	SK4100 PK-4000 -
Cover glass, Ø18 mm	VWR International	631-0153

2.2 Molecular biology

See Section **2.1**, Chapter 2 for detailed list of reagents.

2.2.1 General solutions

LB agar and broth:

LB agar and broth were prepared according to the manufacturers instructions and autoclaved. Autoclaved LB agar was cooled to ~50˚C solution before the relevant selection antibiotic was added. Agar was then poured into 10 cm bacteriological petri dishes and allowed to cool. Kanamycine and carbenicillin were dissolved in ddH_2O and kept as a stock solution of 100 mg/ml. Working concentration was 100 µg/ml.

TAE buffer:

1x TAE buffer (40 mM Tris acetate, 1mM EDTA) was used for casting agarose gels, and 0.5x TAE buffer used as running buffer for agarose gel electrophoresis.

TE buffer:

TE buffer (10 mM Tris-HCL and 1 mM EDTA) was prepared from sterile Tris-HCL and EDTA solutions and was used for storage of DNA.

2.2.2 Cloning of MT1-pHluorin-RFP

Templates used:

- pSG5-MT1F-RFP: MT1-MMP tagged with mRFP- and FLAG. FLAG-tag is inserted between Arg111 and Lys112, whereas mRFP is inserted between Cys574 and Gln575 with 2 Gly as an N-terminal linker. pSG5-MT1F-RFP was kindly provided by Dr Itoh and has been described in[130].
- pGEX-2T-pHluorinS: Superecliptic pHluorin[131] in pGEX-2T was a kind gift from Professor Gero Miesenbock, University of Oxford.

Superecliptic pHluorin was inserted between Gly541 and Gly542 of MT1F-RFP with a 2 Gly N-terminal linker and a 1 Gly C-terminal linker. Cloning strategy for MT1-pHluorin RFP is outlined in **Figure 10**.

Primers used:

Y0001: 5'- GTCGAATTCCACCATGTCTCCCGCCCCAAGA-3'
Y5-BglII: 5'-GACAGATCTTCATCAGACCTTGTCCAGCAGG-3'
E: 5'-TACTCATTCCTCCGCCCTCCTCGTCCACCTCAA-3'
F: 5'-GAGGGCGGAGGAATGAGTAAAGGAGAAGAACTTTTC-3'
G: 5'-CCCCGCCTCCTTTGTATAGTTCATCCATGCC-3'
H: 5'-CTATACAAAGGA GGCGGGGCGGTGAGCGCGGC-3'

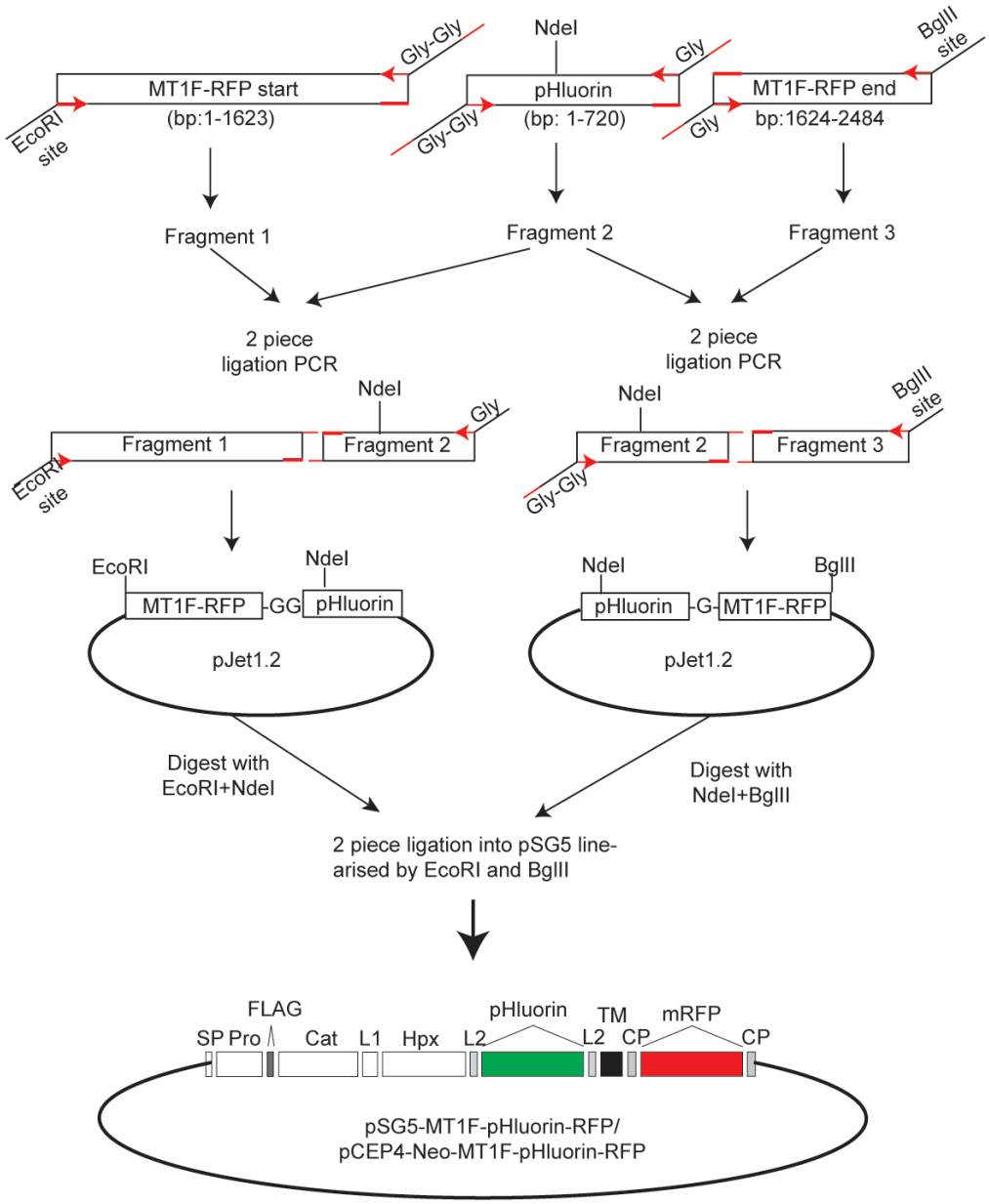


Figure 10. Cloning strategy to create pSG5-MT1F-pHluorin-RFP. The following 3 DNA fragments were generated by PCR: bp 1-1623 of MT1F-RFP (fragment 1, primer Y0001+E), full length superecliptic pHluorin (fragment 2, primer F+G) and bp 1624-2484 of MT1F-RFP (fragment 1, H+Y5-BglII). The PCR products were then gel purified before fragment 1+2 and 2+3 were joined by PCR using primer Y0001+ G and F+Y5-BglII respectively. These two fragments were gel purified and ligated into pJet1.2. The two generated fragments were then cut from pJet1.2 with EcoRI and NdeI or BglII and NdeI respectively, and combined as MT1-pHluorin-RFP in pSG5 using rapid DNA ligation kit (Thermo Fisher). MT1-pHluorin-RFP was further subcloned into pCEP4-neo to allow for stable expression in mammalian cell lines. This was done by restriction digestion of pSG5-MT1F-pHluorin-RFP with EcoRI followed by bluntending with T4 polymerase. The resulting linearised plasmid was then further digested with BglII to yield the MT1F-pHluorin-RFP fragment. This fragment was purified and ligated into pCEP4 linearised by PvuII and BamHI.

2.2.3 Restriction digestion

Restriction enzymes cut specific sequences of nucleic acids and leave overhangs/blunt ends. FastDigest restriction enzymes from ThermoFisher Scientific were used according to manufacturers instructions in ThermoFisher FastDigest buffer. Restriction enzymes were heat-inactivated when necessary in order to avoid star activity.

2.2.4 DNA fragment purification

1-2% agarose gels were prepared by solubilising agorose in 1x TAE buffer by microwaving. Once solubilised, the DNA intercalator GelRed was added to allow for DNA to be visualised. DNA was electrophoresed at 100 V in 0.5x TAE buffer for 10-60 minutes depending on size of the DNA of interest. DNA was visualised by a UV transilluminator, and DNA fragments of interest were excised. GeneJet gel extraction kit (ThermoFisher Scientific) was used to purify DNA. DNA was eluted in ddH_20.

2.2.5 Blunt-ending of DNA

Blunt-ending was used to make DNA overhangs generated by non-blunting restriction enzymes compatible for ligation with blunt-ended DNA. 1 U T4 polymerase was used per 20 µl reaction. T4 polymerase (ThermoFisher Scientific) has 100% activity in ThermoFisher FastDigest buffer and was thus added directly into restriction digestion mixture together with 100 µM dNTP. Enzyme was heat-inactivated after 5 minutes at room temperature.

2.2.6 Ligation of DNA fragments into pJET, pSG5, pCEP4 and pCEP4-neo

Fragments generated by PCR were ligated into the cloning vector pJET1.2 using the CloneJet PCR cloning kit (ThermoFisher Scientific) according to manufacturers instructions. For ligation of inserts into pSG5, pCEP4 and pCEP4-neo the Rapid DNA

ligation kit was used following manufacturers instruction. A molar ratio of at least 3:1 DNA insert to vector was used.

2.2.7 Transformation of bacteria by electroporation

The elecrocompetent E. Coli strain DH5-α was used for transformation. 1-2 µl of ligation mixture was added to bacteria on ice and pipetted into a cold electroporation cassette. Bacteria were pulsed in a BTX Electro Cell Manipulator (Qbiogene) by 2100 V for 5 milliseconds. 500 µl LB medium was then added to the cuvette and culture agitated at 37˚C for 1 hour. Transformed bacteria was then spread on agar plates containing appropriate antibiotics.

2.2.8 DNA isolation from small-scale culture (mini-prep) by alkaline lysis with SDS

A swipe of bacteria from a glycerol stock or a distinct colony picked on an agar plate was cultured in 5 ml LB medium with 100 µg/ml carbenicillin or kanamycine at 37˚C with agitation overnight. Bacteria were pelleted by centrifugation. Plasmids for transfection were extracted by resuspending pellet completely in cold solution I (25 mM Tris-HCL (pH 8), 10 mM EDTA). Bacteria were then lysed by adding 2 volumes of freshly prepared solution II (0.2 N NaOH, 1 % SDS) with mixing and <5 minutes incubation on ice. This disrupts the cell membrane and denatures DNA. 1.5 volume of solution III (3M potassium acetate, 11.5% v/v acetic acid) was then added. Re-acidification allows for renaturation of plasmid, but not the large genomic strands due to their large size and precipitation by denatured DNA-binding proteins. Potassium further precipitates SDS. Chloroform was added to remove protein, and mixture was then centrifuged to isolate the plasmid-containing supernatant. DNA was precipitated by adding 2 volumes of 100% EtOH to the supernatant and further washed with 70% EtOH.

The DNA pellet was dried completely, dissolved in TE with RNaseA and incubated at 37˚C for 30 minutes to allow removal of RNA before storage at -20˚C.

2.2.9 RT-PCR

Total RNA was extracted from cells using the RNAqueous Micro Kit (Invitrogen, ThermoFisher Scientific) according to the manufacturers instructions. RNA was reversed transcribed using the High Capacity cDNA Reverse Transcription Kit from AB applied Biosciences (ThermoFisher Scientific). cDNA was then used as template for PCR using the DreamTaq Polymerase (ThermoFisher Scientific). Primers for GADPH were used as a housekeeping gene for normalisation to the total amount of RNA. The following primers were used:

Primers: β-casein:
Fwd: GACTACATTTACTGTATCCTCTGAG
Rev: GTGCTACTTGCTGCAGAAAGTACAG

Primers PKCα:
Fwd: CTGATCCCAAGAATGAAAGC
Rev: CACCATGAGGAAATTGAAGTC

Primers PKCβ:
Fwd: AAAACCTTGTACCTATGGACC
Rev: CATGAAGTCATTCCTGCTGG

Primers GADPH (canine):
Fwd: TTCACCACCATGGAGAAGGC
Rev: GGTCCCTCCGATGCCTGC

Primers GADPH (human):
Fwd: TTCACCACCATGGAGAAGGC
Rev: GGCATGGACTGTGGTCATGA

2.3 SDS-PAGE and western blotting

Reagents are listed in Section **2.1**, Chapter 2

2.3.1 General solutions

Upper gel buffer

84 mM Ammediol, 62 mM HCl, 0.02% NaN_3, pH: 8.8

Lower gel buffer

110 mM Ammediol (2-amino-2-methyl-1,3-propanedial), 47 mM HCl, 0.02% NaN_3, pH: 9.5

2x SDS sample buffer

SDS (2%), 2x Upper gel buffer, Bromophenol blue (0.05%), Glycerol (40%), 2-β-mercaptethanol (1%)*, dH_2O

*Added fresh before each use

Sucrose solution

50% Sucrose, 0.03% Toluene, 0.02% NaN_3

APS solution

10% Ammonium persulfate (APS) in dH_2O

Upper reservoir buffer

10 mM Ammediol, 10 mM Glycine, 0.1% SDS, pH: 10

Lower reservoir buffer

16 mM Ammediol, 12.5 mM HCl, pH: 8.8

TBS

50 mM Tris-HCl, 150 mM NaCl, pH: 8

TBS-T

50 mM Tris-HCl, 150 mM NaCl, 0.05% Tween, pH: 8

2.3.2 Preparation of cell lysates

2x SDS buffer was diluted to 1x with TBS and salt concentration adjusted to 150 mM by addition of NaCl. β-mercaptoethanol, protease inhibitor cocktail, sodium orthovanadate and okadaic acid was added fresh where applicable.

Cells were washed with PBS before adding 1x SDS lysis buffer to cells on ice. Plates were scraped and incubated 3-5 minutes on ice before isolating lysates. Where

lysates were used for detection of protein phosphorylation, proteinase inhibitor cocktail III (Sigma, 1:1000) and the following phosphatase inhibitors were included: 1 mM sodium orthovanadate (tyrosine phosphatase inhibitor) or 100 nM okadaic acid (serine/threonine phosphatase inhibitor). Lysates were boiled for 20 minutes and stored at -20˚C. For detection of phosphorylation, samples were analysed by Western blot immediately.

2.3.3 SDS-PAGE gel composition and procedure

Buffers and solutions are listed in Section **2.3.1**.

Lower gel composition (7.5% separation gel):

7.5% Acrylamide/Bis, 1x lower gel buffer, 12% sucrose, 0.065% APS, 0.075% TEMED,

Upper gel composition (5% stacking gel):

5% Acrylamide/Bis, 1x upper gel buffer, 12% sucrose, 0.065% APS, 0.17% TEMED,

All glassware was carefully cleaned before use. Lower gels were cast first with APS and TEMED added last. Gels were overlayed with dH_2O-saturated butanol, to ensure an even surface and facilitate polymerisation by excluding oxygen, and left to set for 30-60 minutes at room temperature. Upper gels were made according to recipe above and the solution quickly added on top of the lower gel. Combs were fitted immediately. Gels were set at room temperature for 15-30 minutes and either used directly or stored wrapped in wetted plastic film at 4˚C for up to 24 hours before use.

Gels were secured in running tank and lower (anode) and upper (cathode) reservoir buffers (as listed in Section **2.3.1**) added. A current of 100-150 V was applied for 60-90 minutes or until the bromophenol marker from the sample buffer reached the bottom of the gel.

2.3.4 Western blotting procedure

Proteins were transferred to PVDF membranes by use of the Trans-blot Turbo Transfer System from BioRad. Immediately after transfer, the membrane was incubated 0.5-2 hours in blocking solution (10% milk in TBS) at room temperature, before incubation with primary antibodies in antibody dissolving solution (1 % BSA in TBS-T with 0.02 % azide) overnight at 4˚C. The next day, the membrane was washed 3x10 minutes in TBS-T followed by incubation with secondary antibodies conjugated to alkaline phosphatase. After washing in TBS-T, the membrane was incubated with alkaline phosphatase (AP)-linked secondary antibodies for 1-2 hours. The membrane was washed with TBS-T before development with Western Blue alkaline phosphatase substrate (Promega). The reaction was stopped by washing the membrane in running water. The membrane was dried and scanned using a Canon CanoScan LiDE 210 scanner at 600 DPI. Antibodies used are listed in Section **2.1**.

2.4 Cell biology

2.4.1 Culture of cell lines

All reagents used were tissue culture grade and sterile. Reagents used are listed in Section **2.1**. See **Table 1** at the end of this section) for a list of cell lines used in this study.

All MDCK lines were cultured in DMEM supplemented with 10% fetal calf serum (FCS) and Penicillin/Streptomycine (P/S). MDCK-NT-shRNA and MDCK-DDR1-shRNA cell lines (previously established in the Itoh lab) were maintained in the presence of 4 μg/ml puromycin. MDCK-MT1pH cells were maintained in presence of 800 μg/ml G418. MCF-10A cells were cultured in DMEM/F12 supplemented with 5% FCS, P/S, 20 ng/ml EGF, 0.5 μg/ml Hydrocortisone, 100 ng/ml cholera toxin and 10 μg/ml insulin. CaCO-2 cells were cultured in DMEM supplemented with 20% FCS and P/S. HC11 cells

were cultured in RPMI 1640 medium supplemented with 10% FCS, 5 μg/ml Insulin, 10 mM HEPES, 10 ng/ml epidermal growth factor (EGF). HT1080 and COS-7 cells were cultured in DMEM supplemented with 10% FCS and P/S. 3F2/D8 hybridoma cells were maintained in Iscove's DMEM (IMDM), 20% FCS, 50 mg/ml gentamycin.

All cells were passaged by Trypsin-EDTA every 2-4 days and always kept <80% confluence. Cells used for tubulogenesis assays were split 1:10 from an 60-70% confluent 10 cm dish 24 hours prior to setting up experiments.

Table 1 List of cell lines used in this thesis

Cell lines used:	Description
MDCK cells	MDCK cells were originally obtained from ATCC. This strain has further been subcloned in Dr Itoh's lab to select for tube formation capacity. This was done by culturing cells in 3D collagen type I and isolating clones that formed tubular structures. These MDCK cells were parental to additional strains used in this study.
MDCK-NT-shRNA	Clonal cell line expressing non-targeting shRNA after lentiviral introduction
MDCK-DDR1-shRNA clone 1-3	Clonal cell line expressing shRNA against DDR1 afterlentiviral introduction
MDCK-DDR1-shRNA clone 1-4	Clonal cell line expressing shRNA against DDR1 after lentiviral introduction
MDCK-Flp-Mock	No gene introduced into clonal parent cell line with FlpIN site
MDCK-Flp-DDR1	Gene encoding DDR1 introduced into FlpIN site of clonal parent cell line with FlpIN site
MDCK-Flp-DDR1ΔC	Gene encoding DDR1ΔC (dominant negative DDR1) introduced into FlpIN site of clonal parent cell line with FlpIN site
MDCK-MT1pH	MDCK stably cells expressing pCEP4neo-MT1F-pHluorin RFP based on G418 resistance
MDCK-NT-shRNA clone 2 and 3	2 clonal lines of MDCK cells stably expressing NT shRNA. Established at the same time as MDCK-PKCα-shRNA and MDCK-PKCβ-shRNA
MDCK-PKCα-shRNA clone 4 and 6	MDCK cells stably expressing shRNA against PKCα after lentiviral transduction. Clonal cells isolated
MDCK-PKCα-shRNA clone 4.1.3 and 4.1.6	MDCK-PKCα-shRNA clone 4 was transduced a second time with PKCα shRNA. Clonal cell lines isolated
MDCK-PKCβ-shRNA clone 5, 7, 10 and 11	MDCK cells stably expressing shRNA against PKCα after lentiviral transduction. Clonal cell lines isolated
CaCO-2	Human colorectal carcinoma cells. Cells were a kind gift from Professor Karl Matter (UCL, UK)
MCF-10A	Non-tumorigenic mammary epithelial cells line from patient with fibrocystic disease. Cells obtained from ATCC
HC11	Immortalised, non-transformed mammary epithelial cell line. Cells obtained from ATCC

2.4.2 Cryopreservation and thawing

Frozen stocks of cells were made by trypsinising cells and resuspending them in medium adjusted for cell freezing (50% complete growth medium, 40% FCS and 10% DMSO). Aliquots of 500-1000 µl cell suspension were frozen at -80˚C in cryotubes in a CoolCell Freezing Container (Biosision). Aliquots were later transferred to storage in liquid nitrogen. Cells were thawed by quick transfer from liquid nitrogen to a warm water bath and added to 10 ml pre-warmed growth medium. Cells were pelleted by centrifugation and resuspended in growth medium to remove DMSO. Cells were passaged 1-2 times before use in experiments.

2.4.3 Transfection of plasmid DNA

HT1080 and COS-7 cells were transfected using the TransIT-2020 reagent (Mirus). Cells were seeded in 12-well plates. The next day, cells were transfected by diluting 250 ng plasmid DNA in 50 µl OptiMEM. 1.5 µl transfection reagent was added to this mixture before a 15-30 minute incubation at room temperature. 50 µl DNA/transfection reagent dilution was then added dropwise to wells containing 1 ml complete growth medium. Transfection efficiency was tested 48 hours after transfection.

Lipofectamine 2000 (Thermo Fischer Scientific) was used to transfect MDCK cells. $1*10^4$ cells/cm^2 MDCK cells were seeded in 6-well plates for 50% confluence the following day. Transfection was performed the day after seeding. Growth medium was replaced with 700 µl serum- and antibiotics-free medium. 2 µg plasmid was diluted in 150 µl OptiMEM and mixed with 150 µl OptiMEM containing 6 µl Lipofectamine 2000 transfection reagent. DNA/transfection reagent mixture was incubated 5 minutes at room temperature. 300 µl of DNA/transfection reagent dilution was then added dropwise to wells. After 24 hours, medium was replaced with complete growth medium.

2.4.4 siRNA transfection of MDCK cells

$1*10^4$ cells/cm^2 were seeded in a 12-well plate. The next day, medium was replaced with 800 µl/well of complete growth medium. Transfection reagent was warmed to room temperature and mixed by gentle vortex. siRNA was diluted in to 100 µl OptiMem for a final concentration of 20 nM. In a separate tube, 4 µl RNAimax was diluted in 100 µl OptiMem. Diluted transfection reagent was added to DNA and incubated 15-20 minutes at room temperature before dropwise addition to cells. Medium was changed 24 hours after transfection. Knock down efficiency was analysed by RT-PCR or Western blot after 72 hours.

2.4.5 Generation of MDCK cell lines stably expressing plasmid DNA

MDCK cells were transfected with plasmid DNA as described in Section **2.4.3**. The day after transfection, antibiotics appropriate for the used vector were added. Fresh medium was supplied every 2 days and the concentration of antibiotics (up to 800 µg/ml for G418 and 1 mg/ml hygromycine B) gradually increased. Non-transfected cell were used as a control to ensure that the concentration of antibiotics was sufficient to kill all cells. Control cells perished within 1-2 weeks. Gene expression was confirmed by fluorescence microscopy and Western blot analysis.

For generation of stable cell lines either the pCEP4 or pCEP4-neo (modified from pCEP4) vector was employed. pCEP4 contains the hygromycine B resistance gene, whereas pCEP4-neo in addition contains the neomycine resistance gene. These plasmids thus allow for selection based on resistance to hygromycine B or G418 respectively. pCEP4 and pCEP4-neo additionally encode the Epstein-Barr Virus replication origin (oriP) and nuclear antigen (EBNA-1) gene which allows for extra-chromosomal replication. Cells can thus express the construct without it integrating into the genome,

which eliminates the risk of the DNA integrating into important sites in the genome. pCEP4-neo was used for expression of MT1-pHluorin-RFP.

2.4.6 Transduction of MDCK cells with adenovirus

Adenoviral virus particles for expression of FLAG-tagged MT1-MMP (Ad-MT1F) have previously been generated in our group by Sarah Weaver using the AdEasy vector system (MP Biomedicals).

Multiplicity of infection (MOI) is the average number of virus particles per cell. A MOI of 5 was here used for transduction. The number of infectious units (IFU) needed per well was calculated as: Number of cells*MOI.

$4*10^4$ MDCK cells/cm^2 were seeded for achieving 100% confluence the following day. Virus particles were diluted in serum-free medium and 400 µl of virus suspension was added to cells. After 2 hours incubation at 37˚C, 400 µl medium with 20% FCS was added for a final serum concentration of 10%.

2.4.7 Transduction of MDCK cells with lentivirus

SMARTvector Lentiviral shRNA particles for knock down of PKCα and PKCβ as well as a non-targeting control particles were bought from Dharmacon (ThermoFisher Scientific). $1*10^4$ cells/cm^2 were seeded in a 96-well plate for 50% confluence the following day. The day after seeding, lentiviral particles were thawed on ice and diluted in 50 µl transduction medium (DMEM, 5% FCS, 3 ng/ml Polybrene). A MOI of 500 was used. Transduction medium with lentiviral particles was incubated 10-20 minutes at room temperature before it was added to the cells. The next day the medium was replaced with 100 µl normal growth medium.

2.4.8 Generation of MDCK cell lines stably expressing shRNA

MDCK cells were seeded in 96-well plates and transduced with SMARTvector Lentiviral shRNA particles (Dharmacon (ThermoFisher Scientific)) as described in Section **2.4.7**. 48 hours after transduction, the cells were split into 10 cm dishes in order to dilute the cells enough for clonal growth. Puromycine (4 μg/ml) was added to select shRNA-expressing cells. Once colonies had grown to a size >100 cells, these were isolated using cloning rings (Sigma) and expanded. 10-15 colonies were picked for each shRNA. Knockdown was tested by RT-PCR and Western blotting.

2.4.9 Culture of cells on gelatin-coated coverslips and culture inserts

Coverslips were coated with gelatin by incubation on drops of gelatin (50 μg/ml, Sigma) dissolved in dH_2O at room temperature for 20 minutes. Coverslips were then transferred to drops of 1% glutaraldehyde and incubated at room temperature for 15 minutes before a final 15 minute incubation with 1 M ammonium chloride. Coverslips were transferred to a 12-well dish, sterilised in ethanol and rinsed in serum-free DMEM. The same procedure was followed for coating culture inserts.

2.4.10 Gelatin degradation assay in 2D culture

Coverslips were coated with fluorescently labelled gelatin (gelatin conjugated with Alexa405 dye (Molecular Probes, ThermoFisher)) as described in Section **2.4.9**. Transiently transfected COS-7 cells were seeded on Alexa405-labelled gelatin in the presence of GM6001 (10 μM, Calbiochem). Cells were allowed to adhere for 3 hours in the presence of GM6001. Hereafter, GM6001 was washed out and the culture medium changed to DMEM with 10% FCS. Culture was continued for 5 hours before cells were fixed in 4% paraformaldehyde (PFA). F-actin was stained with Alexa 647-labelled phalloidin after permeabilisation as described in Section **2.5**. Images were captured using

a 60X objective lens a spinning disc confocal microscope (SDCM) using the same exposure times and laser intensity for all images.

2.4.11 Culture of cells on collagen I-coated coverslips and culture inserts

Neutralised collagen I was prepared by adding 1 volume 10X RPMI to 9 volumes of ice-cold acid-extracted type I collagen (CellMatrix) and adjusting pH to 7.5 with NaOH. Collagen was diluted with serum-free DMEM to a concentration of 1.5 mg/ml and pipetted into wells with sterilised coverslips or into culture inserts (0.8 μm pore size, BD Falcon). Coated coverslips/culture inserts were incubated at 37˚C for 1 hours before cells were seeded. $1*10^4$ MDCK cells/cm^2 were seeded for 50% confluence after 24h culture. For 100% confluence $4*10^4$ cells/cm^2 were seeded.

For collagen degradation assays a 1:1 mixture of undiluted, neutralised PureCol and CellMatrix collagen I was used, and collagen dried for 3 hours at 37˚C.

2.4.12 Collagen degradation assay in 2D culture

Corning CellBIND culture 12-well plates (CoStar) were coated with 200 μl of collagen I (1:1 ratio of protease extracted PureCol and acid extracted CellMatrix collagen I) as described in Section **2.4.11**. Collagen was set for 3 hours at 37˚C.

MDCK cells were seeded to confluence in the presence of relevant inhibitors. The next day, the confluent cells were infected with Ad-MT1F at a MOI of 5 (as described in Section **2.4.6**) in the presence of GM6001 (10 μM) in serum-free medium. After 24 hours culture, GM6001 was washed out and cells incubated for a further 16 hours in the presence or absence of HGF (50 ng/ml) and relevant inhibitors. Cells were removed by >24 hours trypsination followed by a 30 minute fixation of the remaining collagen with 4% PFA in PBS. Collagen was stained with Coomassie blue (0.125% (w/v) Coomassie Brilliant Blue, 62.5% (v/v) methanol, 25% (v/v) acetic acid) mixed 1:1 with destaining

solution (30% (v/v) methanol, 1% (v/v) formic acid). Wells were washed with destaining solution followed by water and dried. To analyse, images were captured on a Nikon TE-2000E microscope widefield microscope using a 20x objective lens.

2.4.13 Immunoprecipitation of DDR1

MDCK cells were cultured to 70% confluence in one 10 cm dish per sample. In experiments where DDR1 activity was stimulated by collagen I, cells were serum starved overnight before 100 µg/ml of collagen I (PureCol) was added to the medium for 4 hours. Cells were lysed in 1 ml RIPA buffer (1% Triton X-100, 0.1% SDS, 1% Deoxycholic acid, 0.02% NaN_3, 50 mM Tris-HCl, pH 8.0, 150 mM NaCl,) with freshly added sodium orthovanadate (1 mM), proteinase inhibitor cocktail III (Sigma, 1:1000) and marimastat (Sigma, 10 µM) to prevent shedding of DDR1. Samples were then sonicated with 3, 15 second pulses of 28% amplitude. Samples were centrifuged at 16000 g for 5 minutes to precipitate debris. Supernatant was pre-cleared by incubation with 30 µl of ProteinG magnetic Dynabeads (ThermoFisher Scientific) on a rotor for 1 hours at 4˚C. This removes proteins binding non-specifically to the beads. Beads were removed and samples incubated with 5 µg of DDR1 antibody (cytoplasmic domain, Santa Cruz, sc-532) overnight at 4˚C on a rotor. Next day 30 µl of beads were added to capture DDR1 antibody and sample incubated for 2 hours at 4˚C on a rotor. Beads were washed 3 times with 1000 µl RIPA buffer with protease inhibitor and sodium orthovanadate, followed by 1 wash with 1000 µl TBS with protease inhibitor and sodium orthovanadate. Beads were then resuspended in 60 µl 1X SDS buffer. From each sample the total lysate, lysate after pre-clear, flow-through after antibody capture with beads and eluate were analysed by Western blot.

2.4.14 Transepithelial resistance (TER) measurements

All TER measurements were performed in the lab of Prof. Karl Matter (UCL). Cell culture inserts (Corning, Sigma-Aldrich) were coated with acid-extracted type I collagen (1.5 mg/ml) or left untreated before seeding $4*10^4$ MDCK cells/cm^2 with appropriate inhibitors in triplicate. The next day, TER was measured with a sterile electrode. 3 measurements were done for each well and the mean value noted. TER measured in an insert without any cells were used as background value for subtraction. Medium was changed after measurements, to limit effects from temperature change and sheer stress.

For the Ca^{2+}-switch assay, cells were trypsinised and resuspended in low Ca^{2+} medium (Sigma spinner culture medium with 2 mM Glutamine, 1 mM sodium-pyruvate, 10% dialised FCS, P/S). Centrifugation and resuspension in low Ca^{2+} medium was repeated to deplete internal Ca^{2+} stores before seeding cells in low Ca^{2+} medium. The next morning, low Ca^{2+} medium was replaced with normal medium (DMEM, 10% FCS). After 15 minutes incubation TER was measured at one-hour intervals.

2.4.15 Standard tubulogenesis assay

Tubulogenesis assays with MDCK cells were set up as in Kadono et al., 1998[43]. Cells were trypsinised and resuspended in neutralised, acid-extracted type I collagen (CellMatrix, prepared as described above) to a final concentration of 10^4 cells/ml in 2 mg/ml acid-extracted collagen I. 500 µl of cell/collagen mixture was added to 24-well plates. For 3D tubulogenesis assays used for immunocytochemistry, 75 µl of cell/collagen suspension was added to a 8 µm pore 24-well culture insert (0.8 µm pore size, BD Falcon). Collagen was allowed to gel by incubation for 60 minutes at 37˚C, before overlaying gels with complete growth medium (DMEM with 10% FCS). Medium was replaced every 2 days. Where indicated, 50-100 ng/ml HGF and inhibitors were added to

the collagen mixture as well as to the culture medium. After 3-7 days of growth, samples were analysed by widefield microscopy on a Nikon TE-2000E microscope operated by Volocity Acquisition module software using a 4x or 10x objective lens. At least 3 independent experiments were carried out for all tested conditions.

2.4.16 Tubulogenesis assay on microcarrier beads

This assay was modified from Palmisano and Itoh, 2010[132]. Gelatin-coated Cytodex3 microcarrier beads (Sigma) were incubated with cells suspended in complete growth medium (ratio 250 cells/bead and 500 beads/ml) at 37˚C with gentle agitation (45 RPM). After overnight incubation, it was confirmed by microscopy that cells had formed confluent layers on the beads. Cell-coated beads were washed 3 times with serum-free DMEM to remove floating cells and debris. Beads were gently resuspended in 150 µl growth medium per 400 beads. 150 µl bead suspension was added to 500 µl neutralised, acid-extracted collagen (final collagen concentration 2 mg/ml, CellMatrix collagen) containing appropriate growth factors/inhibitors and mixed thoroughly by gentle pipetting. 500 µl of bead/collagen mixture per well was added to a 24-well plate followed by a 60 minute incubation at 37˚C before overlaying gels with complete growth medium and culturing for 3-7 days. For tubulogenesis with MCF10A cells, EGF was excluded from the culture medium. Medium was replaced every second day.

Samples were analysed after 2-4 days culture by widefield microscopy on a Nikon TE-2000E microscope operated by Volocity Acquisition module software using a 4x or 10x objective lens.

Protrusion length was quantified by measuring the length of the 10 longest protrusions on 5 structures per condition using ImageJ software with the starting point defined as the point in the outer layer of cells from which the tubular structure extends. Measurements were pooled and comparison between conditions done with a Kruskal test

(non-parametric alternative to ANOVA) before localising differences with a pairwise Wilcoxon test with Holm correction of the p-value to correct for multiple testing.

The area of the structures was measured using ImageJ software, using the outermost periphery of the structures as the border. Similarly, the area of the beads was measured using ImageJ software. The area of the structures was normalised to the area of bead to compensate for variations in bead size and thereby variation in starting number of cells and area. 5-7 structures per condition were used for quantification and the ratios of structure/bead area were compared between the different conditions with a Kruskal test before localising differences with a pairwise Wilcoxon test with Holm correction of the p-value to correct for multiple testing.

2.4.17 Lactogenic differentiation of HC11 cells to form mammospheres.

A 70% confluent 10 cm dish of HC11 cells was trypsinised and cells divided into 6 wells in a 6-well plate for cells to form a confluent monolayer the next day. Cells were cultured for 5 days in RPMI 1640 with 10% FCS, 5 μg/ml Insulin and 10 ng/ml epidermal growth factor (EGF) and appropriate inhibitors. On day 6 after seeding, cells were washed with PBS and medium replaced with EGF-free medium. 24 hours later, medium without EGF, but containing dexamethasone (10 μM), insulin (5 μg/ml) and prolactin (5 μg/ml) (DIP medium) was added to induce lactogenic differentiation. Mammosphere formation was monitored by widefield microscopy using a 10X objective lens on a Nikon TE-2000E microscope on day 3, 4 and 5 after addition of DIP medium. 10-20 fields were captured in each well, and the number of mammospheres per field counted in order to compare mammosphere formation in individual conditions based on the mean number of mammospheres per field. The average mean number of mammospheres per field from 3 independent experiments was compared between the tested conditions.

2.4.18 Branching morphogenesis of primary mammary organoids

C57Bl/6J mice were bred as described in **2.6.1**. Wildtype, female C57Bl/6J mice between aged 12-14 weeks were euthanized in a gradient of CO_2. The 2nd, 3rd and 4th pair of mammary glands were dissected out and rinsed in ice-cold PBS. The lymph nodes in the 4th pairs of mammary gland were removed, before mincing gland tissue with a scalpel. Glands were transferred to a collagenase solution (DMEM/F12, 5% FCS, insulin (5 µg/ml), Trypsin (2 mg/ml) and collagenase (2 mg/ml)) and incubated 1 hours at 37˚C with agitation. Epithelial organoids were then pelleted by centrifugation at 520 g for 10 minutes at 25 ˚C. The fatty layer on top and the aqueous phase was removed, and pellets resuspended in DNase solution (DMEM/F12 with DNase I (4 U/ml). Mixture was shaken for 2-5 minutes before a 10 minute centrifugation (520 g). Differential centrifugations were then performed to wash out enzymes and unwanted single cells: organoid suspension was pulse centrifuged to 530 g and stopped after 30 seconds. Supernatant was discarded and organoids resuspended in DMEM/F12. Pulse centrifugation was repeated, reducing the time at 350 g to 20 and finally 10 seconds. The purity of organoids was examined under the microscope after each centrifugation, and the step repeated until the suspension mainly contained organoids. The concentration of organoids was determined under the microscope and resuspended in a volume of 1:2 matrigel/collagen I (acid extracted, CellMatrix) to ensure a final concentration of 1000 organoids/ml. 50 µl organoid suspension was added on top of 96-well plate well pre-coated with 30 µl 1:2 matrigel/collagen I (acid extracted, CellMatrix). Gels were set at 37˚C for 30 minutes before overlaying gels with organoid medium (DMEM/F12 medium with 1X ITS supplement (insulin, transferrin and selenium). bFGF (2.5 nM), DDR1-IN-1 (0.5 µM) and GM6001 (10 µM) were included as indicated. Medium was renewed every second day. Progress of tubular morphogenesis was documented by capturing widefield images

throughout the well on a Nikon TE-2000E widefield microscope from day 5-9. Analysis was done by categorising organoids as either undergoing branching morphogenesis or not based on the appearance of 3 or more branches, and calculating the percentage of organoids undergoing tubular morphogenesis in each condition. The mean value of 3 independent experiments was plotted and used for statistical analysis.

2.5 Immunocytochemistry

Reagents including primary antibodies are listed in Section **2.1**, Chapter 2. 4% PFA was prepared by dissolving PFA in dH_2O at 60˚C before adding 10x PBS to a final concentration of 1x. Aliquots of 4% PFA were kept at -20˚C and discarded after thawing.

Staining of cells in 2D culture on coverslips or in inserts:

Cells were briefly washed in PBS before fixation in 4% PFA in PBS for 10 minutes. After washing in PBS, samples were permeabilised with 0.1% Triton-X100 in PBS for 10 minutes and washed in PBS. A 1 hours blocking step was performed (blocking solution: 3 % (w/v) BSA, 5 % (v/v) goat serum in TBS), before incubation with primary antibodies in blocking solution at 4˚C overnight. After extensive washing in PBS, samples were incubated with Alexa dye-conjugated secondary antibodies (Molecular Probes, ThermoFisher Scientific), Alexa dye-conjugated phalloidin (Molecular Probes, ThermoFisher Scientific) and DAPI in blocking solution for 2-4 hours at room temperature. After extensive washing in PBS, coverslips were mounted on glass slides using Prolong Gold/Diamond Anti-fade mounting medium (Molecular Probes, ThermoFisher Scientific). For culture inserts, the membrane was cut out using a scalpel and mounted with a coverslip on top.

Staining of live 2D cultures to examine surface localisation of MT1-MMP

In order to only detect MT1-MMP on the cell surface, incubation with primary antibodies was performed on live cells on ice. Inserts were washed in PBS before incubation with 4 μg/ml anti-FLAG-M2 (Sigma-Aldrich) in 10% FBS-DMEM on ice for 2 hours. Inserts were washed thoroughly with PBS 3 times before fixation with 4% PFA in PBS for 10 minutes. After washing with PBS, a 1 hours blocking step (blocking solution: 3% (w/v) BSA, 5% (v/v) goat serum in TBS) was performed at room temperature, followed by incubation with Alexa dye-conjugated, secondary antibodies (Molecular Probes, ThermoFisher Scientific) for 2 hours at room temperature. After washing in PBS, an incubation with Alexa dye-conjugated phalloidin (Molecular Probes, ThermoFisher Scientific) and DAPI in blocking solution with 0.1% triton was performed for 30 minutes at room temperature. After extensive washes with PBS, cultures were cut from inserts and mounted on glass slides with a coverslip on top using Prolong Gold/Diamond Anti-fade mounting medium (Molecular Probes, ThermoFisher Scientific).

Immunocytochemistry on cells in 3D culture

Wells and inserts were rinsed with PBS before fixation in 4% PFA in PBS for 30 minutes at room temperature on a shaker. Wells and inserts were rinsed 3 times with PBS before 1 hour incubation in permeabilisation/blocking solution (0.5% Triton-X100 and 10% FCS in PBS) on a shaker at room temperature. Primary antibodies diluted in permeabilisation solution were added to wells and inserts and plates were incubated on a shaker overnight at 4˚C. After 3 washes in permeabilisation solution at room temperature the gels were incubated for 4 hours with secondary Alexa dye-conjugated antibodies (Molecular Probes, ThermoFisher Scientific), Alexa dye-conjugated phalloidin (Molecular Probes, ThermoFisher Scientific) and DAPI in permeabilisation solution. After 3 quick washes and 3 15-minute washes in permeabilisation solution, the inserts

were washed for 30 minutes in PBS. Membranes were cut from inserts and mounted on glass slides using Prolong Gold/Diamond Anti-fade mounting medium (Molecular Probes, ThermoFisher Scientific).

2.6 Immunohistochemistry (IHC)

2.6.1 Source and breeding of mice

LEXKO-1928 mice (DDR1-null) were obtained from The Wellcome Trust Knockout Resource. The parental strain of these mice is C57Bl/6J. DDR1 expression has been abolished by insertion of a Neo-casette into the DDR1 gene. Since DDR1-null females are infertile, breeding pairs were set up with heterozygous females and genotyping performed to identify wildtype, hetero- or homozygous animals. Genotyping was done with 3 primers, allowing for detection of both the presence or absence of the Neo-casette by bands of difference size (2 bands observed in heterozygous animals, wildtype or null animals discerned by size of band). The following 3 primers were used:

Primer Neo3a: GCAGCGCATCGCCTTCTATC
Primer 19: AGACAATCTCGAGATGCTGG
Primer 18: GTTGCGTTACTCCCGAGATG

2.6.2 Tissue isolation and staining

Wildtype and DDR1-null C57Bl/6J female mice of 13-14 weeks age were mated with wild type males. 3 days after giving birth, the female was euthanised in a rising gradient of CO_2. The 4^{th} pair of mammary glands was dissected out and rinsed in ice-cold PBS before fixation in formalin. Tissue was embedded in paraffin and sections cut. Sections were deparaffinised by sequential incubation 2x5 minutes in xylene, 2x2 minutes in 100% ethanol, 5 minutes in 95%, 85% and 70% ethanol before transfer to PBS. Endogenous peroxidase activity was then quenched by a 20 minute incubation in 3%

H_2O_2 in dH_2O. Antigen retrieval was performed by incubating slides in pre-warmed citrate buffer (0.01 M trisodium citrate dehydrate, 0.05% Tween, pH 6) in a 92˚C water bath for 20 minutes. Slides were then allowed to cool at room temperature for 30 minutes. Slides were washed in PBS before performing a 2 hours blocking step by incubating slides in blocking buffer (10% normal goat serum or FCS in TBS) in a humid chamber at room temperature. Primary antibodies (Section **2.1**, Chapter 2) were diluted in blocking buffer and sections incubated with antibodies overnight in a humid chamber at 4 ˚C. The next day, the sections were washed in PBS for 3x5 minutes and incubated with biotinylated secondary antibodies (Vector Laboratories) in blocking solution in a humid chamber at room temperature for 2 hours. After 3x5 minute washing in PBS slides were incubated 30 minutes with avidin/biotin/HRP complex reagent (ABC staining kit, Vector Laboratories). Slides were then washed and reaction developed with DAB substrate (Vector Laboratories) until reaction was stopped by rinsing slides in water. Sections were counter-stained with haematoxylin, dehydrated and mounted using DPX mounting medium (Sigma-Aldrich).

For staining with primary antibodies raised in mouse, the DAKO ARK Peroxidase for Mouse Primary Ab kit (DAKO) was used according to the manufacturers instructions. Briefly, this procedure followed the same protocol as above, except that primary antibodies were pre-incubated with biotinylated secondary antibodies (supplied in DAKO ARK kit) and blocked with normal mouse IgG (supplied in DAKO ARK kit) before applying antibodies to tissue sections. Tissue sections were then washed in PBS and incubated with streptavidin-linked peroxidase before washing and development with DAB substrate as described above.

Stained sections were analysed capturing images by brightfield microscopy and white balance adjusted by applying the same filter to all images in Photoshop (Adobe). ImageJ was used for automatic detection and measurement of alveolar area.

2.7 Imaging and analysis

Widefield microscopy

All widefield images were captured on an inverted Nikon TE2000-E widefield microscope with Volocity Acquisition software (Perkin Elmer, UK). Following objective lenses were used: 4X objective lens (Plan Fluor 4x /NA 0.13), 10x objective lens (UPLSAPO 10x/NA 0.30 DIC) and 20x objective lens (UPLSAPO 20x/NA 0.45). For illumination during imaging a CoolLED pE-4000 illumination (365 nm, 460 nm, 525 nm, 635 nm) was used.

Confocal laser scanning point microscopy (CSLM)

All CSLM imaging employed a FluoView Spectral FV1200 CSLM based on Olympus IX83 motorized inverted microscope CSLM. Following objective lenses were used: 60X objective lens (UPLSAPO 60x/NA 1.4) and a 30x objective (UPLSAPO 30x/NA 1.05 Silicone Immersion). Following lasers were used for imaging: violet diode laser 405 nm (25 mW), blue diode laser 473 nm (50 mW), green DPSS laser 559 nm (25 mW) and a red diode laser 635 nm (25 mW).

Spinning disc confocal microscopy (SDCM)

All SDCM imaging was done on a PerkinElmer Spinning Disk Confocal Microscope based on a Nikon TE 2000-U Eclipse motorized inverted microscope with DIC optics. The following objective lens was used: 60X (Plan Apo 60x/NA 1.40). Volocity software (Perkin Elmer, UK) was used for Acquisition. Following lasers were

used for imaging: violet diode laser 405 nm, blue diode laser 473 nm, green DPSS laser 559 nm and a red diode laser 635 nm.

2.7.1 Image Processing and analysis

Volocity (Perkin Elmer, UK), Adobe Photoshop (Adobe, Berkshire, UK) and ImageJ were used for image processing, visualisation and analysis. The same adjustments were applied to all images within the same experiment unless otherwise stated. Original intensity values were used for quantification.

2.7.2 Statistical analysis

Unless otherwise stated in the figure legends, results are representative of 3 independent experiments. R software (The R Foundation) was used for statistical analysis and data visualisation.

Chapter 3 Collagen signalling through DDR1 plays a role in establishment of apicobasal polarity during epithelial 3D morphogenesis

3.1 Introduction

As described in Chapter 1, MDCK cells in a collagen I matrix can undergo tubulogenesis in a manner relying on MT1-MMP-driven invasion[43]. Posttranslational regulation of MT1-MMP restricts its matrix-degrading activity to the tip of protruding tubules by ensuring that MT1-MMP only localises to the basal, ECM-abutting membrane domain of cells at the tip of protruding tubules[93]. Apicobasal polarity of epithelial cells is thus a prerequisite for the spatial regulation of MT1-MMP during 3D morphogenesis. Details of the molecular mechanisms that govern the polarised distribution of MT1-MMP are not understood, but preliminary findings in the Itoh lab suggests that signalling from the ECM participates in this regulation (PhD thesis by Dr Sarah Weaver). HGF stimulation of MDCK cells cultured on fibrillar collagen I thus induced an increase in MT1-MMP at the basal cell surface, whereas cells cultured on glass or gelatin retained MT1-MMP in its default, apical localisation in the presence of HGF (PhD thesis by Dr Sarah Weaver). This suggests that a collagen receptor activated by fibrillar collagen can affect the polarised distribution of MT1-MMP. However, the receptor transmitting this signal, its mode of action or impact on epithelial morphogenesis has not been identified.

In this chapter I aimed to investigate how signals from the ECM contribute to guiding the apicobasal distribution of MT1-MMP, and particularly whether the collagen receptor DDR1 is involved. To address this question, I developed a novel tool for specific visualisation of MT1-MMP at the cell surface. Using this tool, I confirmed the previous finding that a fine spatiotemporal regulation of MT1-MMP according to apicobasal polarity operates during epithelial morphogenesis. I then tested the hypothesis that a signal from fibrillar collagen mediated through DDR1 could be involved in this regulation. Finally, I explored the role of DDR1 in epithelial tubulogenesis and whether this involves a role in organising apicobasal polarity.

3.2 Results

3.2.1 HGF induces MDCK cells to undergo MMP-dependent tubulogenesis in 3D collagen I matrices

Madin Darby canine kidney (MDCK) cells are a well-polarised epithelial cell line, which will form monolayers with continuous functional cell-cell junctions and intact polarity when cultured in 2D. HGF (also known as "scatter factor") causes MDCK cells to scatter in 2D culture, whereas HGF stimulation in 3D collagen culture induces MDCK cells to undergo tubular morphogenesis[34,35]. MDCK cells are thus a useful model for the study of epithelial tubulogenesis and have been extensively used for this purpose.

To confirm the effects of HGF in our system, I first tested the ability of HGF to induce scattering of MDCK cells in 2D culture. MDCK cells were cultured on plastic or a thin film of fibrillar collagen I (1.5 mg/ml) in the presence or absence of HGF (50 ng/ml). Control cells adhered and grew as islands of cells on both plastic and collagen I. Upon stimulation with HGF, cells in islands scattered out regardless of substratum (**Figure 11**). Scattering on neither plastic nor collagen I depended on MMP activity, as treatment with GM6001 (10 μM), a pan-MMP inhibitor, did not affect this (**Figure 11**).

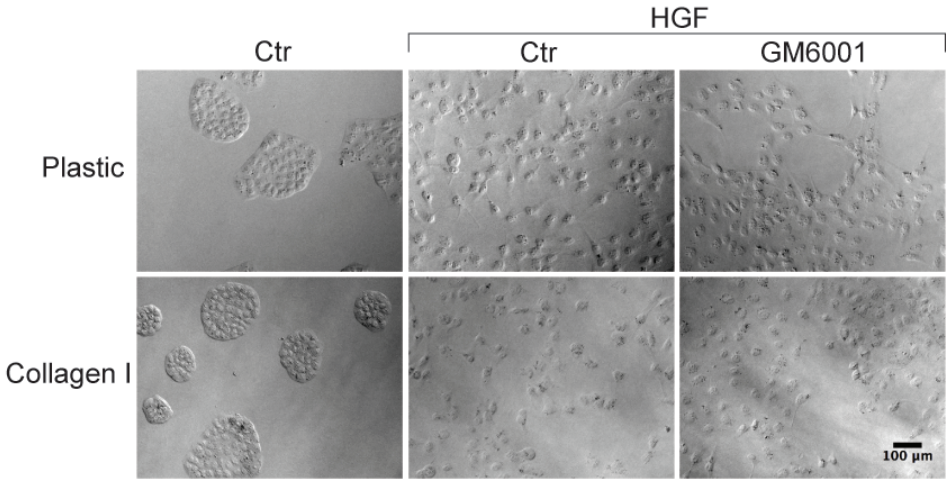


Figure 11. HGF induces scattering of MDCK cells in 2D. MDCK cells were cultured on plastic or a film of collagen I (1.5 mg/ml) in the presence or absence of HGF (50 ng/ml) and GM6001 (10 μM) in DMEM with 10% FCS for 48 hours. A 10x objective was used to capture brightfield images on a widefield microscope. Representative images are shown.

Next, I confirmed that HGF induces tubulogenesis by MDCK cells in 3D collagen. MDCK cells were cultured in a 3D collagen matrix (2 mg/ml collagen I) for 5 days in the presence or absence of HGF. Control cells formed small, cyst-like structures, whereas HGF stimulation caused cells to form branching tubular structures (**Figure 12**). In agreement with previous studies[43], tubulogenesis required MMP-dependent degradation of collagen I, as seen by GM6001 treatment preventing it (**Figure 12**).

Collagen degradation in this model relies on the activity of MT1-MMP[43]. However, causing exaggerated MT1-MMP activity by overexpression of MT1-MMP can also disturb tubulogenesis in this model[43,93]. Thus, a precise regulation of MT1-MMP is required in order for cells to form tubules, making tubulogenesis an interesting model to study how such regulation of MT1-MMP is achieved.

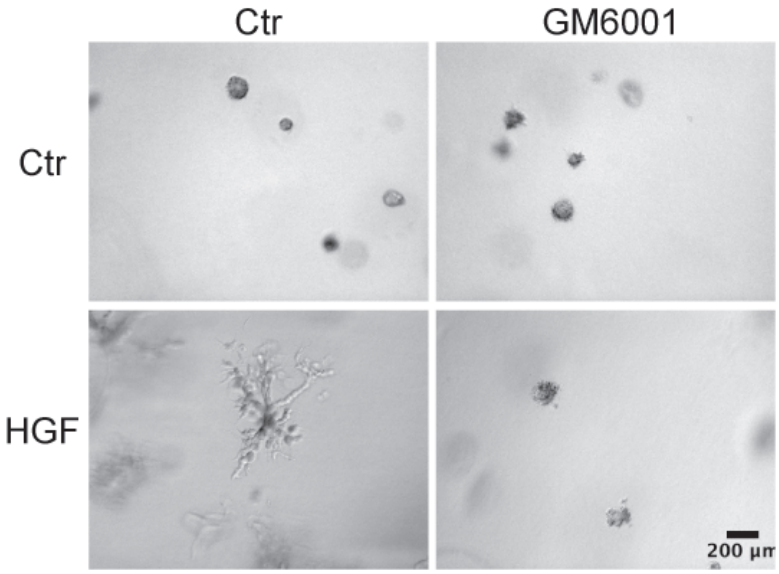


Figure 12. HGF induces MMP-dependent tubulogenesis by MDCK cells in 3D collagen I. MDCK cells were cultured in 3D collagen I gels (2 mg/ml) in DMEM with 10% FCS in the presence or absence of HGF (50 ng/ml) and GM6001 (10 µM). Cells were cultured for 5 days before imaging using a 4X objective on a widefield microscope. Representative images are shown.

3.2.2 MT1-pHluorin-RFP: A tool to study surface localisation of MT1-MMP during 3D tubulogenesis

Our group has previously shown that spatial regulation of MT1-MMP activity during tubulogenesis includes controlling the localisation of the enzyme to the ECM-facing surface of the cells (basal surface) or the surface facing the lumen of the tubule (apical surface)[93]. In order to study this spatial regulation in further detail, I wished to be able to differentiate between vesicular and surface-exposed MT1-MMP. This distinction is important since a prerequisite for ECM degradation is exposure of the enzyme to its substrate at the cell surface. The resolution of confocal microscopy does not facilitate distinguishing MT1-MMP at the cell surface from MT1-MMP in vesicles just below the surface. A way to achieve this distinction is to make vesicular and surface MT1-MMP detectable at different wavelengths. Specific staining of surface-exposed MT1-MMP can be done by immunocytochemistry (ICC) without permeabilisation[93]. However, ICC in 3D is time-consuming and leaving out the permeabilisation step means that apically localised MT1-MMP will not be detected. I therefore developed a flexible tool to readily differentiate vesicular and surface-exposed MT1-MMP in living cells: MT1F-pHluorin-RFP. This mutant MT1-MMP contains a pH-sensitive GFP mutant (superecliptic pHluorin[131]) in the L2 region of MT1-MMP in the ectodomain and a monomeric RFP1 (RFP) in the cytoplasmic domain (principle shown in **Figure 13**). Superecliptic pHluorin is a pH-sensitive green fluorescent protein, which fluoresces at neutral pH when excited at Ex_{475} nm. In contrast, at pH <6 the emission intensity is almost negligible (~2.5% fluorescence left[133])[131]. This allows for specific detection of MT1-MMP at the cell surface, whilst eliminating the signal from MT1-MMP in secretory/endocytic vesicles based on the difference in pH between these compartments (pH ~7.0 on the cell surface, whilst vesicular pH ranges from 4.7 in lysosomes, over 5.5 in secretory granules up to 6.5

in recycling endosomes[134]). The RFP-tag in the cytoplasmic domain enables detection of total MT1-MMP regardless of its localisation (**Figure 13**).

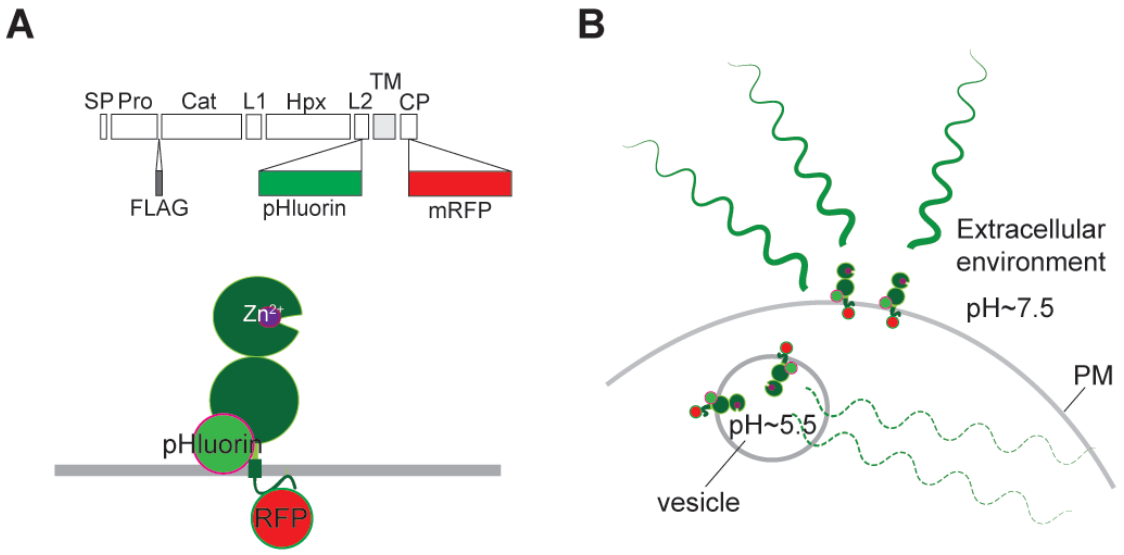


Figure 13. MT1F-pHluorin-RFP: A tool for specific detection of MT1-MMP at the cell surface. A) Structure of MT1-pHluorin-RFP**:** MT1F-pHluorin-RFP consists of MT1-MMP with a FLAG-tag inserted between Arg111 and Lys112 of MT1-MMP and superecliptic pHluorin[131] inserted close to the plasma membrane in the extracellular domain between Gly541 and Gly542 with a 2 Gly N-terminal linker and a 1 Gly C-terminal linker. In addition RFP is inserted in the cytoplasmic domain between Cys574 and Gln575 with a 2 Gly N-terminal linker. **B)** When MT1F-pHluorin-RFP is located at the plasma membrane, the extracellular pHluorin-tag is exposed to neutral pH and fluoresces brightly. In contrast, MT1F-pHluorin-RFP in vesicles will be oriented with the extracellular domain inside the acidic environment of the vesicle, which eliminates fluorescence from pHluorin. The RFP-tag of MT1F-pHluorin-RFP is in both cases located in the cytoplasm and will thus be detectable. Given the high concentration of MT1-MMP in vesicles compared with that on the cell surface, this effectively allows for detection of surface MT1-MMP at $Ex_{475\ nm}$ and vesicular MT1-MMP at Ex_{568}. PM: plasma membrane.

As a proof of concept, I transfected HT1080 cells with MT1F-pHluorin-RFP and measured fluorescence intensity by confocal live cell imaging with varying pH of the extracellular environment. At pH 7.5, the pHluorin signal was mainly detected at the membrane (**Figure 14A**, arrowhead), however, additional background signal in the perinuclear region was also detected (**Figure 14A**, arrow). This may be due to large amounts MT1F-pHluorin-RFP being present in the ER and Golgi apparatus. To test the pH-dependency of fluorescence intensity, cells were imaged every 3.16 seconds for 10 time points at different pHs: the initial buffer was pH 6.4 and the pH was then increased

to 7.5, lowered to pH 5.8 and changed back to neutral pH 7.5. As a control, images were continuously captured at pH 7.5 throughout the same time frame. Representative cells are shown in **Figure 14B**. When imaging was initiated at pH 6.4, weak fluorescence was observed along the cell membrane (**Figure 14B**, arrowhead). Changing the buffer to pH 7.5 markedly increased fluorescence at the cell membrane as expected, whereas a decrease to pH 5.8 almost eliminated the signal (**Figure 14B**, arrowhead). However, changes in extracellular pH also seemed to confer slight changes to the background fluorescence in the perinuclear region. To rule out that changes in fluorescence intensity at the cell membrane were solely due to changes in overall fluorescence, I plotted the ratio of intensity measured in a region of interest (ROI) at the cell membrane and an identical size ROI in the perinuclear region with strong background (**Figure 14C**). This graph shows that fluorescence at the cell membrane is decreased when pH is lowered below pH 7.5. A larger drop in pH confers a larger decrease in fluorescence. In contrast, fluorescence at the cell membrane at constant pH 7.5 does not vary much within the time frame measured (**Figure 14C**). This confirms that fluorescence intensity of pHluorin is pH-dependent and that MT1F-pHluorin-RFP on the cell surface can be selectively visualised.

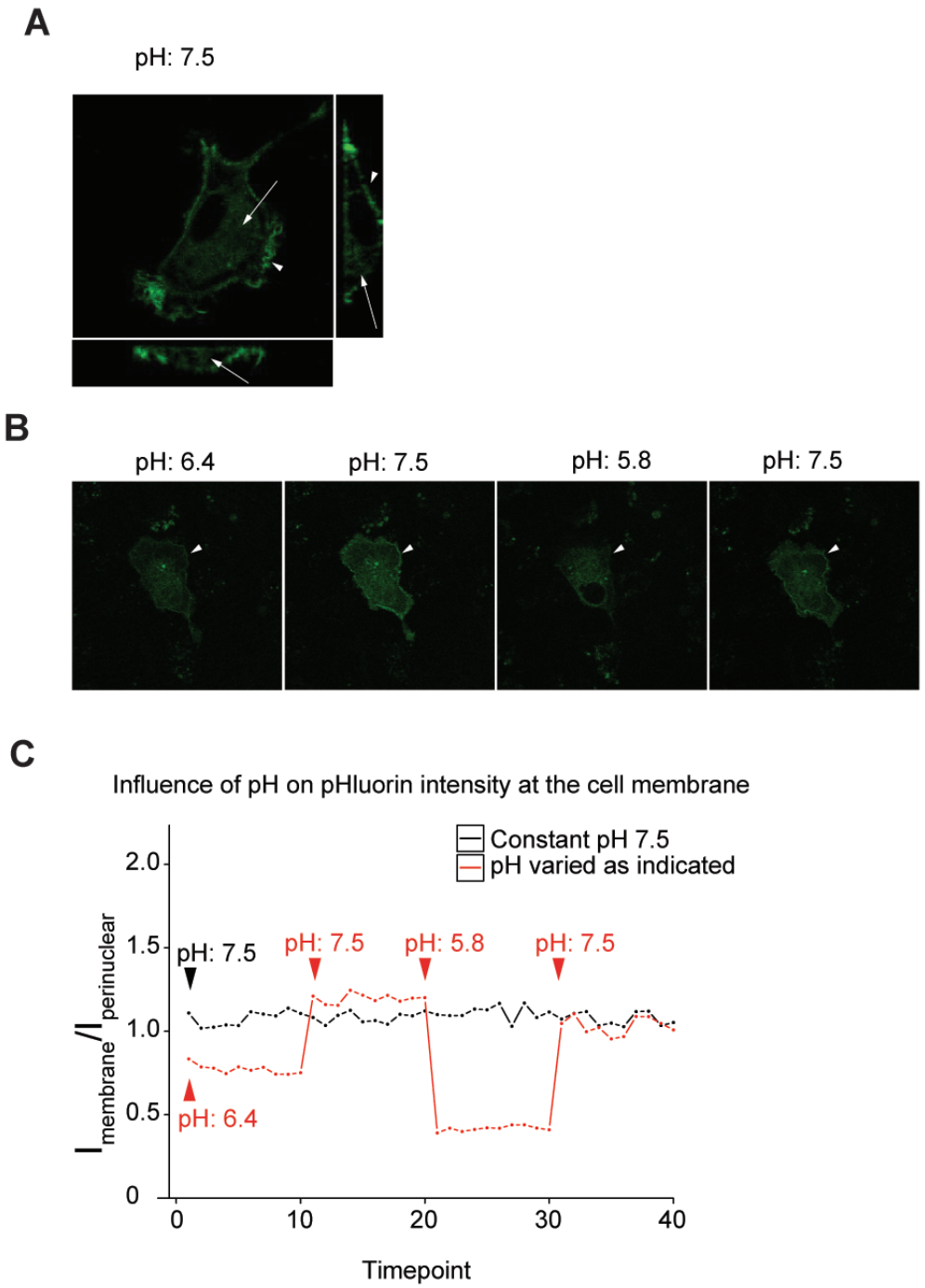


Figure 14. MT1-pHluorin-RFP can be visualised at the cell membrane at neutral, but not acidic extracellular pH. HT1080 cells were seeded in an Ibidi glass-bottom µ-slide and transiently transfected with MT1F-pHluorin-RFP. 48 hours after transfection, growth medium was replaced by imaging buffer (25 mM HEPES, 120 mM NaCl, 2.5 mM KCl, 2 mM $CaCl_2$, 2mM $MgCl_2$, 30 mM Glucose) with pH adjusted to 5.8, 6.4 or 7.5 as indicated in the Figure. Imaging was done with a 60X objective on a CSLM. **A)** Confocal stack captured at Ex_{488} nm at pH 7.5 shows membrane localisation of MT1F-pHluorin-RFP. Arrows point to potential background staining in the region around the nucleus. Image of a representative cell is shown. **B)** Images were captured at 10 time points with 3.13 second intervals before each buffer change. Images of a representative cell are shown. **C)** For the cell shown in B) the ratio between the intensity in a ROI at the cell membrane and the intensity in a same-sized ROI in the region around the nucleus was plotted (red track). The intensity ratio for a cell at pH 7.5, which was not subjected to any changes in buffer pH, is also shown as control (black track).

To test whether cell surface enzymatic activity of MT1-pHluorin-RFP is maintained, MT1F-RFP (as a positive control) or MT1-pHluorin-RFP was expressed in COS-7 cells and the cells seeded on fluorescent gelatin. After 5 hours the level of gelatin film degradation was examined. In contrast to mock-transfected cells, cells transfected with either MT1-pHluorin-RFP or MT1F-RFP degraded gelatin (**Figure 15**). This suggests that insertion of pHluorin did not prevent cell surface activity of MT1-MMP, and MT1-pHluorin-RFP can thus be used to monitor MT1-MMP localisation.

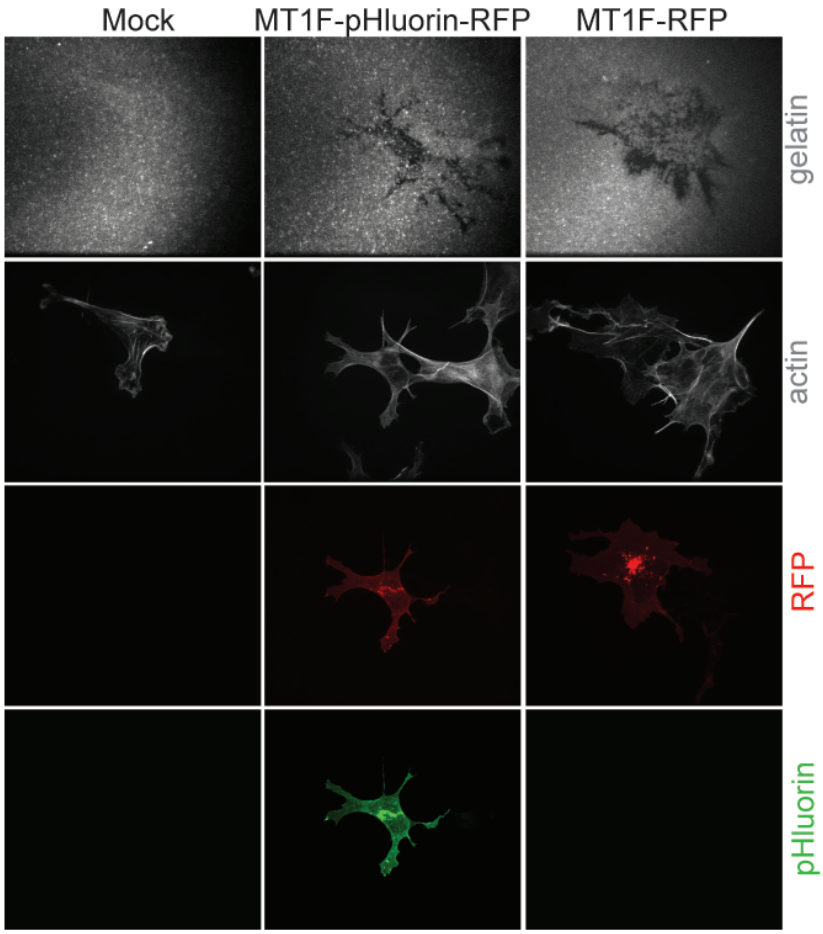


Figure 15. MT1F-pHluorin-RFP displays functional gelatinase activity. COS-7 cells transiently transfected with pSG5, pSG5-MT1F-RFP or pSG5-MT1F-pHluorin-RFP were seeded on Alexa405-labelled gelatin in the presence of GM6001 (10 µM). Cells were allowed to adhere for 3 hours in the presence of GM6001. Hereafter medium was changed to DMEM with 10% FCS and culture continued for 5 hours before fixing cells in 4% PFA. F-actin was stained with Alexa 647-labelled phalloidin after permeabilisation. Images were captured using a 60X objective a SDCM. Gelatin degradation is shown as dark areas against a grey background. Actin is depicted in gray, RFP in red and pHluorin in green. Same exposures and laser intensity were used for all images. Representative images are shown. **Note that the pHluorin signal is not surface specific due to processing for immunocytochemistry.**

3.2.3 MT1-MMP localises to the basal surface of cells at the tip of protruding tubules during HGF-induced epithelial tubulogenesis

To analyse surface localisation of MT1-MMP during epithelial morphogenesis, I generated an MDCK cell line stably expressing MT1-pHluorin-RFP (MDCK-MT1pH cells). Analysis of lysates by Western blot confirmed that MT1F-pHluorin-RFP is expressed at the expected size of ~125 kDa, and processed to the lower molecular weight forms like MT1F-RFP and endogenous MT1-MMP (**Figure 16A**). Live cell imaging of MDCK-MT1pH cells on collagen I film gave a signal corresponding to MT1-MMP in vesicles at Ex_{568} nm (RFP), while the signal at Ex_{488} (pHluorin) localised to the cell membrane as expected (**Figure 16B**). The RFP signal could also be detected at the cell membrane. However, due to the concentration of MT1-MMP molecules in vesicles being much higher than at the cell membrane, the RFP signal at the membrane was very dim when exposure time and laser intensity were adjusted to be appropriate for visualising RFP in vesicles. The major site of pHluorin signal was at the apical membrane, but some signal was also detected in lateral membranes (**Figure 16B**).

To analyse MT1-MMP localisation during 3D morphogenesis, I cultured MDCK-MT1pH cells in a 3D collagen I matrix. After 2 days the cells had formed small cysts with discernable lumens. Confocal imaging of these cysts showed that surface-exposed MT1-MMP (shown in green) localised at the apical membrane (**Figure 16C**). HGF was then added and culture continued for a further 20 hours before the localisation of MT1-MMP again was examined by confocal microscopy. Upon HGF treatment, tubular protrusions began to extend from the cysts. Interestingly, a switch in MT1-MMP localisation to the basal surface was seen on cells at the tip of protruding tubules (**Figure 16C**, arrowheads). HGF treatment thus induces a switch in the apicobasal distribution of MT1-MMP, which brings the enzyme into contact with the ECM at the basal cell surface and thereby allows

matrix degradation to occur. This switch in localisation only occurred in the distinct areas where new tubules began to extend and ECM degradation therefore was required. These results confirmed that MT1-MMP activity in epithelial tubulogenesis is controlled by local changes in the apicobasal distribution of the enzyme.

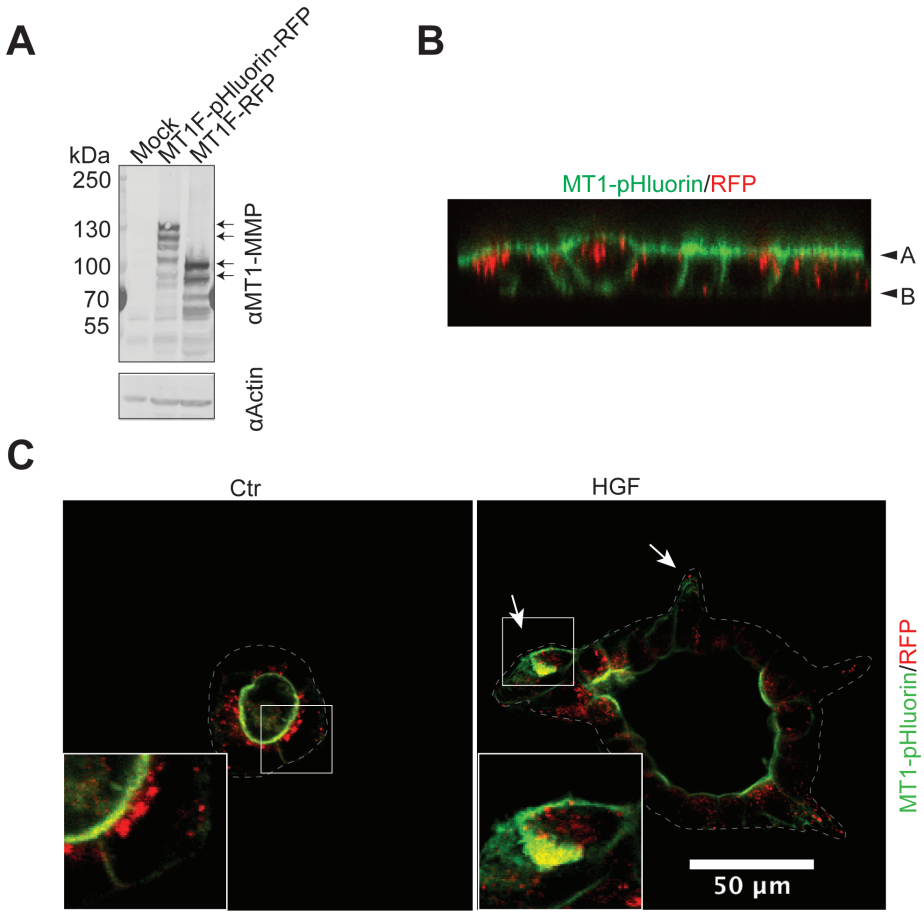


Figure 16. Generation of MDCK-MT1pH cells. A) MDCK cells stably expressing pCEP4neo-MT1-pHluorin-RFP (MDCK-MT1pH cells) were established based on resistance to G418 (800 µg/ml). Lysates were analysed by Western blotting using anti-MT1-MMP antibody recognising the MT-Loop region of MT1-MMP within the catalytic domain. Arrows point to pro- and mature forms of MT1-MMP. **B)** MDCK-MT1pH cells were seeded in an Ibidi glass-bottom µ-slides in 2D culture on a collagen I film. After 24 h, line scan images were captured at Ex_{488} nm (shown in green) and Ex_{568} nm (shown in red) using a 60X objective on a CLSM. Representative image is shown. A: apical, B: basal. **C)** MDCK-MT1pH cells were seeded in 3D collagen I (2 mg/ml) and cultured for 48 hours. Live cell images were captured using a 60X objective on CLSM. Hereafter HGF (50 ng/ml) was added, and culture continued for further 20 hours before images were captured using a 60X objective lens on a CLSM. Representative images are shown. A line has been drawn to mark circumference of the structure. Arrows point to surface MT1-MMP at the basal cell membrane. Ex_{488} nm and Ex_{568} nm are shown in green and red respectively.

3.2.4 HGF induces a collagen-dependent change in the apicobasal distribution of MT1-MMP in polarised monolayers of MDCK cells

I next investigated if the type of matrix that cells are exposed to influences the apicobasal distribution of MT1-MMP. To do this I compared the localisation of MT1-MMP in cells cultured on a film of gelatin, fibrillar collagen I or on uncoated plastic/glass.

In the initial examination of MT1-pHluorin-RFP localisation in monolayers of MDCK-MT1pH cells (Section **3.2.3**), I observed that the enzyme primarily located at the apical cell surface (**Figure 16B**) in accordance with previous studies[93]. However, as mentioned previously, some MT1-pHluorin-RFP was also observed along the lateral surface of cells. This is most likely due to the high level of MT1-pHluorin-RFP expression in MDCK-MT1pH cells overloading the normal secretory machinery of MT1-MMP in MDCK cells, since low level of ectopic expression of MT1-MMP did not result in lateral localization[93]. Therefore, I also employed an adenoviral vector system to express FLAG-tagged MT1-MMP (MT1F) (Ad-MT1F) with a low multiplicity of infection (MOI) of 5. This system allows for better control of expression levels to ensure a low but detectable expression of MT1F (thesis by former student of Dr Itoh, Dr Sarah Weaver).

MDCK cells were seeded either directly into culture inserts or in inserts coated with gelatin or fibrillar collagen I and infected with Ad-MT1F in the presence of GM6001 (10 μM). After 24 hours culture GM6001 was washed out and cells incubated for a further 24 hours in the presence or absence of HGF (50 ng/ml). To specifically detect MT1F on the cell surface, staining was done before fixation by incubating live cells on ice with anti-FLAG antibody. Hereafter cells were fixed and further processed for indirect immunofluorescence. Without HGF treatment, cells cultured on collagen I exclusively localised MT1F (shown in green) at the apical surface with little MT1F detected in

confocal sections captured at the basal side (**Figure 17A**). This suggests that the default secretory pathways of MT1-MMP favour its presence at the apical surface. In contrast, HGF stimulation induced an increase in the appearance of MT1F at the basal surface (**Figure 17A**). Quantification of the percentage of total surface MT1F present at the basal side found this HGF-induced increase to be significant (**Figure 17B**). The concept of HGF bringing MT1-MMP into contact with the ECM as observed in 3D culture (**Figure 16C**), is thus consistent in epithelial monolayers. Interestingly, when cells were seeded on gelatin or plastic, HGF treatment did not induce basal localisation of MT1F (**Figure 17A** and -**B**), suggesting that a signal from fibrillar collagen I is involved in this regulation.

Studying the localisation of MT1F-pHluorin-RFP in MDCK-MT1pH cells on collagen I, gelatin or glass reproduced the results with MT1F (**Figure 17C**): HGF stimulation caused an increase in the percentage of MT1-pHluorin-RFP at the basal surface of cells seeded on collagen I, whereas no change was observed in cells seeded on gelatin or glass. However, the increase in basal localisation of MT1F-pHluorin-RFP induced by HGF treatment was much smaller compared to the change observed for MT1F (55% increase for MT1F-pHluorin-RFP in **Figure 17C** compared to a 763% increase for MT1F in **Figure 17B**). In addition the base levels of MT1-pHluorin-RFP at the basal surface were approximately double of those observed for MT1F in **Figure 17B** and in previous studies[93]. Again, overexpression of MT1F-pHluorin-RFP likely saturates endocytic pathways and thus causes the enzyme to "leak" to the basal side. However, MT1-pHluorin-RFP is still useful to detect surface MT1-MMP in 3D culture conditions, particularly to detect MT1-MMP at the apical cell surface.

These results suggest that regulation of the apicobasal distribution of MT1-MMP is collagen-dependent and that a receptor transmitting signals from fibrillar collagen I is likely to be involved.

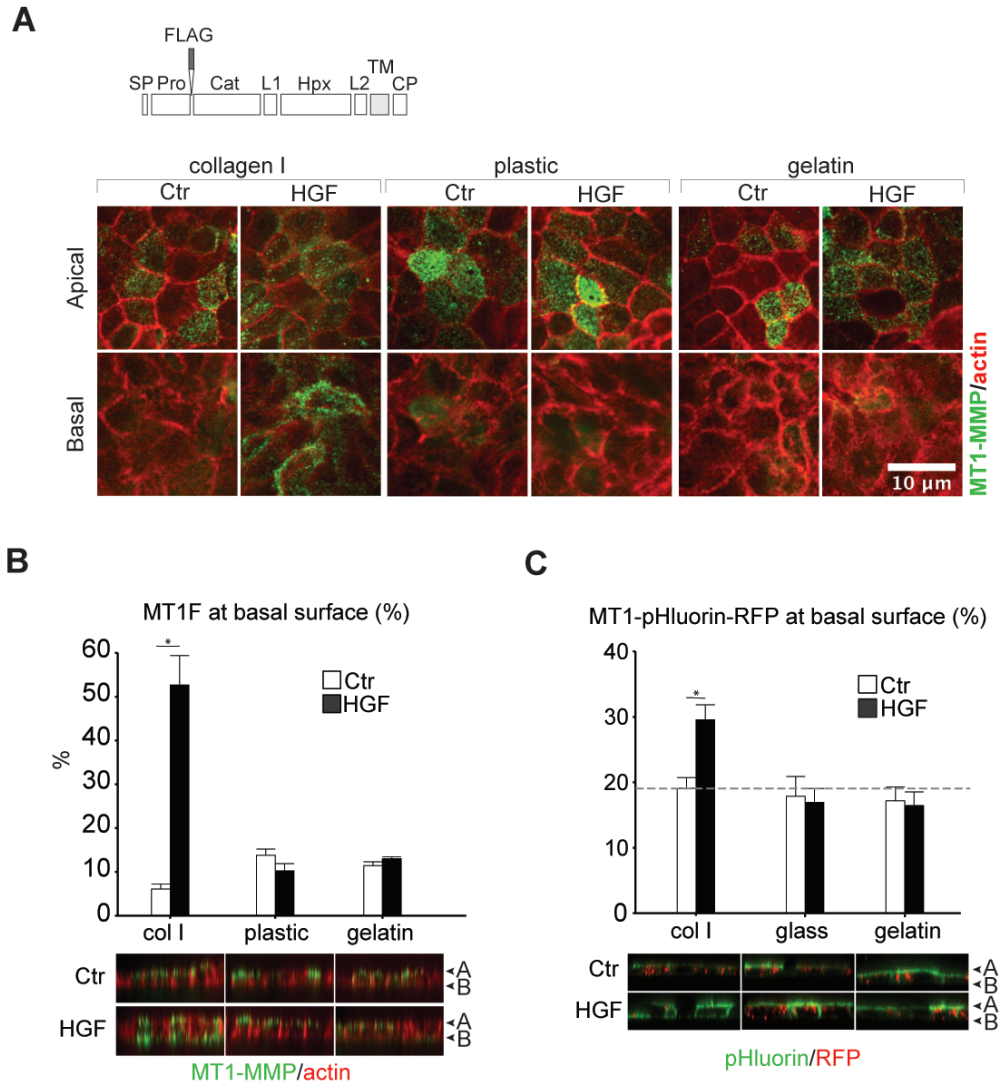


Figure 17. HGF- induces a collagen-dependent increase in basal localisation of MT1-MMP at the basal cell surface. A) Top: Structure of MT1F. FLAG-tag is inserted between Arg111 and Lys112 of MT1-MMP. Bottom: MDCK cells were seeded in culture inserts coated with collagen I (1.5 mg/ml), gelatin (50 µg/ml) or left uncoated. Once 100% confluent, cells were infected with Ad-MT1F at a MOI of 5 in the presence of GM6001 (10 µM). After 24 hours culture, GM6001 was washed out and cells incubated a further 24 hours in the presence or absence of HGF (50 ng/ml). Cells were then stained with anti-FLAG-M2 antibody in ice-cold serum-free DMEM on ice for 1 hour. Cells were fixed and stained with Alexa dye-conjugated secondary antibody and phalloidin. Confocal images were captured using a 60X objective on a SDCM and analysed using Volocity and ImageJ software. MT1F is shown in green, actin in red. Confocal sections at the apical (A) and basal (B) surface in the absence or presence of HGF are shown. **Note basal localisation of MT1F upon HGF treatment. B**) Results in A were quantified by measuring the intensity of the 488 nm channel in identical volumes at the apical and basal surface in 10 confocal stacks per condition. Volumes were selected based on the signal in the channel representing actin. The percentage of total surface MT1F present at the basal surface was calculated as: basal intensity/(apical+basal intensity). Note that MT1-MMP at lateral surfaces thus is ignored in this calculation. Graph represents one of two independent experiments. Representative XZ-sections for each condition are shown underneath the graph. The tested conditions were compared with a Kruskal-Wallis rank sum test ($p< 2*10^{-16}$) before localising differences with a pairwise Wilcoxon test with Holm correction of the p-value to correct for multiple testing. Asterisks (*) depict statistically significant differences ($p<0.05$). Col I: collagen I. **C**) MDCK-MT1pH cells were seeded in IBIDI µ-slide wells coated with collagen I (1.5 mg/ml), gelatin (50 µg/ml) or left uncoated. After 24 h, HGF was added and culture continued for a further 24 hours before capturing line-scan images by live-cell microscopy using a 60X objective on a CLSM and analysed using ImageJ. Representative images from each condition are shown with Ex_{488} nm shown in green and Ex_{568} nm shown in red. Results in A were quantified by measuring the intensity of the 488 nm channel in identical ROIs at the apical and basal surface

in 15 line scans per condition. The percentage of total surface MT1F present at the basal surface was calculated as: basal intensity/(apical+basal intensity). Note that MT1-MMP at lateral surfaces thus is ignored in this calculation. The tested conditions were compared with a Kruskal-Wallis rank sum test ($p=0.005731$) before localising differences with a pairwise Wilcoxon test with Holm correction of the p-value. * depicts statistically significant differences ($p<0.05$). Graph represents one of three independent experiments.

3.2.5 Inhibition of signalling from the collagen receptor DDR1 disturbs the polarised distribution of MT1-MMP

The major collagen receptors expressed in epithelial cells are β1-integrin and DDR1[23]. Epithelial cells attaching to either gelatin or fibrillar collagen form integrin-dependent adhesions and integrins would thus be expected to transmit signals from either substrate. However, the data here indicates that fibrillar collagen, but not gelatin, allows epithelial cells to localise MT1-MMP to the basal surface upon HGF treatment. DDRs are specifically activated by fibrillar collagen I, but not heat-denatured collagen (gelatin)[45] and could thus be involved in the observed collagen I-specific change in MT1-MMP localisation. I therefore tested if inhibition of DDR1-mediated signalling would affect the spatial regulation of MT1-MMP. As a crude means to investigate this, I employed the chemical inhibitor, DDR1-IN-1, which is a selective inhibitor of DDR1 and DDR2 (IC_{50} of 105 nM and 413 nM respectively)[135]. First I confirmed the effect of DDR1-IN-1 on activation of DDR1 in our system. To do this, cells were seeded on plastic in the presence or absence of DDR1-IN-1 (1 μM) and serum-starved overnight. The next day, 100 μg/ml collagen I was added to the medium for 4 h, followed by immunoprecipitation of DDR1 from the cell lysates. The phosphorylation of DDR1 in response to collagen stimulation was analysed by Western blot using an anti-phosphotyrosine antibody. As shown in **Figure 18A** collagen I clearly induced phosphorylation of DDR1 in control cells, whereas treatment with DDR1-IN-1 strongly inhibited this phosphorylation. In addition, the low level of constitutive phosphorylation seen in non-stimulated control cells was also reduced by DDR1-IN-1 (**Figure 18A**).

I next examined the effect of DDR1-IN-1 on the apicobasal distribution of MT1-MMP in monolayers of MDCK cells. This experiment was conducted using the Ad-MT1F system as described in **3.2.4**. Interestingly, when DDR1 was inhibited in cells cultured on collagen I, MT1-MMP localised both at the apical and the basal cell surface of un-stimulated cells (**Figure 18B**). This is in contrast to the primarily apical localisation previously observed in inert epithelial cells (**Figure 17B**). Furthermore, HGF-treatment did not induce any additional change in the apicobasal distribution of MT1-MMP in the presence of DDR1-IN-1 (**Figure 18B**). Inhibition of DDR1 thus appears to disturb the polarised distribution of MT1-MMP. This effect of the inhibitor depends on the presence of collagen since no change in MT1F localisation was observed when cells were seeded on gelatin or plastic (**Figure 18B**). This data suggest that MT1-MMP secretory pathways in cells cultured on fibrillar collagen I in the presence of DDR1-IN-1 are different from secretory pathways in cells cultured on gelatin or plastic. A likely explanation for this is that other collagen-mediated signals are involved in controlling trafficking of MT1-MMP. A precise balance between such collagen-induced signals may thus determine the apicobasal MT1-MMP distribution in epithelial cells on collagen I.

The effect of DDR1-inhibition was corroborated in MDCK-MT1pH cells, which displayed a similar pattern: inhibition of DDR1 in cells on collagen I, but not gelatin or glass, caused increased levels of MT1-pHluorin-RFP at the basal cell surface regardless of HGF stimulation (**Figure 18C**). However, similar to the results in **Figure 17**, the base levels of MT1-pHluorin-RFP at the basal surface were higher than those observed for MT1F, and the size of the change induced by DDR1 inhibition was smaller (**Figure 18C**).

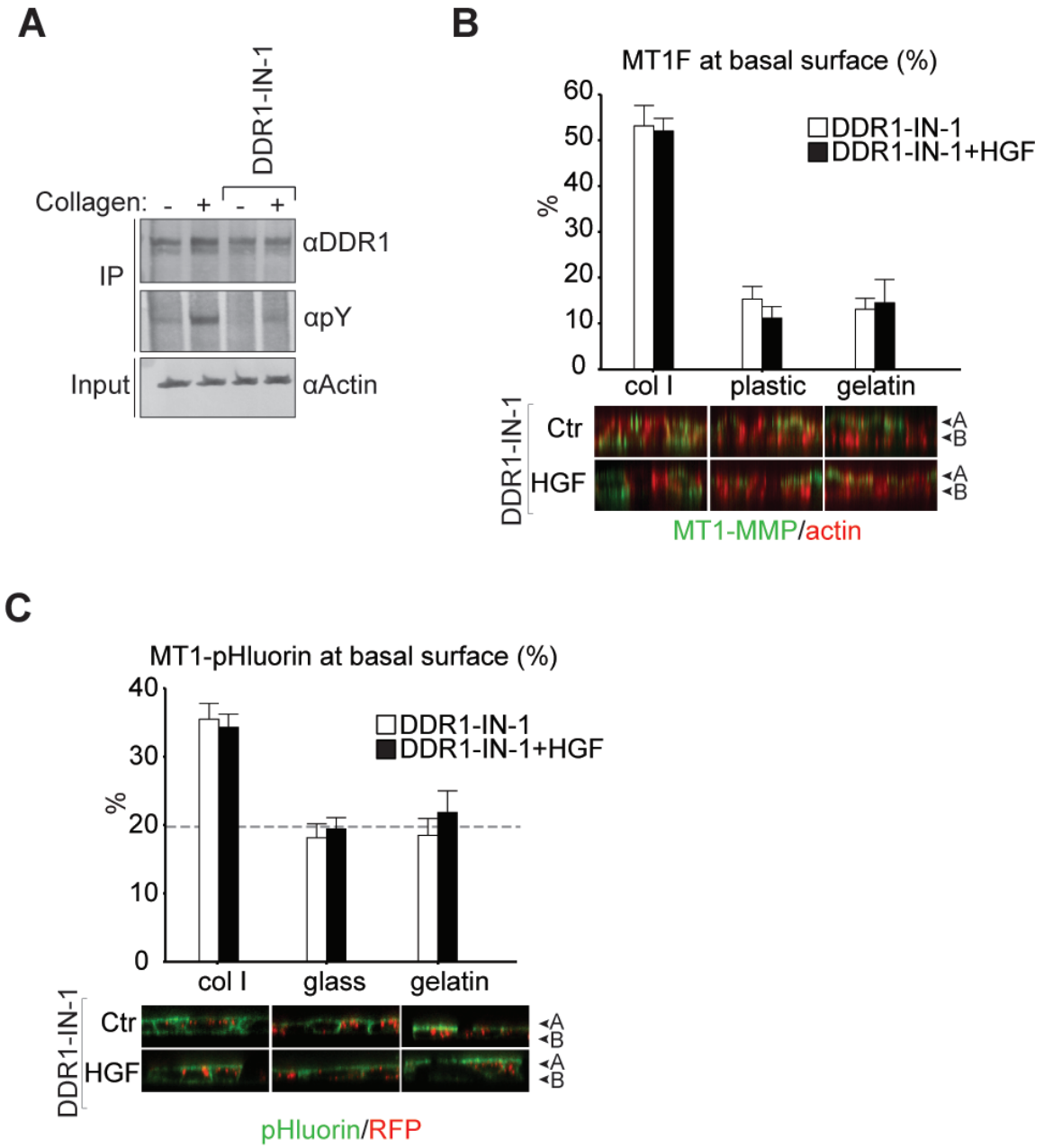


Figure 18. Inhibition of DDR1 disturbs the polarised distribution of MT1-MMP. **A)** MDCK cells were seeded on plastic in the presence of DMSO or DDR1-IN-1 and serum-starved overnight. The next day, cells were stimulated with collagen I (100 µg/ml) for 4 hours or left untreated. DDR1 was immunoprecipitated (IP'ed) from cell lysates using a DDR1 antibody against the cytoplasmic domain. Input and IP eluates were analysed by Western blot with primary antibodies against DDR1 and phosphotyrosine. **B)** MDCK cells were seeded in culture inserts coated with collagen I (1.5 mg/ml), gelatin (50 µg/ml) or left uncoated in the presence of DDR1-IN-1 (1 µM). Infection with Ad-MT1F, HGF treatment and further processing and analysis was done as described in **Figure 17**A-B. Graph depicts the percentage of total surface MT1F present at the basal surface. Error bars represent standard deviation. Representative XZ-sections for each condition are shown underneath the graph. Result from one out of two independent experiments shown. A: apical, B: basal. **C)** MDCK-MT1pH cells were seeded in IBIDI µ-slide wells coated with collagen I (1.5 mg/ml), gelatin (50 µg/ml) or left uncoated in the presence of 1 µM DDR1-IN-1. After 24 hours, HGF was added and culture continued further 24 hours before capturing line-scan images by live-cell imaging using a 60X objective on a CLSM and analysed as in **Figure 17C**. Ex_{488} nm and Ex_{568} nm are shown in green and red respectively in representative images from each condition. Graph depicts the percentage of total surface MT1-MMP present at the basal surface. Error bars represent standard deviation. Representative XZ-sections for each condition are shown underneath the graph. A: apical, B: basal.

3.2.6 Alteration of MT1-MMP distribution upon inhibition of DDR1 is functionally significant

Localisation of MT1-MMP at the basal cell surface is required for MDCK cells to degrade ECM. Indeed, our lab has previously established that an HGF-induced increase in basal localisation of MT1-MMP enhances degradation of collagen in 2D culture[93]. An increase in basal localisation of MT1-MMP upon DDR1 inhibition would therefore also be expected to mediate increased collagen degradation. To test this, I compared HGF-induced degradation of a collagen I film by MDCK cells in the presence or absence of DDR1 inhibitor. MDCK cells were seeded on a thin film of fibrillar collagen I at 100% confluence in the presence or absence of DDR1-IN-1 (1 μM). The next day, cells were infected with Ad-MT1F (MOI: 5) in the presence of GM6001 (5 μM). 24 hours after infection, GM6001 was washed out and cells incubated for a further 16 hours with or without HGF (50 ng/ml). Cells were then removed by extensive trypsination and the remaining collagen I was fixed with PFA and stained with Coomassie blue. Collagen degradation can be seen as white areas against dark collagen I. Non-infected MDCK cells were used as a negative control and no collagenolytic activity was detected in these cells after 16 hours incubation in neither the absence nor the presence of HGF (**Figure 19**). This is most likely due to insufficient incubation time for endogenous MT1-MMP to cleave collagen. Control cells transduced with Ad-MT1F degraded small areas of collagen in the absence of HGF stimulation, whereas HGF markedly enhanced degradation (**Figure 19**). This confirms that the HGF-induced increase in basal localisation of MT1-MMP increases collagen film degradation. In accordance with this, DDR1-IN-1 caused high levels of degradation both in the absence and presence of HGF (**Figure 19**). This finding suggests that the role of DDR1 signalling in regulating the polarised distribution of MT1-MMP has functional consequences for its matrix degrading activity of the cells.

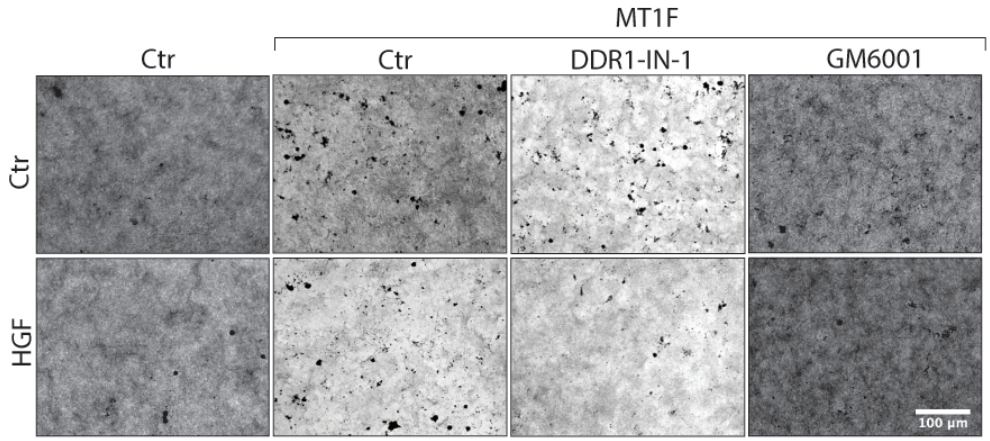


Figure 19. Increased localisation of MT1-MMP to the basal surface in the absence of DDR1 signalling is functionally significant. MDCK cells were seeded in Corning CellBIND culture plates coated with 200 µl of collagen I (1:1 ratio of protease-extracted PureCol and acid-extracted CellMatrix collagen I) in the presence of either DMSO or DDR1-IN-1 (1 µM). Once 100% confluent, cells were infected with Ad-MT1F at a MOI of 5 in the presence of GM6001 (10 µM) in serum-free medium. After 24 hours culture, GM6001 was washed out and cells incubated for a further 16 hours in the presence or absence of HGF (50 ng/ml) with DMSO or DDR1-IN-1. Cells were removed by >24 hours trypsination followed by fixation of remaining collagen and staining of the collagen with Coomassie blue. Digested areas were visualised with a 20X objective on a widefield microscope. Images were processed in Photoshop (Adobe) by applying the same white balance filter to all images. Representative images from one of >3 independent experiments are shown.

3.2.7 DDR1 is required for HGF-induced, MMP-dependent tubulogenesis of MDCK cells

Given that fine spatiotemporal regulation of MT1-MMP is required for proper epithelial tubulogenesis[93], the spatial disorganisation of MT1-MMP activity seen in the absence of DDR1 signalling in 2D culture could likely affect morphogenesis in 3D culture. I therefore tested whether the presence of DDR1-IN-1 would affect the HGF-induced tubulogenesis of MDCK cells in 3D collagen gels. Cells were embedded in collagen I and cultured in the presence of HGF as described in Section **3.2.1**. After 5 days, control cells formed branching tubular structures (**Figure 20A**). In contrast, inhibition of DDR1 resulted in formation of compact, multicellular aggregates rather than tubular structures (**Figure 20A**).

To confirm that this effect of DDR1-IN-1 on tubulogenesis is due to inhibition of DDR1, I examined the effect of knocking down DDR1 by shRNA. MDCK cells stably expressing shRNA against DDR1 (MDCK-DDR1-shRNA) have previously been

established in our lab. First, I confirmed that expression of DDR1 was decreased in a clonal line of MDCK-DDR1-shRNA cells (**Figure 20B**, left).). Next I compared tubulogenesis by cells expressing non-targeting (NT) shRNA (MDCK-NT-shRNA) and MDCK-DDR1-shRNA cells. MDCK-NT-shRNA formed branching tubular structures in response to HGF treatment, while knockdown of DDR1 caused formation of aggregates similar to those observed with DDR1-IN-1 treatment (**Figure 20B**, right). I further validated this in MDCK cells stably expressing a dominant negative DDR1 mutant (DDR1ΔC), which lacks the cytoplasmic domain and therefore cannot signal. MDCK cells expressing DDR1ΔC (MDCK-DDR1ΔC) and empty vector (MDCK-Mock) (**Figure 20C**, left) were stimulated with HGF to undergo tubulogenesis in 3D collagen I gels. Similar to what was seen for DDR1-IN-1 treatment or knockdown of DDR1, the expression of DDRΔC caused MDCK cells to form compact cellular aggregates (**Figure 20C**, right). This data indicate that DDR1 is required for epithelial cells to undergo tubulogenesis in 3D collagen I. This is in agreement with a previous study reporting that expression of dominant negative DDR1 in MDCK cells impedes HGF-induced tubulogenesis[32]. In contrast to knockdown of DDR1, DDR1-IN-1 treatment blocks only the signalling activity of DDR1, and the phenotype of DDR1-IN-1 treatment thus suggests that the kinase activity of DDR1 is important for tubulogenesis.

Stable overexpression of DDR1 (MDCK-DDR1 cells) resulted in cells dying within the collagen I matrix with few cells surviving and forming tubular structures under these experimental conditions (not shown). Aggregate formation was not observed in DDR1 overexpressing cells (not shown).

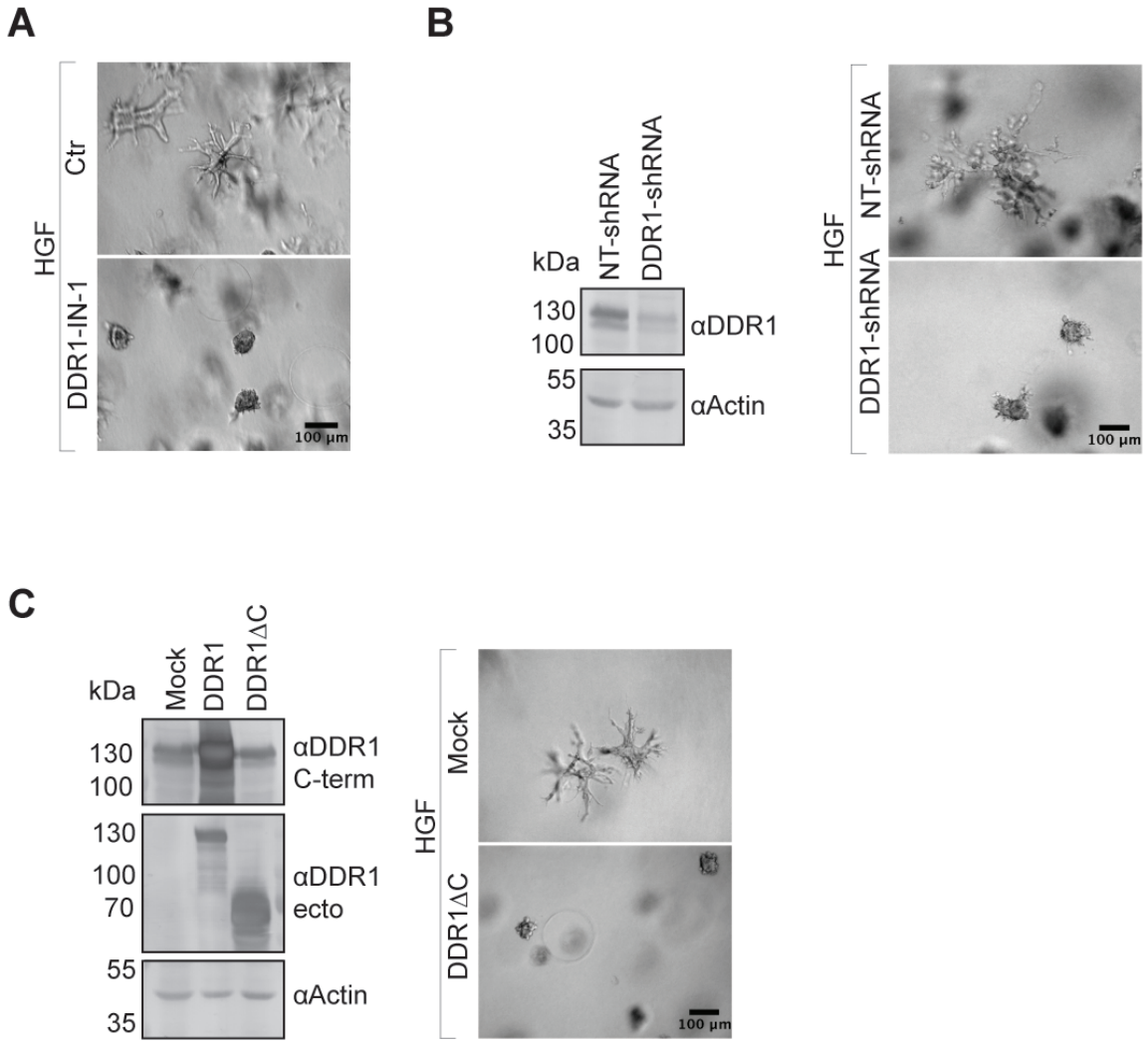


Figure 20. DDR1 is required for tubulogenesis in 3D collagen I. A) MDCK cells in the presence of DMSO or DDR1-IN-1 (1 µM) were cultured in 3D collagen I gels (2 mg/ml) in DMEM with 10% FCS in the presence of HGF (50 ng/ml). Cells were cultured 5 days before imaging using a 10X objective on a widefield microscope. Representative images are shown from one of at least three independent experiments. **B)** Left: clonal lines of MDCK cells stably expressing NT-shRNA (MDCK-NT-shRNA) or DDR1 shRNA (MDCK-DDR1-shRNA) were seeded on plastic. After 24 h, lysates were recovered and subjected to Western blot analysis using an antibody against the cytoplasmic domain of DDR1 with an AP-linked secondary antibody. Right: MDCK-NT-shRNA cells and MDCK-DDR1-shRNA cells were subjected to tubulogenesis assay as described in A) **C)** Left: Lysates from MDCK-Mock, MDCK-DDR1 and MDCK-DDR1ΔC cells were analysed by Western blot using primary antibodies against the cytoplasmic domain of DDR1 (recognises endogenous and overexpressed DDR1, but not DDR1ΔC due to the lack of cytoplasmic domain), the ectodomain of DDR1 (only recognises exogenously expressed DDR1) and actin. Secondary antibodies were AP-linked. Note that size of DDR1ΔC is smaller due to the lack of the cytoplasmic domain. Right: MDCK-Mock and MDCK-DDR1ΔC cells were subjected to tubulogenesis assays as described in A)**.**

3.2.8 DDR1 signalling is required for tubulogenesis of MDCK and MCF-10A cells in a modified tubulogenesis assay on microcarrier beads

To further explore the role of DDR1 in tubulogenesis, I set up an alternative tubulogenesis assay, based on a fibroblast invasion assay described by Palmisano and Itoh[132]. This involved culturing MDCK cells to confluence on gelatin-coated microcarrier beads before suspending the cell-coated beads in a 3D collagen gel (setup depicted in **Figure 21A**). This method benefits from a more homogenous starting point due to the relatively consistent size of the beads (~175 μm in diameter) causing tubular extensions to originate from a similar number of cells. Furthermore, the cells are allowed to establish polarity in a confluent monolayer on the beads before being exposed to the 3D collagen environment. Under these conditions, DDR1 overexpressing cells survive equally well as MDCK-Mock and MDCK-DDR1ΔC cells, and their capacity to undergo tubular morphogenesis can thus be examined.

Beads with confluent MDCK cells were embedded in 3D collagen I (2 mg/ml) in the presence or absence of HGF. 72 hours later, HGF-treated control cells had undergone clear changes compared to non-stimulated cells: in addition to the monolayer in contact with the gelatin-coated bead a second layer of cells formed (**Figure 21B**). The two cell layers were in many places separated by a narrow lumen (**Figure 21B**, arrow), and large, tubular structures protruded from the outer layer (**Figure 21B**, arrowheads). Interestingly, HGF-treated MDCK-DDR1 cells did not form tubular structures, but instead formed large, hollow structures around the bead (**Figure 21B**). These structures consisted of a cell layer on the bead and an additional outer layer similar to control structures; however, the lumen separating these two layers was much larger for MDCK-DDR1 cells (**Figure 21B**, arrow). The outer layer appeared smoother with fewer and shorter protrusions compared to MDCK-Mock cells. This suggests that DDR1 overexpression causes cells along the

entire periphery of the structure to invade into the surrounding matrix, rather than invasive activity being restricted to distinct leader cells at the tip of protruding tubes. DDR1 signalling may thus have a promoting role in collective invasion. In contrast, cells expressing DDR1ΔC performed very limited tubulogenesis regardless of HGF treatment (**Figure 21B**). DDR1-IN-1 treatment inhibited tubulogenesis of both MDCK-Mock and -DDR1 cells resulting in a phenotype similar to MDCK-DDR1ΔC structures (**Figure 21B,** bottom panel). This underlines the importance of the kinase activity of DDR1 in tubulogenesis. Quantification of the results in **Figure 21B** confirms a significant decrease in length of tubular structures upon overexpression of DDR1 or DDR1ΔC (**Figure 21C**, left), whilst DDR1 overexpression causes a significant increase in the size of the structures (**Figure 21B**, right), supporting a potential role for DDR1 in collective invasion.

Similar effects of DDR1 inhibition on tubulogenesis were observed for the MCF-10A cell line of human mammary epithelial cells (**Figure 21D**). The requirement for DDR1 kinase activity in tubular morphogenesis may thus be a general feature for epithelial cell lines.

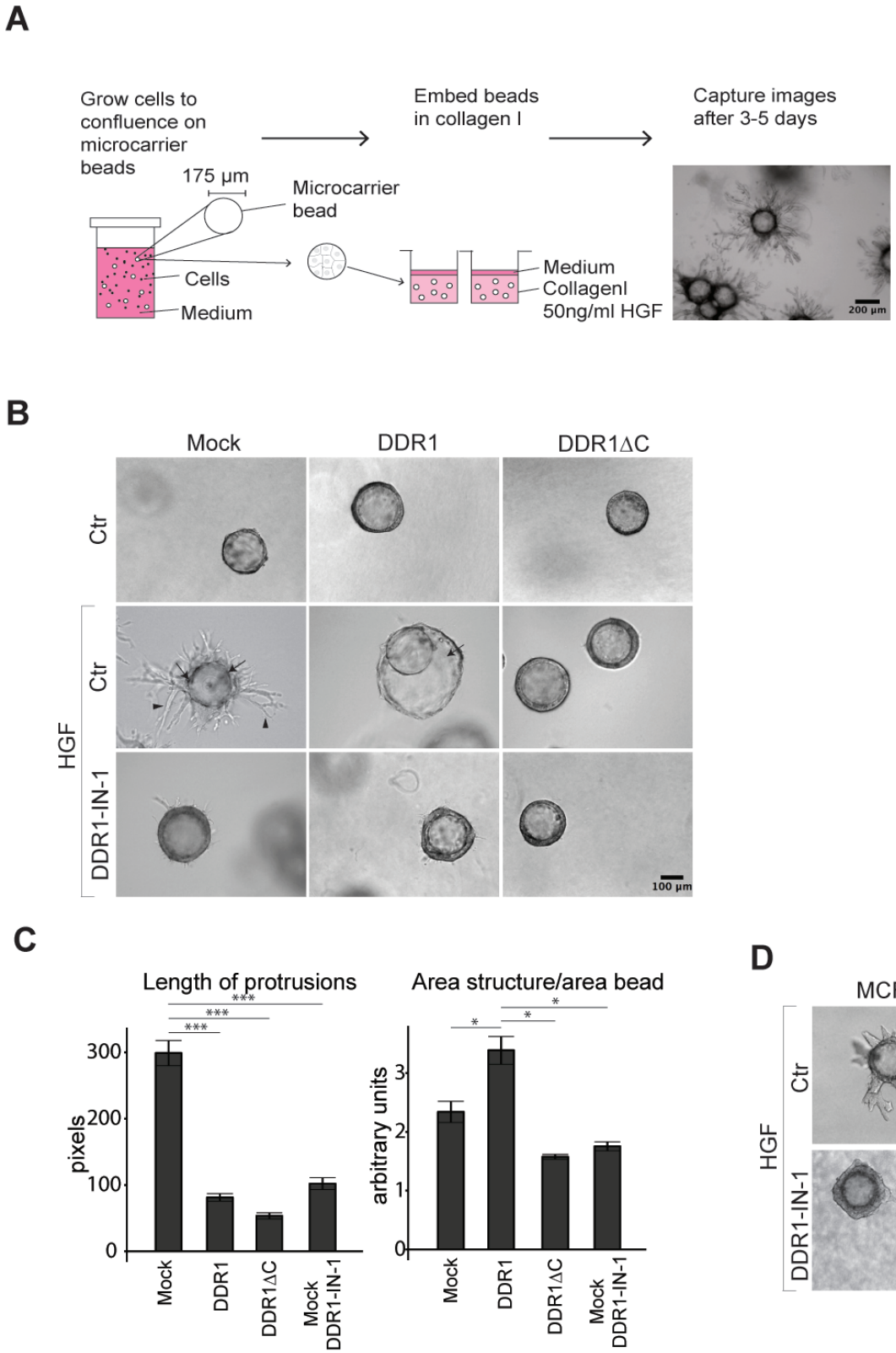

A
Grow cells to confluence on microcarrier beads
175 µm
Microcarrier bead
Cells
Medium
Embed beads in collagen I
Medium
CollagenI
50ng/ml HGF
Capture images after 3-5 days
200 µm
B
Mock
DDR1
DDR1ΔC
Ctr
HGF
Ctr
DDR1-IN-1
100 µm
C
Length of protrusions
pixels
300
200
100
0
***
***
***
Mock
DDR1
DDR1ΔC
Mock DDR1-IN-1
Area structure/area bead
arbitrary units
3
2
1
0
*
*
*
Mock
DDR1
DDR1ΔC
Mock DDR1-IN-1
D
MCF10A
HGF
Ctr
DDR1-IN-1
100 µm

Figure 21. **DDR1 is required for tubulogenesis on microcarrier beads and may positively affect collective invasion. A)** Setup for tubulogenesis assay on microcarrier beads: Cells were cultured to confluence on gelatin-coated microcarrier beads by suspending cells and beads in DMEM with 10% FCS with gentle agitation. Beads were then embedded in 2 mg/ml collagen gels containing 50 ng/ml HGF with or without DDR1-IN-1 (1 μM). Gels were overlayed with complete growth medium in the presence or absence of HGF and DDR1-IN-1. Images were captured using a 10X objective lens on a widefield microscope after 3-5 days. **B)** MDCK-Mock (Mock), MDCK-DDR1 (DDR1), MDCK-DDR1ΔC (DDR1ΔC) and DDR1-IN-1-treated MDCK-Mock (DDR1-IN-1) cells were cultured and analysed as described in A) for 72 hours with or without HGF (50 ng/ml) and DDR1-IN-1 (1 μM) as indicated. Representative images are shown. Arrows point to the narrow lumen formed between the cells in contact with the bead and the additional outer layer of cells. Arrowheads point to tubular structures. Representative images from one of >3 independent experiments shown. **C)** Quantification of experiment shown in B). Left: the lengths of the 10 longest protrusions of 5 different structures per condition were measured using ImageJ software. Each measurement was plotted as a point. Error bars represent standard error of the mean. Kruskal test revealed a significant difference on the distribution of the groups ($p<2.2*10-16$), and differences were localised with a pairwise Wilcoxon test with Holm correction for multiple testing (*** represents p-values <0.001). Right: the areas of 5-7 structures per condition were measured using ImageJ software. To correct for differences in bead size and thereby different number of cells at the starting point, the area of the each structure was normalised to the area of the bead. The average value of this ratio is plotted as a bar graph and error bars represent standard error of the mean. Kruskal test revealed a significant difference on the distribution of the groups ($p=0.0004$), and differences were localised with a pairwise Wilcoxon test with Holm correction for multiple testing (* represents p-value <0.05). **D)** MCF-10A cells were cultured as described in A) for 7 days in the presence of HGF with or without DDR1-IN-1 (1 μm) as indicated. Representative images are shown.

3.2.9 DDR1 inhibition disturbs the distribution of apicobasal markers and lumen formation during MMP-dependent epithelial tubulogenesis

Aggregates forming upon inhibition of DDR1 appeared to contain a large number of cells, suggesting that impaired tubulogenesis is not caused by failure of the cells to grow or survive in 3D collagen I. It rather appeared that proper epithelial organisation was disrupted by DDR1 inhibition. To investigate whether aggregates forming upon DDR1 inhibition displayed correct epithelial polarity, I examined the distribution of apical and basal markers during HGF-induced tubulogenesis. A gold standard marker of the apical surface is the transmembrane glycoprotein GP135 (podocalyxin), which is involved in the earliest steps of establishing apical membrane identity with continuous localisation to the apical domain in polarised, epithelial cells[136]. Control cells formed tubular structures consisting of a monolayer of cells surrounding a central lumen. The surface of cells facing the central lumen is the apical side, whereas the side facing the ECM is basal. The apical surface of control cells was positive for GP135 staining (**Figure 22A**, top left, arrow), suggesting that apicobasal polarity is oriented correctly in these structures. In contrast,

cell aggregates formed in the presence of DDR1-IN-1 failed to establish a central lumen and displayed a disorganised distribution of GP135, which in many places localised to the interface between the cell and the ECM (**Figure 22A**, bottom left, arrowheads). In addition, acetylated tubulin was stained to visualise primary cilia. Primary cilia are structures associated with the apical membrane of confluent, fully differentiated MDCK cells and defect ciliogenesis is associated with aberrant 3D morphogenesis[137,138]. In control cells primary cilia extended towards the lumen (**Figure 22A**, middle panel, arrow), whereas DDR1 inhibition caused a diffuse staining pattern of acetylated tubulin and a lack of primary cilia (**Figure 22A**). Interestingly, decreased formation of primary cilia has previously been observed in chondrocytes from DDR1-null mice[139]. Staining for laminin as a marker of the basement membrane revealed a diffuse distribution in DDR1-IN-1-treated cells compared to the basal localisation in structures formed by control cells (**Figure 22A**, right). Similar phenotypes were observed when DDR1 function was inhibited by knockdown (**Figure 22B**) or overexpression of DDR1ΔC (**Figure 22C**). This suggests that DDR1 is important for epithelial cells to correctly orient apicobasal polarity according to their surroundings during epithelial tubulogenesis.

This effect of DDR1 inhibition on establishment of apicobasal polarity was confirmed in MDCK cells cultured on microcarrier beads. Structures formed on microbeads by MDCK-Mock cells in the presence of HGF displayed GP135 towards the lumen of structures (**Figure 22D**). Multiple GP135-positive lumens can be seen in some of the protruding tubules, suggesting that tubes do not "bud out" from the established lumen whilst continuously maintaining the lumen. Rather, tubulogenesis appears to follow a previously proposed model for tubulogenesis by MDCK cells[39] in which chains of cells extend into the matrix and divide to form cords. Cells in these cords then establish new, small lumens between them, which eventually merge into a continuous lumen. The

large hollow structures formed around the beads by DDR1-overexpressing cells displayed correct polarity with GP135 localising at the apical cell surface towards the lumen, both in the cell layer on the bead and in the outer, invading layer (**Figure 22D**, arrows). Interestingly, examination of the structures formed by MDCK-DDR1ΔC cells revealed a multilayered phenotype: while two monolayers of cells separated by a lumen were seen for MDCK-Mock and MDCK-DDR1 cells, MDCK-DDR1ΔC cells grew in multiple layers on top of each other without a clearly defined apical or basal side (**Figure 22D**). In addition, several microlumens were formed (**Figure 22D**, arrowheads). This multilayered phenotype was observed for MDCK-DDR1ΔC cells both in the presence and absence of HGF, suggesting that the function of DDR1 in establishing polarity is not restricted to HGF-induced morphogenesis. Examination of structures formed by MCF-10A cells on microcarrier beads revealed a similar multi-layered phenotype upon DDR1 inhibition (**Figure 22E**).

These findings suggest that signalling from DDR1 is required for epithelial cells to establish apicobasal polarity in a 3D collagen matrix, and that this DDR1-mediated polarity is essential during HGF-induced tubulogenesis.

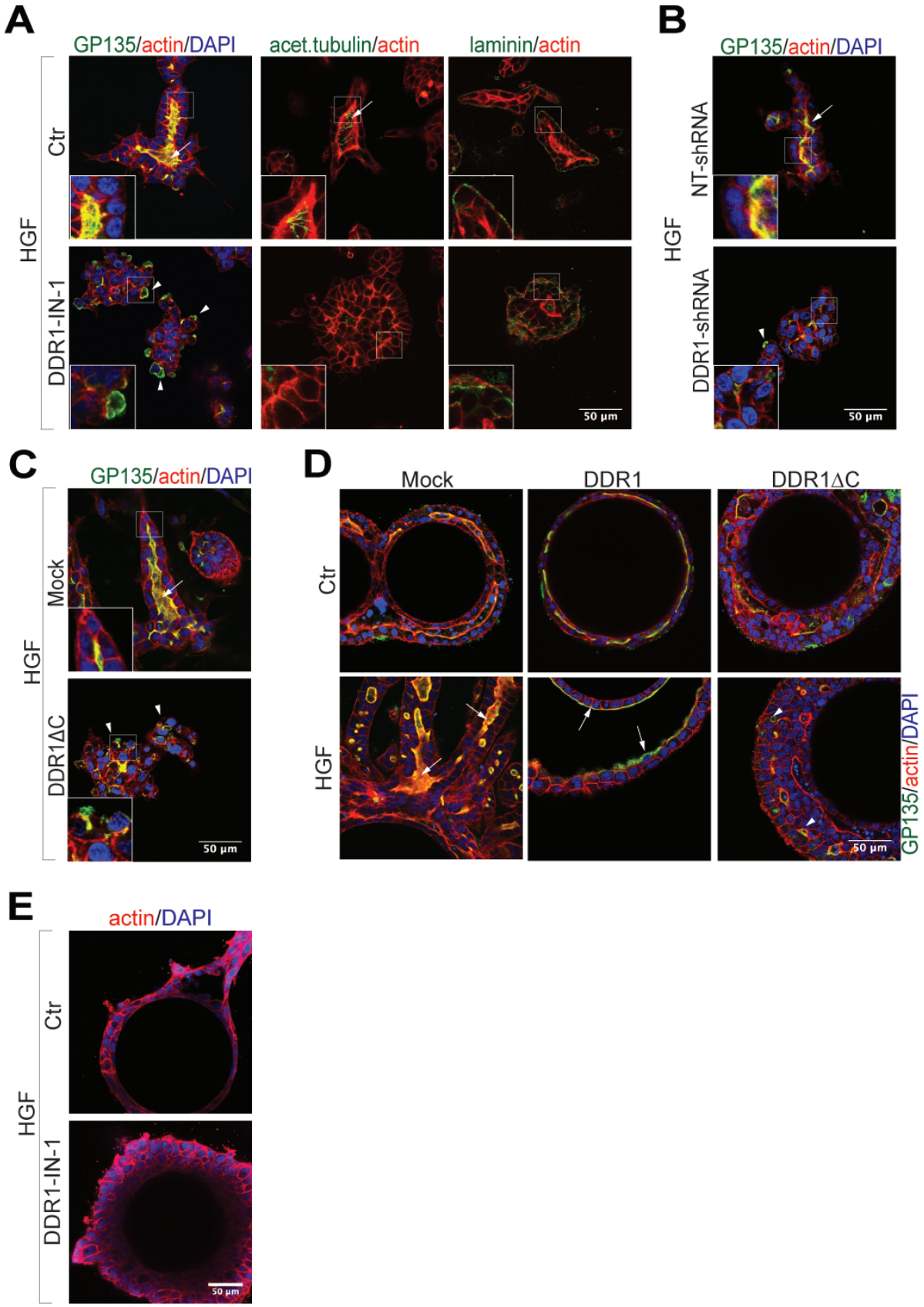

A
GP135/actin/DAPI
acet.tubulin/actin
laminin/actin
HGF
Ctr
DDR1-IN-1
50 µm
B
GP135/actin/DAPI
NT-shRNA
HGF
DDR1-shRNA
50 µm
C
GP135/actin/DAPI
HGF
Mock
DDR1ΔC
50 µm
D
Mock
DDR1
DDR1ΔC
Ctr
HGF
50 µm
GP135/actin/DAPI
E
actin/DAPI
HGF
Ctr
DDR1-IN-1
50 µm

Figure 22. DDR1 inhibition leads to disorganised apicobasal polarity during HGF-induced tubular morphogenesis. A) MDCK cells were grown in thin 3D collagen I (2 mg/ml) gels in culture inserts in the presence of 50 ng/ml HGF and DMSO or 1 μM DDR1-IN-1 for 72 hours. Gels were fixed and stained against GP135/acetylated tubulin/laminin (green), f-actin (red) and DAPI (blue) and analysed by a 60X objective on a CSLM. Arrow points to luminal GP135 staining whereas arrowheads point to basal staining of GP135 when DDR1 is inhibited. Representative images shown from one of >3 independent experiments. **B)** MDCK-NT-shRNA and MDCK-DDR1-shRNA cells were cultured and processed as described in A). Arrow points to luminal GP135 staining whereas arrowheads point to basal staining of GP135 when DDR1 is inhibited. **C)** MDCK-Mock and MDCK-DDR1ΔC were cultured and processed as described in A). Arrow points to luminal GP135 staining whereas arrowheads point to basal staining of GP135. **D)** MDCK-Mock, MDCK-DDR1 and MDCK-DDR1ΔC cells were cultured on microcarrier beads as described in **Figure 21A** in the presence or absence of HGF (50 ng/ml). Gels were fixed and stained against GP135 (green), actin (red) and DAPI (blue) and analysed by a 60X objective on a CSLM. Arrows point to luminal GP135 staining whereas arrowheads point to basal staining of GP135 when DDR1 is inhibited. **E**) MCF-10A cells were cultured as described in A) in the presence of DMSO or 1 μM DDR1-IN-1 for 7 days. Gels were fixed and stained against f-actin (red) and DAPI (blue) and analysed by a 60X objective on a CSLM. Representative images are shown from one of two independent experiments.

3.2.10 DDR1 is required for lumen formation and polarisation during HGF-independent formation of cysts by MDCK and CaCO-2 cells

Since establishment of apicobasal polarity is a prerequisite for 3D morphogenesis, I hypothesised that DDR1 also is required for 3D morphogenesis not depending on HGF stimulation. To examine this, MDCK cells were cultured in 3D collagen I (2 mg/ml) for 7 days to allow the cells to form hollow cysts (**Figure 23A**, arrows point to lumens). Control cells formed cysts consisting of a single monolayer of cells with well-organised polarity. GP135 thus localised to the apical/luminal surface of cysts, whereas laminin lined the basal cell surface (**Figure 23A**, left). In contrast, cells treated with DDR1-IN-1 formed cellular aggregates without a central lumen and with disorganised staining patterns of GP135 and laminin (**Figure 23A**, left), suggesting that apicobasal polarity is not established. In addition to laminin and GP135, I examined the localisation of the Golgi apparatus, which in polarised epithelial cells localises apical to the nucleus in a manner depending on polarised organisation of the microtubule network[140]. In control cells, the cis-Golgi resident protein GM130 localised in the apical part of the cytoplasm towards the cyst lumen as expected (**Figure 23A,** right, top, arrow). In the presence of DDR1-IN-1, where an apical membrane domain is not defined, this organised localisation of GM130 was not observed (**Figure 23A**, right, bottom). This suggests that disorganised

apicobasal polarity in the absence of DDR1 signalling is accompanied by aberrant arrangement of intracellular organelles. Similarly, the formation of primary cilia was lost when DDR1 signalling was inhibited. Acetylated tubulin thus displayed a diffuse distribution in DDR1-IN-1-treated cells compared to control cells, which extend primary cilia towards the lumen of cysts (**Figure 23A**, right). The requirement for DDR1 in correct organisation of apicobasal markers was confirmed in MDCK-DDR1ΔC cells, which similarly formed structures with lack of a central lumen, aberrant GP135 localisation and loss of primary cilia (**Figure 23B**).

To ensure that the effect of DDR1 inhibition on epithelial cystogenesis holds true in other epithelial cell lines, CaCO-2 cells were also analysed. CaCO-2 cells are well-differentiated human colorectal carcinoma cells, which can form polarised cysts when embedded in a 3D Matrigel matrix. Matrigel contains 30% type IV collagen, which is a ligand for DDR1[48]. CaCO-2 cells were cultured in 2% Matrigel in the presence or absence of DDR1-IN-1 (1 μM). After 9 days, cells were fixed and processed for imaging. Control cells formed cysts with lumens clearly detectable under brightfield microscopy (**Figure 23C**, upper panel, arrows point to lumen). Staining for actin and the tight junction marker ZO1, confirmed that cysts are composed of a monolayer of cells surrounding a central lumen, with tight junctions forming apically, towards the lumen. Formation of polarised cysts in Matrigel was not dependent on MMP activity as seen by GM6001 treatment having no effect (**Figure 23C**). In contrast, inhibition of DDR1 caused formation of cellular aggregates with no central lumen. Furthermore, tight junctions formed at the interface between the cells and the ECM, indicating that the organisation of apicobasal polarity is disrupted (**Figure 23C**, arrowhead). In line with this, the Golgi marker GM130 was diffusely distributed in DDR1-IN-1-treated cell aggregates, compared to its localisation in the apical part of the cytoplasm in cysts formed by control cells (**Figure**

23C). DDR1-dependent signalling thus appears to be critical for establishment of epithelial polarity in both HGF-induced, MMP-dependent tubulogenesis and in 3D morphogenesis, which is independent of both HGF stimulation and MMP activity.

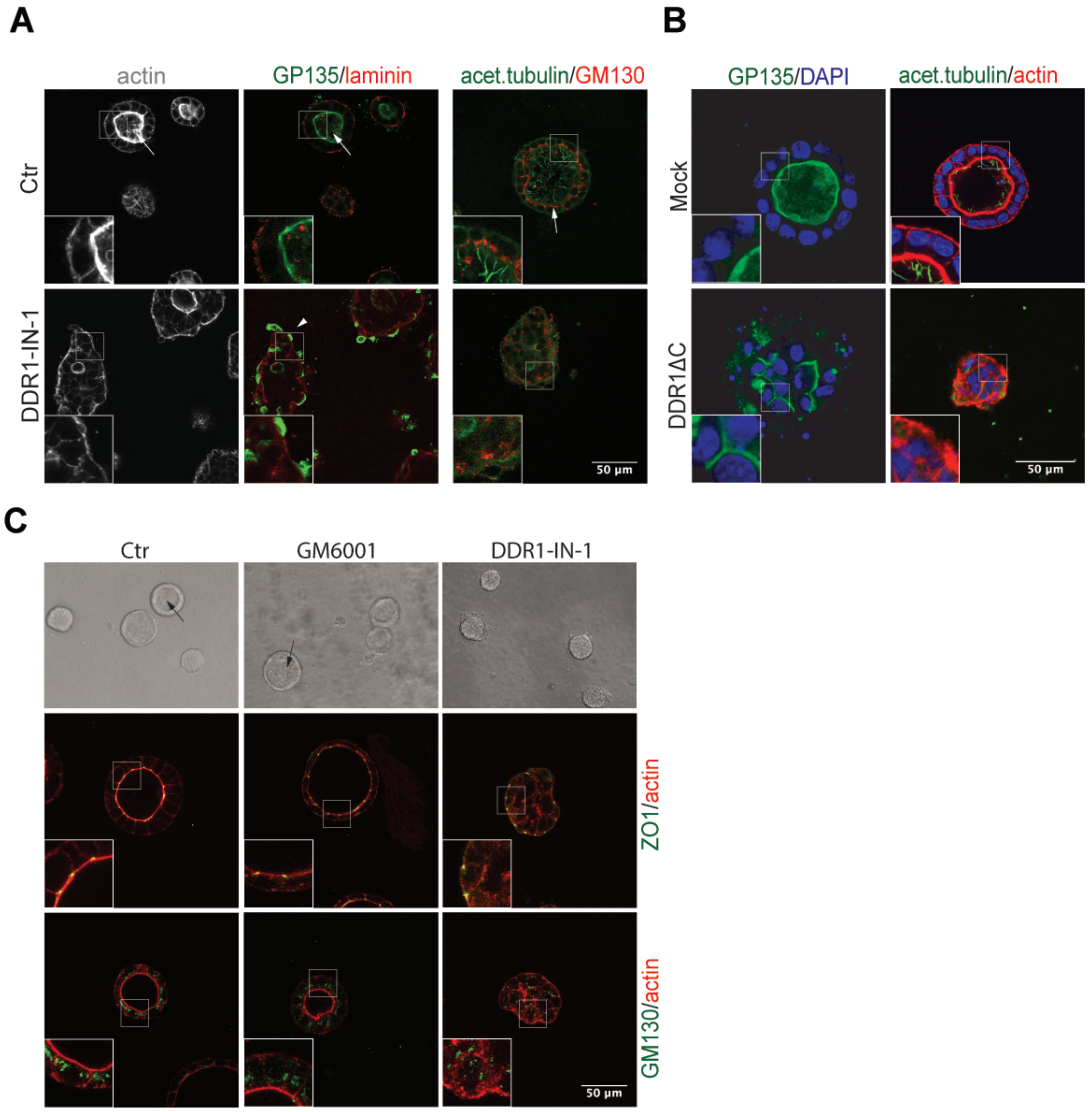


Figure 23. DDR1 is required for lumen formation and polarisation in MMP-independent morphogenesis. A) MDCK cells were grown in thin 3D collagen I (2 mg/ml) gels in transwell culture inserts in the presence of DMSO or 1 µM DDR1-IN-1 in DMEM with 10% FCS for 7 days. Gels were fixed and stained and images were captured using a 60X objective on a CSLM. Left: Gels were stained for F-actin (gray), GP135 (green) and laminin (red). Arrows point to the lumen of cysts, whereas arrowheads point to basal staining of GP135 in the presence of DDR1-IN-1. Right: Gels were stained for acetylated tubulin (green) and GM130 (red). Fluorescent images were captured using a 60X objective on a CSLM and processed using ImageJ. Representative images from one of >3 independent experiments are shown. **B**) MDCK-Mock and MDCK-DDR1ΔC were cultured and processed as described in A). Left: Gels were stained for GP135 (green) and nuclei (blue). Right: Gels were stained for acetylated tubulin (green), f-actin (red) and nuclei (blue). **C**) CaCO-2 cells were seeded on glass coated with 100% matrigel and overlayed by DMEM with 20% FCS and 2% matrigel. Cells were cultured 9 days before fixation and staining. Brightfield images were captured using a widefield microscope. Fluorescent images were captured using a 60X objective on a CSLM and processed using ImageJ. Representative images from one of two independent experiments are shown.

3.3 Discussion

In this chapter, I have confirmed previous work describing that epithelial cells during tubulogenesis can create a gradient of ECM-degrading activity towards the tip of protruding tubules through local changes in the apicobasal distribution of MT1-MMP[93]. This is an efficient way for cells to restrict ECM degradation by MT1-MMP to the right time and place. It is still unclear what specifies a cell to become a tip cell, that localises MT1-MMP to the basal domain and leads invasion into the surrounding matrix, but local endogenous non-canonical TGFβ signalling has been suggested to play a role[93]. Recent studies have also suggested that the choice of leader cell is affected by collective organisation of the cytoskeleton between multiple cells, which creates local differences in tension that are favourable or unfavourable for development into a leader cell[141]. It would be interesting to study if such differences correlate with local TGFβ signalling and MT1-MMP localisation. Other factors likely to contribute to the choice of leader cells include subtle differences in the microarchitecture of the surrounding ECM, which may favour or discourage invasion. This would be a plausible scenario during wound healing, where damaged ECM could stimulate cells to invade into that area for the repair process to happen. Such stimulation may be mediated by ECM receptors being activated by cryptic epitopes revealed during physical or proteolytic damage of ECM components. In favour of the ECM playing an important role, I found that HGF-induced changes to the apicobasal distribution of MT1-MMP required cells to be in contact with collagen I, rather than gelatin or plastic/glass. Specifically, I found that the collagen-binding receptor tyrosine kinase DDR1 contributes to controlling the polarised distribution of MT1-MMP in 2D culture systems. Importantly, DDR1 inhibition disturbed the polarised distribution of MT1-MMP in the absence of HGF stimulation, whereas no change was seen in its presence (**Figure 17B** and **Figure 18B**). This suggests that DDR1 plays a role in

controlling the polarised distribution of MT1-MMP in inert epithelial cells. It is not clear how DDR1 mediates this effect, but several explanations can be proposed:

1) DDR1 signalling is required for establishment of polarity, and is thus a prerequisite for the polarised distribution of MT1-MMP
2) DDR1 affects targeting of MT1-MMP to specific membrane domains
3) DDR1 affects the half-life of MT1-MMP at the apical or basal membrane
4) A balance between signalling from DDR1 and other collagen receptors regulate MT1-MMP localisation

Below, I will discuss these 4 scenarios:

1) DDR1 signalling is required for establishment of polarity, and is thus a prerequisite for the polarised distribution of MT1-MMP

Inhibition of DDR1 led to complete disorganisation of apicobasal polarity in 3D culture (**Figure 22** and **Figure 23**). Since MT1-MMP distribution is regulated according to apicobasal polarity[93], a similar loss of polarity in 2D culture would be expected to cause a non-polarised distribution of MT1-MMP. However, we will in the next chapter see that in contrast to the 3D culture setup, traditional markers of polarity are not affected by DDR1 inhibition in 2D culture. The non-polarised distribution of MT1-MMP upon inhibition of DDR1 in 2D culture is thus not likely to be caused by a complete loss of polarity.

2) DDR1 affects targeting of MT1-MMP to specific membrane domains

The polarised secretion of proteins in epithelial cells depends on vesicle transport. Although DDR1 signalling has not previously been suggested to affect intracellular trafficking of any proteins, the switch in MT1-MMP distribution upon DDR1 inhibition could be a result of influence on the targeting of MT1-MMP to the apical or basal surface. Previously our group reported that targeting MT1-MMP to the basal side of MDCK cells

and focal adhesions in fibroblasts depends on an 8 amino acid region in the catalytic domain (loop region)[93,96]. This loop region was hypothesised to interact with an adaptor molecule, which could link MT1-MMP to kinesins and thus affect the sorting of MT1-MMP into specific vesicles. Given the membrane localisation of DDR1, DDR1 is not an obvious candidate to affect sorting of MT1-MMP into vesicles. Rather, DDR1 signalling could be thought to participate in the formation of protein complexes that help specify receipt or rejection of distinct vesicles. An example of a membrane protein with this function is E-cadherin, which together with nectin recruits the Sec6/8 complex to epithelial junctions, where they aid specific docking of vesicles and thus ensure basal delivery of proteins such as the LDL-receptor[142]. The importance of membrane proteins in determining localisation of such docking complexes was demonstrated by expression of E-cadherin and nectin in fibroblasts leading to recruitment of Sec6/8 to cell-cell junctions in this cell type[143]. It may be that DDR1 is involved in localising such docking complexes, however, no research has addressed this so far.

3) DDR1 affects the half-life of MT1-MMP at the apical or basal membrane

Rather than affecting the targeting of MT1-MMP-containing vesicles to specific membrane domains, DDR1 could also affect the half-life of MT1-MMP at the apical or basal membrane by influencing the rate of its endocytosis.

I found inhibition of DDR1 to increase the percentage of surface MT1-MMP at the basal surface (**Figure 18B**), which would suggest that endocytosis is either decreased at the basal surface or increased at the apical surface. DDR1 has previously been reported to influence endocytosis of the insulin growth factor I receptor, however, the mechanism was not identified[144].

There was no additive effect of DDR1-IN-1 and HGF, since the distribution of MT1-MMP was unchanged by HGF stimulation of DDR1-IN-1-treated cells (**Figure**

18B). This could suggest, that DDR1 and HGF converge on the same aspect of regulating MT1-MMP localisation. Our group have previously shown that the HGF-induced increase in MT1-MMP at the basal surface is unlikely to involve changes in the rate of endocytosis. This was based on the observation that the cytoplasmic domain of MT1-MMP, which is required for clathrin-mediated endocytosis[127], was dispensable for the HGF-induced recruitment of MT1-MMP to the basal cell surface[93]. HGF is thus more likely to affect targeting of MT1-MMP. This means that if DDR1 inhibition affected the rate of MT1-MMP endocytosis, addition of HGF would still be expected to alter targeting of MT1-MMP and thus result in a net change in the distribution of MT1-MMP. Given that this was not the case (**Figure 18B**), DDR1 signalling is not likely to affect endocytosis of MT1-MMP. This should however be clarified by determining whether DDR1 inhibition induces changes in the localisation of a cytoplasmic domain deletion mutant of MT1-MMP.

4) A balance between signalling from DDR1 and other collagen receptors regulate MT1-MMP localisation.

It is possible that the distribution of MT1-MMP is controlled by signals from several collagen receptors, and that the inhibition of DDR1 is causing an imbalance between such signals which disturbs the polarised distribution of MT1-MMP. Indeed, I found that DDR1-IN-1 treatment changed MT1-MMP distribution in cells seeded on fibrillar collagen, but not on gelatin or plastic (**Figure 18B**). Since DDR1 is inactive in the presence of DDR1-IN-1 on all three substrates, the altered distribution of MT1-MMP on collagen is likely caused by involvement of another collagen receptor(s). Signalling from this other collagen receptor would be expected to promote basal MT1-MMP localisation, since inhibition of DDR1 in cells on collagen caused an increase in basal MT1-MMP localisation (**Figure 18B**). This would suggest that DDR1 under normal conditions

promotes apical localisation of MT1-MMP. Given that HGF stimulation of control cells caused an increase in basal MT1-MMP (**Figure 17**), it is possible that signalling induced by HGF is able to either override or switch off the DDR1 signalling that otherwise favour apical localisation of MT1-MMP.

Likely candidates to mediate collagen signalling besides DDR1 could be integrins, which previously have been found to associate with MT1-MMP in specific cellular structures in fibroblasts, epithelial and endothelial cells[96,129,145,146]. Addressing the cross talk between DDR1 and other collagen receptors in future studies will be essential to gain a more thorough understanding of the spatial regulation of MT1-MMP. It would for example be interesting to know if inhibition of collagen-binding integrins, both on their own and in combination with DDR1-IN-1, influences the apicobasal distribution of MT1-MMP.

In this part of the study, DDR1 was found to be essential for morphogenesis of epithelial cells in 3D culture and aggregates with disorganised polarity formed in its absence. Since MT1-MMP distribution is regulated according to apicobasal polarity, 3D structures with disorganised polarity will display a disorganised distribution of MT1-MMP. In 2D culture, I observed that such lack of polarised MT1-MMP distribution caused an increase in basal localisation of MT1-MMP (**Figure 18**) resulting in more degradation of a thin collagen film (**Figure 19**). In line with this, ECM degradation in 3D culture appeared to occur along the edge of the cell aggregates formed upon inhibition of DDR1. This can be seen by the presence of GM6001 reducing the size of aggregates formed by MDCK-DDR1ΔC cells (personal communication with Dr Itoh). Furthermore, matrix degradation is clearly seen in the phenotype of MDCK-DDR1ΔC cells cultured on beads (shown in **Figure 22D** and **Figure 23D**), where multiple, stratified cell layers form, resulting in

large structures that require displacement of the ECM. The effect of DDR1 inhibition on 3D morphogenesis is however not solely due to uncontrolled MT1-MMP activity, since inhibition of DDR1 causes a very different phenotype from MT1-MMP-overexpressing cells, which form large cyst structures in 3D culture[43]. Rather than this, the major role of DDR1 appeared to be establishment of apicobasal polarity. In support of this DDR1 inhibition also caused formation of disorganised cell aggregates during cystogenesis by CaCO-2 cells in matrigel, which does not require ECM degradation (**Figure 23C**).

While cells in the absence of DDR1 signalling had ECM-degrading activity, they appeared to migrate and invade into their surroundings in a less efficient manner than control or DDR1-overexpressing cells as evaluated by the area into which the cells invaded (**Figure 21**). This may be explained by a loss of polarity impeding the spatial coordination of cellular events (cytoskeletal remodelling, junction dis/reassembly etc.) required for efficient collective migration. DDR1 has indeed previously been reported to promote collective invasion by A431 cells in 3D culture through a role in coordinating cytoskeletal organisation across multiple cells[77].

In line with a role for DDR1 in migration, our group has previously reported that DDR1 mediates cell adhesion during migration on collagen I with knockdown of DDR1 reducing cell migration[60]. Interestingly, the promoting role of DDR1 in cell migration requires its ectodomain to be shed by ADAM10, suggesting that DDR1 is needed to attach to the matrix, but that DDR1-mediated cell adhesion also must be released by shedding for efficient cell migration. Overexpression of DDR1, but not DDR1ΔC enhanced cell migration, suggesting that signalling from DDR1 plays a role in the process[60]. In line with a promoting role of DDR1 in cell migration in 2D culture, DDR1 overexpression caused an increase in collective invasion of MDCK cells in 3D culture,

where MDCK-DDR1 cells formed large, polarised structures around the beads (**Figure 21B** and **Figure 22D**). Given that DDR1 is overexpressed in a range of epithelial cancers and associated with poor prognosis[48], it will be important to specify its role in collective invasion/migration in the future.

The role of DDR1 in 3D morphogenesis involved establishment of epithelial cell polarity. DDR1 has previously been reported to localise to cell-cell junctions where it interacts with the polarity regulators Par3 and -6[77]. Par3 was required for junctional localisation of DDR1 and conversely knockdown of DDR1 displaced Par3 from cell-cell junctions[77]. Similarly, DDR1 and E-cadherin have been reported to interact and stabilise each other at adherens junctions[81,147]. Despite being associated with such proteins characteristic of the epithelial phenotype, DDR1 has not previously been demonstrated to be required for establishment of apicobasal polarity. This is thus a novel role for DDR1, and I will in the next chapter explore what signalling downstream of DDR1 may be involved.

Chapter 4 Signalling downstream of DDR1 in epithelial polarisation and morphogenesis

4.1 Introduction

In the previous chapter I found a role for DDR1 signalling in establishing apicobasal polarity of epithelial cells in a 3D collagen environment. DDR1 signalling may thus modulate the activity of pathways involved establishment of apicobasal polarity. However, as described in Chapter 1, the signalling pathways downstream of DDR1 are not well understood and have not previously been suggested to affect epithelial polarity. An important function of DDR1 in epithelial cells is reported to be the regulation of cell morphology through effects on stabilisation of junction proteins including E-cadherin, Par3 and -6 as well as effects on cytoskeletal organisation through regulation of RhoGTPases [70,77,81,147]. Cell-cell interactions and cytoskeletal dynamics play an essential role in establishment of epithelial polarity, and effects of DDR1 on regulators of these processes could thus also contribute to its role in polarisation. In this chapter, I aimed to find candidate molecules with a role in epithelial polarisation downstream of DDR1.

In the first part of this chapter, I employed chemical inhibitors of signalling pathways that previously have been associated with DDR1 to test if these could recapitulate the effect of inhibiting DDR1 in the MDCK tubulogenesis model. The effects of inhibiting candidate pathways were further tested on establishment of apicobasal polarity, and knockdown was used to validate the specificity of the inhibitors.

The inhibitors used in this first part of the chapter did not target the role of DDR1 in cytoskeletal organisation. In the second part of this chapter, I therefore analysed the effect of DDR1 inhibition on cell morphology including polarity, junction integrity and organisation of the actin cytoskeleton in 2D culture of MDCK cells. Through this approach, I aimed to identify regulators of these phenotypes, which may influence establishment of polarity downstream of DDR1.

4.2 Results part 1: Identification of molecules involved in DDR1 signalling using chemical inhibitors

4.2.1 Inhibitor screening suggests PKCαβ as signalling molecules downstream of DDR1

To identify molecules involved in DDR1 signalling, chemical inhibitors for different signalling molecules were examined in the MDCK tubulogenesis assays (**Figure 24**A). Tested inhibitors are listed in the following table:

Inhibitor	**Target**	**Concentrations tested**
Wortmannin	PI3K	50 nM, 200 nM
PP2	Src	2.5 μM, 10 μM
PD325901	MEK	5 μM, 10 μM, 20 μM
go6870	PKCαβγδ and -ε	2 μM
go6976	PKCα and -β	1 μM
CAS 257879-35-9	PKCβ	0.5 μM, 1 μM

DDR1-signalling has been linked to both PI3K and Src signalling[48], and I therefore tested the effect of inhibiting these kinases using wortmannin and PP2 respectively. In contrast to the aggregate formation observed in the presence of DDR1-IN-1 (**Figure 24A**), tubulogenesis was unaffected by inhibition of PI3K or Src, suggesting that the role of DDR1 in tubulogenesis is not mediated through these pathways (**Figure 24B** and **C**). In contrast, inhibition of MEK prevented tubulogenesis, but structures formed in the presence of MEK inhibitor had clearly discernible lumens at all concentrations tested (**Figure 24A** and -**D**, arrows point to lumens). Thus, signalling through MAP kinases cannot fully account for the phenotype observed by DDR1 inhibition. Interestingly, a pan-PKC inhibitor (go6870) resulted in aggregate formation similar to those observed upon DDR1 inhibition (**Figure 24E**). Collagen I was recently reported to promote PKCα signalling through DDR1[148], and PKCα and –β have previously been implicated in establishment of apicobasal polarity in MDCK cells[37].

PKCs would thus be interesting candidates to relay signalling downstream of DDR1 in epithelial tubulogenesis. To narrow down which PKC isoform might be involved, I further tested the effect of go6967, which only inhibits PKCα and –β. This inhibitor recapitulated the effect of the pan-PKC inhibitor (**Figure 24E**), suggesting that PKCα or –β is involved. Applying a PKCβ-selective inhibitor did not affect tubulogenesis (**Figure 24E**), indicating PKCα as the more likely candidate to mediate this effect. Unfortunately, PKCα-selective inhibitors are not available, and I was thus unable further corroborate this by inhibitor studies. Instead knockdown of PKCα (see Section **4.2.4**) will be a more reliable way to confirm that this PKC isoform is mediating the effects of go6976.

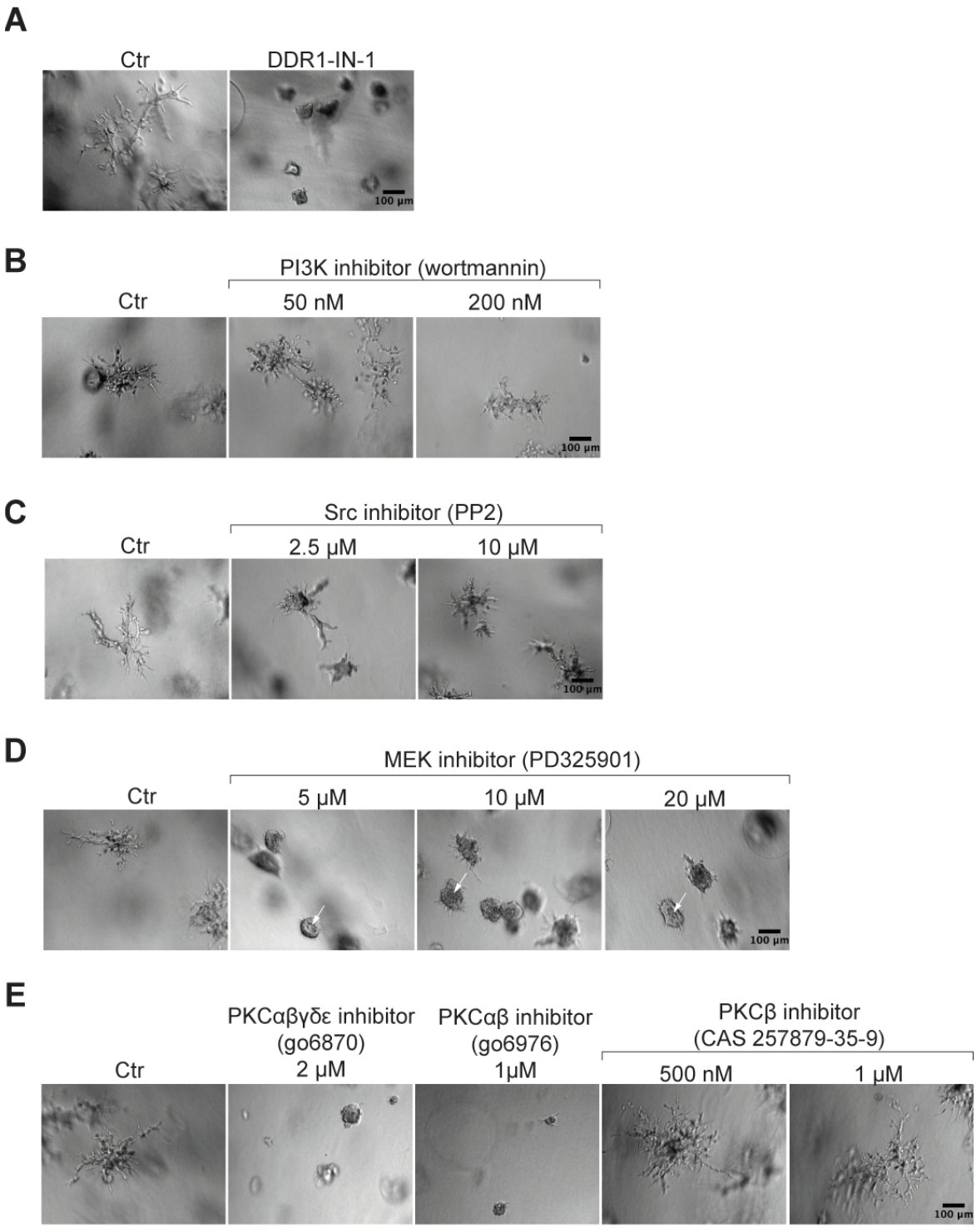


Figure 24: Screening of signalling pathway inhibitors in MDCK tubulogenesis assay. A-E) MDCK cells were cultured in 2 mg/ml collagen I matrices for 5 days in the presence of HGF (50 ng/ml) and the indicated inhibitors. DMSO was used as control. Images were captured using a 10X objective on a widefield microscope. Representative images are shown of 2-4 independent experiments are shown. The following inhibitors were tested: **A)** DDR1-IN-1 (1 µM). **B)** PI3K inhibitor wortmannin (50 and 200 nM). **C)** Src inhibitor PP2 (2.5 and 10 µM). **D)** MEK inhibitor PD325901 (5, 10 and 20 µM). **E)** PKCαβγδε inhibitor go6870 (2 µM), PKCαβ inhibitor go6976 (1 µM) or PKCβ inhibitor CAS 257879-35-9 (500 and 1000 nM).

4.2.2 Inhibition of PKCαβ disturbs polarisation and lumen formation in MDCK and CaCO-2 cells similarly to inhibition of DDR1

To validate that aggregates formed upon PKC inhibition are similar to those formed in the presence of DDR1-IN-1, I examined the distribution of the apical marker GP135. MDCK cells were stimulated by HGF to undergo tubulogenesis in 3D matrices in the presence of the pan-PKC inhibitor, PKCαβ inhibitor or PKCβ inhibitor. 3D cultures were fixed and subjected to indirect immunofluorescence followed by imaging by confocal microscopy. Similar to my previous observations, control cells formed hollow tubular structures with GP135-positive lumens (**Figure 25A**, arrows point to lumen). In contrast, the pan-PKC inhibitor caused cells to form compact aggregates without a central lumen (**Figure 25A**). Similar to the phenotype observed upon DDR1 inhibition, the distribution of GP135 was not restricted to apical surfaces suggesting that polarity is disturbed (**Figure 25A**, arrowheads point to GP135 at the cell-matrix interface). This effect was recapitulated upon inhibition of PKCα and -β, but not PKCβ alone (**Figure 25A**). A potential role for PKCα and/or β in 3D morphogenesis was confirmed in CaCO-2 cells, which failed to form cysts with central lumens upon treatment with go6976 (**Figure 25B**). These data suggest that PKCα and/or β could be potential downstream mediators of DDR1 signalling during polarisation in 3D matrices.

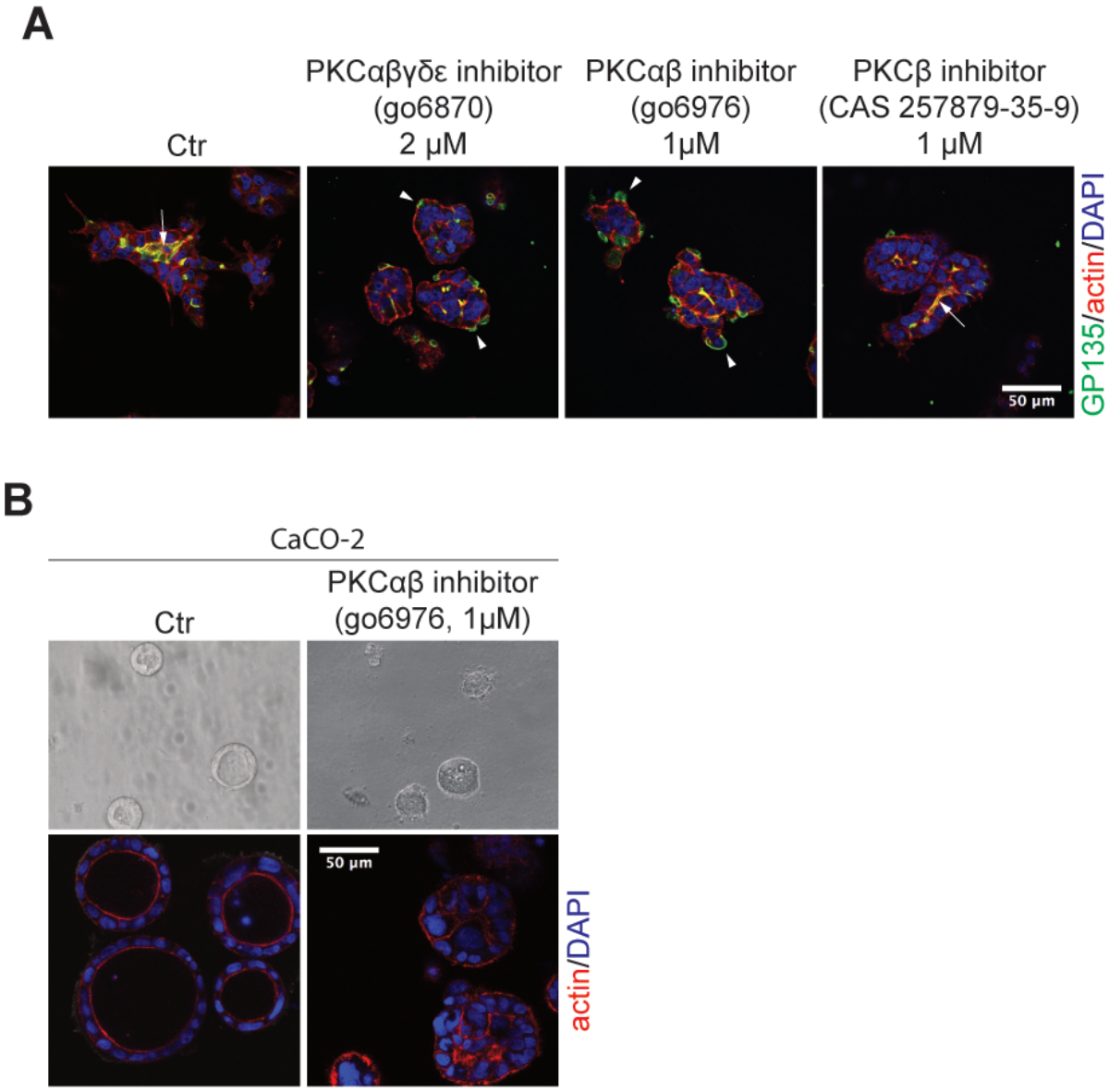


Figure 25: Apicobasal polarity of epithelial cells is disturbed by inhibition of PKCα and –β during tubulogenesis in 3D matrices. A) MDCK cells were cultured in 2 mg/ml collagen I gels for 5 days in the presence of HGF (50 ng/ml) and the indicated inhibitors. DMSO was used as a control. Gels were fixed and stained against actin (red) and DAPI (blue) and analysed by a 60X objective on a CSLM. Representative images from one of >3 independent experiments are shown. **B)** CaCO-2 cells were seeded in IBDI µ-slide wells coated with 100% Matrigel and overlayed by DMEM with 20% FCS and 2% Matrigel and DMSO or go6976 (1 µM). Cells were cultured for 9 days before fixation and staining for actin (red) and nuclei (blue). Images were captured with a 60X objective on a CLSM. Representative images from one of 3 independent experiments are shown.

4.2.3 Inhibition of PKCα and -β attenuates tubulogenesis on microcarrier beads and prevents increased collective invasion by MDCK-DDR1 cells

To further confirm that inhibition of PKCα and –β causes effects similar to the inhibition of DDR1, I tested the effect of the inhibitors in the modified tubulogenesis assay on microcarrier beads. MDCK-Mock, MDCK-DDR1 and MDCK-DDR1ΔC cells were cultured on beads in 3D collagen I as described in Section 3.2.8, Chapter 3. Control cells extended multicellular tubules from the beads as described previously (**Figure 26** left), whereas inhibition of PKCα and –β prevented this formation of tubular structures (**Figure 26**, left). Consistent with a role for PKCα and/or –β downstream of DDR1, the PKCαβ inhibitor attenuated the increased collective invasion observed in cells overexpressing DDR1 (**Figure 26**, middle panels). No effect of inhibiting PKCα and –β was observed for MDCK-DDR1ΔC cells (**Figure 26**, right).

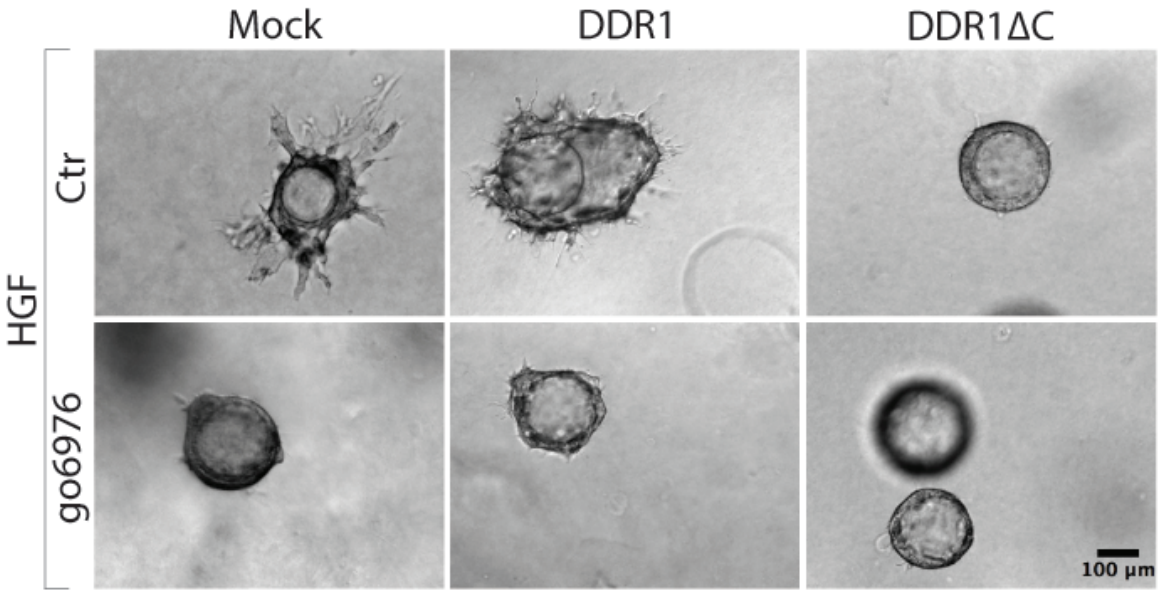


Figure 26. Inhibition of PKCα and -β prevents HGF-induced tubulogenesis and attenuates increased collective invasion by MDCK-DDR1 cells. MDCK-Mock, MDCK-DDR1 and MDCK-DDRΔC cells were cultured to confluence on microcarrier beads. Beads were then embedded in 3D collagen I (2 mg/ml) gels and overlaid with DMEM with 10% FCS and HGF (50 ng/ml) and PKCαβ inhibitor go6976 (1 µM) where indicated. Images were captured on a 20X objective on a widefield microscope. Representative images from one of 3 independent experiments are shown.

4.2.4 Generation of MDCK lines with stable knock-down of PKCα or -β

The above data suggested PKCα as a potential signalling molecule downstream of DDR1, since a PKCαβ inhibitor, but not a PKCβ inhibitor mimicked the phenotype seen upon DDR1 inhibition. To investigate this further, I aimed to knock down PKCα and –β expression in MDCK cells. Since transfection of siRNA for transient knockdown is not efficient in MDCK cells, I used a lentiviral shRNA vector against PKCα or –β to create stable clonal cell lines.

MDCK cells tolerated transduction with PKCα shRNA well, and 5 clonal cell lines were established: MDCK-PKCα-shRNA clone 2-6. Few colonies of cells stably expressing PKCβ-shRNA survived (as evaluated by resistance to antibiotics). However, 4 clonal cell lines were established: MDCK-PKCβ-shRNA clone 5, 7, 10 and 11. Additionally, clonal cell lines expressing non-targeting shRNA were generated as controls (MDCK-NT-shRNA).

The knockdown efficiency of PKCα was tested in MDCK-PKCα-shRNA clone 2-6 cells by Western blot. Compared to cells expressing NT-shRNA, expression levels of PKCα were reduced about 50% (**Figure 27A**). To improve knockdown efficiency, a second transduction was done to introduce an additional copy of the gene encoding the shRNA. Since the knockdown efficiency was highest in MDCK-PKCα-shRNA clone 4 and -6, I chose these for the second transduction. This resulted in two heterogeneous lines of double transfected cells: clone 4.1pool and clone 6.1pool respectively. Additionally 4 clonal cell lines were derived from clone 4.1pool cells: clone 4.1.3, 4.1.6, 4.1.8 and 4.1.9. Lysates of these cells were made and analysed by Western blot to see if the second transduction with shRNA had improved the knockdown efficiency for PKCα. This showed a strong downregulation of PKCα in 2 clonal cell lines with double transduction of PKCα shRNA, namely 4.1.3 and 4.1.6 (**Figure 27B**). These two clones also displayed

the biggest decrease in mRNA levels, when the amount of PKCα mRNA was evaluated by RT-PCR and compared with GADPH mRNA (**Figure 27**C). I therefore chose MDCK-PKCα-shRNA clone 4.1.3 and 4.1.6 for further analysis. Additionally, MDCK-PKCα-shRNA clone 4 was included to detect potential dose-dependent effects. No decrease in PKCα mRNA was detected in cells transduced with shRNA against PKCβ.

Unfortunately, PKCβ could not be detected at protein level with any of the tested antibodies, and I therefore resorted to evaluating PKCβ mRNA levels by RT-PCR. Surprisingly, no decrease in mRNA levels was detected in any PKCβ shRNA clones (**Figure 27D,** left). The primers used for RT-PCR were validated by analysing mRNA in HEK293 cells transiently transfected with siRNA against PKCβ. In these cells the band for PKCβ weakened upon transfection with PKCβ siRNA, but not non-targeting or PKCα siRNA (**Figure 27D**, right), suggesting that the band observed in MDCK cells indeed represents PKCβ. It is unclear why transduction with shRNA did not reduce PKCβ mRNA. Given the high levels of cell death upon transduction with PKCβ shRNA, it is possible that knockdown of PKCβ is toxic to the cells, and that the few surviving clones are ones that somehow attain antibiotic resistance without expressing the shRNA.

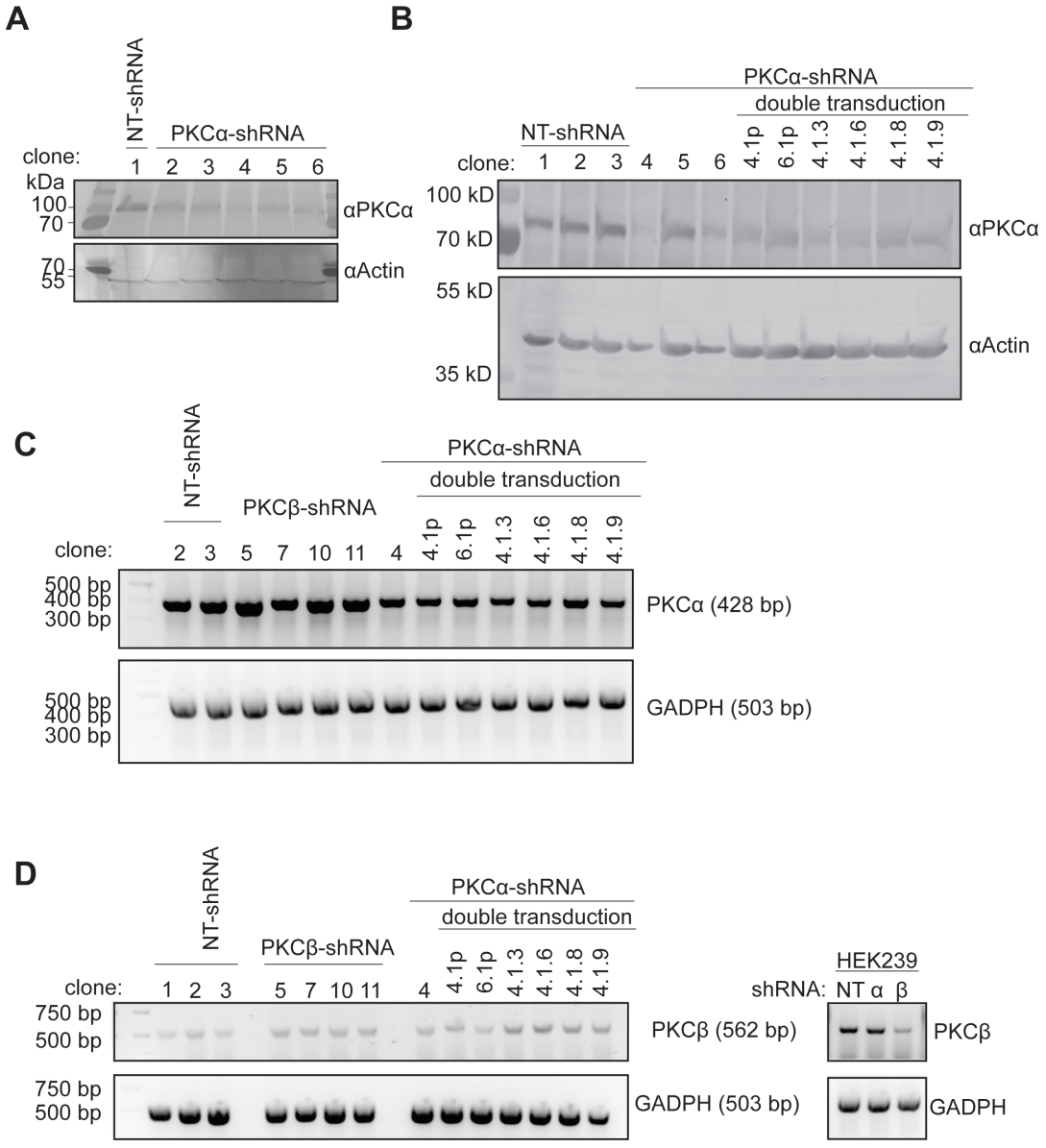


Figure 27. Stable knockdown of PKCα and –β in MDCK cells. A) MDCK cells were transduced with lentivirus at MOI 500 to introduce shRNA targeting PKCα, PKCβ or non-targeting shRNA. Transduced cells were selected based on resistance to puromycin and diluted to isolate clonal cell lines originating from 1 transduced cell. The following cell lines were created: MDCK-NT-shRNA clone 1-3, MDCK-PKCα-shRNA clone 2-6, MDCK-PKCβ-shRNA clone 5, 7, 10 and 11. Lysates were generated and analysed by Western blot with primary antibodies against PKCα and actin. **B**) MDCK-PKCα-shRNA clone 4 and 6 were transduced a second time with shRNA targeting PKCα. Pooled double–transduced cells are denoted clone 4.1p and 6.1p. 4 clonal cell lines were generated from MDCK-PKCα-shRNA clone 4.1p (clone 4.1.3, 4.1.6, 4.1.8 and 4.1.9 respectively). Lysates were made from 3 clonal lines of MDCK-NT-shRNA and single/double transduced MDCK-PKCα-shRNA lines. Lysates were analysed by Western blot with primary antibodies against PKCα and actin. **Note that more total protein is loaded from lysates from double-transduced cell lines.** Western blot representative of 2 experiments**. C**) mRNA levels of PKCα were evaluated by RT-PCR. RNA was extracted from the generated cell lines and reverse transcribed into cDNA. PCR with primers for PKCα were used to amplify a 428 bp fragment of PKCα mRNA. Primers for the housekeeping gene, GADPH, were used as control. Representative result from 3 experiments. **D**) Left: mRNA levels of PKCβ were evaluated by RT-PCR as described in **C**), except primers for a 562 bp fragment of PKCβ were used. Right: The same primers were used to assess levels of PKCβ mRNA in HEK239 cells transiently transfected with siRNA against PKCα or -β or non-targeting siRNA. **Note that PKCβ mRNA decreases upon transfection with PKCβ siRNA in HEK293 cells, suggesting that the primers can detect PKCβ**.

4.2.5 Knockdown of PKCα or β in MDCK cells does not recapitulate the effect of chemical inhibition of PKCα and β on epithelial tubulogenesis

To test whether knockdown of PKCα recapitulated the effects of go6976, I analysed the ability of MDCK-PKCα-shRNA clone 4, 4.1.3 and 4.1.6 to undergo HGF-induced tubulogenesis. MDCK-NT-shRNA cells formed round cysts in the absence of HGF, whereas HGF stimulation induced formation of tubular structures (**Figure 28A)**. In contrast to the aggregate formation observed in cells treated with go6976 (**Figure 24E**), the cell lines expressing shRNA against PKCα were able to form tubular structures in response to HGF stimulation (**Figure 28A**). These structures, however, appeared to have reduced branching compared to MDCK-NT-shRNA cells, suggesting that PKCα knockdown does mediate some attenuation of tubulogenesis without fully reproducing the effect of go6976 (**Figure 28A**). It is difficult to quantify the results from this type of tubulogenesis assay, and thus hard to numerically evaluate the correlation between reduced branching and the expression level of PKCα. Cell lines expressing shRNA against PKCα survived poorly in 3D collagen I in the absence of HGF, suggesting that PKCα also may play a role in proliferation or survival of MDCK cells in 3D collagen I. In line with mRNA levels of PKCβ being undisturbed, MDCK-PKCβ-shRNA cells underwent HGF-induced tubulogenesis similar to MDCK-NT-shRNA cells (**Figure 28B**). Cyst formation in the absence of HGF was also not affected in these cells (**Figure 28B**). Similar observations were done in the tubulogenesis assay on microcarrier beads, where slightly less sprouting of tubules were observed in MDCK-PKCα-shRNA clone 4.1.3 and 4.1.6 compared to MDCK-NT-shRNA (**Figure 28C**). However, compared to the results with go6976 (**Figure 26**), the effect of PKCα knockdown was modest. It thus appears that knocking down PKCα only has slight effects on tubulogenesis, and thus does not fully recapitulate the effects of go6976. This could be due to insufficient knockdown efficiency

for PKCα or to the effect of go6976 being caused by co-inhibition of PKCα and - β. Alternatively the effect of go6976 may be mediated through off-target effects of the inhibitor.

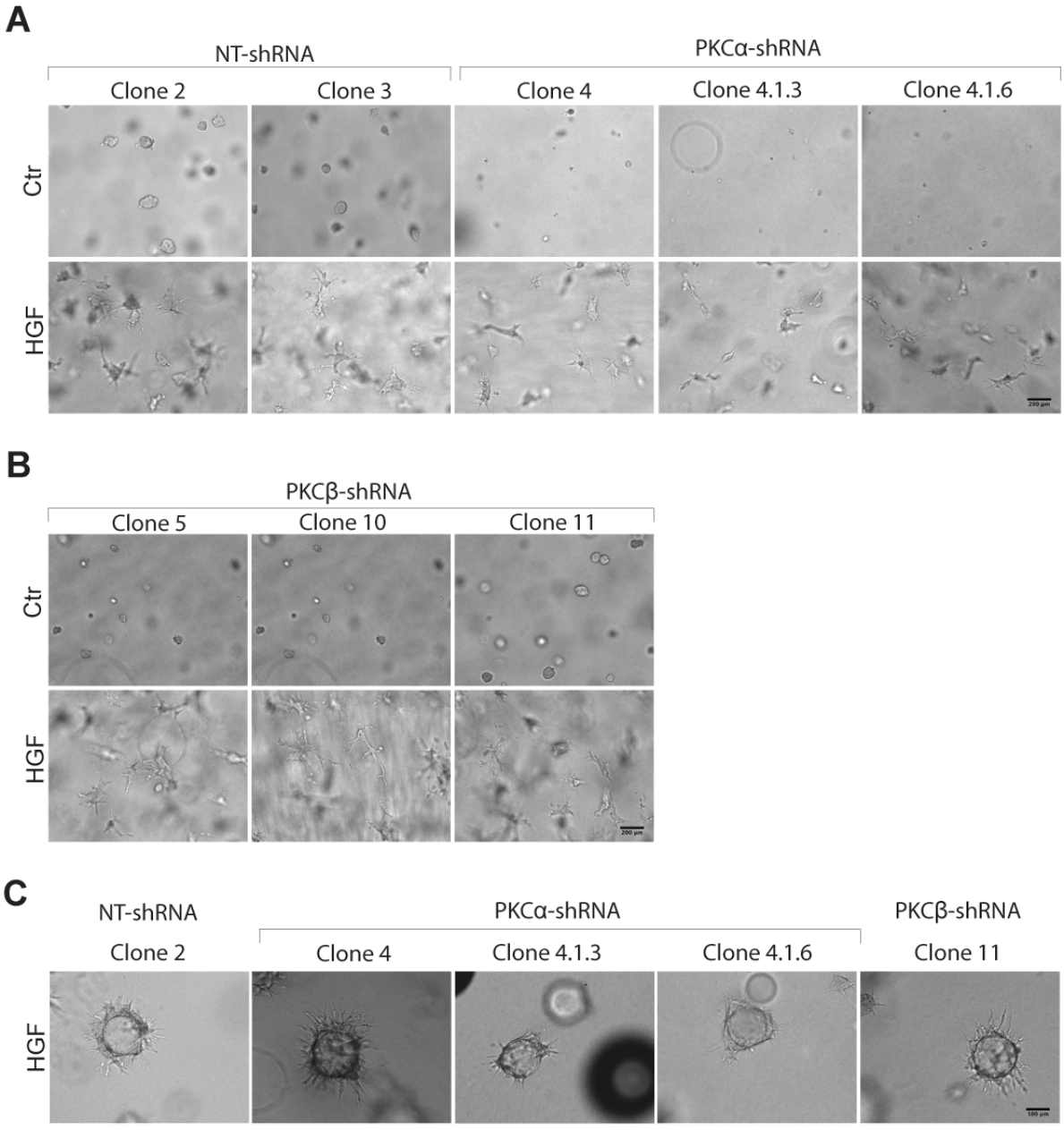


Figure 28. Knockdown of PKCα does not inhibit tubulogenesis. A) Clonal lines of MDCK-NT-shRNA, MDCK-PKCα-shRNA and MDCK-PKCβ-shRNA cells were cultured in 2 mg/ml collagen I gels for 5 days in DMEM with 10% FCS and HGF (50 ng/ml) where indicated. Brightfield images were captured with a 10X objective on a widefield microscope. Representative images from one of 2 independent experiments are shown. **B)** Clonal lines of MDCK-NT-shRNA, MDCK-PKCα-shRNA and MDCK-PKCβ-shRNA cells were cultured to confluence on microcarrier beads. Beads were then embedded in 3D collagen I (2 mg/ml) gels and overlaid with DMEM with 10% FCS and HGF (50 ng/ml) and cultured for 48 hours. Images were captured on a 20X objective on a widefield microscope. Representative images from one of 2 independent experiments are shown.

It thus appears, that whereas go6976 fully reproduced the phenotype of DDR1 inhibition in MDCK cells, conclusive evidence suggesting either PKCα or -β as a molecule involved in DDR1 signalling could not be obtained. In the next section of this chapter, I therefore attempt a second approach to understand how DDR1 signalling affects epithelial polarity.

4.3 Results part 2: Identification of polarity-modulating targets of DDR1 by analysis of its role in epithelial organisation in 2D culture

4.3.1 DDR1 inhibition does not disturb apicobasal polarity in monolayers of MDCK cells

In the previous chapter, I described that DDR1 plays a role in establishment of apicobasal polarity of MDCK cells in 3D collagen gels. To further characterise this function of DDR1, I examined the phenotype of DDR1 inhibition on epithelial organisation in 2D culture in more detail.

First, I examined whether polarity was affected by DDR1 inhibition in 2D culture of MDCK cells, by analysing the distribution of the apical marker GP135, the tight junction component ZO1 and adherens junction protein E-cadherin (**Figure 2**, Chapter 1 schematically depicts the localisation of these proteins in polarised epithelial cells). Cells were cultured on a thin collagen film for 48 hours and processed for confocal microscopy. In contrast to the findings in 3D culture conditions, inhibition of DDR1 did not affect the localisation of GP135 to the apical cell surface (**Figure 29A**). Similarly, ZO1 and E-cadherin localised in apical and lateral structures at cell-cell interfaces respectively regardless of DDR1-IN-1 treatment (**Figure 29A**). Similar observations were made with MDCK-DDR1ΔC cells (**Figure 29B**). MDCK cells are thus able to form cell-cell junctions and to polarise in the absence of DDR1 signalling in 2D culture.

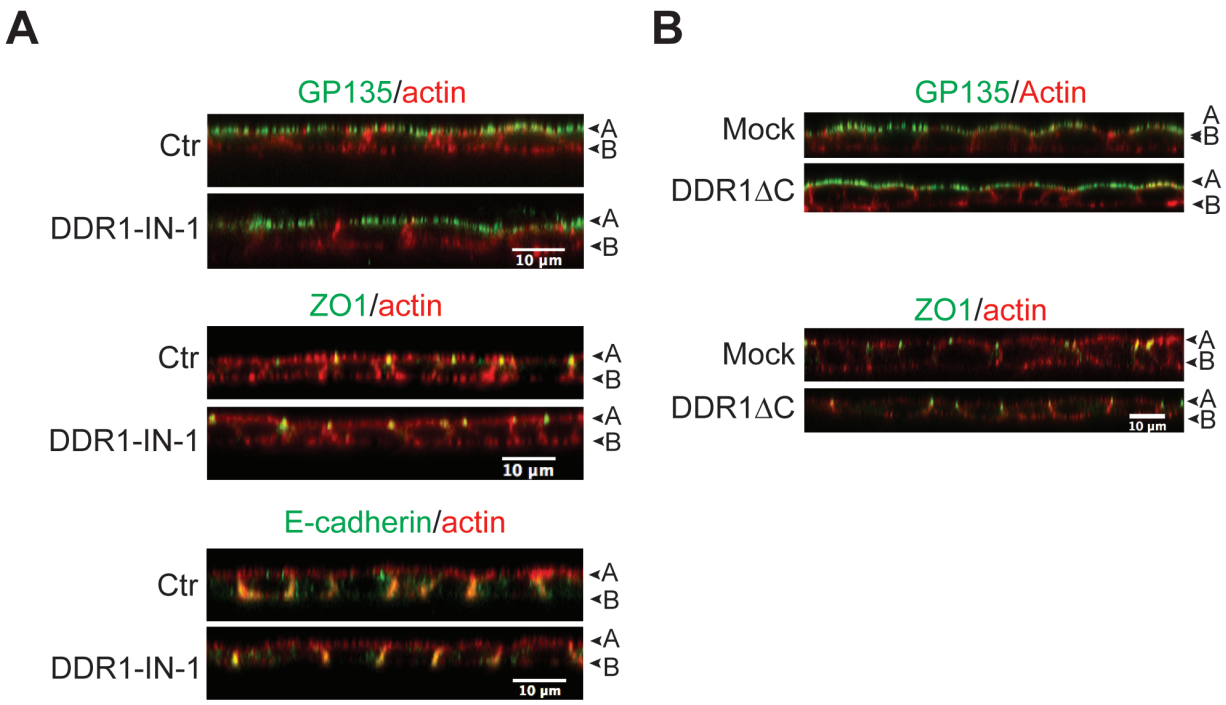


Figure 29 DDR1 inhibition does not disturb polarity in MDCK cells in 2D culture. A) MDCK cells were cultured at 100% confluency in culture inserts coated with collagen I (1.5 mg/ml) in DMEM with 10% FCS in the presence of DMSO or DDR1-IN-1 (1 µM) as indicated. After 4-6 days, cells were fixed and stained against: Top: GP135 (green) and actin (red). Middle: ZO1 (green) and actin (red). Bottom: E-cadherin (green) and actin (red). Samples were analysed by a 60X objective on a CSLM and processed in ImageJ. Representative XZ sections from one of >3 independent experiments are shown. **B)** MDCK-Mock and MDCK-DDR1ΔC cells were cultured as in A). After 3 days, cells were fixed and stained against: Top: GP135 (green) and actin (red). Bottom: ZO1 (green) and actin (red). Samples were analysed by a 60X objective on a CSLM and processed in ImageJ. Representative XZ sections from one of >3 independent experiments are shown.

4.3.2 DDR1 inhibition delays the formation of a mature, polarised monolayer of MDCK cells

Correct localisation of E-cadherin and ZO1 to adherens and tight junctions does not rule out that the functionality of epithelial junctions may be affected by DDR1 inhibition. I therefore evaluated the barrier function of epithelial monolayers by measuring transepithelial resistance (TER). This is done by applying a voltage over a monolayer of epithelial cells whilst measuring the ion flow across the cell layer. Since the plasma membrane is highly impermeable to charged ions, the majority of ion flux will occur at cell-cell junctions, and the integrity of epithelial junctions can thus be evaluated.

To examine the earliest phase of polarisation, MDCK cells were seeded onto collagen-coated culture inserts in Ca^{2+}-free medium, which prevents formation of cell-cell

junctions. The next day, medium was switched to Ca^{2+}-containing medium and TER was measured every hour from 0 hours to 8 hours and again after 20.5 hours to 25.5 hours (**Figure 30Aa**). To look at more long-term effects, MDCK cells were seeded in normal Ca^{2+}-containing medium and TER measurements performed after 23-69 hours culture (**Figure 30Ab**). In control cells, TER values rose within the first 8 hours after the Ca^{2+}-switch in accordance with formation of epithelial junctions (**Figure 30Aa**). Between 20 and 25 hours after the Ca^{2+}-switch, TER values decreased rapidly (**Figure 30A**). After this, TER values continued to decrease until it reached a homeostatic level, indicating complete polarisation/maturation of the monolayer (**Figure 30Ab**). This decrease in TER before it reaches a plateau is potentially due to incorporation of claudins, ion channels and other ion-permeable molecules into their correct positions in the plasma membrane as the monolayer polarises and matures. A rise in TER similar to control cells was observed in DDR1-IN-1-treated cells on collagen I within the first 6 hours after the Ca^{2+}-switch, however, between 6-8 hours a slight delay was observed in DDR1-IN-1-treated cells (**Figure 30Aa**). After 69 hours culture, little difference was seen between control and DDR1-IN-1 treatment (**Figure 30Ab**), suggesting that junctions with full barrier-function are able to form in the absence of DDR1 signalling. However, DDR1-IN-1-treated cells were noticeably slower to reach a homeostatic level of TER (**Figure 30A**). This suggests that DDR1 inhibition causes a delay in formation of a fully mature epithelial monolayer, although this delay eventually is overcome.

Interestingly, control cells on plastic also reached a homeostatic TER level faster than DDR1-IN-1-treated cells on plastic (**Figure 30B**), suggesting that the function of DDR1 in this case does not depend on collagen. It was also noted that cells on plastic had higher TER values than cells on collagen I (compare **Figure 30B** with **Figure 30A**). Since similar background values were measured in uncoated and collagen-coated inserts with no

cells seeded, this difference in TER values is not due to the collagen layer itself. More likely, collagen signalling affects the junctional properties during the polarisation/maturation process. The difference between uncoated and collagen-coated inserts disappeared at 45 hours (**Figure 30A** and -**B**), which may imply that cells have deposited their own matrix at this time point.

To further corroborate that DDR1 has a role in maturation of the epithelial monolayers, I used the formation of primary cilia as another readout of epithelial maturation. As previously mentioned, primary cilia are subcellular structures found at the apical membrane, which form at the last stage of polarisation[137]. The appearance of primary cilia was examined by staining MDCK cells cultured in collagen-coated culture inserts for 24 hours, 48 hours and 4 days (96 hours) against acetylated tubulin. Samples were analysed by widefield microscopy (**Figure 30C**, left). The percentage of cells with primary cilia structures (both punctate pro-cilia and elongated cilia counted) was compared between control and DDR1-IN-1-treated cells at each time point (**Figure 30C**, right). 24 hours after seeding, few cells formed primary cilia structures in both control and DDR1-IN-1-treated samples. Under control conditions, the percentage of cells with cilia increased to 45% after 40 hours and to 65% after 4 days culture. Upon treatment with DDR1-IN-1, no increase from 24 hours to 40 hours was seen, but after 4 days culture, cilia formation by DDR1-IN-1-treated cells had caught up with that control cells (**Figure 30C**), suggesting that DDR1 inhibition causes a delay in the initial increase in cilia formation. These findings are in line with the concept that inhibition of DDR1 may cause a delay in the formation of a mature epithelial monolayer.

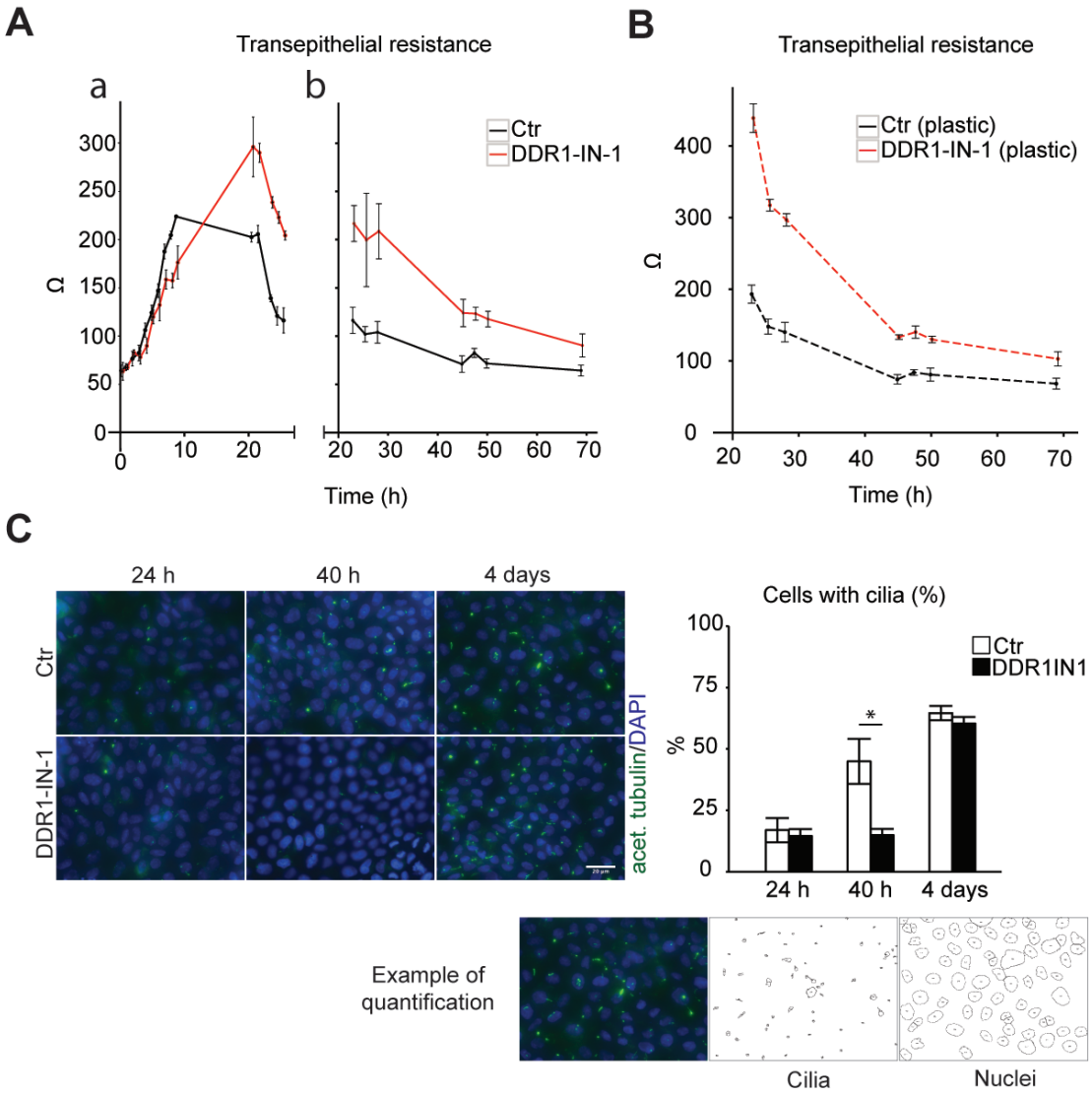


Figure 30. Inhibition of DDR1 causes a delay in maturation of epithelial monolayers. Aa) MDCK cells were trypsinised and resuspended in low Ca^{2+} medium (S-MEM with 2 mM glutamine, 1 mM sodium-pyruvate, 10% dialysed FCS). Cells were spun down and resuspended in low Ca^{2+} medium again to deplete intracellular Ca^{2+} stores. Cells were then seeded in triplicate at 100% confluence in collagen I-coated (1.5 mg/ml) culture inserts in low Ca^{2+} medium in the presence of either DMSO (Ctr) or DDR1-IN-1. Next morning, medium was changed to normal DMEM with 10% FCS and inhibitors as indicated. First TER measurements were done after a 15 minute incubation, and then measured every 1 hours between 1-8 hours and 20.5-25.5 hours after the Ca^{2+} switch. **Ab**) MDCK cells were seeded in triplicate at 100% confluence in collagen I-coated (1.5 mg/ml) culture inserts in DMEM with 10% FCS and DMSO or DDR1-IN-1 (1 µM). TER measurements were done 23, 25.5, 28, 45, 47.5, 50 and 69 hours after seeding. The average TER values of three inserts per condition were plotted against time. Error bars represent standard deviation. Please note that only one experiment with 3 technical replicates was performed for each of Aa and Ab. **B)** MDCK cells were cultured and TER measured and analysed as in Ab, except that cell were cultured in uncoated culture inserts. **C)** MDCK cells were cultured at 100% confluence in culture inserts coated with collagen I (1.5 mg/ml) in DMEM with 10% FCS in the presence of DMSO (Ctr) or DDR1-IN-1 (1 µM) as indicated. Cells were fixed after 24 h, 48 hours or 4 days and stained against: acetylated tubulin (green) and DAPI (blue). Images were captured with a 60X objective on a widefield microscope. Left: Representative images shown. Right: The number of nuclei and cilia was found by automated analysis in ImageJ. An example of the automated detection of nuclei and cilia is shown underneath the graph. The percentage of cells with cilia was found in 15 images per condition. The average percentage of 3 experiments is plotted with error bars representing standard deviation. Conditions were compared with a Kruskal test, and differences localised with a pairwise Wilcoxon test with Holm correction for multiple testing (* represents p-value <0.05). A significant difference between control and DDR1-IN-1-treated cells was found at time point 40 hours (p= 0.02298), but not 24 hours or 4 days.

4.3.3 DDR1 inhibition increases ROCK-dependent ppMLC at cell-cell junctions

Cytoskeletal dynamics are essential during establishment of epithelial polarity. Like many other ECM-receptors, DDR1 has been implicated in regulation of cytoskeletal organisation[70,77,78]. I therefore examined whether organisation of the actin cytoskeleton in epithelial monolayers is affected by inhibition of DDR1. Tension of the actin cytoskeleton is generated by actomyosin contraction, which requires myosin light chain (MLC) to be phosphorylated. I thus investigated actomyosin-generated tension by examining the distribution of diphosphorylated MLC (ppMLC). The time point for analysis was chosen based on the results from the TER measurements. These showed that control cells had nearly reached a steady state after 36 hours culture on collagen I, whilst DDR1-IN-1-treated cells at this time point still retained higher TER values (**Figure 30A**). More pronounced differences may therefore be expected around this time point compared to a fully mature monolayer.

MDCK cells were cultured at 40% confluence on a thin collagen I film in the presence of DMSO or DDR1-IN-1 for 36 hours before fixation and immunofluorescent staining of filamentous actin (red) and ppMLC (green) (**Figure 31A**). Control MDCK cells formed cell islands with a collectively organised cytoskeleton. This comprised a thick, cortical actin band along the periphery of the cell island, which was positive for ppMLC (**Figure 31A**, arrows). In contrast, actin bands along cell-cell junctions within the cell island were weak and showed little ppMLC staining (**Figure 31A**). Interestingly, inhibition of DDR1 signalling appeared to disturb this collective organisation of cytoskeletal tension between neighbouring cells: instead of ppMLC-positive actin bundles being restricted to the periphery of cell islands, DDR1-IN-1-treatment resulted in thicker, ppMLC-positive actin bundles along cell-cell junctions (**Figure 31A**, arrows). RhoA-ROCK signalling is the major promoting regulator of MLC phosphorylation with ROCK

both directly phosphorylating MLC and indirectly inhibiting dephosphorylation of MLC through phosphorylation of the phosphatase MYPT1, which leads to dissociation of MLC from MYPT1[149]. When cells were treated with an inhibitor of ROCK (Y27632) in addition to DDR1-IN-1, the ppMLC signal at cell-cell junctions disappeared (**Figure 31**A). This suggests, that DDR1 has a role in decreasing the phosphorylation of MLC at cell-cell junctions, potentially through suppression of the RhoA-ROCK signalling pathway. Interestingly, a similar increase in ppMLC along cell-cell junctions was seen upon DDR1 inhibition in cells cultured on glass (**Figure 31B**), suggesting that the ROCK-suppressing function of DDR1 is not dependent on collagen stimulation. No consistent change in the total levels of ppMLC was detected by Western blot upon inhibition of DDR1 (data not shown), suggesting that DDR1 is more likely to affect ROCK signalling locally in the junctional area rather than control total RhoA-ROCK activity in the cell.

MDCK cells seeded on coverslips remain flat compared to cells grown in culture inserts. It is thus difficult to get a clear view of the ppMLC distribution along the Z-axis in cells on coverslips. In order to examine if ppMLC increases in the junctional area rather than along the basal cell surface, I examined the distribution of ppMLC in MDCK cells grown at 100% confluence in culture inserts. Compared to control cells, DDR1-IN-1 treatment caused an increase in junctional ppMLC in sections captured towards the apical cell surface, whereas the distribution of ppMLC remained similar in basal sections (**Figure 31C**, left, arrows point ppMLC-positive junctions). This was more clearly seen when the mean intensity in each confocal section was normalised to the highest intensity in the stack and plotted against the Z-axis. In control cells, the highest mean intensities were seen in sections at the basal cell surface, whereas treatment with DDR1-IN-1 switched the highest ppMLC intensity towards the apical cell surface (**Figure 31C**, right).

This suggests that DDR1 contributes to the spatial control of ROCK signalling within the cell by decreasing its activity in the apical, junctional area.

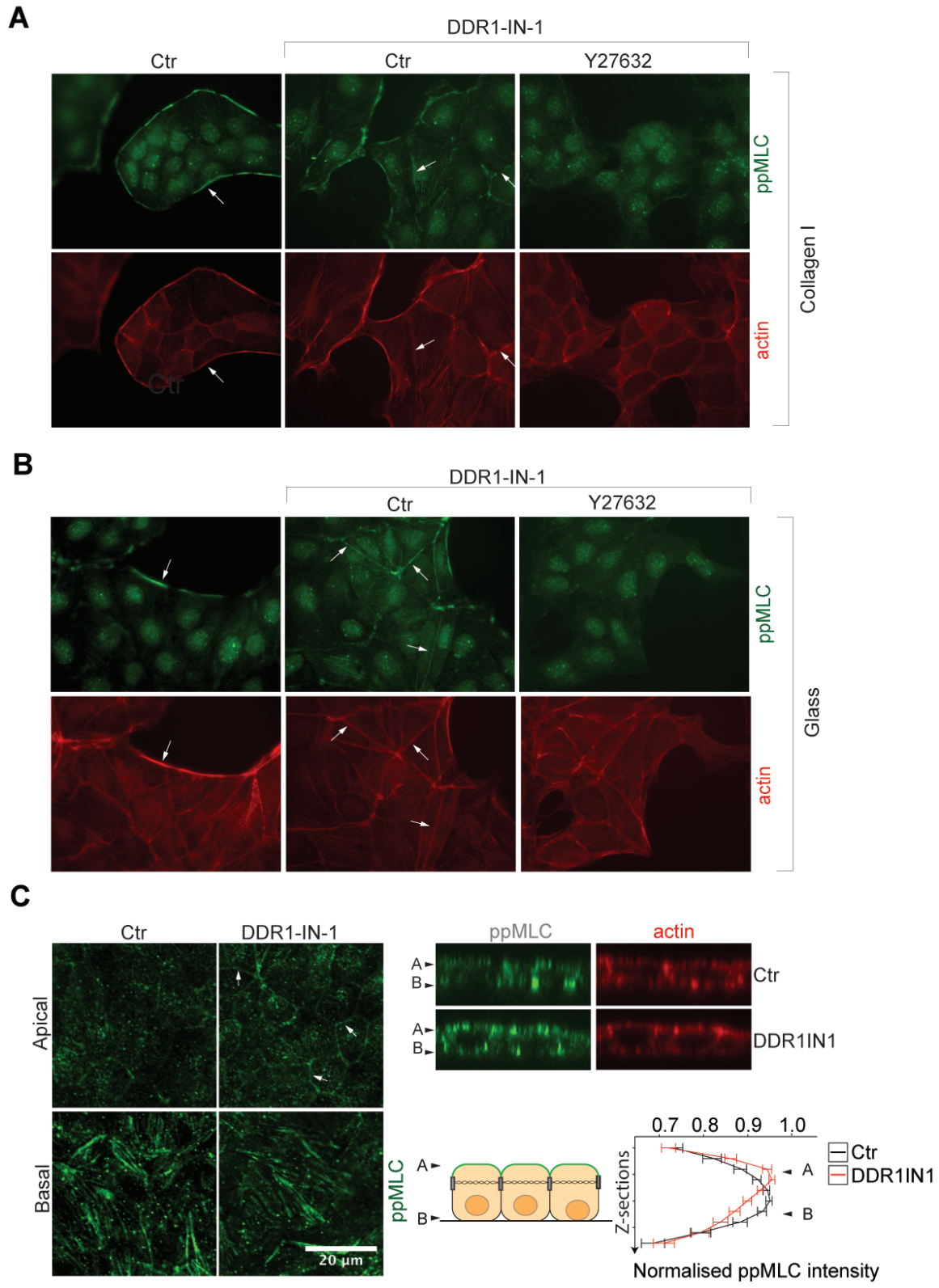


Figure 31: DDR1 inhibition causes increased ROCK activity at cell-cell-junctions. **A+B)** MDCK cells were seeded at 40% confluence on (**A**) collagen-coated or (**B**) uncoated coverslips in DMEM with 10% FCS and indicated inhibitors for 36 hours. Cells were fixed and stained against: ppMLC (Thr18/Ser19) (green) and actin (red). Samples were analysed by a 60X objective on a widefield microscope. Representative images are shown. **C)** MDCK cells were cultured at 100% confluence in culture inserts coated with collagen I (1.5 mg/ml) in DMEM with 10% FCS in the presence of DMSO or DDR1-IN-1 (1 μM) as indicated. Cells were fixed and stained against: ppMLC (Thr18/Ser19) (green) and actin (red). Left: representative confocal sections captured at the apical and basal cell surface are shown. Arrows point to junctional ppMLC. Right, top: representative XZ-sections are shown. Right, bottom: the average intensity in each confocal section was measured in ImageJ. For each stack, the intensities were normalised to the highest average intensity in that stack. Stacks were aligned based on the most apical section and the mean at each Z-section calculated and plotted with error bars representing standard error of the mean. 55-60 stacks per condition pooled from 4 independent experiments were analysed. A and B denotes the apical and basal side respectively.

4.3.4 DDR1 localises to adherens junctions in MDCK cells

Phosphorylated DDR1 interacts with a large range of molecules through its cytoplasmic domain[48] and could thus suppress ROCK activity at cell-cell junctions by recruiting negative regulators of RhoA-ROCK signalling to this location. Indeed, DDR1 has previously been reported to localise and function in epithelial cell junctions[71,77,81,147]. This is an unusual localisation for an ECM-receptor, and I therefore wished to confirm that DDR1 localises in cell-cell junctions in the system used here. Since endogenous DDR1 cannot be detected by immunocytochemistry due to low expression level, I employed MDCK cells overexpressing DDR1. MDCK-DDR1 cells were cultured at 100% confluence in collagen-coated culture inserts for 36 hours before fixation. Cells were then co-stained for DDR1 and E-cadherin or ZO1 as markers of adherens and tight junctions respectively (see **Figure 2**, Chapter 1). Surprisingly, the majority of DDR1 localised in the lateral cell membrane (**Figure 32A** and **B**). E-cadherin and DDR1 had a similar staining pattern and co-distributed at cell-cell junctions. In contrast, ZO1 was found to localise just apical of DDR1 with little colocalisation observed (**Figure 32B**), suggesting that DDR1 localises to adherens junctions (**Figure 32A**).

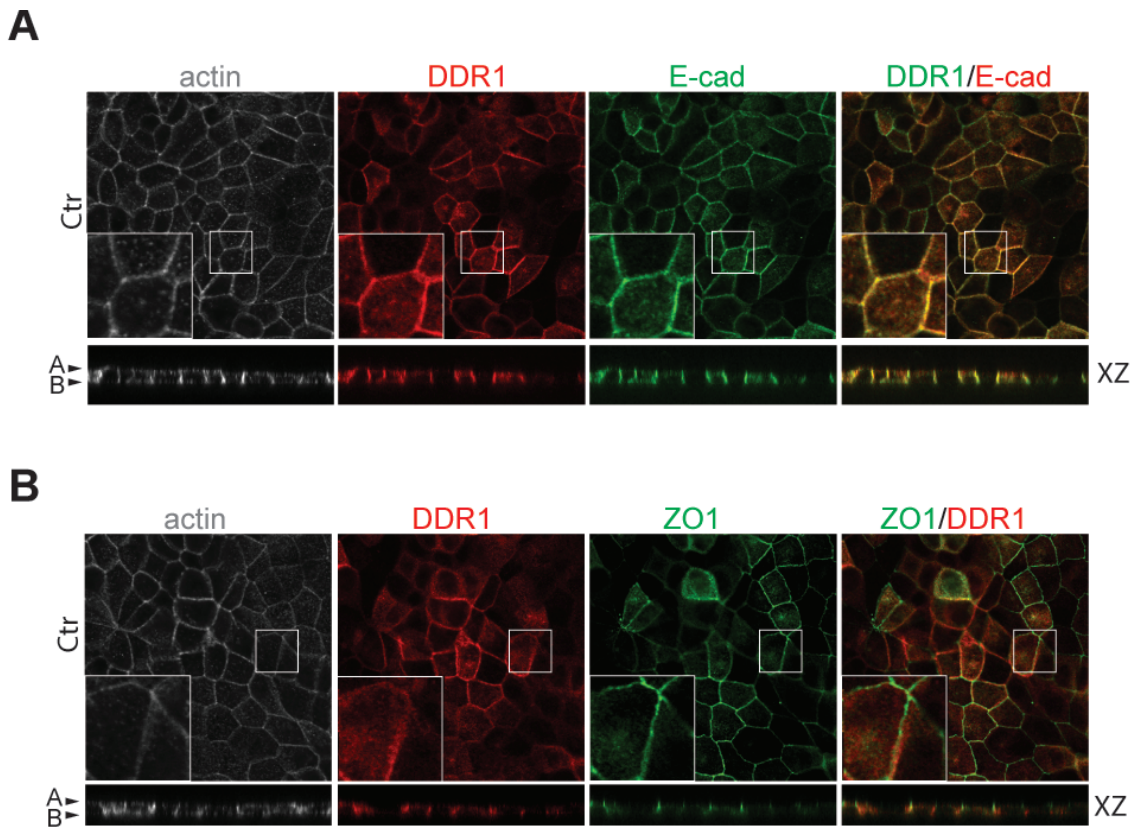


Figure 32. DDR1 localises to adherens junctions. MDCK-DDR1 cells were seeded at 100% confluence in collagen I-coated (1.5 mg/ml) culture inserts and cultured in DMEM with 10% FCS for 36 hours. Cells were fixed and stained against: **A)** E-cadherin (green), DDR1 (cytoplasmic domain, red) and actin (gray). **B)** ZO1 (green), DDR1 (cytoplasmic domain, red) and actin (gray). Samples were analysed by a 60X objective on a CLSM and images processed in ImageJ. Representative XY and XZ planes from one of 3 independent experiments are shown. A: apical, B: basal. Ctr: control

4.3.5 Inhibition of ROCK activity rescues lumen formation and polarisation during cyst formation.

Since adjustment of intracellular tension in response to the stiffness of surrounding matrix is crucial for epithelial morphogenesis[12,150], uncontrolled ROCK activity due to DDR1 inhibition may cause the aberrant epithelial phenotypes observed in 3D matrices. To investigate this, I examined if ROCK inhibition affected the ability of MDCK cells to form polarised cysts in the absence of DDR1 signalling. MDCK cells were cultured in 3D collagen I for 5 days before cells were fixed and stained for actin and nuclei. As observed in the previous chapter, inhibition of DDR1 disrupted the formation of cysts with a central lumen (**Figure 33A**). Interestingly, simultaneous inhibition of ROCK activity with either 3,10 or 30 μM Y27632 rescued the ability of MDCK cells to form cysts (**Figure 33A**).

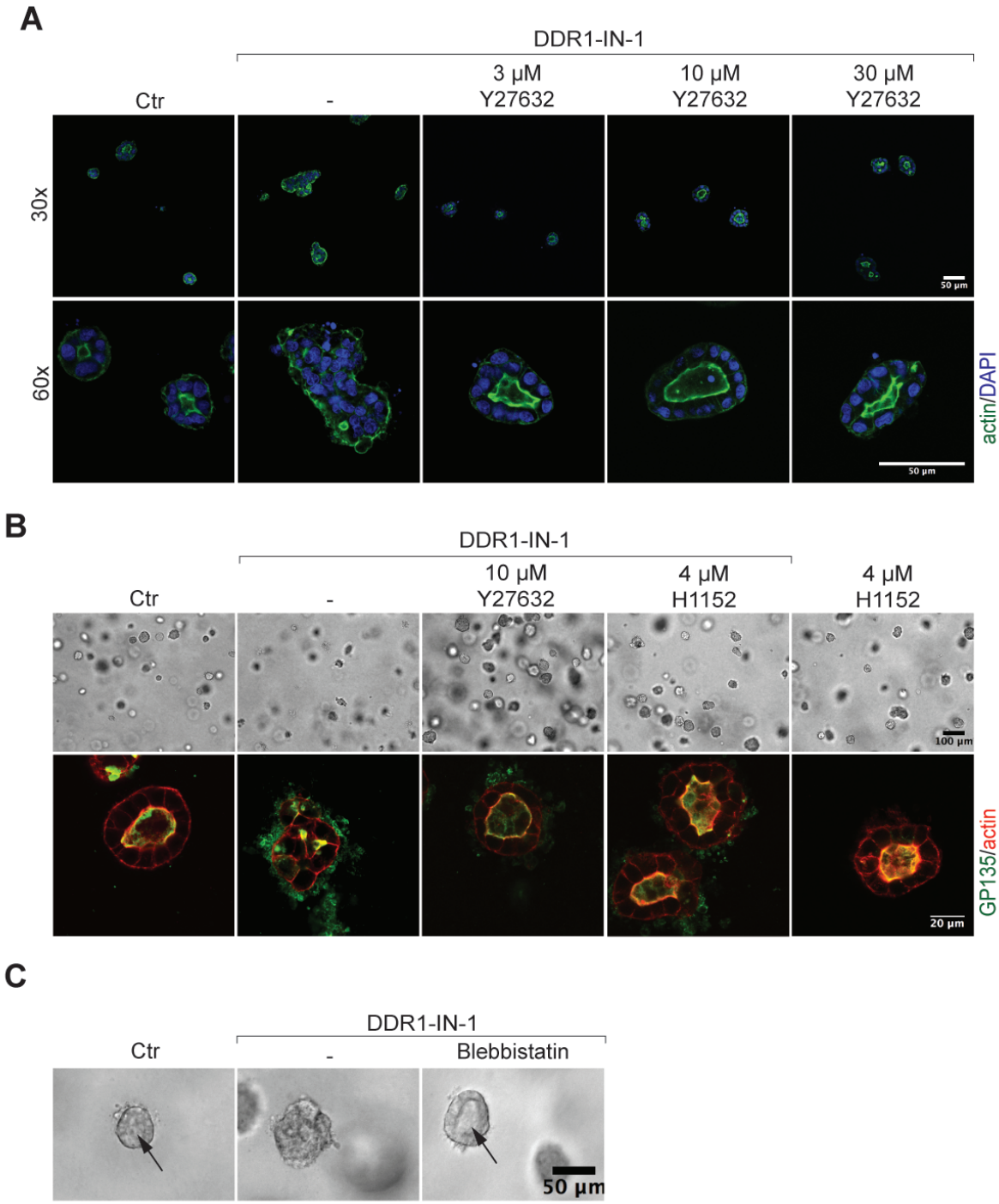


Figure 33. Inhibition of ROCK activity rescues formation of polarised cysts in absence of DDR1 signalling. A) MDCK cells were cultured in 3D collagen I gels (2 mg/ml) for 5 days in the presence of DMSO, DDR1-IN-1 (1 µM) and Y27632 (3, 10 or 30 µM) as indicated. Gels were fixed and stained with f-actin (green) and DAPI (blue). Images were captured with a 30X or 60X objective on a CLSM. Representative images from one of >3 independent experiments are shown. **B)** Cells were cultured as in A) in the presence of DMSO, DDR1-IN-1 (1 µM), Y27632 (10 µM) and/or H1152 (4 µM). Gels were fixed and stained for GP135 (green) and f-actin (red). Confocal images were captured with a 60X objective on a CLSM. Representative images from one of >3 independent experiments are shown. **C**) Cells were cultured as in A) in the presence of DMSO, DDR1-IN-1 (1 µM) or blebbistatin (25 µM). Brightfield images were captured on a widefield microscope. Representative images from one of 2 independent experiments are shown. Arrows point to lumens.

Staining for GP135 confirmed that polarity was restored upon inhibition of ROCK activity with Y27632 as well as with another, more selective, ROCK inhibitor H1152 (**Figure 33B**). Inhibition of ROCK alone did not affect cystogenesis (**Figure 33B**), suggesting that there is no requirement for ROCK activity in establishment of apicobasal polarity in 3D collagen I. The effect of excessive ROCK signalling in absence of DDR1 signalling appears mainly to be mediated by promotion of actomyosin contraction, since the myosin II inhibitor, blebbistatin (25 μM), also rescued cystogenesis in absence of DDR1 signalling (**Figure 33C**, arrow points to lumen).

In contrast to cystogenesis, HGF-induced tubulogenesis by epithelial cells such as T47D, MCF-10A and MDCK cells has been reported to rely on RhoA-ROCK activity[38,151]. In line with this, HGF stimulation activates RhoA[41]. Inhibition of ROCK would therefore be unlikely to restore HGF-induced tubulogenesis. This was confirmed by culturing MDCK cells in 3D collagen I in the presence of HGF and inhibitors for DDR1 and ROCK as indicated in **Figure 34A**. As described previously, control cells formed tubular structures, whereas DDR1 inhibition led to aggregate formation (**Figure 34A**). Additional inhibition of ROCK did not rescue tubulogenesis, and inhibition of ROCK activity alone prevented tubule formation (**Figure 34A**). In contrast to the aggregates formed in the presence of DDR1-IN-1, several spikes and protrusions extended from the aggregates formed upon inhibition of ROCK (**Figure 34A**). This may relate to a reported role of ROCK in controlling the number of protrusions during HGF-induced tubulogenesis[38]. Tubulogenesis requires extensive remodelling of the cytoskeleton as well as disassembly and reassembly of junctions. Since RhoA-ROCK signalling contributes to the regulation of these dynamic processes, it is tempting to speculate that DDR1 contributes to turning off RhoA-ROCK signalling at the right time and place during tubular morphogenesis.

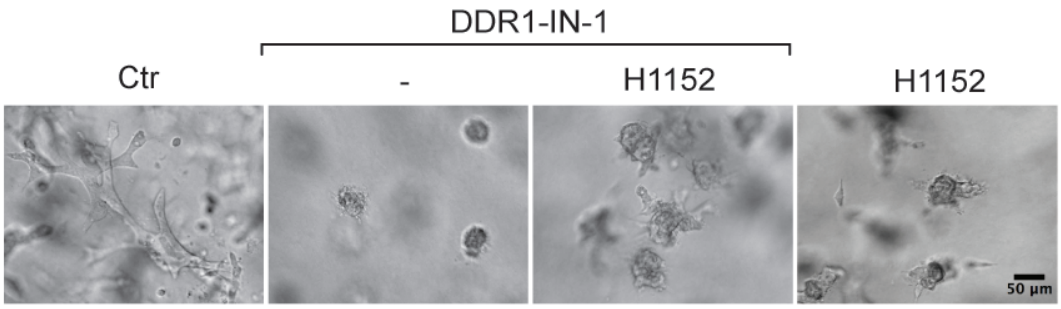


Figure 34. Inhibition of ROCK does not restore HGF-induced tubulogenesis of MDCK cells in absence of DDR1 signalling. MDCK cells were cultured 5 days in 3D collagen I gels (2 mg/ml) in the presence of HGF (50 ng/ml), DDR1-IN-I (1 µM) or H1152 (4 µM) as indicated. Images were captured on a 20X objective on a widefield microscope. Representative images from one of >3 independent experiments are shown.

4.3.6 Inhibition of ROCK restores the polarised distribution of MT1-MMP in inert polarised MDCK cells, but prevents the HGF-induced increase in MT1-MMP at the basal cell surface

I next investigated if the ROCK-suppressing function of DDR1 has relevance for the polarised distribution of MT1-MMP. MDCK cells expressing MT1-pHluorin-RFP were seeded in wells coated with collagen I in the presence of DMSO, DDR1-IN-1 and/or H1152. After 24 hours of culture, HGF was added and cells incubated for a further 24 hours. Localisation of surface MT1-MMP was examined in live cells by capturing XZ-sections on a confocal microscope. As seen previously, DDR1-IN-1 treatment caused an increased level of MT1-MMP at the basal cell surface, which was unaffected by HGF stimulation (**Figure 35A**). Surprisingly, inhibition of ROCK signalling restored the apical localisation of MT1-MMP in the absence of DDR1 signalling. However, ROCK inhibition also prevented the HGF-induced increase in basal MT1-MMP localisation seen under control conditions (**Figure 35A**).

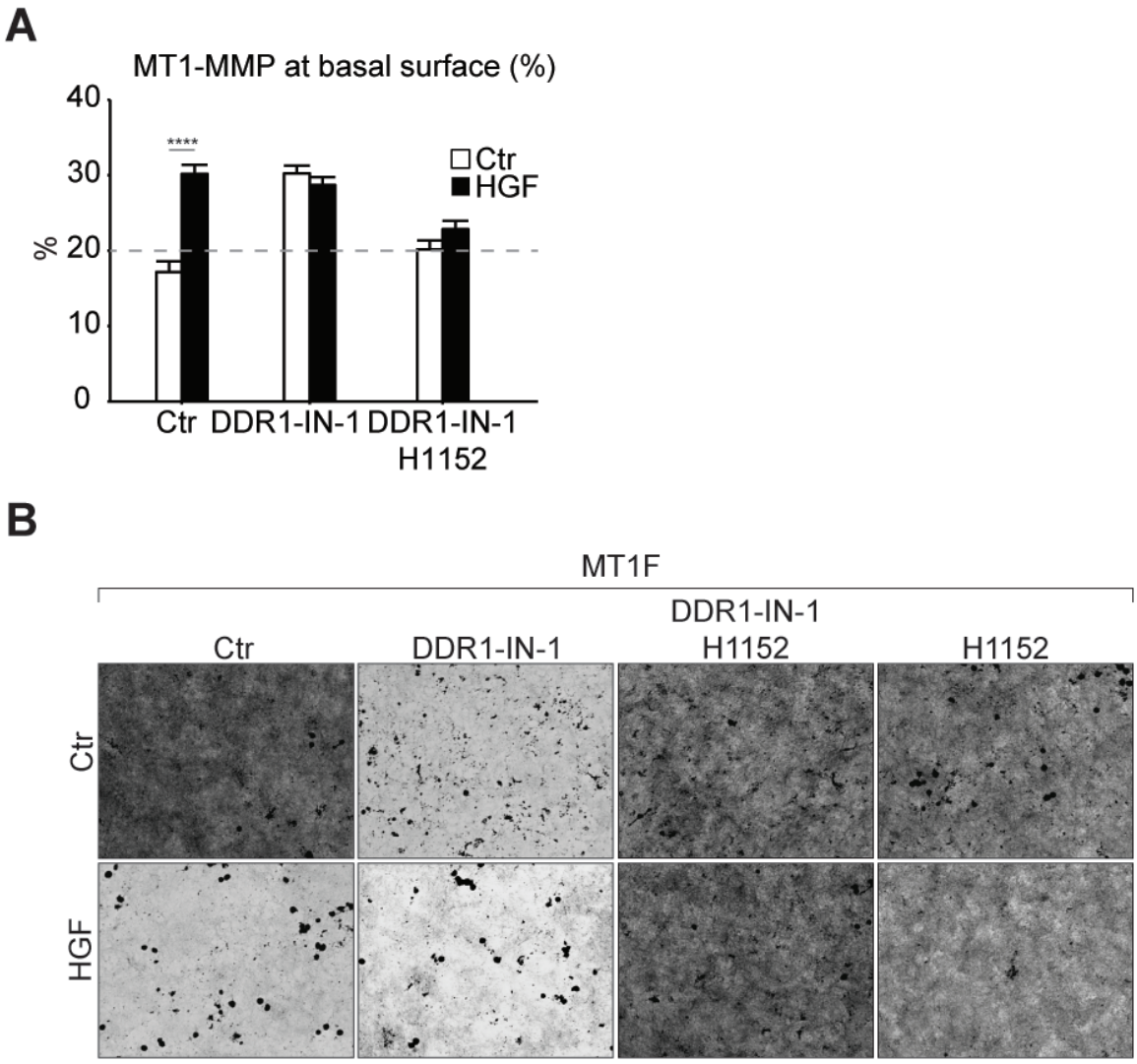


Figure 35. ROCK inhibition prevents recruitment of MT1-MMP to the basal cell surface with consequence for collagen degradation: A) MDCK-MT1pH cells were seeded in IBIDI µ-slide wells coated with collagen I (1.5 mg/ml). Cells were cultured in DMEM with 10% FCS in the presence of DMSO, DDR1-IN-1 (1 µM) and H1152 (4 µM) as indicated. After 24 h, HGF was added and culture continued for a further 24 hours before capturing line-scan images (30 per condition) using a 60X objective on a CLSM and analysed using ImageJ. Graph depicts the percentage of total surface MT1F present at the basal surface. The tested conditions were compared with a Kruskal-Wallis rank sum test ($p=4.852*10^{-14}$) before localising differences with a pairwise Wilcoxon test with Holm correction of the p-value to correct for multiple testing. Results of comparisons are marked by stars or listed in **Table S1**, Section **8.1**. Asterisks *, **, ***. **** depict statistically significant differences of $p<0.05$, $p<0.01$, $p<0.001$ and $p<0.0001$ respectively. **B)** MDCK cells were seeded in Corning CellBIND culture plates coated with 200 µl of collagen I (1:1 ratio of protease-extracted PureCol and acid-extracted CellMatrix collagen I) in the presence of DMSO, DDR1-IN-1 (1 µM) and H1152 (4 µM) as indicated. Once 100% confluent, cells were infected with Ad-MT1F at a MOI of 5 in the presence of GM6001 (10 µM) in serum-free medium. After 24 hours culture GM6001 was washed out and cells incubated a further 16 hours in the presence or absence of HGF (50 ng/ml) with indicated inhibitors. Cells were removed by >24 hours trypsination followed by fixation of remaining collagen and staining of the collagen with Coomassie blue. Remaining collagen I was visualised in gray with a 20X objective on a widefield microscope. Degradation appears as light/white areas. Photoshop was used to enhance contrast with the same settings applied to images from all conditions. Representative images from one of >3 independent experiments are shown.

To confirm these observations, I also compared the ability of MDCK cells to degrade collagen I in response to HGF stimulation. MDCK cells were seeded on a thin film of collagen I at 100% confluence in the presence of DMSO, DDR1-IN-1 (1 μM) and/or H1152 (4 μM) as indicated in **Figure 35B**. Cells were then infected with Ad-MT1F (MOI 5) in the presence of GM6001 (5 μM). After 24 h, GM6001 was washed out and cells incubated for a further 16 hours with or without HGF (50 ng/ml). Cells were then removed by extensive trypsination and remaining collagen I was fixed and stained with Coomassie blue. Collagen was visualised as dark gray against a white background on a widefield microscope (**Figure 35B**). As observed in Chapter 3, collagen degradation correlated with localisation of MT1-MMP: in control cells, collagen degradation was increased by HGF treatment, whereas DDR1-IN-1 treatment resulted in degradation of collagen regardless of HGF treatment (**Figure 35B**). In contrast, ROCK inhibitor prevented degradation of collagen I, both on its own and in combination with DDR1-IN-1 (**Figure 35A**). This suggests that ROCK activity is involved in recruiting MT1-MMP to the basal cell surface with functional significance for the ability of cells to degrade the underlying matrix.

4.3.7 Inhibition of ROCK activity does not rescue lumen formation and polarisation during cyst formation upon inhibition of PKCα and β

In the previous part of this chapter, I found that inhibition of PKCα and -β inhibit establishment of epithelial polarity in 3D matrices. It has previously been reported that inhibition of RhoA-ROCK signalling can rescue defective cystogenesis upon inhibition of PKCα and -β[37]. I therefore tested whether such alleviation of go6976-induced disruption of polarity could be observed in our system. MDCK cells were cultured in 3D collagen I for 5 days in the presence or absence of HGF. Go6976 prevented formation of cysts with discernable lumens in the absence of HGF and caused formation of aggregates in its

presence (**Figure 36A**). Additional inhibition of ROCK activity restored neither cystogenesis nor tubulogenesis (**Figure 36A**). This suggests that the effect of PKCαβ inhibition in our system is not due to an imbalance between PKC and ROCK signalling. This discrepancy may be due to a difference in culture conditions, since the previous study used a 3D Matrigel culture system[37] while 3D collagen gels were used in this study.

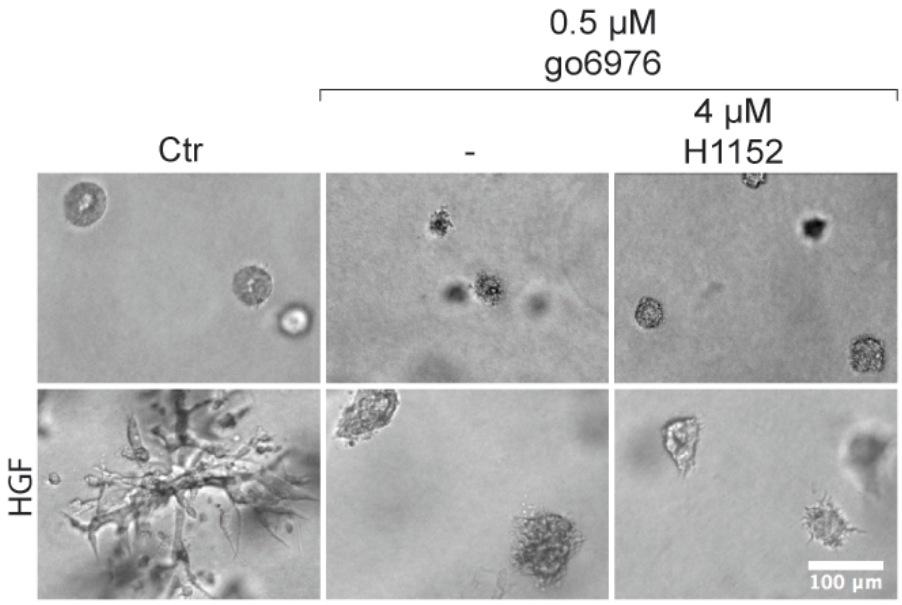


Figure 36. Inhibition of ROCK signalling does not rescue lumen formation and polarisation in the absence of PKCα and β signalling. A) MDCK cells were cultured for 5 days in 3D collagen I gels (2 mg/ml) in the absence or presence of HGF (50 ng/ml), go6976 (0.5 µM) or H1152 (4 µM) as indicated. Images were captured on a 10X objective on a widefield microscope. Representative images from one of 3 independent experiments are shown.

4.4 Discussion

In the first part of this chapter, I found that inhibition of PKC signalling disturbed epithelial morphogenesis in a similar manner to inhibition of DDR1. In particular the inhibitor studies suggested that PKCα could mediate such effects. Interestingly, collagen I was recently reported to promote PKCα signalling through DDR1 in the breast cancer cell lines Erb2 and MDA-MB-231[148]. This was shown to depend on DDR1 forming a complex with an atypical tetraspanin TM4SF and syntenin-2, which allowed for recruitment and activation of PKCα and its substrate JAK2[148]. It should be noted that DDR1-mediated activation of PKCα reported to be independent of kinase activity of DDR12[148]. Future

studies should examine if PKCα is activated by collagen in a DDR1-dependent manner in MDCK cells. Activation of PKCα can be assessed by evaluating the phosphorylation status of immunoprecipitated PKCα or by examining translocation of PKCα to the cell membrane through cellular fractionation or immunocytochemistry.

It was unfortunate that I was unable to confirm the effect of go6976 on tubulogenesis by knockdown of PKCα or –β. It is possible that the knockdown efficiency of PKCα was too low to affect tubulogenesis, however, since I was unable to achieve knockdown of PKCβ it is also possible that the effects of go6976 are due to inhibition of PKCβ rather than -α. I did however not see any effects on tubulogenesis when I treated cells with an inhibitor selective for PKCβ (**Figure 24E**). Simultaneous inhibition of PKCα and –β may also be responsible for the effects of go6976, which could be confirmed by combined knockdown of PKCα and –β. In line with the observations for go6976, PKCα and –β have in a previous study been reported to be involved in establishment of epithelial polarity in MDCK cells[37]. Knockdown of PKCβ and to a lesser extent -α was reported to inhibit formation of cysts with correct apicobasal polarity in 3D Matrigel matrices. This requirement for PKCβ and -α was attributed to phosphorylation of the apical GP135/NHERF/ezrin complex during early polarisation. Phosphorylation of this complex is required for lumen formation, since it allows the complex to disassemble at the cell-ECM interface and relocalise to the preapical patch[37] (**Figure 6**, Chapter 1). This pathway was suggested to work independently from, but in opposition to RhoA-ROCK signalling, with downregulation of RhoA rescuing cystogenesis in the presence of go6976[37]. My inability to reproduce these results in collagen I points to the important impact of matrix properties on morphogenic processes.

More research will be needed to understand if and how PKC signalling is involved in epithelial polarisation and whether PKCs in this case act downstream of DDR1.

In the second part of this chapter, I found that inhibition of DDR1 in epithelial cells in 2D culture did not prevent establishment of apicobasal polarity. This is in contrast to the observations in 3D culture in the previous chapter, where DDR1 signalling was found to be indispensable for polarisation. This may reflect that the polarisation process in 2D is more robust than in 3D culture. The difference between the polarisation process in 2D and 3D was highlighted in a microarray study comparing gene expression between MDCK cells polarising in 2D and 3D culture, revealing at least 99 differentially regulated genes[152]. Similar observations of dramatic effects in 3D contrasted by mild effects in 2D culture have been made by manipulation of other polarity regulators such as the Crumbs3-Pals1[153] complex, Par3[154,155], Cdc42[13] and Rac[15]. In example, the polarity protein Par3 is required during cystogenesis in 3D, whereas the effect of Par3 knockdown in 2D culture is limited to a delay in the initial establishment of apical membrane identity[154,155]. The results on TER and cilia formation (**Figure 30**) suggested that inhibition of DDR1 causes an initial delay in maturation of epithelial monolayers, which is overcome over time. Since cells *in vivo* exist in 3D environments, 3D culture may better reflect the physiological role of DDR1.

Our findings suggest that the role of DDR1 in polarisation and morphogenesis in 3D culture involves regulation of cytoskeletal organisation through spatial control of ROCK activity. This is similar to a previous study in A431 cells, which revealed a role for DDR1 in suppressing ROCK signalling at cell-cell junctions with implications for cytoskeletal coordination[77]. This coordination was shown to be required for collective migration and was shown to be mediated by DDR1 interacting with Par3 and - 6 at cell-cell junctions, where the complex facilitated recruitment of RhoE to junctions[77]. Since RhoE can supress ROCK activity both directly and indirectly via inhibition of RhoA,

DDR1 in this manner contributed to suppression of ROCK activity at cell-cell junctions[77]. However, preliminary investigation of the distribution of mCherry-tagged RhoE in our system suggested, that this is not the mode of action of DDR1 in MDCK cells (data not shown). The ROCK-suppressing function of DDR1 in A431 cells was further found to be independent of DDR1 kinase activity with a kinase-dead DDR1 mutant being able to rescue the phenotype of cells depleted for DDR1[77]. This is in contrast to my finding of DDR1-IN-1 treatment causing increased junctional ROCK activity in MDCK cells. Interestingly, whereas kinase activity of DDR1 was required for ROCK suppression in my study, it did not require collagen stimulation (**Figure 31B**). This may suggest that DDR1 can be activated in cell-cell junctions in a collagen-independent manner. Collagen-independent activation of DDR1 is supported by some constitutive DDR1 activity being present in unstimulated MDCK cells (Chapter 3, **Figure 18A**). Alternatively, cells cultured for 36 hours on plastic may have produced enough matrix on their own to cause some activation of DDR1. Collagen is known to induce changes in the distribution of DDR1 in the cell membrane, which lead to clustering of the receptor. It has been proposed that activation of DDR1 in response to collagen could be mediated by such clustering[44,50,56]. If this is the case, it is possible that a large number of DDR1 molecules locating in adherens junctions could constitute such clustering and lead to activation of DDR1. This activation depends on autophosphorylation of DDR1 in MDCK cells, but since other kinases such as Src, and recently DDR2, have been shown to be able to phosphorylate DDR1 during activation[56,75], one could speculate that hyperactivation of such signalling pathways in cancer cells, such as A431 cells, could lead to phosphorylation of kinase-dead DDR1. This could explain why the similar role of DDR1 in MDCK and A431 cells appear to require kinase activity in one system, but not the other. Additionally, variations in expression and regulation of phosphatases could

contribute to differential regulation of DDR1. It would be interesting to examine whether DDR1 localising in adherens junctions is phosphorylated or not in the two cell types. My attempts to assess this by immunocytochemistry using primary antibodies specific for phosphorylated DDR1 were, however, hampered by failure to validate the specificity of the tested antibodies. Since DDR1 has been reported to interact with E-cadherin[156], an alternative approach could be to isolate the junctional pool of DDR1 by co-immunoprecipitation with E-cadherin followed by sequential immunoprecipitation of DDR1 to assess its phosphorylation status.

In line with a role for DDR1 in adherens junctions, I observed the majority of DDR1 in confluent MDCK cells to be located in adherens junctions. This is in agreement with previous studies reporting DDR1 to interact with and stabilise E-cadherin in cell-cell junctions[81]. Junctional DDR1 could affect ROCK signalling by acting as a scaffold for proteins inhibitory of RhoA-ROCK signalling such as RhoGAPs or by excluding positive regulators such as RhoGEFs. I did not see any effect of DDR1 inhibition on the distribution of the RhoA-activating proteins p114RhoGEF and GEFH1 (data not shown), suggesting that these are not the link between DDR1 and ROCK signalling in MDCK cells. DDR1 has previously been connected to regulation of small RhoGTPases, however, results are inconsistent and appear to vary between different cell types. A study in MDCK cells reports that DDR1 can reduce β1-integrin-dependent increases in Cdc42 and Rac activity in response to collagen I stimulation[70]. In contrast, a study in MDA-MB-231 cells reports DDR1 to increase Cdc42 activity through the RhoGEF TUBA leading to formation of matrix-degrading linear invadosomes[76]. The effect of DDR1 on Cdc42 was found to be independent of DDR1 kinase activity in MDA-MB-231 cells[76], whereas it was attributed to kinase activity of DDR1 in MDCK cells[70]. In Th17 T-cells, collagen

increases RhoA-ROCK signalling in a DDR1-dependent manner[157], which is in contrast to the study in A431 cells[77] and our observations in MDCK cells, which both suggest a ROCK-supressing function of DDR1. A known downstream signalling molecule of DDR1 in MDCK cells is the phosphatase Shp2, which binds phosphorylated DDR1 and mediates DDR1 signalling[67]. Interestingly, Shp2 has been reported to supress RhoA activity in MDCK cells through inhibition of the RhoGEF Vav2[158]. Vav2 is predicted to interact with DDR1[51], and DDR1 could thus promote the RhoA-inhibitory effect of Shp2 at cell-cell junctions by bringing the two proteins into proximity of one another in this location. It would be interesting to assess whether DDR1 inhibition affects the distribution of Vav2 and whether Shp2 is required for DDR1-mediated suppression of ROCK activity at cell-cell junctions.

How DDR1 supresses ROCK activity in MDCK cells will need further attention in the future. Imaging with biosensors for active RhoA such as Anillin-based sensors[159] or FRET-probes[160] could be used to examine if DDR1 inhibition causes an increase in junctional RhoA activity or whether DDR1 suppresses ROCK in a RhoA-independent manner. Similarly, biosensors for ROCK activity[161] could allow for more thorough evaluation of changes in the spatial regulation of ROCK activity and would provide temporal information to understand at what stages of cell polarisation and homeostasis DDR1 affects ROCK activity.

Cytoskeletal organisation is crucial during polarisation, and it is thus not surprising that modulation of RhoA-ROCK signalling can affect this process. Indeed, inhibition of RhoA-ROCK signalling has previously been reported to rescue cystogenesis in MDCK cells where polarity has been disrupted by inhibiting the function of β1-integrin[24,37,162], α2-integrin[162] , PKCα/β[37] or ARF6[163]. In our setup, the disruptive effect of

increased ROCK signalling in the absence of DDR1 signalling appeared to mainly rely on increased actomyosin contraction, since the myosin II inhibitor blebbistatin had similar effects to inhibition of ROCK. This is in contrast to a study which reports that excessive RhoA-ROCK signalling disrupts establishment of polarity in MDCK cells by stabilising NHERF1/Ezrin/GP135 complex at the cell-ECM interface[37]. This difference in modality of ROCK signalling in establishment of polarity may be due to differences in the nature of 3D matrices used. In the mentioned study, Matrigel matrices were used[37], whereas collagen I is used here. Indeed lumen formation has been reported to occur through different mechanisms in MDCK cells cultured in Matrigel or collagen I[164]. These two matrix types vary with regards to matrix stiffness, which confers different requirements for regulation of cytoskeletal tension on the cells[151]. Furthermore, different ECM components are present in the two matrices (collagen I versus laminin and collagen IV), which means that different sets of ECM receptors will provide input in the two scenarios.

How signalling from DDR1 cooperates with other ECM receptors is unclear and depends on the cell type studied. Activation of DDR1 is independent of integrins, but the two receptors appear to modulate each other's downstream effects[48]. In MDCK cells, integrins and DDR1 have been reported to have opposing roles[23]. One study found β1-integrin to increase endocytosis of E-cadherin upon DDR1 knockdown, whereas DDR1 promoted stability of junctional E-cadherin[82]. Similarly, DDR1 suppresses STAT3-phosphorylation induced by β1-integrin[67]. Another study reports that DDR1 suppresses cell spreading, whereas α2β1-integrin promotes it[70]. Since integrins also have been shown to regulate RhoA-ROCK signalling[24,37,162], it would be interesting to study whether this is another pathway on which DDR1 and β1-integrin converge. Integrins have mainly been found to inhibit RhoA-ROCK signalling in MDCK cells. However, given that the majority of DDR1 localises to junctions, whereas β1-integrin mainly is present at the

basal membrane domain, it may be that inhibition of either DDR1 or β1-integrin skews the spatial distribution of RhoA-ROCK activity. It would be interesting to study whether additional inhibition of β1-integrin affects the phenotype of DDR1 inhibition and vice versa.

It was surprising that inhibition of ROCK appeared to prevent basal localisation and collagen degradation by MT1-MMP, since ROCK signalling has not previously been found to regulate trafficking of MT1-MMP in epithelial cells. A study in endothelial cells reports an opposite effect of ROCK, with inhibition causing increased expression and surface localisation of MT1-MMP[165]. The ROCK target LIMK has been found to control recruitment of cortactin to MT1-MMP positive endosomes in MDA-MB-231 cells. This recruitment of cortactin is required for surface delivery of MT1-MMP and formation of invadopodia[166]. It may thus be that ROCK activity affects trafficking of MT1-MMP positive vesicles through activation of LIMK. It would be interesting to investigate if the association of cortactin and MT1-MMP is affected by inhibition of DDR1 and whether inhibition of LIMK affects localisation and collagen degradation by MT1-MMP in MDCK cells.

In conclusion, this chapter revealed that ROCK is an important downstream target of DDR1 with implications for epithelial cells to establish polarity in 3D matrices. In the next chapter, I explore whether the role of DDR1 in the mammary epithelium could involve such suppression of ROCK signalling.

Chapter 5 DDR1 contributes to morphogenesis and differentiation of mammary epithelium

5.1 Introduction

The mammary gland epithelium consists of two cell layers: Luminal epithelial cells form the inner layer of alveoli and are the cells responsible for milk production and secretion during lactation[167]. Basal to the luminal epithelial cells, a layer of myoepithelial cells resides on a basement membrane. These cells are responsible for creating the contractile activity to push milk from alveoli through the ductal tree to be secreted to the exterior of the body[167]. Myoepithelial cells are furthermore the source of laminin-111, which is thought to be a major driver of apicobasal polarisation and differentiation of luminal epithelial cells[167].

Post-natal development of the mammary gland can be divided into two phases, which both involve branching tubular morphogenesis; the first happens during puberty and is characterised by ductal growth and early development of alveoli. The second phase happens during pregnancy and postpartum where alveoli grow, expand and differentiate to produce milk, followed by involution once lactation subsides[168]. Interestingly, the DDR1-null mouse has been reported to display defects in both phases[30]. During puberty, a delay in ductal growth is observed, whereas a more pronounced phenotype is present during pregnancy and lactation. In this phase mammary glands of DDR1-null mice fail to undergo proper remodelling and differentiation and remain largely composed of adipocytes. Alveoli in the lactating DDR1-null mice are condensed, produce less milk and enter involution early, thus rendering the mice unable to sustain viable offspring[30]. These changes to epithelial organisation in the DDR1-null mouse made us speculate, whether the observations in epithelial cell lines *in vitro* may be reflected in the *in vivo* phenotype of the DDR1-null mouse. Given that DDR1-null mice are viable and relatively healthy, the complete disorganisation of polarity seen *in vitro* may be moderated by compensatory mechanisms in the *in vivo* situation. However, it is possible that impaired epithelial

polarisation could contribute to incomplete lactogenic differentiation of the mammary gland in DDR1-null mice.

Interestingly, lactogenic differentiation has previously been associated with a decrease in RhoA-ROCK activity in mammary epithelial cells[151,169,170], which led us to ask whether the ROCK-suppressing function of DDR1 in MDCK cells, also may be present in mammary epithelial cells.

In this chapter, I thus aim to investigate if the *in vitro* observation that DDR1 plays a role in epithelial organisation is reflected in the organisation of the mammary glands in DDR1-null mice. I also address, whether a role for DDR1 in lactogenic differentiation could involve suppression of ROCK activity as observed in MDCK cells in the previous chapter.

5.2 Results

5.2.1 Mammary gland tissue from DDR1-null mice has smaller ducts and displays a diffuse distribution of basement membrane markers

Since the phenotype of DDR1-null mice is reported to be most evident during pregnancy-induced remodelling of the mammary gland[30], mammary gland tissue from wild type and DDR1-null mice were analysed 3 days postpartum. Tissue was dissected from wild type and DDR1-null C57Bl/6J females and processed for HE-staining to allow for a comparison of gland architecture. Mammary glands from wild type mice were at this stage filled with dilated alveoli (**Figure 37A**, left). In contrast, the mammary glands of DDR1-null mice were composed of more fat-tissue relative to epithelial structures. Furthermore, alveoli were noticeably smaller in the DDR1-null mice (**Figure 37A**, left). Quantification of the area of alveoli in wild type and DDR1-null mice showed that the mean size in DDR1-null mice was decreased to approximately a third of the alveoli size in wild type animals (**Figure 37A**, right). This difference was however not significant

(p=0.1), possibly due to the low number of animals used (n=3 for each genotype). The decrease in alveolar size and increase in fat tissue in DDR1-null mice corresponds to the previous reports on involvement of DDR1 in lactogenic remodelling of the mammary gland[30,31].

Lack of DDR1 thus appears to affect epithelial organisation *in vivo*. Since epithelial polarity was affected by DDR1 inhibition *in vitro*, I next asked whether lack of DDR1 would affect the apicobasal distribution of molecules in the mammary gland. To evaluate this, mammary gland tissue sections from lactating mice were stained for collagen IV and laminin as markers of the basement membrane. Collagen IV was localised continuously along the basal side of alveoli in the wild type mammary glands in correspondence with the expected distribution of basement membrane components (**Figure 37B**). In contrast, the staining pattern in DDR1-null mice was more diffuse and had a punctate distribution along the basal side of cells with increased occurrence of intracellular staining (**Figure 37B**). Similar observations were made for laminin, which also appeared to have a disorganised distribution in DDR1-null glands compared to wild type (**Figure 37C**). This suggests that the organisation of the basement membrane in the mammary epithelium is disturbed in DDR1-null animals.

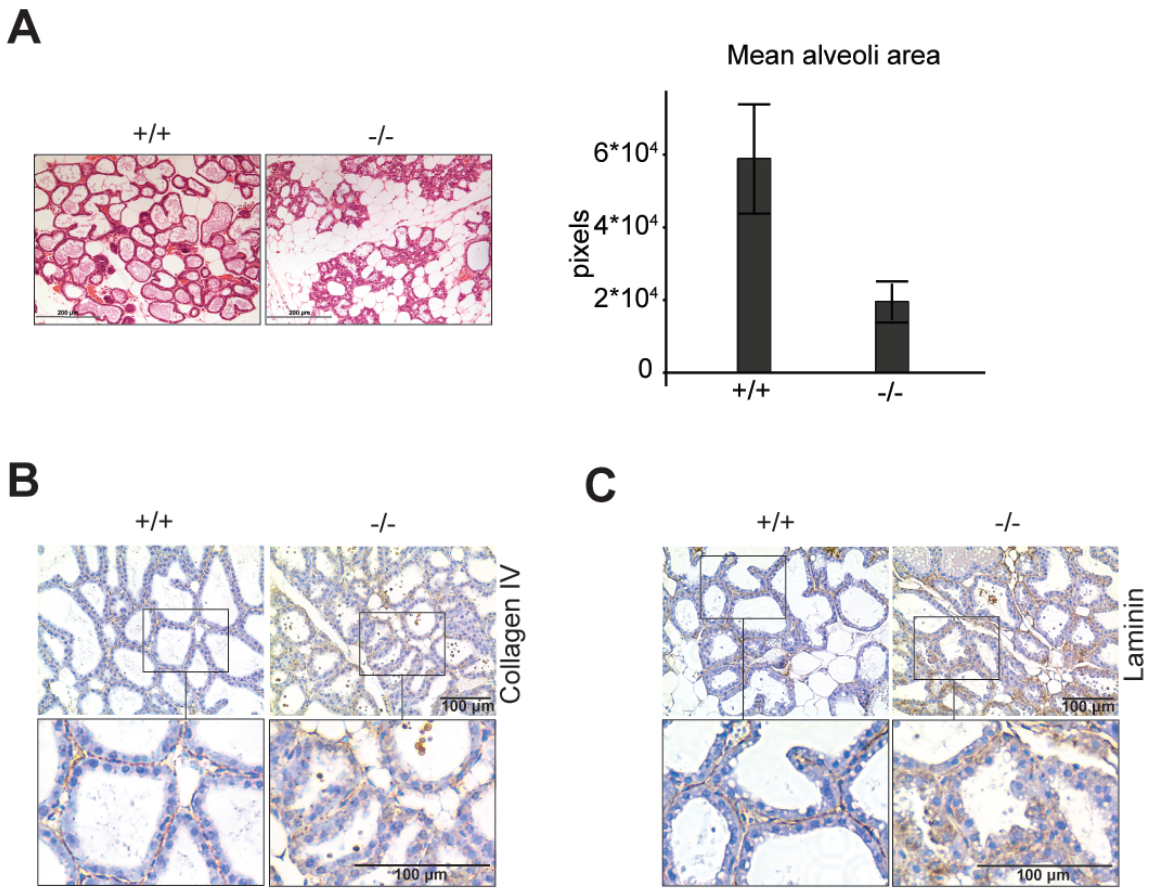


Figure 37. DDR1-null mice have altered epithelial organisation in the mammary gland. The 4th pair of mammary glands from wild type and DDR1-null female C57Bl/6J mice were dissected out 3 days postpartum and fixed in formalin. All mice were 13-14 weeks old. Tissue was embedded in paraffin and processed for IHC. **A)** Left: Tissue sections from wild type (+/+) and DDR1-null (-/-) mice were compared. Images were captured on a widefield microscope. White balance was adjusted using Photoshop software. Scale bars represent 200 µm. Right: The areas of mammary alveoli were measured using ImageJ. The mean alveoli area was determined for 3 wild type (+/+) and 3 DDR1-null (-/-) mice and the mean area of the 3 mice plotted as a bar graph. Error bars represent standard error of the mean. A Wilcoxon rank sum test was applied to compare the means, yielding a non-significant p-value of 0.1. Note that sample size is small (n=3). **B)** Tissue sections were rehydrated and antigen retrieval performed by heating slides to 95˚C in citrate buffer for 20 minutes. After a blocking step, sections were incubated in primary antibody against collagen IV at 4˚C overnight. On the next day, sections were incubated with biotinylated secondary antibody, followed by avidin/biotin/HRP complex and developed using DAB substrate. Sections were counterstained with haematoxylin. Images were captured using a 40X objective on a widefield microscope. White balance was adjusted using Photoshop software. Representative images are shown. **C)** Sections were stained and analysed as in **B)**, except a primary antibody against laminin was used.

5.2.2 Inhibition of DDR1 attenuates branching morphogenesis of primary mammary organoids

In contrast to the *in vitro* situation where epithelial cells alone undergo tubulogenesis in a homogenous collagen I matrix, *in vivo* remodelling of the mammary gland occurs in interaction between many cell types in a complex ECM environment[171]. The phenotype of DDR1-null mice could thus be caused by loss of DDR1 signalling in a

number of cell types. To investigate if there is an intrinsic requirement for DDR1 signalling in primary mammary epithelial cells undergoing branching morphogenesis, I isolated mammary organoids from wild type mice as outlined in **Figure 38A**. The isolated epithelial fragments from wild-type mice were embedded in a mixed matrix of Matrigel and collagen I and stimulated with bFGF to induce branching morphogenesis in the presence or absence of GM6001 (10 μM) or DDR1-IN-1 (0.5 μM). Epithelial organoids reorganised into round structures after overnight incubation. Control organoids remained like this during 9 days culture (**Figure 38B**, left). In contrast, bFGF treatment induced branching morphogenesis in around 50% of the organoids at around 5 days, while the remaining 50% of organoids remained as rounded structures similar to control organoids (**Figure 38B**). In this setup, branching morphogenesis was MMP-dependent as GM6001 treatment caused a 76% reduction in branching morphogenesis (**Figure 38B**, right). Interestingly, DDR1-IN-1 treatment also reduced branching morphogenesis by 47% compared to bFGF-treated organoids (**Figure 38B**, right). This suggests that morphological remodelling of the mammary gland involves DDR1 signalling in the epithelial cells.

Organoids were not compared between wild type and DDR1-null mice. This was due to a large variation observed between organoid preparations from different mice, which would make it difficult to determine if a potential difference between 2 organoid preparations in fact are due to DDR1 status. Comparison between DMSO and DDR1-IN-1-treated organoids from the same preparation allows for isolated evaluation of the effect of DDR1 inhibition.

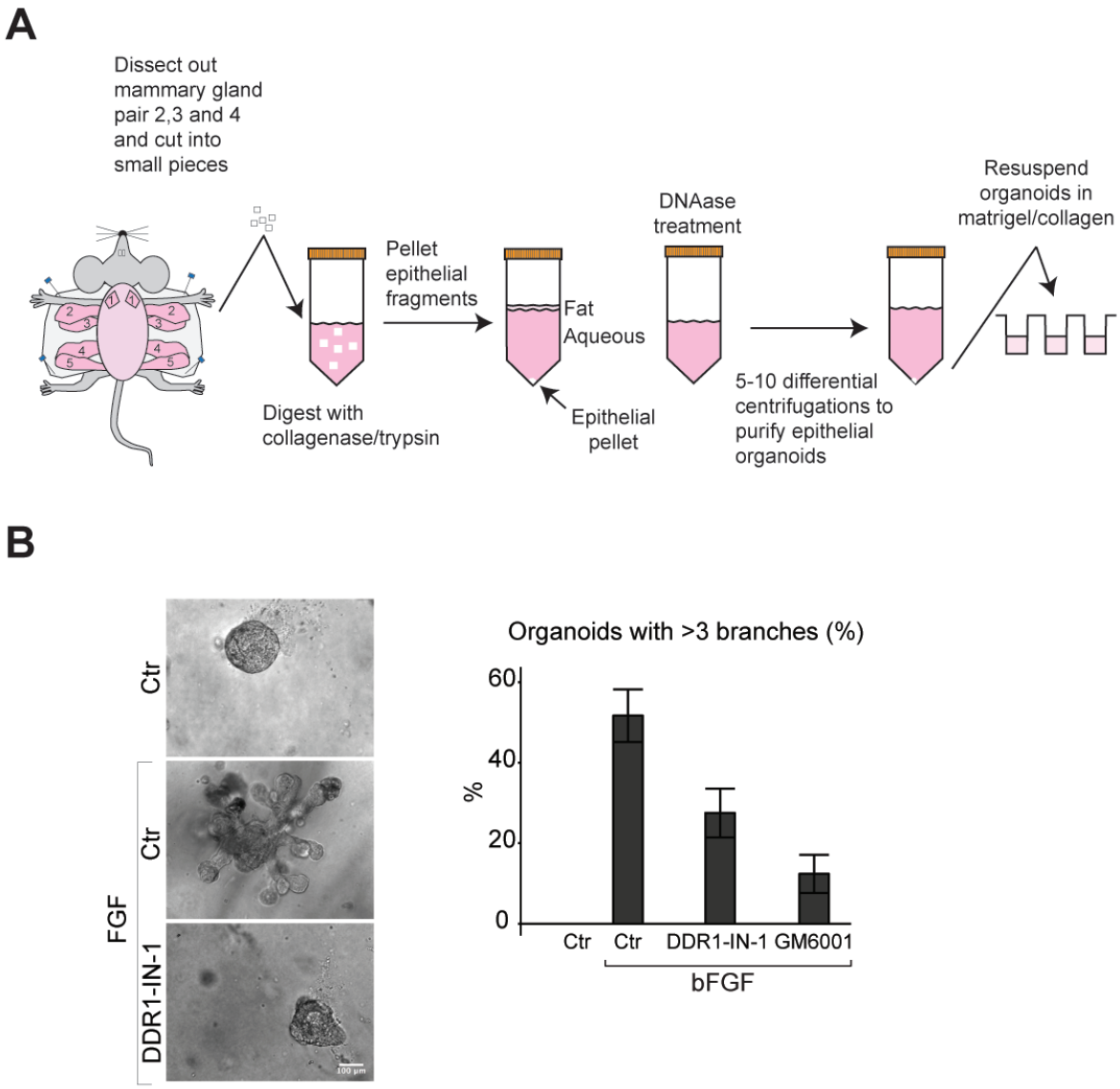


Figure 38. DDR1 inhibition attenuates branching morphogenesis of primary, mammary epithelial organoids. A) The 2nd, 3rd and 4th pair of mammary glands were dissected from two wild type female C57Bl/6J mice between 12-13 weeks of age. The glands were cut into smaller pieces and collagenase-treated before pelleting of epithelial fragments. These were then treated with DNase to avoid clumping, followed by 5-10 differential centrifugations to purify epithelial fragments from stromal cells. Finally the pellet of epithelial organoids was resuspended in a 1:2 mixture of Matrigel and collagen I at a density of 1000 organoids/ml. Solidified gels were overlaid with organoid medium (DMEM/F12 medium with 1X ITS supplement (insulin/transferrin/selenium) with or without bFGF (2.5 nM), DDR1-IN-1 (0.5 µM) and GM6001 (10 µM) as indicated. **B**) Left: Organoids were derived and cultured as described in A). Images were captured after 9 days using a 20X objective on a widefield microscope. Representative images are shown. Right: The percentage of organoids undergoing branching morphogenesis was done by categorising structures in images captured throughout the well (33-70 images per condition), based on the presence of 3 or more branches or less than 3 branches. The average percentage from 3 independent experiments is plotted in the bar graph with error bars representing standard deviation.

5.2.3 DDR1 inhibition attenuates formation of mammospheres by HC11 cells in response to lactogenic stimulation in a ROCK-dependent manner

A role for DDR1 in remodelling of mammary epithelial cells could affect the ability of these cells to undergo lactogenic differentiation, since this process relies on morphogenic events[168,172]. I therefore examined whether DDR1 inhibition affects lactogenic differentiation. To study this, I employed HC11 cells, which are a clonal derivative of the COMMA-1D mouse mammary epithelial cell line. HC11 cells were derived based on their ability to differentiate and produce milk proteins upon stimulation with prolactin. These cells are thus a useful model of lactogenic differentiation[173]. Similar to *in vivo*, lactogenic differentiation of HC11 cells has a morphogenic component with HC11 cells forming dome-shaped 3D structures termed "mammospheres" when treated with lactogenic stimuli[174]. This formation of mammospheres is a visible readout of the degree of lactogenic differentiation[174].

To induce lactogenic differentiation, HC11 cells were first cultured to complete confluence in the presence of EGF for 5 days. EGF was then removed for 24 hours to make cells competent to respond to lactogenic differentiation medium containing prolactin, insulin and dexamethasone (DIP medium). As previously reported[174], mammospheres could be observed after 3 days with numbers increasing until the experiment was terminated at day 5 (**Figure 39A**). Confocal microscopy of DIP-treated HC11 cells stained for actin and DAPI confirmed that mammospheres are dome-shaped structures with a closed, hollow lumen (**Figure 39B**). To analyse the role of DDR1 in the response to lactogenic stimulation, I compared the number of mammospheres per field between control cells and DDR1-IN-1-treated cells. Interestingly, inhibition of DDR1 significantly decreased the number of mammospheres formed (**Figure 39C**), suggesting that DDR1 indeed affects the morphogenic response to lactogenic differentiation.

Given the importance of ROCK suppression by DDR1 for cystogenesis of MDCK cells, I next asked whether the role of DDR1 in mammosphere formation involves suppression of ROCK activity. The effect of the ROCK inhibitor H1152 on DDR1-IN-1-treated cells was therefore evaluated. Interestingly, additional inhibition of ROCK improved the ability of the cells to form mammospheres in the presence of DDR1-IN-1 (**Figure 39C**). This observation suggests that DDR1-mediated suppression of ROCK activity is important during lactogenic differentiation. However, inhibition of ROCK activity on its own also increased the formation of mammospheres to a level higher than that observed for control cells (**Figure 39C**). It is thus also possible, that the improvement of mammosphere formation by ROCK inhibition in DDR1-IN-1-treated cells is the sum of positive effects from ROCK inhibition and negative effects from DDR1 inhibition.

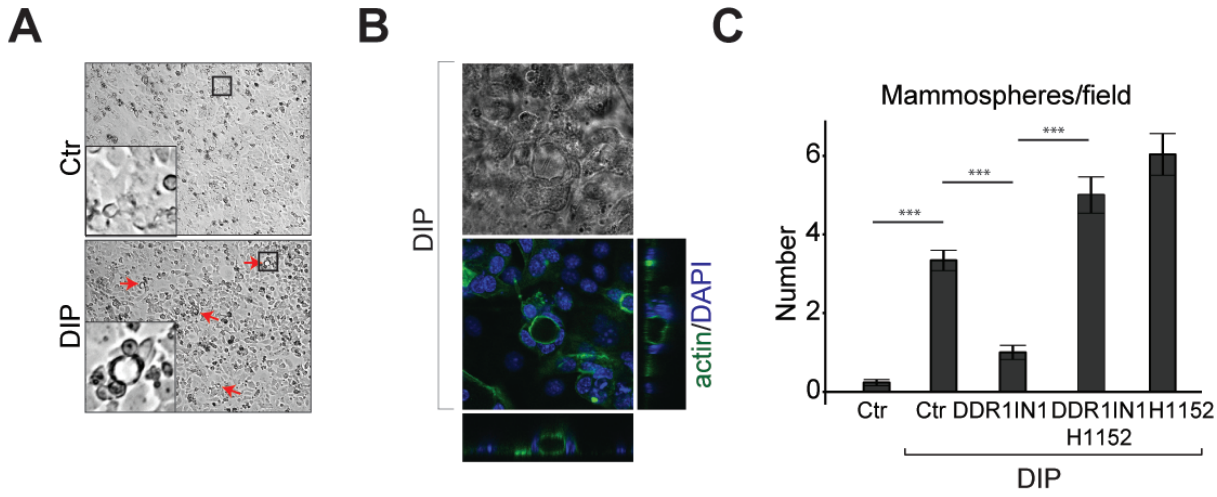


Figure 39. Inhibition of ROCK rescues attenuated mammosphere formation upon inhibition of DDR1 signalling. A-C) HC11 cells were cultured at confluence for 5 days in RPMI 1640 with 10% FCS, 5 µg/ml Insulin and 10 ng/ml epidermal growth factor (EGF) and DMSO, DDR1-IN-1 (1 µM) and/or H1152 (4 µM) as noted in the figure. Medium was replaced with EGF-free medium with appropriate inhibitors and culture continued for a further 24 hours. To induce lactogenic differentiation, medium without EGF, but containing dexamethasone (10 µM), insulin (5 µg/ml) and prolactin (5 µg/ml) was added (DIP medium) in the presence of appropriate inhibitors. Images to follow mammosphere formation were captured 5 days after addition of DIP medium using a 10X objective on a widefield microscope. >3 independent experiments were performed. **A**) Representative brightfield images of control cells in the absence or presence of DIP medium shown. **B**) HC11 cells were cultured as described, except in IBIDI µ-slide wells. 5 days after DIP addition, samples were fixed and stained for actin and DAPI. Confocal images were captured using a 60X objective on a CLSM. Images were processed in ImageJ. XY, XZ and YZ sections from a representative confocal stack are shown. **C**) Formation of mammospheres under different conditions was compared. The mean number of mammospheres per field for each condition was counted on day 4 after adding DIP medium. Graph represents the mean of 3 independent experiments. A Kruskal test followed by a pairwise Wilcoxon test with Holm correction for multiple testing was used to locate significant differences. *** represents p-values<0.001. Additional significant changes in addition to the plotted ones can be found in **Table S2**, Section **8.1**.

5.2.4 DDR1 inhibition causes increased ROCK activity in HC11 cells

To clarify whether DDR1 acts through suppression of ROCK in HC11 cells or whether the two molecules affect mammosphere formation independently, I next examined the level of ppMLC in the presence of DDR1-IN-1. Since the cytoskeleton of HC11 cells in monolayers is disorganised compared to MDCK cells, changes to the apicobasal distribution of ppMLC are difficult to examine by immunocytochemistry. Instead, the total level of ppMLC in HC11 cells was examined by Western blot. HC11 cells were induced to form mammospheres for 5 days as in the previous section and whole cell lysates were analysed. Induction of lactogenic differentiation with DIP medium resulted in slightly lower amounts of ppMLC compared to HC11 cells left unstimulated (**Figure 40A** and **B**). Interestingly, DDR1-IN-1 treatment in HC11 cells treated with DIP medium led to a noticeable increase in the total amount of ppMLC, which disappeared upon treatment with H1152. This suggests that lack of DDR1 signalling indeed does increase ROCK activity in this setup (**Figure 40A**). A quantification of the band intensities from 5 experiments confirmed this pattern (**Figure 40B**). It is thus plausible that DDR1-mediated suppression of ROCK activity contributes to the response of mammary epithelial cells to lactogenic differentiation.

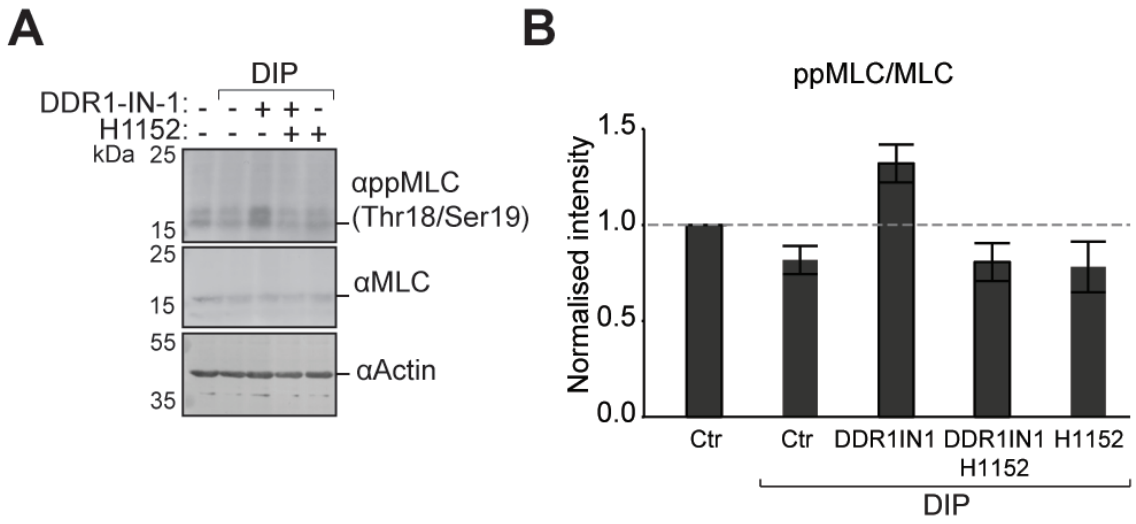


Figure 40. Inhibition of DDR1 increases ROCK activity in HC11 cells. HC11 cells were cultured at confluence for 5 days in RPMI 1640 with 10% FCS, 5 µg/ml insulin and 10 ng/ml epidermal growth factor (EGF) and DMSO, DDR1-IN-1 (1 µM) and/or H1152 (4 µM) as noted in the figure. Medium was replaced with EGF-free medium with appropriate inhibitors and culture continued for a further 24 hours. To induce lactogenic differentiation, medium without EGF, but containing dexamethasone (10 µM), insulin (5 µg/ml) and prolactin (5 µg/ml) was added (DIP medium) in the presence of appropriate growth factors. 5 days after addition of DIP medium, cells were lysed in the presence of the Thr/Ser phosphatase inhibitor okadaic acid. Lysates were immediately subjected to Western blot with primary antibodies against ppMLC, MLC and actin. **A**) Western blot from one of 5 independent experiments is shown. **B**) Band intensities were quantified from 5 experiments using ImageJ and intensities normalised to undifferentiated control cells. The average of 5 experiments is plotted in the bar graph with error bars representing standard error of the mean. The tested conditions were compared with a Kruskal-Wallis rank sum test (p=0.02666) before localising differences with a pairwise Wilcoxon test with Holm correction of the p-value to correct for multiple testing. No statistically significant differences were found.

5.2.5 ROCK inhibition promotes production of β-casein in the absence of DDR1 signalling

To test whether attenuated formation of mammospheres by DDR1-IN-1 corresponds to decreased lactogenic differentiation, the production of the milk component β-casein was examined. Unfortunately, I was unable to detect β-casein expression at protein level in cell lysates. This may be due to low expression level, secretion of the protein into the medium or low sensitivity of the primary antibody used. Instead, I evaluated β-casein expression on mRNA level by RT-PCR. HC11 cells were stimulated with DIP medium in the presence of DMSO, DDR1-IN-1 and/or H1152 as described in the previous section. 5 days after DIP stimulation, total RNA was extracted and reverse transcribed into cDNA for detection of β-casein and GADPH as a housekeeping control. Stimulation with DIP medium led to an increase in expression of β-casein (**Figure 41A**

and -**B**). This increase was reduced by 44% when HC11 cells were cultured in the presence of DDR1-IN-1, confirming the role of DDR1 signalling in lactogenic differentiation. Similar to the observations for mammosphere formation, inhibition of ROCK activity restored expression of β-casein in the presence of DDR1-IN-1 and on its own increased levels of β-casein 3 fold relative to the differentiated control HC11 cells (**Figure 41A** and -**B**). The pattern of the β-casein expression under the conditions tested (**Figure 41B**) corresponds to that of mammosphere formation (**Figure 39C**), confirming that mammosphere formation correlates with the extent of lactogenic differentiation[174].

These data suggest a role for DDR1 in the morphogenic aspects of lactogenic differentiation with consequence for expression of the milk component β-casein. Furthermore, consistent with the findings in MDCK cells, regulation of ROCK activity appears to be a crucial downstream effect of DDR1 signalling in the mammary gland.

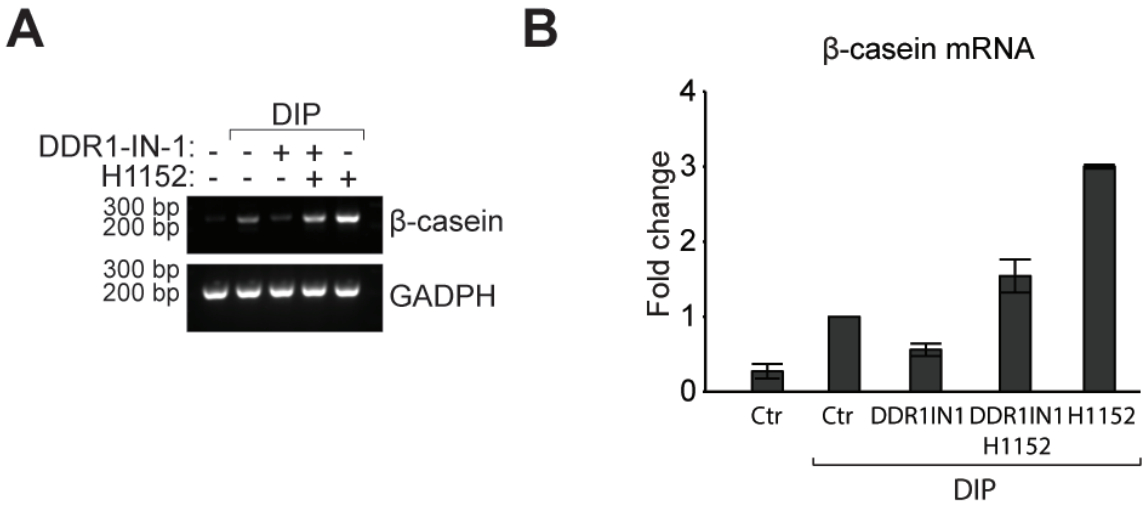


Figure 41. Inhibition of ROCK rescues DIP-induced β-casein expression in the absence of DDR1 signalling. A) HC11 cells were cultured as described in **Figure 39** in the presence of appropriate inhibitors. After 5 days DIP stimulation, RNA was extracted and reverse transcribed into cDNA. Transcripts encoding β-casein and GADPH were examined by PCR. Representative result is shown. **B**) Intensities for PCR products representing β-casein relative to GADPH were analysed using ImageJ and the ratio for each condition normalized to differentiated control cells. The mean of 3 independent experiments is plotted in the bar graph with error bars representing standard error of the mean. The tested conditions were compared with a Kruskal-Wallis rank sum test (p=0.009777) before localising differences with a pairwise Wilcoxon test with Holm correction of the p-value to correct for multiple testing. No statistically significant differences were found.

5.2.6 β-casein staining is not decreased in lactating DDR1-null mice

Given the decrease in β-casein mRNA expression upon DDR1 inhibition in the HC11 cell system, I next examined the expression of β-casein in the mammary glands of lactating DDR1-null mice. Mammary gland tissue from wild type and DDR1-null females 3 days postpartum was analysed by IHC for β-casein. Wild type tissue showed strong staining along the apical cell surface towards the alveolar lumens (**Figure 42**). Unexpectedly, a similar pattern was observed in DDR1-null tissue with no apparent difference in staining intensity (**Figure 42**). As described previously, DDR1-null glands were richer in fat tissue and had smaller alveolar size compared to wild type tissue, despite still producing β-casein. A potential cause for this finding is that production of different milk components have different requirements and time scales[168]. It may thus be that β-casein is not the right milk component to investigate in order to see differences between wild type and DDR1-null mice. This topic will be addressed in more detail in the following discussion.

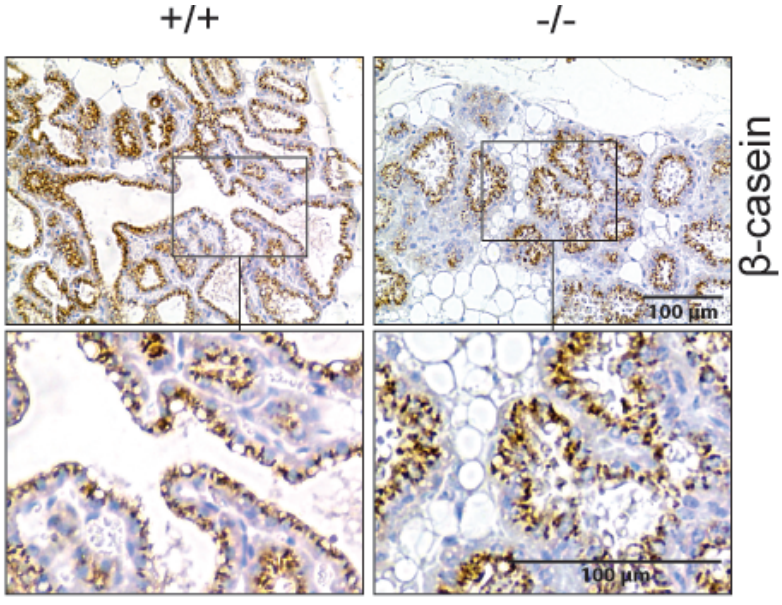


Figure 42. β-casein expression is not decreased in lactating DDR1-null mice. Tissue was harvested and processed as in **Figure 37**. Tissue sections from lactating wild type (+/+) and DDR1-null (-/-) mice were stained with a primary antibody against β-casein and counterstained with haematoxylin. Images were captured using a 40X objective on a widefield microscope. White balance was adjusted using Photoshop software. Representative images are shown.

5.3 Discussion

In line with previous studies[30,31], data in this chapter find a disorganisation of the epithelium in the lactating mammary glands of DDR1-null mice. This suggests that the role of DDR1 in epithelial morphogenesis and polarisation *in vitro* indeed is reflected *in vivo*. Since DDR1 inhibition attenuated branching morphogenesis of primary, epithelial organoids, the function of DDR1 in the mammary gland appeared to be intrinsic to the epithelial cells (**Figure 38**). Such cell-autonomy of DDR1 function was previously shown by transplantation of mammary epithelial tissue from pregnant DDR1-null mice into the cleared fat pad of pregnant wild type mice[31]. This resulted in defects in branching morphogenesis comparable to those observed in mammary glands of DDR1-null mice[31]. Accordingly, DDR1 localises in the luminal epithelial cells during lactation[30]. I was unable to examine DDR1 distribution due to the non-specific nature of the antibody used. It would be interesting to follow the expression and distribution of DDR1 during different stages of lactogenic differentiation *in vivo* upon identifying a specific DDR1 antibody.

In contrast to the phenotype of DDR1 inhibition in MDCK cells in 3D collagen, the overall structure of alveoli with lumens is preserved in DDR1-null mammary tissue. Alveolar structures, however, appeared smaller and less organised than in wild type mice (**Figure 37**). It is possible that other ECM receptors can compensate for loss of DDR1 *in vivo*. It is not known whether lack of DDR1 affects the organisation of luminal and myoepithelial cells in the mammary gland. This could be addressed by IHC for cell-type specific markers such as α-smooth muscle actin (α-SMA) or cytokeratin-5/14 for myoepithelial cells and cytokeratin-8/18 for luminal epithelial cells[175].

IHC data indicated a disorganised distribution of the basement membrane components laminin and collagen IV in DDR1-null mice. This could be due to disturbed

polarised secretion of these components or interferance with their assembly into a basement membrane (**Figure 37B** and **-C**). It would be interesting to investigate this further. Changes in polarised secretion could be revealed by analysing the apical and basal medium from cells growing in culture inserts for secreted matrix components. Additionally, the effects of DDR1 on deposition and assembly of a basement membrane could be evaluated by following the deposition of GFP-tagged laminin. Since no differences in staining intensity of laminin or collagen IV were observed in DDR1-null tissue sections (**Figure 37B** and **C**), DDR1 is less likely to affect the expression level of these components. This could however be addressed by examining whether DDR1 inhibition affects mRNA/protein levels of matrix components in epithelial cells.

Since the basement membrane provides cues for orientation of apicobasal polarity[20], failure to correctly assemble a basement membrane could affect mammary gland function in DDR1-null mice. Laminin in particular has been implicated in lactogenic differentiation and is required, in addition to prolactin receptor (PrlR) activation, for the sustained activation of STAT5, which allows for milk protein transcription[168,176,177]. Disorganised laminin deposition in the absence of DDR1 could thus influence lactogenic signalling. DDR1 has indeed been reported to affect prolactin-induced STAT5 activation. DDR1 overexpression in HC11 cells thus promoted STAT5 phosphorylation and β-casein expression, whereas primary DDR1-null cells failed to activate STAT5[31]. This was suggested to involve a transient interaction between DDR1 and STAT5b leading to activation of STAT5b[31]. In support of such interaction, a proteomic study on human placenta tissue predicts STAT5b to bind phosphorylated tyrosine residues in the kinase and juxtamembrane domains of DDR1[51]. Since STAT5 is a key player in lactogenic signalling which activates transcription of β-casein and genes

involved in morphogenesis[176,178], failure to activate STAT5 may contribute to the mammary gland phenotype of DDR1-null mice.

Morphogenic events are tightly linked to lactogenic differentiation, and reorganisation of mammary epithelial cells into alveolar-like structures including mammospheres correlates with lactogenic differentiation[168,176,179]. Accordingly, my results in HC11 cells revealed that DDR1 inhibition interfered with formation of mammospheres and activation of β-casein transcription (**Figure 39** and **Figure 41**). A role of DDR1 in epithelial morphogenesis could thus also contribute to lactogenic differentiation. A way in which alveolar architecture can enhance lactogenic differentiation is by increasing exposure of the PrlR to prolactin[168,176]. This increased exposure of PrlR is due to the reorientation of the basal cell membrane (where PrlR localises) towards the prolactin-containing medium in cells in mammospheres. In contrast, cells in a monolayer orient the basal membrane towards the bottom of the dish. The importance of the distribution of PrlR matching the spatial availability of prolactin has been demonstrated in Eph4 mammary epithelial cells growing in culture inserts[176]. These cells express PrlR at their basal surface, and accordingly, application of prolactin in the basal medium induces β-casein expression, whereas prolactin in the apical medium does not[176]. Decreased mammosphere formation upon DDR1 inhibition may thus decrease activation of the lactogenic signalling cascade by reducing exposure of PrlR to prolactin. Despite the restricted access of prolactin to PrlR in monolayers of HC11 cells, some activation of signalling is likely to occur, since DIP medium is able to induce mammosphere formation from monolayers of HC11 cells, when initially added to induce differentiation.

Similar to in MDCK cells, the role for DDR1 in lactogenic differentiation *in vitro* involved suppression of ROCK activity (**Figure 39**, **Figure 40** and **Figure 41**). Since lactogenic differentiation requires both remodelling of cell junctions, cell migration and polarisation[178], it is not surprising that regulators of cytoskeletal dynamics are implicated. Indeed, disruption of the actin or microtubule cytoskeleton have been reported to prevent prolactin-induced β-casein expression in primary, mammary epithelial cells[180]. Suppression of ROCK activity has previously been found to positively affect lactogenic differentiation of the mammary epithelium[151,169,170]. The role of ROCK signalling in lactogenic differentiation may relate to its function in controlling cytoskeletal tension according to the stiffness of the surrounding ECM[151]. ECM stiffness affects the ability of mammary epithelial cells to differentiate with higher stiffness having inhibitory effects[181]. For example, mammary epithelial cells cultured in a stiff ECM (collagen concentration >1.8 mg/ml) are unable to differentiate and form tubules, while cells in a more flexible ECM can[151]. Interestingly, RhoA-ROCK activity is decreased in cells in a flexible ECM, but remains high in cells in a stiff ECM[151], suggesting that RhoA-ROCK signalling is part of a tension sensory mechanism in mammary epithelial cells[181]. Similar to our findings in Chapter 4, some RhoA-ROCK activity was required for tubule formation, but too high levels were inhibitory[151]. Like tubule formation, prolactin-induced STAT5 signalling is prevented on rigid substrates where ROCK signalling remains high compared to flexible substrates[169]. The importance of RhoA-ROCK signalling being kept low was demonstrated by chemical inhibition of ROCK allowing cells on rigid substrates to respond to prolactin signalling with phosphorylation of STAT5 and transcription of β-casein[169]. This effect of ROCK was related to cytoskeletal tension, since the myosin inhibitor blebbistatin mediated similar effects[169]. It is possible that DDR1 by regulating

ROCK activity contributes to translating extracellular tension into appropriate intracellular responses required for lactogenic differentiation.

Alveologenesis during pregnancy has been reported to involve a change in junctional properties from being relatively permeable during pregnancy to forming a tight seal after birth[182]. Interestingly, RhoA-ROCK signalling has been reported to affect tight junction properties in mammary epithelial cells, as seen by a RhoE-mediated decrease in ROCK signalling being required for sealing of tight junctions[183]. Excessive ROCK activity could thus affect the tight junction closure at the onset of lactogenic differentiation[182]. It would be interesting to examine whether junction integrity is affected during lactation in DDR1-null mice, despite junctional integrity being unaltered in MDCK cells *in vitro* (**Figure 30A**, Chapter 4). Junctional properties can be analysed *in vivo* by injecting a tracer into the mammary ducts and measuring its diffusion into the blood stream[182]. Such studies could reveal whether the reported sealing of the tight junctions at the onset of lactation[182] happens in DDR1-null mice. There appears to be a correlation between increased tight junction leakiness and decreased milk production[182,184]. A potential increase in leakiness in DDR1-null mice could thus negatively affect production of milk.

DDR1-null mice were previously reported to be incapable of lactation based on the failure of DDR1-null females to nurture pups and the presence of less eosinophilic material in alveoli on HE-stainings of lactating DDR1-null mammary glands[30]. Analysis of mammary gland lysates for milk proteins, further revealed a dramatic decrease in an 82 kDa milk protein in DDR1-null mice, whereas a 26 kDa protein (likely corresponding to β-casein) only was slightly reduced[30]. In contrast to this slight decrease in β-casein *in vivo*[30], another study found that primary mammary epithelial cells from DDR1-null mice

produced markedly less β-casein when subjected to lactogenic differentiation *in vitro*[31]. My results showed a similar discrepancy with inhibition of DDR1 reducing the expression of β-casein in prolactin-stimulated HC11 cells *in vitro* (**Figure 41**), while no difference in amount and distribution of β-casein was found *in vivo* (**Figure 42**). It thus appears that the regulation of β-casein expression in *in vitro* systems cannot be directly compared to the *in vivo* situations. The finding that lysates from DDR1-null mice showed different levels of reduction in different milk components[30] indicates that not all milk proteins are co-regulated[168]. It is thus possible, that production of milk proteins other than β-casein could be affected in DDR1-null mice. An example of differentially regulated milk components is the production of β-casein and whey acidic protein (WAP). While laminin and prolactin signalling is sufficient for β-casein expression, WAP expression additionally requires closure of the tight junctions to firmly separate the apical and basal cell surface[185,186]. This is due to apically secreted TGFα inhibiting WAP expression upon activation of its receptor, EGFR, at the basal cell surface[185,186]. This means that an epithelium with leaky junctions (e.g. mammary epithelium during pregnancy[182]) will respond to prolactin with β-casein expression, but WAP expression will be inhibited by TGFα diffusing from the apical to the basal side and activating EGFR[185,186]. Upon lactation, closure of the tight junctions will inhibit this paracellular diffusion and thus allow for WAP expression[168,185,186]. It may thus be, that while β-casein is expressed in the mammary gland of DDR1-null mice, other milk proteins such as WAP, which require additional differentiation-induced remodelling, may not be produced. It would be interesting to examine the expression of other milk components in lactating DDR1-null mammary glands to test this idea.

In conclusion, this chapter confirms a role for DDR1 in guiding morphogenesis in the mammary gland *in vivo*. *In vitro*, this function of DDR1 was found to have consequences for lactogenic differentiation. Similar to the observations in MDCK cells, this role of DDR1 appears to involve suppression of ROCK activity, suggesting that this is an important function of DDR1 in epithelial cells. Future studies should address whether increased RhoA-ROCK signalling indeed can be observed *in vivo* and whether inhibition of ROCK can alleviate phenotypes in epithelia of the DDR1-null mouse.

Chapter 6 General discussion and future prospects

In this thesis, I investigated how signals from the ECM contribute to regulating the polarised distribution of MT1-MMP during epithelial morphogenesis. Through this, I identified the collagen receptor DDR1 as a modulator of the apicobasal localisation of MT1-MMP. Furthermore, I found DDR1 to be required for establishment of epithelial polarity during both MMP-dependent and -independent 3D morphogenesis. This role of DDR1 was at least partly mediated through effects on cytoskeletal organisation via suppression of ROCK activity. A role for DDR1 in guiding epithelial morphogenesis likely contributes its function in the mammary epithelium *in vivo*. Furthermore, this role of DDR1 may be important during epithelial morphogenesis in pathological settings.

In Chapter 3, I confirmed previous findings from our group, which indicate that regulation of the apicobasal distribution of MT1-MMP modulates its activity during physiological cell invasion such as tubular morphogenesis of epithelial cells[93]. This regulatory mechanism is likely important for physiological ECM remodelling during postnatal growth and wound healing. It follows that disturbing this regulatory mechanism may initiate MT1-MMP-driven ECM degradation in pathological conditions by increasing the presence of MT1-MMP at the ECM-abutting surface. This could facilitate matrix degradation and breach of the basement membrane at the invading front of well-differentiated epithelial tumours during early stages of cancer progression. MT1-MMP is indeed well known to promote the invasive behaviour of carcinoma cells[187,188]. Although an EMT-mediated loss of polarity in epithelial tumour cells could bypass the need for pathways that bring MT1-MMP to the basal domain of polarised cells, well-differentiated carcinomas are known to invade without losing their epithelial phenotype. For example, primary and secondary lesions of invading mammary and prostate carcinomas can maintain cell-cell junctions, apicobasal polarity and glandular organisation[189]. It is likely

that such tumours, in order to acquire invasiveness, must either bypass or disrupt the pathways that favour apical localisation of MT1-MMP in physiological settings.

I found signalling from the ECM through the collagen receptor DDR1 to be important for regulating the apicobasal distribution of MT1-MMP in MDCK cells. Inhibition of DDR1 in 2D culture thus disturbed the polarised distribution of MT1-MMP and led to an increase in the enzyme at the basal cell surface (**Figure 18B-C**, Chapter 3). This consequently promoted degradation of an underlying collagen I film (**Figure 19**, Chapter 3). These results in 2D culture were in accordance with preliminary results on the localisation of MT1-pHluorin in MDCK-DDR1ΔC cells in 3D culture. These cells formed aggregates in which MT1-MMP distribution was disorganised and localised along all cell surfaces including cell-cell and cell-ECM interfaces (data not shown). This would cause matrix degradation to occur in a spatially uncoordinated manner. DDR1 may thus play a role in controlling matrix degradation by epithelial cells through spatial regulation of MT1-MMP. This function of DDR1 has not previously been suggested.

In this study, I examined DDR1-mediated regulation of MT1-MMP localisation in MDCK cells. It will be important to investigate if this regulation also takes place in less polarised epithelial cell types such as carcinoma cells. Two previous studies have reported DDR1 to promote formation of linear invadosomes in a kinase-independent manner in MDA-MB-231 and hepatocellular carcinoma cells[76,190]. This role of DDR1 was proposed by the authors to involve recruitment of proteolytic molecules including MT1-MMP to invadosomes[76], however, no data on MT1-MMP distribution was presented. Similarly, another study found DDR1 to promote formation of ECM-degrading invadopodia in pancreatic carcinoma cells, but did not investigate MT1-MMP localisation[191]. It would be interesting to study if DDR1 signalling can affect the recruitment of MT1-MMP to

invasive structures such as invadopodia or lamellipodia in migrating carcinoma cells and whether this modulates the invasive behaviour of the cells.

DDR1 is found to have altered expression level and activity in many cancers with consequences for malignant behaviour[48,59]. For example, increased phosphorylation of DDR1 is seen in non-small cell lung cancer tumours and cell lines[192] and DDR1-null mice are protected in a k-Ras-induced model of lung adenocarcinoma[193]. For pancreatic adenocarcinoma cells, growth of subcutaneous xenografts *in vivo* was associated with a promoting function of DDR1 on cell proliferation/survival[194], whereas resistance to chemotherapy was linked to DDR1 in breast cancer cell lines[68]. A recent study connected DDR1 to metastatic reactivation of breast cancer cells in a manner depending on activation of the pluripotency factor Sox2, which enabled cancer cells to exit dormancy and reactivate self-renewal at metastatic sites[148]. According to a promoting function of DDR1 in metastasis, silencing of DDR1 in this study prevented metastatic colonisation of bone, brain and lung by breast cancer cells[148]. DDR1 has thus been reported to promote malignant behaviour of cancers through various mechanisms, and DDR1 has accordingly been suggested to be a potential therapeutical target[59]. However, some studies have also found decreased DDR1 expression to confer a poor prognosis in epithelial cancers[59]. Given the heterogeneity of reported functions of DDR1 in cancer progression, further studies are required to determine if inhibition of DDR1 may be a valid strategy.

My data suggested DDR1 to be required for epithelial cells to establish apicobasal cell polarity in 3D matrices (**Figure 33**, Chapter 4). Given the importance of establishing and maintaining polarity during epithelial morphogenesis[11,122], this role of DDR1 could contribute to its functions in remodelling of epithelial structures in the mammary gland *in*

vivo[30]. Conversely, altered expression or localisation of DDR1 in a pathological context could disturb polarity. Loss of polarity as part of EMT is considered to enhance the invasive behaviour of cancer cells[89]. However, my results indicated that inhibition of DDR1 in MDCK cells did not cause EMT, since it did not induce single cell migration or weakening of cell-cell junctions (**Figure 22**, Chapter 3 and **Figure 30**, Chapter 4).

In line with a role for DDR1 in organising epithelial polarity, DDR1 has been reported to interact with Par3 and -6 and promote their junctional localisation in carcinoma cells[77,83]. A loss of DDR1 or change in its distribution could thus cause these polarity proteins to function in aberrant locations. Such hijacking of polarity molecules by other signalling pathways is indeed known to occur in malignancy, where mislocalised determinants of apicobasal polarity can contribute to generating front-rear polarity and enhance migration of cancer cells[195,196]. For example, the Par complex can localise at the leading edge of keratinocytes to generate front-rear polarity and promote directional migration[197]. More studies are required to elucidate the significance of DDR1-mediated effects on the localisation of polarity molecules for motility of carcinoma cells. It would furthermore be interesting to study if DDR1 also affects the distribution of Par proteins in MDCK cells, since this could be important for polarisation. Since endogenous levels of many polarity proteins are too low to detect by immunocytochemistry, studies of these molecules (e.g. Par proteins) are frequently performed using exogenously expressed tagged proteins. Combined with tracking of DDR1, such studies can give information on how these proteins affect each other's localisation.

It has been reported that knockdown of DDR1 in pancreatic carcinoma cells can reverse the cell-cell adhesion-promoting effect of knocking down the heterotrimeric G-protein, Gα13, and thereby enhance MT1-MMP-dependent cell migration in a 3D

collagen I matrix[83]. This effect of DDR1 knockdown was found to involve displacement of Par3 from cell-cell junctions and knockdown of Par3 recapitulated the pro-invasive effect of DDR1 knockdown[83]. This is in line with the general notion that displacement or downregulation of polarity complexes enhances invasive behaviour[195,196]. A similar role for DDR1 in ensuring junctional Par3/6 localisation was found in A431 squamous cell carcinoma cells[77]. In these cells, DDR1 knockdown attenuated collective invasion in mixed collagen/Matrigel 3D matrices, but increased single cell migration[77]. My results also showed DDR1 inhibition to prevent collective invasion of MDCK cells, while DDR1 overexpression increased it (**Figure 21**, Chapter 3). However, I did not observe any single cell migration upon inhibition of DDR1 function by kinase inhibitor, knockdown or expression of a dominant negative mutant. Since induction of a mesenchymal, migratory phenotype through EMT is a multifactorial process, the susceptibility to take on this mode of migration depends on the cellular context[89]. For example, normal epithelial cells such as MDCK and HCE cells are resistant to EMT induced by LEF-1 overexpression, whereas DLD1 carcinoma cells readily undergo EMT upon LEF-1 expression[198]. This was attributed to differences in the efficiency of nuclear export of beta-catenin[198]. Similarly, decreased expression of E-cadherin makes epithelial cells more susceptible to EMT[89]. It is thus possible that the less polarised A431 cells are more susceptible to take on a mesenchymal, migratory phenotype than MDCK cells in response to DDR1 inhibition.

Based on the observations above, it is tempting to speculate that the loss or gain of DDR1 signalling can promote distinct types of migration in different cell types. Well-differentiated cancer cells, which must migrate in a collective manner, may thus become more invasive upon overexpression of DDR1, while a poorly differentiated cancer, relying on EMT-induced single cell migration, could invade more efficiently upon loss of DDR1 expression. A systematic analysis of how DDR1 signalling affects 3D invasion by

epithelial cells with varying differentiation status could shed light on how DDR1 affects cell motility in different cellular contexts.

I did not analyse whether the non-polarised aggregates formed in the absence of DDR1 signalling display any migratory behaviour. Motile behaviour was recently demonstrated for similar aggregates of MDCK cells formed upon inhibition of β1-integrin in Matrigel[37]. These aggregates lost apicobasal polarity and displayed apical markers at the ECM-abutting surface. The apical markers (including pERM and GP135) primarily localised at the migrating front of the aggregates, suggesting that the structures had front-rear polarity[37]. β1-integrin was thus suggested to function as a switch between apicobasal and front-rear polarity. Tracking of the aggregates by live cell microscopy showed these structures to be highly motile compared to control cysts with normal apicobasal polarity[37]. Since the study was done in a loose 2% Matrigel matrix, this migratory behaviour did not depend on matrix degradation. It could be interesting to assess whether the disorganised aggregates observed upon inhibition of DDR1 similarly display front-rear polarity and have a motile phenotype.

It is interesting that both inhibition of β1-integrin and DDR1 in MDCK cells in 3D culture results in formation of cell aggregates with disorganised polarity (**Figure 23**)[37]. This highlights the importance of ECM-sensing for establishment of polarity. As discussed in Section **4.3**, Chapter 4, β1-integrin and DDR1 do not directly influence signalling from each other, but do converge on common targets[23]. In MDCK cells, the two receptors frequently have opposite effects on such common targets[23] and a balance between signalling from DDR1 and β1-integrin may thus be important during polarisation. It would be interesting to study the cross-talk between DDR1 and β1-integrin in the context of polarisation.

I found the role of DDR1 in establishment of apicobasal polarity in MDCK cells to include regulation of cytoskeletal organisation through suppression of junctional ROCK activity (**Figure 31**, Chapter 4). Suppression of RhoA-ROCK signalling by DDR1 agrees with the increase in stress fibre formation reported to result from inhibition of DDR1 function[70,71,81]. Since cytoskeletal organisation is a crucial aspect of cell migration and invasion, local modulation of ROCK activity by DDR1 could affect the motility of cells[12,199]. In line with this, DDR1-mediated suppression of ROCK-dependent phosphorylation of MLC along cell-cell junctions was shown to increase coherence between cells within migrating groups of A431 cells and thus enhance collective cell migration[77]. My results on the effect of DDR1 inhibition on ppMLC-distribution suggested that ROCK activity is subject to a similar spatial organisation in MDCK cells (**Figure 31**, Chapter 4). It is thus possible that the role of DDR1 in collective invasion by MDCK cells undergoing tubulogenesis (**Figure 21D**, Chapter 3) also is related to spatial control of ROCK-mediated cytoskeletal tension. To understand the dynamics of DDR1-dependent ROCK regulation during polarisation and invasion in 3D culture, it would be interesting to employ a biosensor for active ROCK[161]. Furthermore, it would be interesting to identify which of the two ROCK isoforms (ROCK1 or -2) is regulated by DDR1, since these can mediate distinct functions[200].

Negative regulation of ROCK by DDR1 in A431 cells was mediated by a DDR1-Par3/6 complex recruiting RhoE to cell-cell junctions to suppress ROCK activity[77]. As discussed in Chapter 4, Section **4.3**, this mode of ROCK suppression did not appear to occur in MDCK cells. Furthermore, while DDR1-mediated regulation of ROCK was independent from its kinase activity in A431 cells, my data indicate that kinase activity of DDR1 is required for ROCK suppression in MDCK cells[77]. Further investigation is required to understand how DDR1 can downregulate ROCK activity in MDCK cells. One

approach to address this question could be identification of interaction partners of DDR1 in MDCK cells through proteomic analysis. This could identify candidate GTPase regulatory proteins that may associate with DDR1 in MDCK cells. It would be interesting to examine if such interactions depend on kinase-activity and phosphorylation of DDR1.

In agreement with my data suggesting DDR1 to suppress ROCK activity specifically at cell-cell junctions, I found the majority of DDR1 to be present in junctions of confluent monolayers of MDCK cells (**Figure 32**, Chapter 4). A role for DDR1 in cell-cell junctions has been reported by several studies as described in Section **1.2.3**, Chapter 1. However, it is not clear if DDR1 mediates distinct functions in cell-cell junctions compared to cell-ECM contacts or how the intracellular distribution of DDR1 is regulated. It has been proposed that E-cadherin sequesters DDR1 in cell-cell junctions in resting polarised epithelial monolayers and that this reduces collagen-induced phosphorylation of the receptor[147]. In contrast, sub-confluent MDCK cells in the active growth phase localised DDR1 to the apical and basal surfaces, where it was activated by collagen[147]. The localisation of DDR1 and thus its exposure to collagen may in this way vary between sub-confluent and confluent epithelial monolayers. The role of E-cadherin and Par3/6 in ensuring junctional localisation of DDR1[77,83,147] could suggest that DDR1 is relocalised in situations where junctions are disassembled. This could for example occur in wound healing or during remodelling of epithelial structures in the mammary gland. Such processes could in this way displace DDR1 from cell-cell junctions and thereby trigger its activity at the basal cell surface. In support of DDR1 playing different roles in confluent and subconfluent epithelial cells, I found DDR1 inhibition to cause an increase in stress-fibres both at the basal cell surface and at junctions in sub-confluent MDCK cells, while the increase in stress-fibres was restricted to cell-cell junctions in confluent

cells (**Figure 31A** and **-C**, Chapter 4). It would be interesting to follow the dynamics of DDR1 localisation in MDCK cells in wound healing assays to test whether migratory behaviour of cells at the leading edge may be associated with non-junctional localisation of DDR1.

In accordance with previous observations, my results suggested that the function of DDR1 in cell-cell junctions was independent of collagen (**Figure 30** and **Figure 31**, Chapter 4)[77]. It is not known whether DDR1 can be phosphorylated in junctions in a collagen-independent manner. An assessment of the phosphorylation status of DDR1 in these distinct locations could provide insight to how DDR1 mediates its function at cell-cell junctions versus cell-ECM interfaces. If DDR1 indeed is active at cell-cell junctions, the mechanism behind such activation will be important to elucidate.

Similar to the role of DDR1 in cystogenesis and tubulogenesis *in vitro*, DDR1 appeared to have a role in remodelling of epithelial structures in the mammary gland *in vivo*. Mammary glands from lactating DDR1-null mice thus displayed smaller alveoli compared to wild type mice and the basement membrane lining alveoli appeared disorganised (**Figure 37**, Chapter 5). Interestingly, the expression of DDR1 in the mammary gland increases during morphogenically active phases such as pregnancy, whereas involution and resting phases of the mammary gland are accompanied by a decrease in DDR1 expression[30]. Upregulation of DDR1 may thus be associated with growth and morphogenesis, whereas downregulation of DDR1 could be associated with a "stop signal" for such processes. Since cancers have been suggested to aberrantly reactivate physiological morphogenesis programmes[199], an association between high DDR1 expression and the onset of active remodelling may be interesting to investigate in the context of elevated DDR1 expression in cancers.

It was interesting to see that regulation of ROCK activity also appeared to be important for the function of DDR1 in mammary epithelial cells undergoing lactogenic differentiation *in vitro* (**Figure 39**, **Figure 40** and **Figure 41**, Chapter 5). It would be exciting to assess whether ROCK activity is altered *in vivo* in the lactating mammary gland of DDR1-null mice, and whether any phenotypes in the DDR1-null mice can be ameliorated by inhibition of ROCK activity.

While inhibition of DDR1 completely disrupted epithelial polarity in MDCK cells, lack of DDR1 did not appear to severely affect polarity of epithelial tissues *in vivo*. DDR1-null mice are thus viable and apart from the mammary gland, preliminary examination of HE-stained sections from epithelial organs including kidney, lung and intestine by light microscopy did not reveal obvious changes in the organisation of epithelial structures. More detailed analysis by IHC for specific molecules or analysis by electron microscopy may reveal phenotypes in these organs. Analysis of mammary gland morphology suggested that despite the increased presence of fat tissue and alveoli being smaller, the overall glandular organisation is preserved in DDR1-null mice. This relatively mild phenotype may be attributed to other ECM receptors compensating for the lack of DDR1. It would be interesting to address whether upregulation of DDR2 could mediate such compensation. DDR2 has previously been found to be upregulated in chondrocytes of DDR1-null mice, where it was reported to account for increased osteoarthritis in the temporomandibular joint[139]. Additionally, I found that overexpression of DDR2 in MDCK cells had a similar phenotype to DDR1 overexpression in the tubulogenesis assay on beads (data not shown). Overexpression of DDR2 thus caused increased collective invasion resulting in formation of large hollow cysts around the beads, similar to those observed for DDR1-overexpressing cells in **Figure 21D**, Chapter

3. This suggests that DDR1 and -2 may have some overlapping functions in morphogenesis. However, it was recently shown that DDR2 can phosphorylate DDR1 during activation[56]. It is thus also possible that overexpression of DDR2 in MDCK cells may enhance activation of endogenous DDR1 and thereby cause a similar phenotype to overexpression of DDR1. It would be interesting to examine if expression of DDR2 in MDCK cells lacking DDR1 can promote the ability of these cells to polarise and undergo morphogenesis in 3D environments. I was unable to examine if DDR2 is upregulated in mammary gland tissue from DDR1-null animals due to a lack of specific antibodies. This should however be addressed upon identification of a suitable antibody.

Arguing against DDR2 compensating for DDR1 function in the DDR1-null mouse, a double DDR1/DDR2-null mouse was recently generated in Dr Itoh's lab and was found to be born and viable (personal communication with Dr Itoh). A detailed analysis of the phenotype of this mouse remains to be carried out, but preliminary examination suggested that DDR1/2-null mice are markedly smaller than wild type and heterozygous littermates. Given that the DDR1/2-null mouse is viable, it is likely that other ECM receptors can compensate for the lack of DDR1 in epithelial polarisation and morphogenesis, since a complete failure to do this would be expected to have a more severe phenotype. It will be interesting to conduct a detailed analysis of the phenotype of the DDR1/2 double knockout mouse in the future.

Further studies are required to determine whether the spatial regulation of MT1-MMP observed here in MDCK cells undergoing tubulogenesis has relevance during invasion in a pathological context. Additionally, the potential involvement of DDR1 in this regulation under pathological conditions remains unexplored. It would thus be interesting to investigate if MT1-MMP preferentially localises to the ECM-abutting basal

membrane at the invading front of well-differentiated carcinomas and whether DDR1 signalling can affect this. This could be studied *in vitro* by inducing cultures of carcinoma spheroids or tumour explants to invade into 3D collagen matrices[201]. Expression of MT1-pHluorin in such systems would allow for precise tracking of surface MT1-MMP during collective invasion. Collective invasion of cancer cells can furthermore be studied *in vivo* by intradermal injection of HT1080 cells in a modified skinfold chamber model for *in vivo* imaging[202]. Stable expression of MT1-pHluorin in carcinoma cells before injection in such a model could make it possible to follow the dynamics of surface localisation of MT1-MMP during invasion *in vivo* to determine if basal localisation of MT1-MMP indeed is observed at the invading front. One would however have to ensure that overexpression of MT1-MMP in this model does not interfere with the collective mode of migration or epithelial organisation. MDCK cells overexpressing MT1-MMP have previously been shown to display invasive, but non-metastatic behaviour upon subcutaneous injection in mice[203]. Despite the cells invading into the muscular layer in this model, the cells maintained a polarised organisation[203]. This model could thus potentially be useful for studying the apicobasal distribution of MT1-MMP in cells undergoing invasion *in vivo* whilst maintaining polarity. It may however be difficult to obtain sufficient resolution using *in vivo* imaging. Additionally, immunofluorescent staining of MT1-MMP in tissue sections from patients with invasive carcinomas could determine whether MT1-MMP localises to the ECM-facing surface of cells at the invading front of tumours during cancer progression *in vivo*.

Overall, work in this thesis suggests that DDR1 is important for establishment of epithelial cell polarity during physiological, morphogenic events. We hypothesise that a way in which DDR1 contributes to polarisation is by modulating cytoskeletal organisation

and tension via local suppression of ROCK activity at cell-cell junctions of well-polarised epithelial cells. This role of DDR1 likely involves recruitment of regulatory factors for RhoA-ROCK signalling. Many questions still remain regarding the mechanism behind this role of DDR1 in epithelial morphogenesis, as well as its relevance in less differentiated epithelial cells including cancer cells. An increased understanding of this may clarify how DDR1 signalling contributes to disease progression and identify important target molecules downstream of DDR1 in pathological settings. Understanding the physiological role of DDR1 may thus contribute to validating DDR1 as a potential therapeutical target as well as predict potential adverse effects of targeting DDR1 in disease.

Chapter 7 References

1. Alberts, B. *et al. Molecular biology of the cell*. (Garland Science, 2002).
2. Rodriguez-Boulan, E. & Macara, I. G. Organization and execution of the epithelial polarity programme. *Nat. Rev. Mol. Cell Biol.* **15,** 225–42 (2014).
3. Matter, K. & Balda, M. S. Signalling to and from tight junctions. *Nat. Rev. Mol. Cell Biol.* **4,** 225–36 (2003).
4. Arnold, T. R., Stephenson, R. E. & Miller, A. L. Rho GTPases and actomyosin: Partners in regulating epithelial cell-cell junction structure and function. *Exp. Cell Res.* (2017). doi:10.1016/j.yexcr.2017.03.053
5. Sluysmans, S. *et al.* The role of apical cell-cell junctions and associated cytoskeleton in mechanotransduction. *Biol. Cell* **109,** 139–161 (2017).
6. Miller, R. K. & McCrea, P. D. Wnt to build a tube: contributions of Wnt signaling to epithelial tubulogenesis. *Dev. Dyn.* **239,** 77–93 (2010).
7. Horowitz, A. & Simons, M. Branching morphogenesis. *Circ. Res.* **103,** 784–95 (2008).
8. Iruela-Arispe, M. L. & Beitel, G. J. Tubulogenesis. *Development* **140,** 2851–5 (2013).
9. Rodríguez-Fraticelli, A. E., Gálvez-Santisteban, M. & Martín-Belmonte, F. Divide and polarize: recent advances in the molecular mechanism regulating epithelial tubulogenesis. *Curr. Opin. Cell Biol.* **23,** 638–46 (2011).
10. Blasky, A. J., Mangan, A. & Prekeris, R. Polarized Protein Transport and Lumen Formation During Epithelial Tissue Morphogenesis. *Annu. Rev. Cell Dev. Biol.* **31,** 575–591 (2015).
11. Bryant, D. M. & Mostov, K. E. From cells to organs: building polarized tissue. *Nat. Rev. Mol. Cell Biol.* **9,** 887–901 (2008).
12. Zegers, M. M. & Friedl, P. Rho GTPases in collective cell migration. *Small GTPases* **5,** e28997 (2014).
13. Martin-Belmonte, F. *et al.* PTEN-Mediated Apical Segregation of Phosphoinositides Controls Epithelial Morphogenesis through Cdc42. *Cell* **128,** 383–397 (2007).
14. Yu, W. *et al.* Beta1-integrin orients epithelial polarity via Rac1 and laminin. *Mol. Biol. Cell* **16,** 433–45 (2005).
15. O'Brien, L. E. *et al.* Rac1 orientates epithelial apical polarity through effects on basolateral laminin assembly. *Nat. Cell Biol.* **3,** 831–8 (2001).
16. Nakayama, M. *et al.* Rho-Kinase Phosphorylates PAR-3 and Disrupts PAR Complex Formation. *Dev. Cell* **14,** 205–215 (2008).
17. Willenborg, C. & Prekeris, R. Apical protein transport and lumen morphogenesis in polarized epithelial cells. *Biosci. Rep.* **31,** 245–56 (2011).
18. Weisz, O. A. & Rodriguez-Boulan, E. Apical trafficking in epithelial cells: signals, clusters and motors. *J. Cell Sci.* **122,** (2009).
19. Terry, S. J. *et al.* Spatially restricted activation of RhoA signalling at epithelial junctions by p114RhoGEF drives junction formation and morphogenesis. *Nat. Cell Biol.* **13,** 159–66 (2011).
20. Lee, J. L. & Streuli, C. H. Integrins and epithelial cell polarity. *J. Cell Sci.* **127,** (2014).
21. Morrissey, M. A. & Sherwood, D. R. An active role for basement membrane assembly and modification in tissue sculpting. *J. Cell Sci.* **128,** 1661–8 (2015).
22. Kalluri, R. Angiogenesis: Basement membranes: structure, assembly and role in tumour angiogenesis. *Nat. Rev. Cancer* **3,** 422–433 (2003).
23. Yeh, Y.-C., Lin, H.-H. & Tang, M.-J. A tale of two collagen receptors, integrin β1 and discoidin domain receptor 1, in epithelial cell differentiation. *Am. J. Physiol.*

Cell Physiol. **303,** C1207-17 (2012).
24. Yu, W. *et al.* Involvement of RhoA, ROCK I and myosin II in inverted orientation of epithelial polarity. *EMBO Rep.* **9,** 923–9 (2008).
25. Wang, A. Z., Ojakian, G. K. & Nelson, W. J. Steps in the morphogenesis of a polarized epithelium. I. Uncoupling the roles of cell-cell and cell-substratum contact in establishing plasma membrane polarity in multicellular epithelial (MDCK) cysts. *J. Cell Sci.* **95,** (1990).
26. Wang, A. Z., Ojakian, G. K. & Nelson, W. J. Steps in the morphogenesis of a polarized epithelium. II. Disassembly and assembly of plasma membrane domains during reversal of epithelial cell polarity in multicellular epithelial (MDCK) cysts. *J. Cell Sci.* **95 (Pt 1),** 153–65 (1990).
27. Akhtar, N. & Streuli, C. H. An integrin-ILK-microtubule network orients cell polarity and lumen formation in glandular epithelium. *Nat. Cell Biol.* **15,** 17–27 (2013).
28. Naylor, M. J. *et al.* Ablation of beta1 integrin in mammary epithelium reveals a key role for integrin in glandular morphogenesis and differentiation. *J. Cell Biol.* **171,** 717–28 (2005).
29. Weir, M. L. *et al.* Dystroglycan loss disrupts polarity and β-casein induction in mammary epithelial cells by perturbing laminin anchoring. *J. Cell Sci.* **119,** (2006).
30. Vogel, W. F., Aszódi, A., Alves, F. & Pawson, T. Discoidin domain receptor 1 tyrosine kinase has an essential role in mammary gland development. *Mol. Cell. Biol.* **21,** 2906–17 (2001).
31. Faraci-Orf, E., McFadden, C. & Vogel, W. F. DDR1 signaling is essential to sustain Stat5 function during lactogenesis. *J. Cell. Biochem.* **97,** 109–21 (2006).
32. Wang, C.-Z., Hsu, Y.-M. & Tang, M.-J. Function of discoidin domain receptor I in HGF-induced branching tubulogenesis of MDCK cells in collagen gel. *J. Cell. Physiol.* **203,** 295–304 (2005).
33. McAteer, J. A., Evan, A. P. & Gardner, K. D. Morphogenetic clonal growth of kidney epithelial cell line MDCK. *Anat. Rec.* **217,** 229–239 (1987).
34. Montesano, R., Schaller, G. & Orci, L. Induction of epithelial tubular morphogenesis in vitro by fibroblast-derived soluble factors. *Cell* **66,** 697–711 (1991).
35. Montesano, R., Matsumoto, K., Nakamura, T. & Orci, L. Identification of a fibroblast-derived epithelial morphogen as hepatocyte growth factor. *Cell* **67,** 901–8 (1991).
36. Bryant, D. M. *et al.* A molecular network for de novo generation of the apical surface and lumen. *Nat. Cell Biol.* **12,** 1035–1045 (2010).
37. Bryant, D. M. *et al.* A Molecular Switch for the Orientation of Epithelial Cell Polarization. *Dev. Cell* **31,** 171–187 (2014).
38. Yu, W. *et al.* Hepatocyte growth factor switches orientation of polarity and mode of movement during morphogenesis of multicellular epithelial structures. *Mol. Biol. Cell* **14,** 748–63 (2003).
39. Pollack, A. L., Runyan, R. B. & Mostov, K. E. Morphogenetic mechanisms of epithelial tubulogenesis: MDCK cell polarity is transiently rearranged without loss of cell-cell contact during scatter factor/hepatocyte growth factor-induced tubulogenesis. *Dev. Biol.* **204,** 64–79 (1998).
40. Rosário, M. & Birchmeier, W. How to make tubes: signaling by the Met receptor tyrosine kinase. *Trends Cell Biol.* **13,** 328–335 (2003).
41. Zondag, G. C. M. *et al.* Oncogenic Ras Downregulates Rac Activity, Which Leads to Increased Rho Activity and Epithelial–Mesenchymal Transition. *J. Cell Biol.*

149, (2000).
42. Rogers, K. K., Jou, T.-S., Guo, W. & Lipschutz, J. H. The Rho family of small GTPases is involved in epithelial cystogenesis and tubulogenesis. *Kidney Int.* **63,** 1632–1644 (2003).
43. Kadono, Y. *et al.* Membrane type 1-matrix metalloproteinase is involved in the formation of hepatocyte growth factor/scatter factor-induced branching tubules in madin-darby canine kidney epithelial cells. *Biochem. Biophys. Res. Commun.* **251,** 681–7 (1998).
44. Carafoli, F. & Hohenester, E. Collagen recognition and transmembrane signalling by discoidin domain receptors. *Biochim. Biophys. Acta - Proteins Proteomics* **1834,** 2187–2194 (2013).
45. Vogel, W., Gish, G. D., Alves, F. & Pawson, T. The Discoidin Domain Receptor Tyrosine Kinases Are Activated by Collagen. *Mol. Cell* **1,** 13–23 (1997).
46. Shrivastava, A. *et al.* An Orphan Receptor Tyrosine Kinase Family Whose Members Serve as Nonintegrin Collagen Receptors. *Mol. Cell* **1,** 25–34 (1997).
47. Leitinger, B. & Kwan, A. P. L. The discoidin domain receptor DDR2 is a receptor for type X collagen. *Matrix Biol.* **25,** 355–364 (2006).
48. Leitinger, B. Discoidin domain receptor functions in physiological and pathological conditions. *Int. Rev. Cell Mol. Biol.* **310,** 39–87 (2014).
49. Noordeen, N. A., Carafoli, F., Hohenester, E., Horton, M. A. & Leitinger, B. A transmembrane leucine zipper is required for activation of the dimeric receptor tyrosine kinase DDR1. *J. Biol. Chem.* **281,** 22744–51 (2006).
50. Mihai, C., Chotani, M., Elton, T. S. & Agarwal, G. Mapping of DDR1 distribution and oligomerization on the cell surface by FRET microscopy. *J. Mol. Biol.* **385,** 432–45 (2009).
51. Lemeer, S. *et al.* Phosphotyrosine mediated protein interactions of the discoidin domain receptor 1. *J. Proteomics* **75,** 3465–3477 (2012).
52. Xu, H. *et al.* Collagen binding specificity of the discoidin domain receptors: Binding sites on collagens II and III and molecular determinants for collagen IV recognition by DDR1. *Matrix Biol.* **30,** 16–26 (2011).
53. Konitsiotis, A. D. *et al.* Characterization of High Affinity Binding Motifs for the Discoidin Domain Receptor DDR2 in Collagen. *J. Biol. Chem.* **283,** 6861–6868 (2008).
54. Carafoli, F. *et al.* Crystallographic Insight into Collagen Recognition by Discoidin Domain Receptor 2. *Structure* **17,** 1573–1581 (2009).
55. Lemmon, M. A. & Schlessinger, J. Cell Signaling by Receptor Tyrosine Kinases. *Cell* **141,** 1117–1134 (2010).
56. Juskaite, V., Corcoran, D. S. & Leitinger, B. Collagen induces activation of DDR1 through lateral dimer association and phosphorylation between dimers. *Elife* **6,** e25716 (2017).
57. Majkowska, I., Shitomi, Y., Ito, N., Gray, N. S. & Itoh, Y. Discoidin Domain Receptor 2 Mediates Collagen-Induced Activation of Membrane-Type 1 Matrix Metalloproteinase in Human Fibroblasts. *J. Biol. Chem.* jbc.M116.770057 (2017). doi:10.1074/jbc.M116.770057
58. Casaletto, J. B. & McClatchey, A. I. Spatial regulation of receptor tyrosine kinases in development and cancer. *Nat. Rev. Cancer* **12,** 387–400 (2012).
59. Valiathan, R. R., Marco, M., Leitinger, B., Kleer, C. G. & Fridman, R. Discoidin domain receptor tyrosine kinases: new players in cancer progression. *Cancer Metastasis Rev.* **31,** 295–321 (2012).
60. Shitomi, Y. *et al.* ADAM10 controls collagen signaling and cell migration on

collagen by shedding the ectodomain of discoidin domain receptor 1 (DDR1). *Mol. Biol. Cell* **26,** 659–73 (2015).
61. Fu, H.-L. *et al.* Shedding of discoidin domain receptor 1 by membrane-type matrix metalloproteinases. *J. Biol. Chem.* **288,** 12114–29 (2013).
62. Gross, O. *et al.* DDR1-deficient mice show localized subepithelial GBM thickening with focal loss of slit diaphragms and proteinuria. *Kidney Int.* **66,** 102–111 (2004).
63. Gross, O. *et al.* Loss of collagen-receptor DDR1 delays renal fibrosis in hereditary type IV collagen disease. *Matrix Biol.* **29,** 346–356 (2010).
64. Kerroch, M. *et al.* Protective effects of genetic inhibition of Discoidin Domain Receptor 1 in experimental renal disease. *Sci. Rep.* **6,** 21262 (2016).
65. Meyer zum Gottesberge, A. M., Gross, O., Becker-Lendzian, U., Massing, T. & Vogel, W. F. Inner ear defects and hearing loss in mice lacking the collagen receptor DDR1. *Lab. Investig.* **88,** 27–37 (2008).
66. Meyer zum Gottesberge, A. M. & Hansen, S. The collagen receptor DDR1 co-localizes with the non-muscle myosin IIA in mice inner ear and contributes to the cytoarchitecture and stability of motile cells. *Cell Tissue Res.* **358,** 729–736 (2014).
67. Wang, C.-Z., Su, H.-W., Hsu, Y.-C., Shen, M.-R. & Tang, M.-J. A Discoidin Domain Receptor 1/SHP-2 Signaling Complex Inhibits 2beta1-Integrin-mediated Signal Transducers and Activators of Transcription 1/3 Activation and Cell Migration. *Mol. Biol. Cell* **17,** 2839–2852 (2006).
68. Das, S. *et al.* Discoidin Domain Receptor 1 Receptor Tyrosine Kinase Induces Cyclooxygenase-2 and Promotes Chemoresistance through Nuclear Factor- B Pathway Activation. *Cancer Res.* **66,** 8123–8130 (2006).
69. Suh, H. N. & Han, H. J. Collagen I regulates the self-renewal of mouse embryonic stem cells through α2β1 integrin- and DDR1-dependent Bmi-1. *J. Cell. Physiol.* **226,** 3422–3432 (2011).
70. Yeh, Y.-C., Wang, C.-Z. & Tang, M.-J. Discoidin domain receptor 1 activation suppresses alpha2beta1 integrin-dependent cell spreading through inhibition of Cdc42 activity. *J. Cell. Physiol.* **218,** 146–56 (2009).
71. Yeh, Y.-C., Wu, C.-C., Wang, Y.-K. & Tang, M.-J. DDR1 triggers epithelial cell differentiation by promoting cell adhesion through stabilization of E-cadherin. *Mol. Biol. Cell* **22,** 940–53 (2011).
72. Huang, H. *et al.* Up-regulation of N-cadherin by Collagen I-activated Discoidin Domain Receptor 1 in Pancreatic Cancer Requires the Adaptor Molecule Shc1. *J. Biol. Chem.* **291,** 23208–23223 (2016).
73. Koh, M. *et al.* Discoidin domain receptor 1 is a novel transcriptional target of ZEB1 in breast epithelial cells undergoing H-Ras-induced epithelial to mesenchymal transition. *Int. J. Cancer* (2014). doi:10.1002/ijc.29154
74. Roberts, M. E., Magowan, L., Hall, I. P. & Johnson, S. R. Discoidin domain receptor 1 regulates bronchial epithelial repair and matrix metalloproteinase production. *Eur. Respir. J.* **37,** 1482–93 (2011).
75. Lu, K. K., Trcka, D. & Bendeck, M. P. Collagen stimulates discoidin domain receptor 1-mediated migration of smooth muscle cells through Src. *Cardiovasc. Pathol.* **20,** 71–76 (2011).
76. Juin, A. *et al.* Discoidin domain receptor 1 controls linear invadosome formation via a Cdc42-Tuba pathway. *J. Cell Biol.* **207,** 517–533 (2014).
77. Hidalgo-Carcedo, C. *et al.* Collective cell migration requires suppression of actomyosin at cell-cell contacts mediated by DDR1 and the cell polarity regulators Par3 and Par6. *Nat. Cell Biol.* **13,** 49–58 (2011).
78. Huang, Y., Arora, P., McCulloch, C. A. & Vogel, W. F. The collagen receptor

DDR1 regulates cell spreading and motility by associating with myosin IIA. *J. Cell Sci.* **122,** (2009).
79. Coelho, N. M. *et al.* Discoidin Domain Receptor 1 Mediates Myosin-Dependent Collagen Contraction. *Cell Rep.* **18,** 1774–1790 (2017).
80. Wang, C.-Z., Yeh, Y.-C. & Tang, M.-J. DDR1/E-cadherin complex regulates the activation of DDR1 and cell spreading. *Am. J. Physiol. Cell Physiol.* **297,** C419-29 (2009).
81. Eswaramoorthy, R. *et al.* DDR1 regulates the stabilization of cell surface E-cadherin and E-cadherin-mediated cell aggregation. *J. Cell. Physiol.* **224,** 387–97 (2010).
82. Chen, H.-R. *et al.* DDR1 promotes E-cadherin stability via inhibition of integrin-β1-Src activation-mediated E-cadherin endocytosis. *Sci. Rep.* **6,** 36336 (2016).
83. Chow, C. R. *et al.* Cancer Cell Invasion in Three-dimensional Collagen Is Regulated Differentially by Gα13 Protein and Discoidin Domain Receptor 1-Par3 Protein Signaling. *J. Biol. Chem.* **291,** 1605–18 (2016).
84. Shintani, Y. *et al.* Collagen I-mediated up-regulation of N-cadherin requires cooperative signals from integrins and discoidin domain receptor 1. *J. Cell Biol.* **180,** 1277–89 (2008).
85. Xie, R. *et al.* DDR1 enhances invasion and metastasis of gastric cancer via epithelial-mesenchymal transition. *Tumor Biol.* **37,** 12049–12059 (2016).
86. Hu, Y. *et al.* MiR-199a-5p Loss Up-Regulated DDR1 Aggravated Colorectal Cancer by Activating Epithelial-to-Mesenchymal Transition Related Signaling. *Dig. Dis. Sci.* **59,** 2163–2172 (2014).
87. Câmara, J. & Jarai, G. Epithelial-mesenchymal transition in primary human bronchial epithelial cells is Smad-dependent and enhanced by fibronectin and TNF-α. *Fibrogenesis Tissue Repair* **3,** 2 (2010).
88. Maeyama, M. *et al.* Switching in discoid domain receptor expressions in SLUG-induced epithelial-mesenchymal transition. *Cancer* **113,** 2823–31 (2008).
89. Kalluri, R., Weinberg, R. A., Blumenberg, M., Schneider, R. J. & Thiery, J. P. The basics of epithelial-mesenchymal transition. *J. Clin. Invest.* **119,** 1420–8 (2009).
90. Mouw, J. K., Ou, G. & Weaver, V. M. Extracellular matrix assembly: a multiscale deconstruction. *Nat. Rev. Mol. Cell Biol.* **15,** 771–85 (2014).
91. Itoh, Y. & Seiki, M. MT1-MMP: a potent modifier of pericellular microenvironment. *J. Cell. Physiol.* **206,** 1–8 (2006).
92. Itoh, Y. Membrane-type matrix metalloproteinases: Their functions and regulations. *Matrix Biol.* **44,** 207–223 (2015).
93. Weaver, S. A. *et al.* Basal localization of MT1-MMP is essential for epithelial cell morphogenesis in 3D collagen matrix. *J. Cell Sci.* (2014). doi:10.1242/jcs.135236
94. Hotary, K., Allen, E., Punturieri, A., Yana, I. & Weiss, S. J. Regulation of cell invasion and morphogenesis in a three-dimensional type I collagen matrix by membrane-type matrix metalloproteinases 1, 2, and 3. *J. Cell Biol.* **149,** 1309–23 (2000).
95. Itoh, Y. MT1-MMP: a key regulator of cell migration in tissue. *IUBMB Life* **58,** 589–96 (2006).
96. Woskowicz, A. M., Weaver, S. A., Shitomi, Y., Ito, N. & Itoh, Y. MT-LOOP-dependent Localization of Membrane Type I Matrix Metalloproteinase (MT1-MMP) to the Cell Adhesion Complexes Promotes Cancer Cell Invasion. *J. Biol. Chem.* **288,** 35126–37 (2013).
97. Holmbeck, K. *et al.* MT1-MMP-Deficient Mice Develop Dwarfism, Osteopenia, Arthritis, and Connective Tissue Disease due to Inadequate Collagen Turnover.

Cell **99,** 81–92 (1999).
98. Zhou, Z. *et al.* Impaired endochondral ossification and angiogenesis in mice deficient in membrane-type matrix metalloproteinase I. *Proc. Natl. Acad. Sci. U. S. A.* **97,** 4052–7 (2000).
99. Koenig, G. C. *et al.* MT1-MMP-dependent remodeling of cardiac extracellular matrix structure and function following myocardial infarction. *Am. J. Pathol.* **180,** 1863–78 (2012).
100. Rajavashisth, T. B. *et al.* Membrane type 1 matrix metalloproteinase expression in human atherosclerotic plaques: evidence for activation by proinflammatory mediators. *Circulation* **99,** 3103–9 (1999).
101. Hiraoka, N., Allen, E., Apel, I. J., Gyetko, M. R. & Weiss, S. J. Matrix metalloproteinases regulate neovascularization by acting as pericellular fibrinolysins. *Cell* **95,** 365–77 (1998).
102. Castro-Castro, A. *et al.* Cellular and Molecular Mechanisms of MT1-MMP-Dependent Cancer Cell Invasion. *Annu. Rev. Cell Dev. Biol.* **32,** annurev-cellbio-111315-125227 (2016).
103. Hotary, K., Li, X.-Y., Allen, E., Stevens, S. L. & Weiss, S. J. A cancer cell metalloprotease triad regulates the basement membrane transmigration program. *Genes Dev.* **20,** 2673–86 (2006).
104. Rowe, R. G. & Weiss, S. J. Breaching the basement membrane: who, when and how? *Trends Cell Biol.* **18,** 560–574 (2008).
105. Itoh, Y. *et al.* Homophilic complex formation of MT1-MMP facilitates proMMP-2 activation on the cell surface and promotes tumor cell invasion. *EMBO J.* **20,** 4782–93 (2001).
106. Itoh, Y., Ito, N., Nagase, H. & Seiki, M. The second dimer interface of MT1-MMP, the transmembrane domain, is essential for ProMMP-2 activation on the cell surface. *J. Biol. Chem.* **283,** 13053–62 (2008).
107. Wang, Z., Juttermann, R. & Soloway, P. D. TIMP-2 is required for efficient activation of proMMP-2 in vivo. *J. Biol. Chem.* **275,** 26411–5 (2000).
108. Knäuper, V. *et al.* Cellular mechanisms for human procollagenase-3 (MMP-13) activation. Evidence that MT1-MMP (MMP-14) and gelatinase a (MMP-2) are able to generate active enzyme. *J. Biol. Chem.* **271,** 17124–31 (1996).
109. Ratnikov, B. I. *et al.* An Alternative Processing of Integrin v Subunit in Tumor Cells by Membrane Type-1 Matrix Metalloproteinase. *J. Biol. Chem.* **277,** 7377–7385 (2002).
110. Atapattu, L., Lackmann, M. & Janes, P. W. The role of proteases in regulating Eph/ephrin signaling. *Cell Adh. Migr.* **8,** 294–307 (2014).
111. Itoh, Y. Membrane-type matrix metalloproteinases: Their functions and regulations. *Matrix Biol.* **44–46,** 207–223 (2015).
112. Kajita, M. *et al.* Membrane-Type 1 Matrix Metalloproteinase Cleaves Cd44 and Promotes Cell Migration. *J. Cell Biol.* **153,** (2001).
113. Yamamoto, K. *et al.* Inhibition of Shedding of Low-Density Lipoprotein Receptor-Related Protein 1 Reverses Cartilage Matrix Degradation in Osteoarthritis. *Arthritis Rheumatol.* (2017). doi:10.1002/art.40080
114. Koshikawa, N., Minegishi, T., Sharabi, A., Quaranta, V. & Seiki, M. Membrane-type Matrix Metalloproteinase-1 (MT1-MMP) Is a Processing Enzyme for Human Laminin 2 Chain. *J. Biol. Chem.* **280,** 88–93 (2005).
115. Mori, H. *et al.* Transmembrane/cytoplasmic, rather than catalytic, domains of Mmp14 signal to MAPK activation and mammary branching morphogenesis via binding to integrin β1. *Development* **140,** 343–52 (2013).

116. Szabova, L., Yamada, S. S., Birkedal-Hansen, H. & Holmbeck, K. Expression pattern of four membrane-type matrix metalloproteinases in the normal and diseased mouse mammary gland. *J. Cell. Physiol.* **205,** 123–132 (2005).
117. Wiseman, B. S. *et al.* Site-specific inductive and inhibitory activities of MMP-2 and MMP-3 orchestrate mammary gland branching morphogenesis. *J. Cell Biol.* **162,** (2003).
118. Kadono, Y., Okada, Y., Namiki, M., Seiki, M. & Sato, H. Transformation of epithelial Madin-Darby canine kidney cells with p60(v-src) induces expression of membrane-type 1 matrix metalloproteinase and invasiveness. *Cancer Res.* **58,** 2240–4 (1998).
119. Mahimkar, R., Alfonso-Jaume, M. A., Cape, L. M., Dahiya, R. & Lovett, D. H. Graded activation of the MEK1/MT1-MMP axis determines renal epithelial cell tumor phenotype. *Carcinogenesis* **32,** 1806–14 (2011).
120. Ota, I., Li, X.-Y., Hu, Y. & Weiss, S. J. Induction of a MT1-MMP and MT2-MMP-dependent basement membrane transmigration program in cancer cells by Snail1. *Proc. Natl. Acad. Sci. U. S. A.* **106,** 20318–23 (2009).
121. Tanaka, S. S. *et al.* Cell-Cell Contact Down-Regulates Expression of Membrane Type MetaIIoproteinase-1 (MT1-MMP) in a Mouse Mammary Gland Epithelial Cell Line. *Zoolog. Sci.* **14,** 95–99 (1997).
122. Fata, J. E., Werb, Z. & Bissell, M. J. Regulation of mammary gland branching morphogenesis by the extracellular matrix and its remodeling enzymes. *Breast Cancer Res.* **6,** 1–11 (2004).
123. Mori, H. *et al.* CD44 directs membrane-type 1 matrix metalloproteinase to lamellipodia by associating with its hemopexin-like domain. *EMBO J.* **21,** 3949–59 (2002).
124. Terawaki, S., Kitano, K., Aoyama, M., Mori, T. & Hakoshima, T. MT1-MMP recognition by ERM proteins and its implication in CD44 shedding. *Genes to Cells* **20,** 847–859 (2015).
125. Poincloux, R., Lizárraga, F. & Chavrier, P. Matrix invasion by tumour cells: a focus on MT1-MMP trafficking to invadopodia. *J. Cell Sci.* **122,** 3015–24 (2009).
126. Yamaguchi, H. *et al.* Lipid Rafts and Caveolin-1 Are Required for Invadopodia Formation and Extracellular Matrix Degradation by Human Breast Cancer Cells. *Cancer Res.* **69,** 8594–8602 (2009).
127. Uekita, T., Itoh, Y., Yana, I., Ohno, H. & Seiki, M. Cytoplasmic tail–dependent internalization of membrane-type 1 matrix metalloproteinase is important for its invasion-promoting activity. *J. Cell Biol.* **155,** 1345–1356 (2001).
128. Anilkumar, N. *et al.* Palmitoylation at Cys574 is essential for MT1-MMP to promote cell migration. *FASEB J.* **19,** 1326–8 (2005).
129. Bravo-Cordero, J. J. *et al.* MT1-MMP proinvasive activity is regulated by a novel Rab8-dependent exocytic pathway. *EMBO J.* **26,** 1499–510 (2007).
130. Itoh, Y. *et al.* Dimerization of MT1-MMP during cellular invasion detected by fluorescence resonance energy transfer. *Biochem. J.* **440,** 319–26 (2011).
131. Miesenböck, G., De Angelis, D. A. & Rothman, J. E. Visualizing secretion and synaptic transmission with pH-sensitive green fluorescent proteins. *Nature* **394,** 192–5 (1998).
132. Palmisano, R. & Itoh, Y. Analysis of MMP-dependent cell migration and invasion. *Methods Mol. Biol.* **622,** 379–92 (2010).
133. Sankaranarayanan, S., De Angelis, D., Rothman, J. E. & Ryan, T. A. The Use of pHluorins for Optical Measurements of Presynaptic Activity. *Biophys. J.* **79,** 2199–2208 (2000).

134. Casey, J. R., Grinstein, S. & Orlowski, J. Sensors and regulators of intracellular pH. *Nat. Rev. Mol. Cell Biol.* **11,** 50–61 (2010).
135. Kim, H.-G. *et al.* Discovery of a potent and selective DDR1 receptor tyrosine kinase inhibitor. *ACS Chem. Biol.* **8,** 2145–50 (2013).
136. Meder, D., Shevchenko, A., Simons, K. & Füllekrug, J. Gp135/podocalyxin and NHERF-2 participate in the formation of a preapical domain during polarization of MDCK cells. *J. Cell Biol.* **168,** 303–13 (2005).
137. Bacallao, R. *et al.* The subcellular organization of Madin-Darby canine kidney cells during the formation of a polarized epithelium. *J. Cell Biol.* **109,** (1989).
138. Torkko, J. M., Manninen, A., Schuck, S. & Simons, K. Depletion of apical transport proteins perturbs epithelial cyst formation and ciliogenesis. *J. Cell Sci.* **121,** 1193–203 (2008).
139. Schminke, B. *et al.* A discoidin domain receptor 1 knock-out mouse as a novel model for osteoarthritis of the temporomandibular joint. *Cell. Mol. Life Sci.* **71,** 1081–1096 (2014).
140. Barr, F. A. & Egerer, J. Golgi positioning: are we looking at the right MAP? *J. Cell Biol.* **168,** 993–8 (2005).
141. Rausch, S. *et al.* Polarizing cytoskeletal tension to induce leader cell formation during collective cell migration. *Biointerphases* **8,** 32 (2013).
142. Grindstaff, K. K. *et al.* Sec6/8 Complex Is Recruited to Cell–Cell Contacts and Specifies Transport Vesicle Delivery to the Basal-Lateral Membrane in Epithelial Cells. *Cell* **93,** 731–740 (1998).
143. Yeaman, C., Grindstaff, K. K. & Nelson, W. J. Mechanism of recruiting Sec6/8 (exocyst) complex to the apical junctional complex during polarization of epithelial cells. *J. Cell Sci.* **117,** (2004).
144. Malaguarnera, R. *et al.* Novel cross talk between IGF-IR and DDR1 regulates IGF-IR trafficking, signaling and biological responses. *Oncotarget* **6,** 16084–16105 (2015).
145. Gálvez, B. G., Matías-Román, S., Yáñez-Mó, M., Sánchez-Madrid, F. & Arroyo, A. G. ECM regulates MT1-MMP localization with beta1 or alphavbeta3 integrins at distinct cell compartments modulating its internalization and activity on human endothelial cells. *J. Cell Biol.* **159,** 509–21 (2002).
146. Gonzalo, P., Moreno, V., Gálvez, B. G. & Arroyo, A. G. MT1-MMP and integrins: Hand-to-hand in cell communication. *BioFactors* **36,** 248–254 (2010).
147. Wang, C.-Z., Yeh, Y.-C. & Tang, M.-J. DDR1/E-cadherin complex regulates the activation of DDR1 and cell spreading. *Am. J. Physiol. Cell Physiol.* **297,** C419-29 (2009).
148. Gao, H. *et al.* Multi-organ Site Metastatic Reactivation Mediated by Non-canonical Discoidin Domain Receptor 1 Signaling. *Cell* **166,** 47–62 (2016).
149. Julian, L. & Olson, M. F. Rho-associated coiled-coil containing kinases (ROCK). *Small GTPases* **5,** e29846 (2014).
150. Haeger, A., Wolf, K., Zegers, M. M. & Friedl, P. Collective cell migration: Guidance principles and hierarchies. *Trends in Cell Biology* **25,** 556–566 (2015).
151. Wozniak, M. A., Desai, R., Solski, P. A., Der, C. J. & Keely, P. J. ROCK-generated contractility regulates breast epithelial cell differentiation in response to the physical properties of a three-dimensional collagen matrix. *J. Cell Biol.* **163,** (2003).
152. Gálvez-Santisteban, M. *et al.* Synaptotagmin-like proteins control the formation of a single apical membrane domain in epithelial cells. *Nat. Cell Biol.* **14,** 838–849 (2012).

153. Roh, M. H., Fan, S., Liu, C.-J. & Margolis, B. The Crumbs3-Pals1 complex participates in the establishment of polarity in mammalian epithelial cells. *J. Cell Sci.* **116,** (2003).
154. Horikoshi, Y. *et al.* Interaction between PAR-3 and the aPKC–PAR-6 complex is indispensable for apical domain development of epithelial cells. *J. Cell Sci.* **122,** (2009).
155. Sfakianos, J. *et al.* Par3 functions in the biogenesis of the primary cilium in polarized epithelial cells. *J. Cell Biol.* **179,** (2007).
156. Eswaramoorthy, R. *et al.* DDR1 regulates the stabilization of cell surface E-cadherin and E-cadherin-mediated cell aggregation. *J. Cell. Physiol.* **224,** 387–397 (2010).
157. El Azreq, M.-A. *et al.* Discoidin domain receptor 1 promotes Th17 cell migration by activating the RhoA/ROCK/MAPK/ERK signaling pathway. *Oncotarget* **7,** 44975–44990 (2014).
158. Kodama, A. *et al.* Involvement of an SHP-2-Rho small G protein pathway in hepatocyte growth factor/scatter factor-induced cell scattering. *Mol. Biol. Cell* **11,** 2565–75 (2000).
159. Piekny, A. J. & Glotzer, M. *Anillin Is a Scaffold Protein That Links RhoA, Actin, and Myosin during Cytokinesis*. *Current Biology* **18,** (2008).
160. Pertz, O., Hodgson, L., Klemke, R. L. & Hahn, K. M. Spatiotemporal dynamics of RhoA activity in migrating cells. *Nature* **440,** 1069–72 (2006).
161. Li, C. *et al.* A FRET Biosensor for ROCK Based on a Consensus Substrate Sequence Identified by KISS Technology. *Cell Struct. Funct.* **42,** 1–13 (2017).
162. Myllymäki, S. M. *et al.* Two Distinct Integrin-Mediated Mechanisms Contribute to Apical Lumen Formation in Epithelial Cells. *PLoS One* **6,** e19453 (2011).
163. Monteleon, C. L. *et al.* Establishing epithelial glandular polarity: interlinked roles for ARF6, Rac1, and the matrix microenvironment. *Mol. Biol. Cell* **23,** 4495–505 (2012).
164. Martín-Belmonte, F. *et al.* Cell-polarity dynamics controls the mechanism of lumen formation in epithelial morphogenesis. *Curr. Biol.* **18,** 507–13 (2008).
165. Ispanovic, E., Serio, D. & Haas, T. L. Cdc42 and RhoA have opposing roles in regulating membrane type 1-matrix metalloproteinase localization and matrix metalloproteinase-2 activation. *AJP Cell Physiol.* **295,** C600–C610 (2008).
166. Lagoutte, E. *et al.* LIMK Regulates Tumor-Cell Invasion and Matrix Degradation Through Tyrosine Phosphorylation of MT1-MMP. *Sci. Rep.* **6,** 24925 (2016).
167. Inman, J. L., Robertson, C., Mott, J. D. & Bissell, M. J. Mammary gland development: cell fate specification, stem cells and the microenvironment. *Development* **142,** 1028–1042 (2015).
168. Mroue, R. & Bissell, M. J. Three-dimensional cultures of mouse mammary epithelial cells. *Methods Mol. Biol.* **945,** 221–50 (2013).
169. Du, J.-Y. *et al.* The RhoA-Rok-myosin II pathway is involved in extracellular matrix-mediated regulation of prolactin signaling in mammary epithelial cells. *J. Cell. Physiol.* **227,** 1553–1560 (2012).
170. van Miltenburg, M. H. A. M. *et al.* Complete focal adhesion kinase deficiency in the mammary gland causes ductal dilation and aberrant branching morphogenesis through defects in Rho kinase-dependent cell contractility. *FASEB J.* **23,** 3482–3493 (2009).
171. Wiseman, B. S. & Werb, Z. Stromal Effects on Mammary Gland Development and Breast Cancer. *Science (80-.).* **296,** (2002).
172. Morales, F. C., Hayashi, Y., van Pelt, C. S. & Georgescu, M.-M. NHERF1/EBP50

controls lactation by establishing basal membrane polarity complexes with prolactin receptor. *Cell Death Dis.* **3,** e391 (2012).
173. Ball, R. K., Friis, R. R., Schoenenberger, C. A., Doppler, W. & Groner, B. Prolactin regulation of beta-casein gene expression and of a cytosolic 120-kd protein in a cloned mouse mammary epithelial cell line. *EMBO J.* **7,** 2089–95 (1988).
174. Morrison, B. & Cutler, M. Lou. Mouse Mammary Epithelial Cells form Mammospheres During Lactogenic Differentiation. *J. Vis. Exp.* (2009). doi:10.3791/1265
175. Mikaelian, I. *et al.* Expression of Terminal Differentiation Proteins Defines Stages of Mouse Mammary Gland Development. *Vet. Pathol.* **43,** 36–49 (2006).
176. Xu, R. *et al.* Sustained activation of STAT5 is essential for chromatin remodeling and maintenance of mammary-specific function. *J. Cell Biol.* **184,** (2009).
177. Streuli, C. H. *et al.* Laminin mediates tissue-specific gene expression in mammary epithelia. *J. Cell Biol.* **129,** (1995).
178. Oakes, S. R., Hilton, H. N. & Ormandy, C. J. The alveolar switch: coordinating the proliferative cues and cell fate decisions that drive the formation of lobuloalveoli from ductal epithelium. *Breast Cancer Res.* **8,** 207 (2006).
179. Barcellos-Hoff, M. H., Aggeler, J., Ram, T. G. & Bissell, M. J. Functional differentiation and alveolar morphogenesis of primary mammary cultures on reconstituted basement membrane. *Development* **105,** (1989).
180. Zoubiane, G. S. *et al.* A role for the cytoskeleton in prolactin-dependent mammary epithelial cell differentiation. *J. Cell Sci.* **117,** 271–80 (2004).
181. Schedin, P. & Keely, P. J. Mammary gland ECM remodeling, stiffness, and mechanosignaling in normal development and tumor progression. *Cold Spring Harb. Perspect. Biol.* **3,** a003228 (2011).
182. Nguyen, D.-A. D. & Neville, M. C. Tight Junction Regulation in the Mammary Gland. *J. Mammary Gland Biol. Neoplasia* **3,** 233–246 (1998).
183. Rubenstein, N. M., Chan, J. F., Kim, J. Y., Hansen, S. H. & Firestone, G. L. Rnd3/RhoE induces tight junction formation in mammary epithelial tumor cells. *Exp. Cell Res.* **305,** 74–82 (2005).
184. Stelwagen, K. & Singh, K. The Role of Tight Junctions in Mammary Gland Function. *J. Mammary Gland Biol. Neoplasia* **19,** 131–138 (2014).
185. Chen, L. H. & Bissell, M. J. A novel regulatory mechanism for whey acidic protein gene expression. *Cell Regul.* **1,** 45–54 (1989).
186. Lin, C. Q., Dempsey, P. J., Coffey, R. J. & Bissell, M. J. Extracellular matrix regulates whey acidic protein gene expression by suppression of TGF-alpha in mouse mammary epithelial cells: studies in culture and in transgenic mice. *J. Cell Biol.* **129,** 1115–26 (1995).
187. Nabeshima, K., Inoue, T., Shimao, Y., Kataoka, H. & Koono, M. Cohort migration of carcinoma cells: differentiated colorectal carcinoma cells move as coherent cell clusters or sheets. *Histol. Histopathol.* **14,** 1183–97 (1999).
188. Sabeh, F. *et al.* Tumor cell traffic through the extracellular matrix is controlled by the membrane-anchored collagenase MT1-MMP. *J. Cell Biol.* **167,** 769–781 (2004).
189. Christiansen, J. J. & Rajasekaran, A. K. Reassessing Epithelial to Mesenchymal Transition as a Prerequisite for Carcinoma Invasion and Metastasis. *Cancer Res.* **66,** (2006).
190. Ezzoukhry, Z. *et al.* TGF-β1 promotes linear invadosome formation in hepatocellular carcinoma cells, through DDR1 up-regulation and collagen I cross-

linking. *Eur. J. Cell Biol.* **95,** 503–512 (2016).
191. Yang, J. *et al.* TM4SF1 Promotes Metastasis of Pancreatic Cancer via Regulating the Expression of DDR1. *Sci. Rep.* **7,** 45895 (2017).
192. Rikova, K. *et al.* Global Survey of Phosphotyrosine Signaling Identifies Oncogenic Kinases in Lung Cancer. *Cell* **131,** 1190–1203 (2007).
193. Ambrogio, C. *et al.* KRAS-driven lung adenocarcinoma: combined DDR1/Notch inhibition as an effective therapy. *ESMO Open* **1,** (2016).
194. Rudra-Ganguly, N. *et al.* Discoidin domain receptor 1 contributes to tumorigenesis through modulation of TGFBI expression. *PLoS One* **9,** e111515 (2014).
195. Etienne-Manneville, S. Polarity proteins in migration and invasion. *Oncogene* **27,** 6970–6980 (2008).
196. Tanos, B. & Rodriguez-Boulan, E. The epithelial polarity program: machineries involved and their hijacking by cancer. *Oncogene* **27,** 6939–6957 (2008).
197. Pegtel, D. M. *et al.* The Par-Tiam1 complex controls persistent migration by stabilizing microtubule-dependent front-rear polarity. *Curr. Biol.* **17,** 1623–34 (2007).
198. Kim, K., Lu, Z. & Hay, E. D. Direct evidence for a role of beta-catenin/LEF-1 signaling pathway in induction of EMT. *Cell Biol. Int.* **26,** 463–76 (2002).
199. Friedl, P. & Gilmour, D. Collective cell migration in morphogenesis, regeneration and cancer. *Nat. Rev. Mol. Cell Biol.* **10,** 445–457 (2009).
200. Wei, L., Surma, M., Shi, S., Lambert-Cheatham, N. & Shi, J. Novel Insights into the Roles of Rho Kinase in Cancer. *Arch. Immunol. Ther. Exp. (Warsz).* **64,** 259–278 (2016).
201. Friedl, P. *et al.* Migration of coordinated cell clusters in mesenchymal and epithelial cancer explants in vitro. *Cancer Res.* **55,** 4557–60 (1995).
202. Alexander, S., Koehl, G. E., Hirschberg, M., Geissler, E. K. & Friedl, P. Dynamic imaging of cancer growth and invasion: a modified skin-fold chamber model. *Histochem. Cell Biol.* **130,** 1147–1154 (2008).
203. Soulié, P. *et al.* Membrane-type-1 matrix metalloproteinase confers tumorigenicity on nonmalignant epithelial cells. *Oncogene* **24,** 1689–1697 (2005).

Chapter 8 Appendix

8.1 Supplementary tables

Table S1 – summary of statistic analysis in chapter 4, Figure 35A

The tested conditions were compared with a Kruskal-Wallis rank sum test ($p=4.852*10^{-14}$) before localising differences with a pairwise Wilcoxon test with Holm correction of the p-value to correct for multiple testing. Asterisks *, **, ***. **** depict statistically significant differences of $p<0.05$, $p<0.01$, $p<0.001$ and $p<0.0001$ respectively.

	Ctr	DDR1-IN-1	DDR1-IN-1 HGF	DDR1-IN-1 Y27632	DDR1-IN-1 Y27632+HGF
Ctr+HGF	****	NS	NS	****	**
DDR1-IN-1	****	-	-	-	-
DDR1-IN-1+HGF	****	NS	-	-	-
DDR1-IN-1+Y27632	NS	****	****	-	-
DDR1-IN-1+Y27632+HGF	**	****	**	NS	-

Table S2– summary of statistic analysis in chapter 5, Figure 39C

A Kruskal test was performed to compare conditions, followed by a pairwise Wilcoxon test with Holm correction for multiple testing to locate significant differences. *** represents p-values<0.001. Asterisks *, **, ***. **** depict statistically significant differences of $p<0.05$, $p<0.01$, $p<0.001$ and $p<0.0001$ respectively.

	DIP	DIP DDR1-IN-1	DIP DDR1-IN-1 +H1152	DDR1-IN-1 H1152
DIP+DDR1-IN1	****	-	-	-
DIP+DDR1-IN1+H1152	**	****	-	-
DIP+H1152	****	****	NS	-
No DIP	****	***	****	****